

Syracuse University

SURFACE at Syracuse University

Dissertations - ALL

SURFACE at Syracuse University

Summer 7-1-2022

WDR5 Network Analysis Using Ensemble Approaches

Ali Imran

Syracuse University

Follow this and additional works at: <https://surface.syr.edu/etd>



Part of the [Biophysics Commons](#)

Recommended Citation

Imran, Ali, "WDR5 Network Analysis Using Ensemble Approaches" (2022). *Dissertations - ALL*. 1562.
<https://surface.syr.edu/etd/1562>

This Dissertation is brought to you for free and open access by the SURFACE at Syracuse University at SURFACE at Syracuse University. It has been accepted for inclusion in Dissertations - ALL by an authorized administrator of SURFACE at Syracuse University. For more information, please contact surface@syr.edu.

Abstract

Understanding the properties of protein-protein interactions (PPIs) is necessary to deconvolute the processes inside living organisms. As such, research in this regard has significant implications for gaining insight into cancers and other diseases. Once understood, drugs can be designed to target these diseases. In these chapters we focus on the network of interactions of WD40 repeat protein 5 (WDR5), a known hub protein. Several of its interactions are significant for regulation of histone methylation and consequently epigenetic regulation. These interacting partners include the SET1 family of proteins and retinoblastoma binding protein-5 (RbBP5). In this work we used multiple ensemble measurement based bulk-phase techniques to characterize WDR5's interactions. We utilized biolayer interferometry (BLI) and surface plasmon resonance (SPR) to calculate the association and dissociation rate constants. Furthermore, we used fluorescence polarization (FP) to calculate the equilibrium dissociation constants. After characterizing these PPIs under wild-type conditions we quantified the impact of key WDR5 cancer mutants on these interactions. These mutants can impact downstream gene expression, which ultimately controls various cellular processes. Therefore, evaluating their modification of WDR5's kinetics is key to understanding their potential impact on tumor development. Additionally, by using different tether conditions, we have explored the role of surface-tethering in modulating the kinetics of these PPIs. The work shows the impact of tethering on tethered ligand-receptor complexes that are common in biological signaling and

cellular adhesion. Moreover, it shows how surface-tethering can be used to modulate a typical PPI. We also characterized the role of the N-terminal intrinsically disordered region (IDR) of WDR5. Our work explores the self-association behavior catalyzed by this IDR and the potential ramifications of this self-association on WDR5's role inside the nucleus.

WDR5 network analysis using ensemble approaches

By

Ali Imran

B.S., Lahore University of Management Sciences, 2016

M.S., Syracuse University, 2018

Dissertation

Submitted in partial fulfillment of the requirements for the degree of Doctor of
Philosophy in Physics

Syracuse University

July 2022

Copyright © Ali Imran 2022

All Rights Reserved

Acknowledgements

I would like to thank all the people, who have supported me in the writing of this thesis and have made this work possible.

I would like to thank my advisor, Dr. Liviu Movileanu, for giving me the opportunity to perform research in his lab. The guidance, resources, and freedom he gave me, allowed me to pursue and address important research questions.

I am grateful to Dr. Ivan Korendovych, Dr. Jennifer Ross, Dr. Alison Patteson, Dr. Jennifer Schwarz and Dr. Michael Cosgrove who kindly accepted to evaluate my work.

I would like to thank Dr. Aaron Wolfe, Dr. Brandon Moyer and the many people at Ichor whose contributions and expertise were crucial to our projects.

I would like to thank Dr. Thomas Duncan for his advice on my experiments.

I am indebted to the members of Dr. Movileanu's group and Dr. Cosgrove's group for helpful discussions and guidance in this research.

I am grateful to my colleagues in the physics department for fostering a friendly and constructive environment that was conducive to learning and growth.

Last but not least, I would like to thank my family. My parents for their constant support and encouragement. My sister, Hafsa, for keeping me motivated. My brother, Usman, for his helpful advice. And my wife, Maryam, whose love and support kept me going.

Contents

Abstract.....	i
List of Figures.....	viii
List of Tables	xi
List of Publications	xiv
Chapter 1: Introduction	1
1.1 Protein System	1
1.1.1 WDR5	1
1.1.2 SET1 Proteins	3
1.1.3 RbBP5	4
1.2 Theoretical Overview.....	5
1.3 Bulk-phase Techniques.....	6
1.3.1 Biolayer Interferometry.....	6
1.3.2 Surface Plasmon Resonance	8
1.3.3 Steady-state Fluorescence Polarization.....	8
1.4 Thesis Outline	9
1.5 REFERENCES	12
Chapter 2: Kinetics of the multitasking high-affinity Win binding site of WDR5 in restricted and unrestricted conditions	15
2.1 Abstract.....	16
2.2 Introduction.....	17
2.3 Materials and Methods.....	23
2.4 Results and Discussion	35
2.5 Concluding remarks, practical implications, and future prospects	49
2.6 SUPPORTING INFORMATION	52
2.7 REFERENCES	65
Chapter 3: Convergent Oncogenic Alterations of a Protein Hub Produce Divergent Effects Within a Binding Site.....	73
3.1 Abstract.....	74
3.2 Introduction.....	75

3.3 Materials and Methods.....	79
3.4 Results and Discussion	83
3.5 Concluding remarks	99
3.6 SUPPLEMENTARY INFORMATION	100
3.7 REFERENCES	120
Chapter 4: The Interplay of Affinity and Surface Tethering in Protein Recognition	127
4.1 Abstract.....	128
4.2 Introduction.....	129
4.3 Results and Discussion	132
4.4 Conclusion	147
4.5 SUPPLEMENTARY INFORMATION	148
4.6 REFERENCES	172
Chapter 5: N-terminus IDR of WDR5 Impacts its Function and Kinetic Measurements	177
5.1 Abstract.....	178
5.2 Introduction.....	179
5.3 Results and Discussion	181
5.4 Conclusions.....	193
5.5 Materials and Methods.....	193
5.6 SUPPLEMENTARY INFORMATION	196
5.7 REFERENCES	210
Chapter 6: Summary and Future work	212
Curriculum Vitae	216

List of Figures

Chapter 1

Figure 1: WDR5 binding sites.	2
Figure 2: A BLI sensorgram.	7

Chapter 2

Figure 1: Structure of the binary WDR5-MLL1 _{win} complex.....	20
Figure 2: Label-free optical BLI sensorgrams of WDR5-SET1 _{win} interactions.	36
Figure 3: Label-free optoelectronic SPR sensorgrams of the WDR5-SET1 _{win} interactions.	38
Figure 4: Steady-state FP curves of the WDR5-SET1 _{win} interactions.....	43
Figure 5: Quantitative comparisons of dissociation equilibrium constants of WDR5-SET1 _{win} interactions using BLI, SPR, and steady-state FP measurements.	44

Supplementary Information

Figure S1: Structures of WDR5 (green) complexed with MLL1 _{win} peptide (magenta). ..	54
Figure S2: Structures of WDR5 complexed with SET1 _{win} peptides.....	55
Figure S3: Structure of the binding cavity of WDR5.	57
Figure S4: Arginine is a key side chain in trapping the MLL3 _{win} peptide within the WDR5 cavity.	58
Figure S5: Representative SPR sensorgrams and their kinetic fits for the interactions of SET1 _{win} peptides with WDR5.	59
Figure S6: Steady-state SPR measurements for the quantification of the interactions between MLL1 _{win} peptide and WDR5.....	60
Figure S7: Comparisons of kinetic rate constants of association and dissociation between restricted BLI and unrestricted SPR conditions.	61

Chapter 3

Figure 1: The two binding sites of WDR5 and the structure of the WDR5-MLL3 _{win} complex.....	76
Figure 2: Label-free optical BLI sensorgrams of the WDR5 mutant-MLL3 _{win} interactions.....	85

Figure 3: Normalized dissociation rate constants of the WDR5 mutant-SET1 _{win} interactions using BLI sensorgrams.	88
Figure 4: Normalized K_D of the WDR5 mutant-SET1 _{win} interactions using BLI sensorgrams.	89
Figure 5: Normalized K_D of the WDR5 mutant-SET1 _{win} interactions using steady-state FP spectroscopy.	94
Figure 6: Quantitative comparison between affinity data resulting from BLI and FP measurements.	96
Supplementary Information	

Figure S1: Results of mutation clustering for different N_{max} -based mutation subsets.	104
Figure S2: Cartoon illustrating the location of key residues present in the A and B pockets of the WDR5 protein.	109
Figure S3: BLI sensorgrams show either nondetectable or weakly detectable interactions of D92N with SET1 _{win} ligands.	109
Figure S4: Normalized association rate constants of the WDR5-SET1 _{win} interactions using BLI sensorgrams.	112
Figure S5: The effect of the S175L mutation on the SETd1A _{win} -S175L interaction.	114
Figure S6: Steady-state FP anisotropy curves for WDR5-SET1 _{win} ligand interactions.	115
Figure S7: Fraction bound of SET1 _{win} ligands to D92N using steady-state FP spectroscopy experiments.	116
Figure S8: Quantitative comparison between affinity data resulting from BLI and FP measurements.	117

Chapter 4

Figure 1: WDR5 protein interacting with the SET1 _{win} peptide ligands under different conditions.	130
Figure 2: Scatter plots of kinetic and equilibrium constants for ST-SET1 _{win} and LT-SET1 _{win} ligands.	134
Figure 3: Scatter plots of kinetic and equilibrium constants for NT-SET1 _{win} and LT-SET1 _{win} ligands.	140
Figure 4: 3D plots and contour maps of normalized K_D constants.	144

Supplementary Information

Figure S1: BLI sensorgrams of ST-MLL2 _{win} interacting with WDR5 and its mutants.	153
Figure S2: BLI sensorgrams of LT-MLL2 _{win} interacting with WDR5 and its mutants.	154
Figure S3: Scatter plots of the association rate constants versus the dissociation rate constants using a linear-scale representation.	159
Figure 4: Scatter plots of the association rate constants versus the dissociation rate constants using a logarithm-scale representation.	160
Figure S5: SPR sensorgrams of NT-MLL2 _{win} interacting with immobilized WDR5 proteins.	161
Figure S6: 3D plots and contour maps of the normalized association rate constants.	166

Figure S7: 3D plots and contour maps of the normalized association rate constants.	167
Figure S8: Scatter plots of the k_a , k_d , and K_D for the ST and NT conditions.	168
Figure S9: Scatter plots of the equilibrium dissociation constants of S175L data.	169

Chapter 5

Figure 1: BLI Experiment of RbBP5 interacting with WDR5 in the presence of Salt. ...	180
Figure 2: RbBP5 Interaction with WDR5 _{FL}	183
Figure 3: Blocking the Win binding site using ARTEVY.	185
Figure 4: RbBP5 Interaction with WDR5 _{ΔN}	189
Figure 5: Effect of Salt on the RbBP5 Interaction with WDR5 _{ΔN}	192

Supplementary Information

Figure S1: BLI Sensorgrams for RbBP5's interaction with ARTEVY saturated WDR5 _{FL}	198
Figure S2: BLI sensorgrams for MLL3's interaction with WDR5 _{ΔN}	200
Figure S3: Two state fitted BLI sensorgrams for RbBP5's interaction with WDR5 _{FL}	202
Figure S4: Two state analysis of RbBP5-WDR5 _{FL} Interaction.	203
Figure S5: RbBP5 peptide and WDR5 charge distribution.	206
Figure S6: BLI Sensorgrams for different buffer conditions.	207

Chapter 6

Figure 1: BLI sensorgram of the MYC- WDR5 _{ΔN} interaction.	214
---	-----

List of Tables

Chapter 1

Table 1: Design of the SET1 _{win} peptides.	3
---	---

Chapter 2

Table 1: Alignment of the amino acid sequence of SET1 _{win} motifs.	21
Table 2: Kinetic rate constants of association, k_{on} , and dissociation, k_{off} , and equilibrium dissociation constants, K_{D-BLI} , of WDR5 with SET1 _{win} peptides using BLI.	37
Table 3: Kinetic and affinity determinations of WDR5-SET1 _{win} interactions using SPR.	40

Supplementary Information

Table S1: Comprehensive mapping of hydrogen bonding at the WDR5-SET1 _{win} interface.	56
Table S2: Quantitative comparisons of K_D obtained via BLI, SPR, and steady-state FP.	62
Table S3: Determination of the association rate constants using the basal rate constants, k_{on0} , and electrostatic free energies, ΔG_{el}^* , of the transient WDR5-SET1 _{win} complex.	62

Chapter 3

Table 1: Results of mutation clustering of WDR5 for different subsets of N.	84
--	----

Supplementary Information

Table S1: Amino acid sequences of SET1 _{win} motif peptide ligands.	102
Table S2: Location of mutations from tumor samples with $N < 500$	102
Table S3: Distributions of somatic cancer mutations in tumors with a well-defined upper limit of mutations.	103
Table S4: Tumor locations associated with missense WDR5 cancer mutations.	105
Table S5: Mapping of hydrogen bonds at the WDR5-SET1 _{win} interface.	105
Table S6: List of all known noncovalent interactions.	107

Table S7: Kinetic rate constants of association, k_{on} , of WDR5 mutants with the SETd1A _{win} ligands using BLI measurements.....	110
Table S8: Kinetic rate constants of dissociation, k_{off} , of WDR5 mutants with the SET1 _{win} ligands using BLI measurements.....	110
Table S9: Equilibrium dissociation constants, K_{D-BLI} , of the WDR5 mutants with the SET1 _{win} ligands determined from BLI measurements.....	113
Table S10: Equilibrium dissociation constants, K_{D-FP} , of WDR5 mutants with SET1 _{win} ligands determined from steady-state FP measurements.....	116
Table S11: Quantitative comparisons between affinity data resulting from BLI and FP measurements in terms of the ratio of the K_{D-BLI} to the K_{D-FP}	117
Table S12: Quantitative comparisons between affinity data resulting from BLI and FP measurements in terms of the ratio of the normalized K_{D-BLI} to the normalized K_{D-FP} ...	117
Table S13: List of fluorescently labeled SET1 _{win} ligands for steady-state FP studies. ..	118

Chapter 4

Table 1: Table showing the predicted and experimental values of the k_{d-ST} for S175L interacting with ST-SET1 _{win}	146
Table 2: Table showing the predicted and experimental values of the K_{D-ST} for S175L interacting with ST-SET1 _{win}	146

Supplementary Information

Table S1: List of 14-residue SET1 _{win} peptide ligands used in biolayer interferometry (BLI) measurements.....	150
Table S2: This table shows WDR5 mutants used in this study.....	151
Table S3: Kinetic rate constants of association, k_{a-ST} , of WDR5 and its mutants with ST-SET1 _{win} ligands using BLI measurements.....	155
Table S4: Kinetic rate constants of dissociation, k_{d-ST} , of WDR5 and its mutants with ST-MLL ligands using BLI measurements.....	155
Table S5: Equilibrium dissociation constants, K_{D-ST} , of WDR5 and its mutants with ST-SET1 _{win} ligands determined from BLI measurements.....	156
Table S6: Kinetic rate constant of association, k_{a-ST} , of WDR5 and its mutants, for ST-SET1 _{win} ligands divided by the corresponding k_{a-LT} for LT-SET1 _{win} ligands.....	156
Table S7: Kinetic rate constant of disassociation, k_{d-ST} , of WDR5 and its mutants interacting with ST-SET1 _{win} ligands divided by the corresponding k_{d-LT} for LT-SET1 _{win} ligands.....	157
Table S8: Calculations of the differential activation free energies of the dissociation processes, $\Delta\Delta G_d$, of the interactions of ST-SET1 _{win} ligands with respect to those of LT-SET1 _{win} ligands.....	157
Table S9: K_{D-ST} measured with ST-SET1 _{win} ligands normalized to the corresponding K_{D-LT} values measured with LT-SET1 _{win} ligands.....	158
Table S10: Calculations of the differential activation free energies of the ligand-receptor complex formation, $\Delta\Delta G$, of WDR5-SET1 _{win} interactions of ST-SET1 _{win} ligands with respect to those of LT-SET1 _{win} ligands.....	158

Table S11: Kinetic rate constants of association, k_{a-NT} , of immobilized WDR5 receptor and its mutants with NT-SET1 _{win} ligands using SPR measurements.	162
Table S12: Kinetic rate constants of dissociation, k_{d-NT} , of WDR5 and its mutants with the NT-SET1 _{win} ligands using SPR measurements.	162
Table S13: Equilibrium dissociation constants, K_{D-NT} , of WDR5 and its mutants with the NT-SET1 _{win} ligands using SPR measurements.	163
Table S14: Kinetic rate constant of association, k_{a-NT} , of WDR5 and its mutants, determined by SPR measurements divided by the corresponding k_{a-LT} determined by BLI sensorgrams.	163
Table S15: Kinetic rate constants of dissociation, k_{d-NT} , of WDR5 and its mutants, determined by SPR, normalized to the corresponding k_{d-LT} values.	164
Table S16: K_{D-NT} values determined by SPR measurements, which were normalized to the corresponding K_{D-LT} values determined by BLI measurements.	164
Table S17: Differential activation free energies of the ligand-receptor complex formation, $\Delta\Delta G$ (kcal/mol), determined for NT conditions with respect to LT conditions.	165

Chapter 5

Table 1: Peptides.	182
-------------------------	-----

Supplementary Information

Table S1: WDR5 _{FL} and WDR5 _{ΔN} , kinetics and K_D , with RbBP5.	199
Table S2: WDR5 _{FL} and WDR5 _{ΔN} , kinetics and K_D , with MLL3.	201
Table S3: Mapping of the Hydrogen bonds at the RbBP5-WDR5 interface.	204
Table S4: List of all known noncovalent interactions between RbBP5 and WDR5.	204
Table S5: Impact of WBM Inhibitor on RbBP5-WDR5 interaction.	205
Table S6: Salt analysis.	208

List of Publications

1. **Imran, A;** Duncan, T. M.; Movileanu, L. , Characterization of protein-ligand interactions using biolayer interferometry, (*manuscript under preparation*), **2022**
2. **Imran, A;** Cosgrove, M. S.; Movileanu, L, N-terminus IDR of WDR5 Impacts its Function and Kinetic Measurements, (*manuscript under preparation*), **2022**
3. **Imran, A;** Moyer, B. S.; Kalina, D.; Duncan, T. M.; Moody, K. J.; Wolfe, A. J.; Cosgrove, M. S.; Movileanu, L., Convergent Oncogenic Alterations of a Protein Hub Produce Divergent Effects Withing a Binding Site, (*ACS Chem. Bio, Accepted*), **2022**
4. **Imran, A;** Moyer, B. S.; Wolfe, A. J.; Cosgrove, M. S.; Makarov, D. E.; Movileanu, L. The Interplay of Affinity and Surface Tethering in Protein Recognition, *J. Phys. Chem. Lett*, **2022**, 13(18), 4021-4028.
<https://doi.org/10.1021/acs.jpcllett.2c00621>
5. Mayse, L. A.; **Imran, A.;** Larimi, M. G.; Cosgrove, M. S.; Wolfe, A. J.; Movileanu, L. Disentangling the Recognition Complexity of a Protein Hub Using a Nanopore. *Nat Commun* **2022**, 13 (1), 978.
<https://doi.org/10.1038/s41467-022-28465-8>.
6. **Imran, A.;** Moyer, B. S.; Canning, A. J.; Kalina, D.; Duncan, T. M.; Moody, K. J.; Wolfe, A. J.; Cosgrove, M. S.; Movileanu, L. Kinetics of the Multitasking High-Affinity Win Binding Site of WDR5 in Restricted and Unrestricted Conditions. *Biochemical Journal* **2021**, 478 (11), 2145–2161. <https://doi.org/10.1042/BCJ20210253>.
7. **Imran, A.;** Popescu, D.; Movileanu, L. Cyclic Activity of an Osmotically Stressed Liposome in a Finite Hypotonic Environment. *Langmuir* **2020**, 36 (13), 3659–3666. <https://doi.org/10.1021/acs.langmuir.9b03923>.

Chapter 1: Introduction

Protein-protein interactions (PPIs) form the backbone of various cellular processes. Understanding these interactions is key to parsing and disentangling the complex mechanisms inside living organisms. PPIs have a range of properties that can be studied through different techniques. The focus of my thesis is on the binding affinities and kinetics of sets of PPIs obtained through well-established ensemble measurement based bulk-phase techniques. In this work, we explored a known hub-protein, and its network of interactions with a range of different binding partners.

1.1 Protein System

1.1.1 WDR5

WD40 repeat protein 5 (WDR5) is a nuclear hub whose interactions have significant implications for epigenetic regulations.¹⁻⁸ Moreover, WDR5 is overexpressed under various oncogenic conditions and its upregulation catalyzes cancer development.⁹ Its repertoire of known binding partners includes the SET1 family, retinoblastoma binding protein-5 (RbBP5), MYC, 3-phosphoinositide-dependent protein kinase 1 (PDPK1) as well as a host of different proteins¹⁰⁻¹⁴.

This 334 residue protein is formed by a seven-bladed, WD40 repeat-based β propeller structure, surrounding a central cavity. Its interactions are regulated through two known sites: WDR5 interaction (Win) site and WDR5 binding motif

(WBM) site (fig.1).¹⁵ Win site interactions require the presence of the Win motif, shown in Table 1, on the binding partner. Additionally, this motif has a crucial Arginine residue, conserved across all Win site binders, that inserts into the central cavity and forms several stabilizing hydrogen bonds and cation-pi interactions.^{10,11} This motif also displays interactions with the surface residues around the cavity. On the other hand, WBM site interactions require the presence of the WBM motif on the binding partner. For example, RbBP5 has the WBM motif EEVDVT. Bindings to this site consist of primarily surface interactions dominated by electrostatic and hydrophobic contributions^{13,15}.

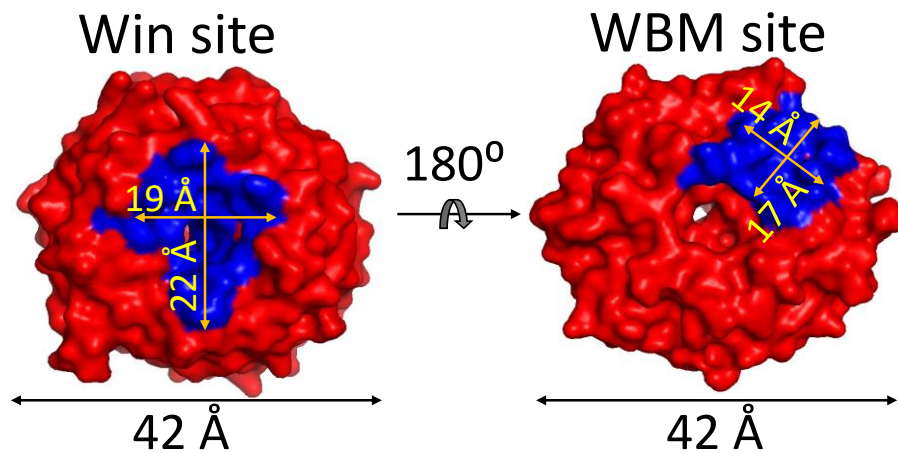


Figure 1: WDR5 binding sites. Surface-representation cartoon of the Win and WBM binding sites of WDR5. Orientations of WDR5 in the two cartoon are 180° with respect to each other. Representations were made using pdb entry 4ERY.¹¹

1.1.2 SET1 Proteins

The SET1 family of proteins' interactions with WDR5, through the Win site, have regulatory implications for histone 3 lysine (H3K4) mono-, di- and tri-methylation. These proteins have the evolutionarily conserved SET domain which is required for lysine methylation.²⁹ There are 6 known SET1 family members: MLL1, MLL2, MLL3, MLL4, SETd1A and SETd1B.¹⁶⁻¹⁸ Because these proteins are hundreds of kDa in size it is not feasible to express and purify them. Therefore, for *in-vitro* studies of the SET1 family, only regions of interest are produced and employed. Particularly, for my work, I used 14 residues sequences, containing the Win motif, from each SET1 protein to create peptides that emulate the interaction of these proteins with WDR5.¹¹ Previous work has shown that these peptides are sufficient to model the interactions of larger regions of these proteins with WDR5. The design of the peptides is shown in the table below.¹⁰

SET1 _{Win} Peptide	Sequence
MLL1 ³⁷⁵⁸⁻³⁷⁷¹	L N P H G S A R A E V H L S*
MLL2 ⁵³³³⁻⁵³⁴⁶	I N P T G C A R S E P K I L
MLL3 ⁴⁷⁰³⁻⁴⁷¹⁶	V N P T G C A R S E P K M S
MLL4 ²⁵⁰⁴⁻²⁵¹⁷	L N P H G A A R A E V Y L S*
SETd1A ¹⁴⁸⁸⁻¹⁵⁰¹	E H Q T G S A R S E G Y Y P
SETd1B ¹⁶⁹⁸⁻¹⁷¹¹	E H V T G C A R S E G F Y T

Table 1: Design of the SET1_{Win} peptides. The table of peptide sequences chosen to represent the different SET1 proteins. The part of the sequence in blue

represents the Win motif on each protein.*For MLL1 and MLL4 the last residues was changes from Arginine to Serine to prevent any artifacts from the C-terminus free Arginine inserting into the Win site cavity.

The extent of the impact of SET1-WDR5 interactions on H3K4 methylation has been studied before. The MLL1-WDR5 interaction is crucial for the assembly of the MLL1 complex with RbBP5 and ASH2L and therefore for the methylation behavior of this complex. On the other hand, the MLL3 complex with RbBP5 and ASH2L is unaffected by the lack of WDR5 or the inhibition of the Win site. The peptides.^{18,27} SET1 proteins are also seen frequently mutated in certain cancers, for example, MLL3 is one of the top 10 proteins seen mutated in breast cancers.³⁰ Therefore, studying their interactions can help us disentangle the different contributions to those cancers.

1.1.3 RbBP5

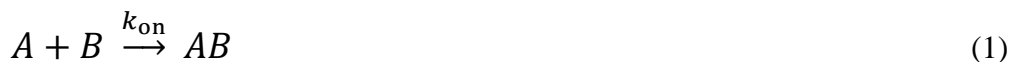
RbBP5 is a member of the SET1 family core complex, along with WDR5, ASH2L and DPY-30.¹⁶ It is a 538 residue protein that interacts with WDR5 through the WBM site¹³. RbBP5 is an integral part of the complex, and its presence has been established to be crucial to the methylation function of the SET1 proteins.¹⁸ The RbBP5-ASH2L hetero-dimer is an essential sub-unit that allows for the SET1 complex to come together.²⁸

This is one of the interactions stabilizing the SET1 complex and consequently important for their function.^{13,15,18} Therefore, studying the RbBP5-WDR5

interaction allows us to better understand the assembly and function of the SET1 complexes.

1.2 Theoretical Overview

All protein-protein interactions can be broken down into association rates and dissociation rates. A simple 1:1 binding can be represented as follows:



Here A and B represent the binding partners while AB represents their complex.¹⁹⁻

²¹ The first equation shows the forward reaction which is controlled by the association rate constant k_{on} . The second equation represents the corresponding reverse reaction controlled by the dissociation rate constant k_{off} . These constants are collectively known as the kinetics of the interaction. Using the notation for concentrations, we see that the rate of complex formation is given by:

$$\frac{d[AB]}{dt} = k_{\text{on}}[A][B] - k_{\text{off}}[AB] \quad (3)$$

At equilibrium the forward and backward rates are equal; the rate of complex formation is 0. This gives us:

$$k_{\text{on}}[A][B] = k_{\text{off}}[AB] \quad (4)$$

Some rearrangement here can give us the equilibrium dissociation constant, K_D as shown below:

$$K_D = \frac{k_{\text{off}}}{k_{\text{on}}} = \frac{[A][B]}{[AB]} \quad (5)$$

The derivation shows that we can obtain the K_D by taking a ratio of the dissociation rate constant and the association rate constant.¹⁹ K_D can be used as a measure of the strength of the interaction. The smaller the value, the stronger the interaction.

1.3 Bulk-phase Techniques

There are several well established bulk-phase techniques that are used, by academic labs and pharmaceutical companies alike, to characterize PPIs. All techniques have their own advantages and disadvantages. This work uses biolayer interferometry (BLI), surface plasmon resonance (SPR) and fluorescence polarization (FP). BLI and SPR allow the characterization of kinetics while FP directly obtains the equilibrium dissociation constant.

1.3.1 Biolayer Interferometry

BLI is an optics based sensing method. It uses the interference of light to quantify the protein bound to a biosensor. White light passes through the sensor and gets reflected by two different interfaces. The first interface is a part of the sensor while the second interface is formed by the bound molecules. The interference of these two reflected lights gives us an absorbance spectrum. This spectrum experiences a shift when more molecules bind to the sensor surface and plotting this shift against time gives us a BLI sensorgram.²²

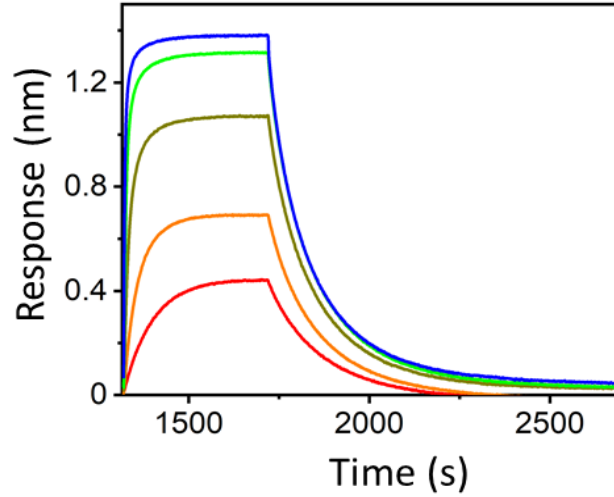


Figure 2: A BLI sensorgram. This BLI sensorgram shows us the association and dissociation phases of an interaction.

For a simple 1:1 binding, the BLI association and dissociation curves look like those shown in fig. 2. To see how these results can be analyzed, we can look at the differential equation underlying the process. The response (R) seen by the biosensor is directly proportional to the amount of complex and the maximum R possible (R_{\max}). If B is the immobilized ligand, then we can say that R_{\max} is directly proportional to the concentration of B . This simplification gives us:

$$\frac{dR}{dt} = k_{\text{on}}[A](R_{\max} - R) - k_{\text{off}}R \quad (6)$$

²³ For the association and dissociation phases we get the analytical solutions:

$$R = (R_{\max} - R_0)e^{-(k_{\text{on}}[A] + k_{\text{off}})t} + R_0 \quad (7)$$

$$R = (R_{\max} - R_0)e^{-k_{\text{off}}t} + R_0 \quad (8)$$

. Here R_0 is the response seen after B is immobilized onto the surface but no complex has formed. Fitting the BLI sensorgrams with these equations gives us the association and dissociation rates.

1.3.2 Surface Plasmon Resonance

SPR is another technique for measuring association and dissociation rates. It is also an optical technique however its measurement principle is based on the SPR angle of reflected light. In this case, an incident light is bounced off a sensor chip and the SPR angle is measured. Presence of proteins on the other side chip shifts the critical angle. This shift in the SPR angle when plotted against time gives us a SPR sensorgram.²⁴

The data obtained from SPR is very similar to that obtained from the BLI and is analyzed the same way. It can provide kinetics of an interaction which can then be used to calculate the equilibrium dissociation constant as well.^{22,23}

1.3.3 Steady-state Fluorescence Polarization

Steady-state Fluorescence Polarization (FP) can be used to measure the K_D of an interaction. The method looks at the polarization of light emitted by a rotating fluorophore-labelled ligand after excitation. The anisotropy, r , of the emitted light is calculated using the following equation.

$$r = \frac{I_{||} - GI_{\perp}}{I_{||} + GI_{\perp}} \quad (9)$$

Here $I_{||}$ represents the intensity of the emitted light parallel to the polarization of the light used for excitation, I_{\perp} represents the intensity of the light perpendicular to the polarization and G is a calibration factor.^{19,25} When the ligand binds to an analyte, the rotational rate slows down and it increases the anisotropy of the emitted light. By mapping out the anisotropy values of the ligand population when exposed to a range of concentrations of analyte we can calculate the fractional occupancy α of the ligand. This number represent the proportion of the ligand that is bound to the analyte. At α equals 0.5, half the ligand population is bound, and the corresponding analyte concentration gives us the K_D of the interaction.²⁶

1.4 Thesis Outline

WDR5's interactions with other binding partners have been studied before. While previous studies have focused on the mechanisms of the interaction using crystal structures and binding affinities of the interactions using ITC or FP, a thorough exploration of the kinetics of these interactions has not yet been performed. This gap in knowledge is what we sought to fill with this work.

In chapter 2, we look at the kinetics of wild-type WDR5's interaction with SET1 proteins. Using BLI and SPR, we examined these PPIs and looked at the contributions of the association and dissociation rates towards the strengths of the interactions. Additionally, for further validation we obtained K_D values for these interactions using FP. These values were then compared to those K_D values indirectly calculated from the kinetics obtained through BLI and SPR. Our work allowed us to look at the impact of restrictions on these interactions. Ranging from

most restricted for the BLI to least restricted for the FP. Furthermore, having multiple bulk-phase methods allows us to account for any biases introduced from one. The agreement of our results across multiple techniques strengthens our conclusions.

In chapter 3, we dive into deviations from wild-type behavior of WDR5 induced by oncogenic mutations. We looked at the mutations in WDR5 seen in tumors and quantified the impact of those mutations on WDR5-SET1 interactions. First, we used computational clustering techniques to identify a region of interest. Then we selectively isolated mutations in that region for further *in vitro* study. These WDR5 mutants were expressed and purified. The kinetics of their interactions with SET1 were then studied using BLI. Not only did we measure the impact of these mutations on the strengths of the interactions, but we were also able to break down the impact in terms of effects on association and dissociation rates. Moreover, by extracting K_D via FP, we were able to validate our findings and perform an accurate determination of the impact of the oncogenic mutations. These results allow us to understand the possible consequences of the mutations on H3K4 methylation.

In chapter 4, we look at the effect of surface tethering on PPIs. Surface-tethered ligand-receptor complexes are important elements in biological signaling and adhesion. We explored the impact of tethers, of different lengths, on the kinetics of different PPIs. Our work with WDR5 (Wild-type and mutants) and SET1 proteins gave us a range of PPIs with varying binding strengths. Leveraging that, we observed these interactions under short-tether, long-tether, and no-tether conditions. For the design of this study, the SET1_{win} peptides were tethered.

Moreover, we used WDR5 wild-type and 3 mutants to establish the impact of the tethers. Additionally, we used the interactions of a 4th mutant to test how effectively we can predict the effect of the tether. The work shows that this tethering can separately modulate the association and dissociation rates of the interactions.

In chapter 5, we shift focus on to the WBM site of WDR5. We looked at the interaction of WDR5 with RbBP5 through WBM site. However, in this case we noticed a deviation from expected behavior. Through a hypothesis-based design approach we explored likely possibilities and identified that this divergence was caused by the N-terminal intrinsically disordered region (IDR) of WDR5. Additionally, using orthogonal experiments, we further confirmed the role of this IDR in affecting our measurements of WDR5-RbBP5 binding. We discuss the relevance of our results for future explorations of WBM interactions as well as for understanding the role of WDR5 inside the cell.

1.5 REFERENCES

1. Crawford, B.D. and Hess, J.L. (2006) 'MLL Core Components Give the Green Light to Histone Methylation', *ACS Chemical Biology*, 1(8), pp. 495–498.
2. Cosgrove, M.S. and Patel, A. (2010) 'Mixed lineage leukemia: a structure-function perspective of the MLL1 protein', *The FEBS journal*, 277(8), pp. 1832–1842.
3. Li, Y. *et al.* (2016) 'Structural basis for activity regulation of MLL family methyltransferases', *Nature*, 530(7591), pp. 447–452.
4. Vedadi, M. *et al.* (2017) 'Targeting human SET1/MLL family of proteins', *Protein Science : A Publication of the Protein Society*, 26(4), pp. 662–676.
5. Xue, H. *et al.* (2019) 'Structural basis of nucleosome recognition and modification by MLL methyltransferases', *Nature*, 573(7774), pp. 445–449.
6. Jiang, H. (2020) 'The complex activities of the SET1/MLL complex core subunits in development and disease', *Biochimica et biophysica acta. Gene regulatory mechanisms*, 1863(7), p. 194560.
7. Sha, L. *et al.* (2020) 'Insights on the regulation of the MLL/SET1 family histone methyltransferases', *Biochimica et biophysica acta. Gene regulatory mechanisms*, 1863(7), p. 194561.
8. Mayse, L.A. *et al.* (2022) 'Disentangling the recognition complexity of a protein hub using a nanopore', *Nature Communications*, 13(1), p. 978.
9. Chen, X. *et al.* (2015) 'Upregulated WDR5 promotes proliferation, self-renewal and chemoresistance in bladder cancer via mediating H3K4 trimethylation', *Scientific Reports*, 5(1), p. 8293.
10. Patel, A., Dharmarajan, V. and Cosgrove, M.S. (2008) 'Structure of WDR5 bound to mixed lineage leukemia protein-1 peptide', *The Journal of Biological Chemistry*, 283(47), pp. 32158–32161.
11. Dharmarajan, V. *et al.* (2012) 'Structural Basis for WDR5 Interaction (Win) Motif Recognition in Human SET1 Family Histone Methyltransferases', *The Journal of Biological Chemistry*, 287(33), pp. 27275–27289.
12. Guarnaccia, A.D. *et al.* (2021) 'Impact of WIN site inhibitor on the WDR5 interactome', *Cell Reports*, 34(3), p. 108636

13. Odho, Z., Southall, S.M. and Wilson, J.R. (2010) 'Characterization of a novel WDR5-binding site that recruits RbBP5 through a conserved motif to enhance methylation of histone H3 lysine 4 by mixed lineage leukemia protein-1', *The Journal of Biological Chemistry*, 285(43), pp. 32967–32976.
14. Thomas, L.R. *et al.* (2015) 'Interaction with WDR5 promotes target gene recognition and tumorigenesis by MYC', *Molecular Cell*, 58(3), pp. 440–452.
15. Guarnaccia, A. duPuy and Tansey, W.P. (2018) 'Moonlighting with WDR5: A Cellular Multitasker', *Journal of Clinical Medicine*, 7(2), p. 21.
16. Dou, Y. *et al.* (2006) 'Regulation of MLL1 H3K4 methyltransferase activity by its core components', *Nature Structural & Molecular Biology*, 13(8), pp. 713–719.
17. Patel, A. *et al.* (2009) 'On the mechanism of multiple lysine methylation by the human mixed lineage leukemia protein-1 (MLL1) core complex', *The Journal of Biological Chemistry*, 284(36), pp. 24242–24256.
18. Shinsky, S.A. *et al.* (2015) 'Biochemical reconstitution and phylogenetic comparison of human SET1 family core complexes involved in histone methylation', *The Journal of Biological Chemistry*, 290(10), pp. 6361–6375.
19. Rossi, A.M. and Taylor, C.W. (2011) 'Analysis of protein-ligand interactions by fluorescence polarization', *Nature Protocols*, 6(3), pp. 365–387.
20. Jarmoskaite, I. *et al.* (2020) 'How to measure and evaluate binding affinities', *eLife*. Edited by S. Deindl and J. Kuriyan, 9, p. e57264.
21. Myszka, D. G. Kinetic analysis of macromolecular interactions using surface plasmon resonance biosensors. *Curr. Opin. Biotechnol.* 8(1), 50–57.
22. Sultana, A. and Lee, J.E. (2015) 'Measuring protein-protein and protein-nucleic Acid interactions by biolayer interferometry', *Current Protocols in Protein Science*, 79, p. 19.25.1-19.25.26.
23. Karlsson, R.; Michaelsson, A.; Mattsson, L. Kinetic analysis of monoclonal antibody-antigen interactions with a new biosensor based analytical system. *J. Immunol. Methods* 1991, 145, 229–240

24. Singh, P. (2016) 'SPR Biosensors: Historical Perspectives and Current Challenges', *Sensors and Actuators B: Chemical*, 229, pp. 110–130.
25. Wolfe, A.J., Parella, K.J. and Movileanu, L. (2019) 'High-Throughput Screening of Protein-Detergent Complexes Using Fluorescence Polarization Spectroscopy', *Current Protocols in Protein Science*, 97(1), p. e96.
26. Hall, M.D. *et al.* (2016) 'Fluorescence polarization assays in high-throughput screening and drug discovery: a review', *Methods and applications in fluorescence*, 4(2), p. 022001.
27. Alicea-Velázquez, N.L. *et al.* (2016) 'Targeted Disruption of the Interaction between WD-40 Repeat Protein 5 (WDR5) and Mixed Lineage Leukemia (MLL)/SET1 Family Proteins Specifically Inhibits MLL1 and SETd1A Methyltransferase Complexes', *The Journal of Biological Chemistry*, 291(43), pp. 22357–22372.
28. Jiang, H. (2020) 'The complex activities of the SET1/MLL complex core subunits in development and disease', *Biochimica et biophysica acta. Gene regulatory mechanisms*, 1863(7), p. 194560.
29. Dillon, S.C. *et al.* (2005) 'The SET-domain protein superfamily: protein lysine methyltransferases', *Genome Biology*, 6(8), p. 227.
30. Tate, J.G. *et al.* (2019) 'COSMIC: the Catalogue Of Somatic Mutations In Cancer', *Nucleic Acids Research*, 47(Database issue), pp. D941–D947.

Chapter 2: Kinetics of the multitasking high-affinity Win binding site of WDR5 in restricted and unrestricted conditions

Ali Imran,¹ Brandon S. Moyer,² Ashley J. Canning,³ Dan Kalina,^{2,4} Thomas M. Duncan,³ Kelsey J. Moody,^{1,2,4} Aaron J. Wolfe,^{1,2,4} Michael S. Cosgrove,³ and Liviu Movileanu^{1,5,6*}

¹ *Department of Physics, Syracuse University, 201 Physics Building, Syracuse, New York 13244-1130, USA*

² *Ichor Therapeutics, Inc., 2521 US Route 11, LaFayette, New York 13084, USA*

³ *Department of Biochemistry and Molecular Biology, State University of New York - Upstate Medical University, 4249 Weiskotten Hall, 766 Irving Avenue, Syracuse, New York 13210, USA*

⁴ *Department of Chemistry, State University of New York, College of Environmental Science and Forestry, 1 Forestry Dr., Syracuse, New York 13210, USA*

⁵ *The BioInspired Institute, Syracuse University, Syracuse, New York, 13244, USA*

⁶ *Department of Biomedical and Chemical Engineering, Syracuse University, 329 Link Hall, Syracuse, New York 13244, USA*

This chapter is adapted from “Imran, A.; Moyer, B. S.; Canning, A. J.; Kalina, D.; Duncan, T. M.; Moody, K. J.; Wolfe, A. J.; Cosgrove, M. S.; Movileanu, L. Kinetics of the Multitasking High-Affinity Win Binding Site of WDR5 in Restricted and Unrestricted Conditions. *Biochemical Journal* 2021 <https://doi.org/10.1042/BCJ20210253>.”

2.1 Abstract

Recent advances in quantitative proteomics show that WD40 proteins play a pivotal role in numerous cellular networks. Yet, they have been fairly unexplored and their physical associations with other proteins are ambiguous. A quantitative understanding of these interactions has wide-ranging significance. WD40 repeat protein 5 (WDR5) interacts with all members of human SET1/MLL methyltransferases, which regulate methylation of the histone 3 lysine 4 (H3K4). Here, using real-time binding measurements in a high-throughput setting, we identified the kinetic fingerprint of transient associations between WDR5 and 14-residue WDR5 interaction (Win) motif peptides of each SET1 protein (SET1_{Win}). Our results reveal that the high-affinity WDR5-SET1_{Win} interactions feature slow association kinetics. This finding is likely due to the requirement of SET1_{Win} to insert into the narrow WDR5 cavity, also named the Win binding site. Furthermore, our explorations indicate fairly slow dissociation kinetics. This conclusion is in accordance with the primary role of WDR5 in maintaining the functional integrity of a large multisubunit complex, which regulates the histone methylation. Because the Win binding site is considered a key therapeutic target, the immediate outcomes of this study could form the basis for accelerated developments in medical biotechnology.

2.2 Introduction

WD40 repeat protein 5 (WDR5) is a conserved chromatin-associated protein that is involved in a number of transient protein-protein interactions [1]. However, WDR5 is notoriously known for its regulatory role in multisubunit epigenetic complexes, such as Suppressor of Variegation, Enhancer of Zeste, and Trithorax 1 (SET1) lysine methyltransferases (KMT) of histones [2-8]. There are six SET1 family members in humans: MLL1, MLL2, MLL3, MLL4, SETd1A, and SETd1B. Each member forms a large multisubunit complex with functions that appear to have diverged in target gene localization and product specificity. However, features common among the complexes are a C-terminal catalytic SET domain that is regulated by interaction with a conserved subcomplex consisting of WDR5, retinoblastoma binding protein-5 (RbBP5), absent-small-homeotic-2-like protein (Ash2L), and dumpy-30 (DPY-30) (WRAD₂) [7, 9-20]. WDR5 functions to bridge the interaction between the SET domain and other WRAD₂ subunits by the recognition of an evolutionarily conserved WDR5-interaction (Win) motif found in all SET1 family members [21-25]. Formation of this core complex is required for optimal methyltransferase activity [9, 11, 26]. Therefore, small molecules targeting the Win motif-WDR5 protein-protein interaction show promise as anticancer therapeutic candidates.

Interestingly, recent studies have revealed that WDR5 is involved in numerous interactions with other proteins [27-29], including the transcription factor MYC oncoprotein [30-35], 3- phosphoinositide-dependent protein kinase 1 (PDK1)

[36], and interacting partners involved in phosphatidylinositol 3-kinase (PI3K) signaling [36]. Moreover, WDR5 is implicated in nongenomic activities, such as regulatory mechanisms of cellular shape, polarity, and migration [37, 38]. Therefore, WDR5 is a multitasking protein with diverse roles in cellular processes [36, 39, 40]. Its highly conserved sequence across multiple organisms suggests the fundamental significance of its multiple roles [40].

An essential structural archetype of WDR5 is its internal cavity that hosts a high-affinity binding pocket for an evolutionarily conserved Arg-containing peptide segment of the six SET1 proteins [21-23]. Interestingly, this binding cavity of WDR5, here named the Win binding site, is the same [21, 23] as that previously suggested to bind histone H3 [41-46]. Yet, the WDR5-SET1 interaction is required for the stability and functional operation of the C-terminal catalytic SET domain [11, 21, 22]. Moreover, it has only recently been identified that the Win binding site is implicated in transient protein-protein interactions with dozens of proteins, including those involved in PI3K signaling [36]. Given that WDR5 is overexpressed under various oncogenic conditions [47-49], the Win binding site has become a key therapeutic target for different cancers [24, 25, 50-59]. Therefore, a better mechanistic and quantitative understanding of the interactions of the Win binding site with other Win motif partners has fundamental and clinical significance [60-64].

Several research groups have previously examined interactions of WDR5

protein with Win motif SET1 (SET1_{win}) peptides using a variety of approaches, such as analytical ultracentrifugation (AUC) [22], isothermal titration calorimetry (ITC) [21, 24, 65], surface plasmon resonance (SPR) [23], and X-ray crystallography [21, 23, 24, 65]. These explorations have confirmed the high affinity of the Win binding site for different Win motif interaction partners [24, 65]. In this study, we determined the kinetic fingerprint and affinities of these interactions using high-throughput optical and fluorescence approaches, which included biolayer interferometry (BLI), SPR, and steady-state fluorescence polarization (state-state FP).

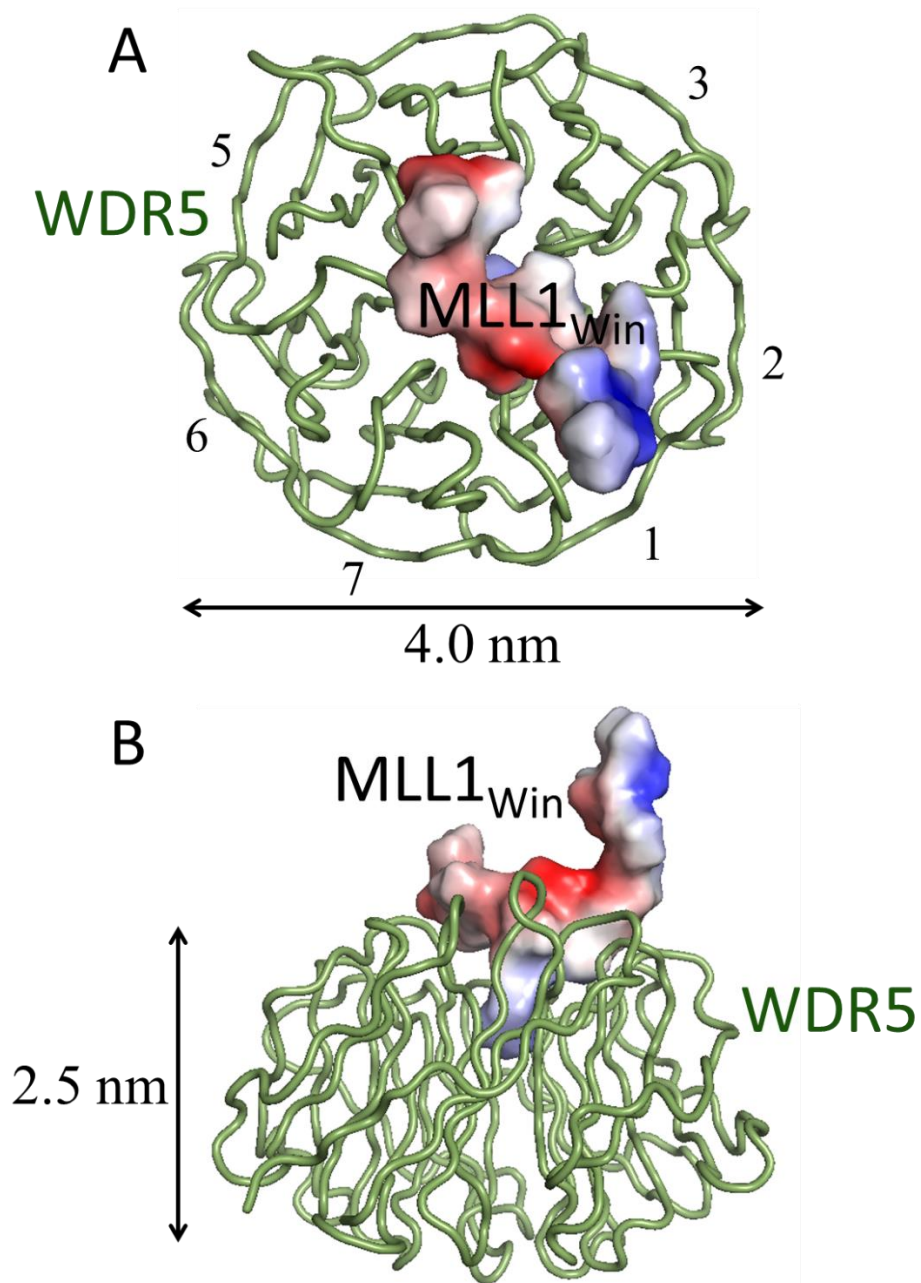


Figure 1: Structure of the binary WDR5-MLL1_{Win} complex. (A) The insertion of MLL1_{Win} into the WDR5 cavity is shown from the top. (B) The same interaction is shown from the side. These graphic representations were made using the pdb code 4ESG.⁶³

Table 1: Alignment of the amino acid sequence of SET1_{Win} motifs.

Peptide	P ₋₇ P ₋₆ P ₋₅ P ₋₄ P ₋₃ P ₋₂ P ₋₁ P ₀ P ₁ P ₂ P ₃ P ₄ P ₅ P ₆	Charge
MLL1_{Win} : MLL1 ³⁷⁵⁸⁻³⁷⁷¹	L N P H G S A R A E V H L S*	0
MLL2_{Win} : MLL2 ⁵³³³⁻⁵³⁴⁶	I N P T G C A R S E P K I L	+1
MLL3_{Win} : MLL3 ⁴⁷⁰³⁻⁴⁷¹⁶	V N P T G C A R S E P K M S	+1
MLL4_{Win} : MLL4 ²⁵⁰⁴⁻²⁵¹⁷	L N P H G A A R A E V Y L S*	0
SETd1A_{Win} : SETd1A ¹⁴⁸⁸⁻¹⁵⁰¹	E H Q T G S A R S E G Y Y P	-1
SETd1B_{Win} : SETd1B ¹⁶⁹⁸⁻¹⁷¹¹	E H V T G C A R S E G F Y T	-1

S* This is a R3771S substituted MLL1_{Win} peptide.

S* This is a R2517S substituted MLL4_{Win} peptide.

WDR5 is a 334-residue protein that has a 7-bladed, WD-40 repeat-based β propeller structure surrounding a central cavity (**Figure 1A**) [29, 66-68]. Each blade contains four anti-parallel β strands. A segment of the central cavity serves as the high-affinity Win binding site for the SET1_{Win} peptides (**Figure 1B**; **Supplementary Figures S1-S2**) [21, 23, 24, 65]. Here, we performed a systematic kinetic analysis of the interactions of WDR5 with six 14-residue SET1_{Win} peptides, which include an evolutionarily conserved Arg residue at P₀ (**Table 1**). Moreover, this Arg residue has been shown to be critical to WDR5-SET1_{Win} interactions (**Supplementary Table S1, Figure S3**) [22, 26, 69, 70]. In addition, SET1_{Win} sequences contain a highly conserved 6-residue Win motif peptide, at positions P₋₃ through P₂, along with 8 residues on their flanking sides, at positions P₋₇ through P₆.

₄ and P₃ through P₆. These flanking residues diverge among SET1 family members, accounting for differences in the binding affinity of WDR5-SET1_{win} interactions [24, 65]. The highly conserved 6-residue Win motif peptide has to insert into the WDR5 binding cavity to facilitate these highly specific WDR5-SET1_{win} interactions [24, 65]. Therefore, the choice of a 14-residue length of SET1_{win} was based on the requirement of the minimal 6-residue Win motif sequence, along with four residues on each flanking side. This also facilitated the interpretation of our results in light of a prior crystallographic study [24], which was conducted with an identical SET1_{win} length.

Here, we employed multiple techniques to probe the effect of the surface immobilization on the kinetic fingerprint of WDR5-SET1_{win} interactions as well as to establish the efficacy of each technique for the measurement of the kinetic rate constants and binding affinities. We provide a critical analysis of each approach with respect to the kinetics of the Win binding site. BLI and SPR require surface immobilization, while steady-state FP does not. On the other hand, steady-state FP is free from this limitation, but is unable to provide real-time kinetic measurements. Furthermore, the use of multiple approaches allowed us to provide quantitative and qualitative validations of our conclusions and to obtain more generalizable outcomes that were not restrained by any one approach. Finally, we also show that distinctions in the kinetic rate constants of these interactions are correlated with unique sequences on the SET1_{win} peptides' flanking sides.

2.3 Materials and Methods

Protein Expression and Purification

Human WDR5 (UniProtKB - P61964; WDR5_HUMAN) was expressed and purified, as follows. pET3aTr vectors containing the 6×His-TEV-WDR5 sequence were transformed into Rosetta™ 2 BL21(DE3)pLysS (Novagen, Cat #71403) competent *E. coli* cells. Rosetta™ 2 BL21(DE3)pLysS (Novagen, Cat #71403) competent *E. coli* cells were grown overnight on Luria-Bertani (LB) agar carbenecillin/chloramphenicol selection plates at 37°C. 50 mL LB broth starter cultures (one per 10 L bioreactor growth) containing 50 µg/mL each of carbenecillin and chloramphenicol were inoculated with 5 colonies and grown for 3-5 hours until turbid at 37°C. 10 L Luria broth bioreactors (Eppendorf BioFlo, Enfield, CT) containing 50 µg/mL each of carbenecillin and chloramphenicol, in addition to Antifoam 204 (Sigma-Aldrich, St. Louis, MO), were then inoculated at 37°C and 800 rpm with the entire turbid starter culture. When the culture attained $OD_{600} = 0.8$, agitation was decreased to 600 rpm and the temperature was rapidly dropped to 18°C. Induction of target proteins was initiated with 100 µM Isopropyl-β-d-1-thiogalactopyranoside (IPTG; Goldbio, St. Louis, MO) at 18°C. After 12-24 hours post-induction at 18°C, cells were pelleted by centrifugation at 4,465×g using a J6-MI centrifuge (Beckman Coulter, Brea, CA) for 30 minutes at 4°C. The pellet was resuspended in 50 mM Tris-HCl (pH 7.4), 300 mM NaCl, 10 mM βME, and 20 mM imidazole. The resuspended cells were frozen on dry ice and stored at -80°C until purification.

Cell pellets were lysed with a Qsonica Sonicator Q700 (FisherBrand, Pittsburg, PA) on ice. 5 L of thawed, resuspended pellets were resuspended in 160 mL of 50 mM Tris-HCl (pH 7.4), 300 mM NaCl, 3 mM DTT, and 30 mM imidazole (lysis/Ni-NTA Buffer A/dialysis buffer) containing an additional 200 μ L of phenylmethylsulfonyl fluoride (PMSF; Sigma-Aldrich) and two Pierce™ Protease Inhibitor Mini Tablets (EDTA-free; Thermo Fisher Scientific, Waltham, MA). The cell suspensions were stirred at 4°C for 15 minutes until homogeneous and then sonicated for 10 minutes at 90% power (2 seconds on, 4 seconds off). Lysate was then centrifuged for 1 hour at 4,465 \times g and 4°C, and the supernatant was stored at 2-8°C for purification. A Ni-NTA purification process was followed. A Kontes 25 x 200 mm column with 30-40 mL Ni-NTA resin (Qiagen, Hilden, Germany) was equilibrated with at least 10 resin-bed volumes (RBVs) of 0.22 μ m filtered de-ionized (DI) H₂O to remove ethanol, and then at least 5 RBVs of Ni-NTA Buffer A (above). After equilibration, lysate was added to the column and washed with 5-10 RBVs of Ni-NTA Buffer A. Sample was eluted using at least 5 RBVs of Ni-NTA Buffer B (50 mM Tris-HCl (pH 7.4), 300 mM NaCl, 3 mM DTT, and 500 mM imidazole). 5 mL fractions were collected, analyzed via SDS-PAGE, and pooled. Then, sample was dialyzed, as follows. WDR5-containing fractions were pooled into 12-14 kDa MWCO dialysis tubing (Repligen, Waltham, MA), then 2.5 mg of GST-6H-TEV protease (per 5 L of culture; expressed and purified in-house) was added to cleave the His-tag, and the solution was dialyzed against 4 L of dialysis buffer (above) overnight for 12-18 hours at 2-8°C. Dialyzed protein was

analyzed via SDS-PAGE to ensure complete cleavage. A negative Ni-NTA was then conducted. The resulting cleaved WDR5 solution was passed through a Bio-Rad Ni-NTA IMAC cartridge (Bio-Rad, Hercules, CA) using a Bio-Rad NGC chromatography system (Bio-Rad) to remove the cleaved His-tag and GST-6H-TEV protease. The flowthrough was collected, analyzed via SDS-PAGE and UV-Vis, and concentrated for size-exclusion chromatography (SEC) purification. As a final polish, the WDR5 proteins were purified via SEC using a HiLoad® 26/600 Superdex® 200 pg column (GE Healthcare, Chicago, IL) into 20 mM Tris-HCl (pH 7.5), 300 mM NaCl, 1 μ M ZnCl₂, 1 mM TCEP. Fractions of interest were analyzed via SDS-PAGE and UV-Vis, pooled, concentrated where necessary, aliquoted to 1 mL, flash-frozen in liquid nitrogen, and stored at -80°C.

Peptide synthesis, labeling, purification, and analysis for BLI measurements

All peptides for biolayer interferometry measurements were synthesized by GenScript (Piscataway, NJ). The peptides were purified to $\geq 95\%$ purity. Amino acid analysis, purity confirmation, and solubility testing were provided by GenScript. All peptides were biotinylated at the N terminus. Their C terminus was amidated.

Peptide synthesis, labeling, purification, and analysis for SPR and FP measurements

For Fmoc-SPPS, peptides were synthesized at theoretical 100 μmol scale using the standard double coupling workflow pre-programmed on the Biotage Syro I peptide synthesizer (Biotage, Charlotte, NC). 278 mg of Rink Amide AM Resin LL (100-200 mesh, 0.36 mmol/g functionalization; Novabiochem (EMD Millipore)) was loaded into each 10 mL reactor vial, corresponding to the 100 μmol synthesis scale. Each resin aliquot was swelled with DMF for 30 minutes, followed by an initial resin deprotection step using 40% piperidine in DMF. Each double coupling cycle was comprised of two independent, 45-minute coupling sub-steps that differed in the choice of activation reagents: 1) DIC/Oxyma (1:2 ratio with respect to Fmoc-[AA]), followed by 2) HBTU/DIPEA (0.95:2 ratio with respect to Fmoc-[AA]). For each coupling sub-step, four molar equivalents of each respective 0.5 M Fmoc-[AA] stock was added to each vial. Each coupling cycle terminated with a double Fmoc deprotection step using 40% piperidine in DMF. Coupling reactions proceeded with interspersed vortexing of the vials and under an air atmosphere at ambient temperature. Following the conclusion of peptide synthesis, resins were washed with three successive aliquots of DCM, followed by three minutes under vacuum to dry.

Each peptidyl-resin aliquot was swelled with DMF for 30 minutes and drained. DMF (1,200 μL) was added to each aliquot, followed by 300 μL of DIPEA in NMP (6 molar equivalents, 600 μmol), then followed by 600 μL of Lissamine Rhodamine B sulfonyl chloride in DMF (3 molar equivalents, 300 μmol). The mixture was shielded from light and allowed to react with intermittent vortexing overnight at

ambient temperature. Following conjugation, the resin bed was drained, washed successively with DMF until no further change in the color of the flowthrough was observed (faint pink), washed successively with DCM, and then held under vacuum for three minutes to dry.

Cleavage cocktail containing 90% TFA, 5% TIS, 2.5% DODT, and 2.5% H₂O was freshly prepared. 4 mL of cleavage cocktail was added to each peptidyl-resin aliquot, sealed, and placed on a rocking platform to react for 4 hours at ambient temperature. After incubation, the contents of each reactor vial were plunged into separate 50 mL conical tubes. The resin was then treated with an additional 2 mL of cleavage cocktail and allowed to react on the rocking platform for 30 minutes at ambient temperature. Following the second incubation, the contents of each reactor vial were pooled into their respective 50 mL conical tubes and the resin containing reactor vials were discarded. Cleavage aliquots were triturated by the fast addition of ~45 mL cold (-80°C) diethyl ether. Precipitate was compacted by centrifugation at 1,000×g for 10 minutes at 0°C using an Allegra X-22R centrifuge (Beckman Coulter, Brea, CA). The supernatant was discarded, and the peptide pellets were washed with a second ~30 mL aliquot of cold diethyl ether, centrifuged, and decanted as before. The resulting peptide pellets were flash frozen in liquid nitrogen and lyophilized using a FreeZone 2.5L lyophilizer (Labcono, Kansas City, MO) overnight to remove residual solvents. The crude lyophilized peptide was stored at -80°C until purification.

Crude peptide aliquots were purified using reversed-phase chromatography through two stages: 1) Flash chromatography using a Biotage Isolera One (Biotage AB, Uppsala, Sweden), 2) Semi-preparative HPLC using a Waters 2695 separations module equipped with a Waters 2996 photodiode array detector (PDA).

1) Biotage Isolera One purifications: Each crude peptide aliquot was solubilized in 2.5 mL total of either DMSO or DMF (DMF only if the peptide contained oxidizable Cys or Met residues) and loaded onto a Biotage Sfär C₁₈ Samplet for 25 g Column (Biotage, Uppsala, Sweden) with the aid of a vacuum. Each samplet was placed in a Biotage Sfär Bio C₁₈ D Duo (300 Å, 20 µm) 25 g column (Biotage). Peptides were eluted using a 15-column volume (CV) gradient of 9-90% MeCN in H₂O containing 0.1% TFA at a flowrate of 30 mL/min. The collection threshold was 75 mAU for $\lambda = 200-400$ nm, with monitoring at $\lambda = 215$ nm and 355 nm (rhodamine). Rhodamine labeled fractions were pooled and MeCN was removed using a rotary evaporator for 30 minutes at 25°C. Samples were flash-frozen in liquid nitrogen and lyophilized using a FreeZone 2.5L lyophilizer (Labcono) for three days. The semi-pure lyophilized peptide was stored at -80°C until further purification.

2) Semi-preparative HPLC: Peptide samples were resuspended in 50-80 µL aliquots of DMSO or 1:2 DMSO/H₂O. Aliquots were injected onto a Waters XBridge Peptide BEH C₁₈ OBD Prep Column (5 µm, 300 Å, 10 mm x 150 mm). A gradient of 10-50% MeCN containing 0.1% (v/v) TFA in H₂O containing 0.1% (v/v) TFA was applied over 40 minutes ($\Delta 1\%/min.$) at a flow rate of 4.73 mL/min. at ambient temperature using a Waters 2695 separations module. Sample detection occurred at 215 nm, 280 nm, 355 nm (rhodamine), and 560 nm (rhodamine) using

a Waters 2996 photodiode array detector (PDA). Sample purity was determined by baseline integration using Waters Empower 3 software (>90% purity in all cases). Rhodamine containing fractions were analyzed by MALDI-TOF mass spectroscopy for the identity and purity confirmatory tests. Target fractions were flash-frozen in liquid nitrogen and lyophilized using a FreeZone 2.5L lyophilizer (Labcono) for three days. The resulting purified, lyophilized peptides were reconstituted as concentrated stocks in ultrapure water, aliquoted, flash-frozen in liquid nitrogen, and stored at -80°C until use.

For MALDI-TOF mass spectroscopy of the purified peptides, 1 μ L of peptide stock in H₂O (1-100 μ M) was mixed with 9 μ L spotting matrix (10 mg/mL α -cyano-4-hydroxycinnamic acid (CHCA) in 50:50 MeCN/0.1% (v/v) TFA in H₂O). 2 μ L of each peptide spotting solution was spotted onto a Bruker MTP 384 Target Plate, which was calibrated using Anaspec Peptide Mass Standard Kit, and allowed to dry at room temperature for at least 30 minutes prior to analysis. Samples were analyzed on a Bruker Autoflex iii Mass Spectrometer as an average of 1200 shots using 35% laser power, an m/z range from 840-6000 Da with suppression <400 Da in linear mode, 3.6x detector gain, 2.00 sample rate, and medium gating strength.

Biolayer interferometry (BLI)

Octet RED384 (FortéBio, Fremont, CA) was used for the BLI studies [71-73]. Streptavidin (SA) sensors were presoaked in buffer for ~30 minutes. The buffer

solution contained 150 mM NaCl, 20 mM Tris-HCl, 1 mM TCEP, 1 mg/mL bovine serumalbumin (BSA), pH 7.5. 5 nM tagged peptide was then loaded onto sensors for 15 minutes. Sensors were then dipped in buffer again for 5 minutes to wash off unbound peptides from the surface. A 3-fold serial dilution of WDR5 was conducted ranging from 0.1 μ M to 9 μ M for the association process and then placed into the buffer solution for the dissociation process. The association and dissociation processes were \sim 200 and \sim 600 seconds long, respectively. For all WDR5 concentrations, unloaded sensors were run concurrently as controls and were used to subtract the baseline and the drift in the sensorgrams to extract the binding curves. The BLI experiments were performed at 24°C. All reagents were prepared in the above- mentioned buffer and were loaded into 96-well flat bottom black plates for the sensorgram recordings. The binding curves were fitted using the Octet Data Analysis software (FortéBio). The curves of the association process, which were recorded for various analyte concentrations, $[C]$, were fitted using the following equation [74]:

$$Y = Y_{\infty} - (Y_{\infty} - Y_0)e^{-k_{\text{obs}}t}$$

(1)

Here, Y_0 and Y_{∞} are the BLI response signals at time zero and infinity, respectively, of the association process. t denotes the cumulative time of the association reaction. k_{obs} is the apparent first-order reaction rate constant of the association process. The curves of the dissociation process were fitted using the following equation:

$$Y = Y_{\infty} + (Y_0 - Y_{\infty})e^{-k_{\text{off}}t}$$

(2)

Here, Y_0 and Y_∞ are the BLI response signals at time zero and infinity, respectively, of the dissociation process. k_{off} indicates the dissociation rate constant. Finally, the association rate constant, k_{on} , was determined using the slope of the linear curve [75, 76]:

$$k_{\text{obs}} = k_{\text{on}}[C] + k_{\text{off}}$$

(3)

Global fitting, which was conducted using several analyte concentrations, provided the corresponding k_{on} and k_{off} values. The dissociation constant, K_D , were indirectly determined using the k_{on} and k_{off} values. Three distinct BLI measurements were conducted for all inspected interactions.

Surface plasmon resonance (SPR)

All SPR experiments [77-79] were conducted on a Cytiva Biacore 8K (Cytiva Life Sciences, Marlborough, MA). All buffers and dilutions were freshly made in-house using ultrapure water obtained from an IQ 7000 Milli-Q system (Millipore-Sigma, Burlington, MA). WDR5 protein was immobilized onto the active flow cell of each channel of a Cytiva Series S Sensor Chip CM5 (Cytiva Life Sciences) according to the following parameters and protocol. A CM5 chip was inserted into the instrument and equilibrated for 1 h at 25°C in PBS-P+ running buffer (PBS-P+ Buffer 10×, Cytiva Life Sciences). The chip surface was activated using an injection of 1:1 N-hydroxysuccinimide (NHS)/1-ethyl-3-(3-dimethylaminopropyl)carbodiimide (EDC) (Cytiva Amine Coupling Kit, Cytiva Life Sciences) for 420 seconds at 10 $\mu\text{L}/\text{min}$ across both active and reference flow

cells. This activation process was followed by a wash of the microfluidics with 1 M ethanolamine-HCl (pH 8). Following activation, wild-type WDR5 (1.75-2.50 $\mu\text{g/mL}$; analyte dependent) in 50 mM sodium phosphate (pH 6.5), 50 mM NaCl was then injected across the active flow cell for 150 seconds at 10 $\mu\text{L/min}$. Following ligand immobilization, both active and passive flow cells were chemically deactivated with an injection of 1 M ethanolamine-HCl (pH 8) for 420 seconds at 10 $\mu\text{L/min}$. SET1_{win} peptide dilutions were freshly prepared from HPLC- purified peptide stocks in ultrapure water; the peptides were identical to those used in the steady-state FP experiments and contained an N-terminal sulforhodamine B and a C-terminal amide. Titrations of each labeled SET1_{win} peptide analyte were conducted to span an approximate range of $0.1-10 \times K_D$ (approximately 1 nM to 7 μM ; 40 μM for MLL1). Each SET1_{win} peptide was analyzed in a separate channel. Multicycle kinetic analyses were conducted at a flow cell temperature of 25°C and a sample compartment temperature of 20°C in a running buffer composed of 20 mM Tris- HCl (pH 7.5), 150 mM NaCl, 1 mM TCEP, 0.05% Tween 20. Each analysis cycle consisted of the following steps: 1) SET1_{win} peptide analyte injection: 120-second association, 360-second dissociation, 30 $\mu\text{L/min}$.; 2) regeneration injection with 100% ethylene glycol for 15 seconds at 10 $\mu\text{L/min}$. (high viscosity setting); 3) wash of the microfluidics system with running buffer; 4) regeneration injection with 1 μM ZnCl₂ for 30 second at 10 $\mu\text{L/min}$. Prior to curve fitting, all data generated from the active flow cell of each channel are double referenced to both the appropriate buffer blanks (first/last) and the reference flow cell. For MLL2_{win}, MLL3_{win}, MLL4_{win},

SETd1A_{Win}, and SETd1B_{Win}, the affinity constants, K_D , were calculated indirectly using $K_D = k_{\text{off}}/k_{\text{on}}$. For MLL1_{Win}, a plot of relative response versus the MLL1_{Win} analyte concentration was constructed and data were fitted using a four-parameter logistic regression to obtain the K_D . Therefore, an affinity analysis (relative response vs. concentration dose-response curve) was used to calculate the K_D , in this instance due to kinetic rate constants falling outside of the instrument detection range. All interactions were independently determined in triplicate (*e.g.*, separate ligand immobilizations). Experimental data and fits were plotted using GraphPad Prism 8 (GraphPad Software).

Steady-state fluorescence polarization (steady-state FP) measurements

All steady-state fluorescence polarization (FP) measurements were recorded using a SpectraMax i3x plate reader (Molecular Devices, San Jose, CA).[80, 81] HPLC-purified peptides, which contained an N-terminal sulforhodamine B and a C-terminal amide, were reconstituted as concentrated stocks in ultrapure water and used in all subsequent experiments. All steady-state FP assays were conducted in a buffer containing 20 mM Tris-HCl (pH 7.5), 150mM NaCl, 1 mM TCEP, 0.005% Tween 20 and plated in black untreated 96-well polystyrene microplates (Corning Inc., Corning, NY). Steady-state FP assays were conducted in triplicate, 24-point serial dilution for each of the six SET1_{Win} peptides against WDR5. 200 μL of WDR5 stock solutions, ranged from 21.6 to 131 μM , were added to each well on the first column of one of two adjacent black 96-well dilution plates, and 100 μL

of the assay buffer was added to wells A2-H24 over the two plates. WDR5 variants were then diluted down the two plates by transferring 100 μL from each well to the next, for a total of 24, 2-fold dilutions which range from low μM to low pM (variant specific). Following dilutions, 100 μL of the appropriate 20 nM labeled SET1_{win} peptide, which was dissolved in the assay buffer, was added to each well on each set of plates at a final concentration of 10 nM. The steady-state FP anisotropy was measured on the plates after a 1 h incubation at room temperature in the dark. The resulting dose-response data were averaged and fitted using a four-parameter logistic regression to obtain the binding affinity (K_D) for each interaction. Data were plotted and analyzed using GraphPad Prism 8 (GraphPad Software, San Diego, CA).

Molecular graphics

All cartoons showing molecular graphics were prepared using the PyMOL Molecular Graphics System (Version 2.4.0 Schrödinger, LLC).

2.4 Results and Discussion

The kinetic fingerprint of WDR5 – SET1_{win} interactions

We first explored the association (k_{on}) and dissociation (k_{off}) rate constants of WDR5-SET1_{win} interactions using BLI measurements [71, 72]. This technology probes ligand-receptor interactions that lead to accumulations of bimolecular complexes at the surface of the BLI sensor. This process is facilitated by immobilizing one interacting partner (ligand) onto the surface of the BLI sensor and supplying the analyte partner (receptor) from solution. In this way, the association and dissociation phases of the ligand-receptor complex are optically measured in real time using alterations in the interference pattern between reflected light waves at the surface of the BLI sensor. The N-terminus of each SET1_{win} was biotinylated and their C-terminus was amidated (**Table 1**). A 9-residue Gly/Ser-rich peptide spacer was inserted between the biotinylated site and the SET1_{win} sequence. This 3 nm-long spacer ensures that there is a satisfactory distance between the BLI sensor and SET1_{win} for WDR5 to interact without steric hinderance from the sensor surface.

The association binding curves were acquired through a 3-fold serial dilution of WDR5 (**Figure 2**). After the BLI response reached a saturation level, individual dissociation binding curves were recorded when sensors were placed in a WDR5-free buffer. The association and dissociation BLI phases underwent a time-dependent single-exponential increase and decrease, respectively. The binding

curves were fitted using the Octet Data Analysis software (**Materials and Methods; eqns. (1)-(3)**). The equilibrium dissociation constants using BLI, K_{D-BLI} , were indirectly determined using k_{on} and k_{off} .

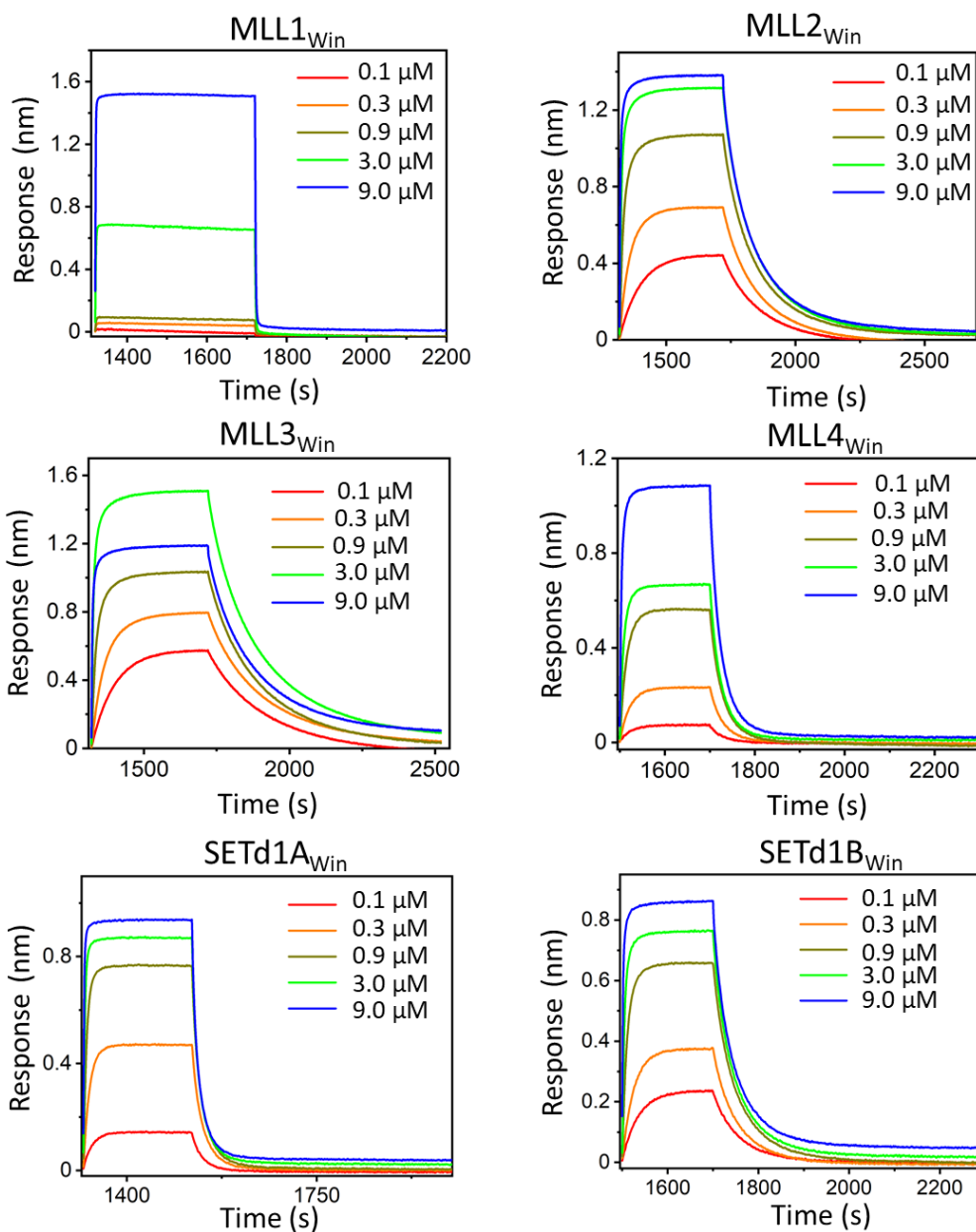


Figure 2: Label-free optical BLI sensorgrams of WDR5-SET1_{win} interactions. 5 nM biotin-tagged SET1_{win} peptides were loaded onto streptavidin (SA) sensors for 15 minutes. Titration series of WDR5 were injected as analytes and the corresponding association and dissociation curves are shown for the six SET1_{win}

peptides.

Table 2: Kinetic rate constants of association, k_{on} , and dissociation, k_{off} , and equilibrium dissociation constants, $K_{\text{D-BLI}}$, of WDR5 with SET1_{Win} peptides using BLI. Numbers represent mean \pm s.d. determined from three independent experiments.

Peptide sequence	k_{on} ($\text{M}^{-1}\text{s}^{-1}$) $\times 10^{-4}$	k_{off} (s^{-1}) $\times 10^3$	$K_{\text{D-BLI}}$ (nM)
Biotinyl-(GGS) ₃ MLL1 _{Win-NH2}	ND*	ND**	ND***
Biotinyl-(GGS) ₃ MLL2 _{Win-NH2}	4.4 \pm 0.4	7.7 \pm 0.2	170 \pm 20
Biotinyl-(GGS) ₃ MLL3 _{Win-NH2}	5.4 \pm 0.6	5.3 \pm 0.1	100 \pm 5
Biotinyl-(GGS) ₃ MLL4 _{Win-NH2}	2.3 \pm 0.2	39 \pm 2	1,700 \pm 200
Biotinyl-(GGS) ₃ SETd1A _{Win-NH2}	8.2 \pm 0.8	51 \pm 6	620 \pm 20
Biotinyl-(GGS) ₃ SETd1B _{Win-NH2}	7.1 \pm 0.5	17 \pm 1	250 \pm 30

ND* k_{on} was not quantitatively determined. Although WDR5-MLL1_{Win} interactions were detectable using a BLI measurement (**Fig. 2**), no accurate quantitative determination was made due to the limited time resolution of this approach. In this case, we assume that the k_{on} was in the same order of magnitude with the k_{on} of the other SET1_{Win} peptides ($\sim 10^4 \text{ M}^{-1}\text{s}^{-1}$).

ND** k_{off} was not quantitatively determined due to a fast dissociation rate constant. The upper-limit value for the detection of k_{off} is 1 s^{-1} according to instrument specifications.

ND*** $K_{\text{D-BLI}}$ was not quantitatively determined due to the limited time resolution of the approach. In this case, $K_{\text{D-BLI}}$ determined by BLI for WDR5-MLL1_{Win} interactions should be greater than $\sim 10^5 \text{ nM}$. This value results from dividing the upper-limit value of detection of k_{off} (ND**) by the value of the k_{on} approximation (ND*).

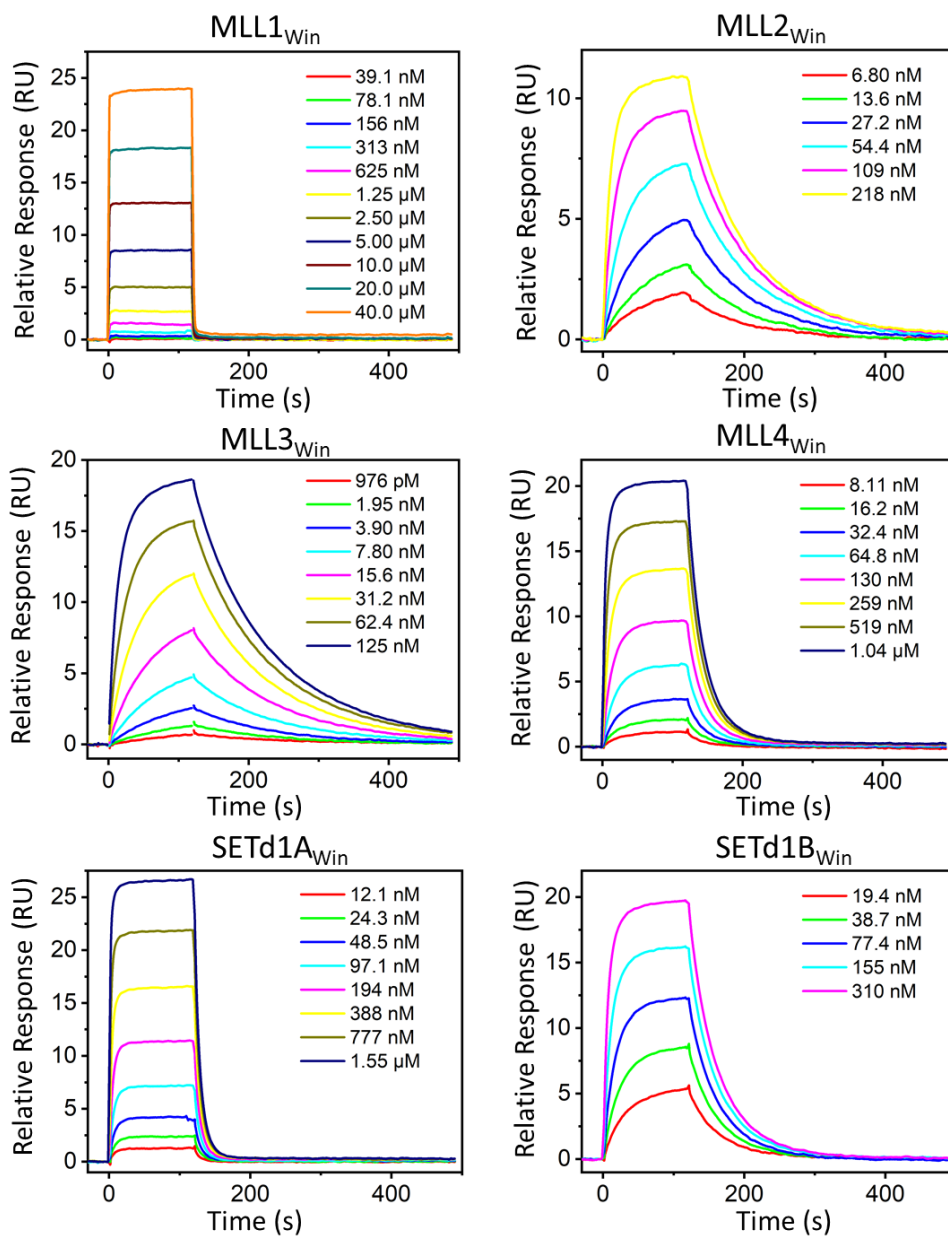


Figure 3: Label-free optoelectronic SPR sensorgrams of the WDR5-SET1_{win} interactions. Titration series of the respective SET1_{win} peptides were injected as analytes and the corresponding association and dissociation curves are shown for the six SET1_{win} peptides.

Association rate constants

The BLI-determined k_{on} values were in the order of $10^4 \text{ M}^{-1}\text{s}^{-1}$, clearly

indicating slow association kinetics for a protein-peptide system (Table 2). It is likely that this outcome resulted from two distinct physical restrictions: (i) tethering SET1_{Win} onto the surface of the BLI sensor, thus reducing its local mobility, and (ii) partitioning of SET1_{Win} into the WDR5 cavity. The latter physical process was illustrated in early crystallographic studies [21], which revealed that an MLL1_{Win} peptide penetrates into the WDR5 cavity to undergo a bimolecular association process. Here, we were unable to acquire an accurate mean value of k_{on} for the WDR5-MLL1_{Win} interaction due to its relatively fast k_{off} constant, whose binding time constant was shorter than the time-resolution limit of this approach (~1 s). Furthermore, k_{on} measured by BLI for various SET1_{Win} peptides were within the same order of magnitude, suggesting a similar insertion mechanism of the 6-residue Win motif peptide into the Win binding site (Table 1; Supplementary Figures S1-S2) [24, 65].

Dissociation rate constants

In contrast, k_{off} values spanned between two and three orders of magnitude (Table 2), highlighting significant distinctions in the WDR5-SET1_{Win} interactions. This assumes that the k_{off} of the WDR5-MLL1 interactions is faster than 1 s^{-1} , showing that MLL1_{Win} has the weakest interaction with WDR5 among all SET1_{Win} peptides. On the other hand, the strongest WDR5-SET1_{Win} interactions were monitored with MLL2_{Win} and MLL3_{Win}, which had average k_{off} values of $(7.7 \pm 0.2) \times 10^{-3}\text{ s}^{-1}$ and $(5.3 \pm 0.1) \times 10^{-3}\text{ s}^{-1}$, respectively. This finding provides unusually long binding times of ~130 s and ~190 s, respectively.

It was previously demonstrated that WDR5-SET1_{Win} interactions have a common archetype: a highly conserved Arg residue at P₀ (Table 1) [22]. This Arg residue is the pivotal player of WDR5-SET1_{Win} interactions, contributing to most of the binding affinity through a complex network of contacts with neighboring residues (Supplementary Table S1, Figure S3) [22, 24]. To test this hypothesis, we conducted BLI measurements using a control MLL3_{Win} peptide, whose native form exhibited the longest binding time with WDR5. The key Arg residue at P₀ was replaced by an Ala residue, resulting in the R4710A MLL3_{Win} mutant. No interaction was detected with this R4710A MLL3_{Win} mutant (Supplementary Figure S4), confirming the critical role of Arg at P₀ for the strength of WDR5-SET1_{Win} interactions. In addition, this finding validates the efficacy of our BLI measurements for examining the kinetic landscape of the Win binding site of WDR5.

Table 3: Kinetic and affinity determinations of WDR5-SET1_{Win} interactions using SPR. Values represent mean \pm s.d. acquired from at least three independent experimental determinations (separate receptor immobilizations). For MLL2_{Win}, n = 4 independent experimental determinations were used.

Peptide sequence	k_{on} ($M^{-1}s^{-1}$) $\times 10^{-5}$	k_{off} (s^{-1}) $\times 10^3$	K_D -SPR (nM)
Sulforhodamine B-(GGS) ₃ MLL1 _{Win-NH2}	ND*	ND**	16,000 \pm 3,000***
Sulforhodamine B-(GGS) ₃ MLL2 _{Win-NH2}	3.7 \pm 0.3	12 \pm 1	33 \pm 2
Sulforhodamine B-(GGS) ₃ MLL3 _{Win-NH2}	4.9 \pm 0.4	9 \pm 1	19 \pm 1
Sulforhodamine B-(GGS) ₃ MLL4 _{Win-NH2}	2.1 \pm 0.3	41 \pm 3	190 \pm 20
Sulforhodamine B-(GGS) ₃ SETd1A _{Win-NH2}	3.1 \pm 0.2	110 \pm 10	350 \pm 10
Sulforhodamine B-(GGS) ₃ SET1dB _{Win-NH2}	3.4 \pm 0.3	24 \pm 1	69 \pm 6

ND* k_{on} was not quantitatively determined. Although the WDR5-MLL1_{win} interactions were detectable using an SPR measurement (**Fig. 3**), no accurate quantitative determination was made due to the limited time resolution of the approach. In this case, we assume that the k_{on} was in the same order of magnitude with the k_{on} of other SET1_{win} peptides ($\sim 10^5 \text{ M}^{-1}\text{s}^{-1}$).

ND** k_{off} was not quantitatively determined due to a fast dissociation rate constant. The upper-limit value for the detection of k_{off} is 0.5 s^{-1} according to instrument specifications. The Biacore 8K+ cannot measure rate constants of dissociation, k_{off} , faster than 0.5 s^{-1} .

***Here, $K_{\text{D-SPR}}$ was determined using a steady-state SPR measurement (**Supplementary Figure S6**).

Does the tethering restriction of SET1_{win} onto the surface of the BLI sensor impact the kinetic rate constants?

Association rate constants

We postulated above that the slow association kinetics of WDR5-SET1_{win} interactions were caused at least in part by the immobilization of SET1_{win} onto the surface of the BLI sensor. To assess this hypothesis, we next employed SPR [77-79] as an orthogonal, label-free approach for examining these interactions of SET1_{win} peptides with WDR5. SPR is an optoelectronic technique that monitors accumulation of bimolecular ligand-receptor complexes onto the surface of the SPR sensor by changes in the refractive index. In this case, SET1_{win} analyte is supplied by using a flow-driven fluidic device. WDR5 was immobilized onto the surface of the SPR chips as the "receptor" (**Materials and Methods**). In this way, we recorded the association and dissociation phases in real time when SET1_{win} was not immobilized onto a surface (**Figure 3**). BiacoreTM Software was used to analyze and fit the SPR sensorgrams using a 1:1 binding interaction model to provide the

k_{on} and k_{off} rate constants (**Supplementary Figure S5**). In accord with our expectation, k_{on} values obtained by SPR were significantly increased by almost an order of magnitude to quantities greater than $10^5 \text{ M}^{-1}\text{s}^{-1}$ (**Table 3; Supplementary Figure S6, Figure S7A**). Again, k_{on} measured by SPR for various SET1_{Win} peptides were within the same order of magnitude, potentially indicating an identical insertion mechanism of the 6-residue Win motif peptide into the Win binding site (**Table 1; Supplementary Figures S1-S2**) [24, 65]. In addition, this insertion mechanism prevails no matter whether SET1_{Win} is in either physically restricted (e.g., BLI) or unrestricted (e.g., SPR) conditions.

Dissociation rate constants

Interestingly, with the exception of SETd1A, the k_{off} values acquired by the SPR measurement of WDR5-SET1_{Win} interactions closely resembled those measured by BLI (**Table 3; Supplementary Figure S7B**). Moreover, this finding provides indirect evidence that WDR5 did not undergo denaturation upon its immobilization onto the surface of the SPR sensor. Tethering SET1_{Win} onto the surface of the BLI sensor via its C-terminus was considered inconvenient, because prior crystallographic information indicated the interaction of the C-terminus residues (**Table 1**) with the WDR5 surface [24]. However, does the SET1_{Win} tethering onto the surface of the BLI sensor via its N-terminus impose an additional physical restriction on the binding mechanism? Since the k_{off} measured by BLI and SPR are almost identical, we conclude that the SET1_{Win} tethering onto the surface

of the BLI sensor via its N-terminus did not produce any additional restrain on the detachment mechanism of SET1_{Win} from the high-affinity Win binding site.

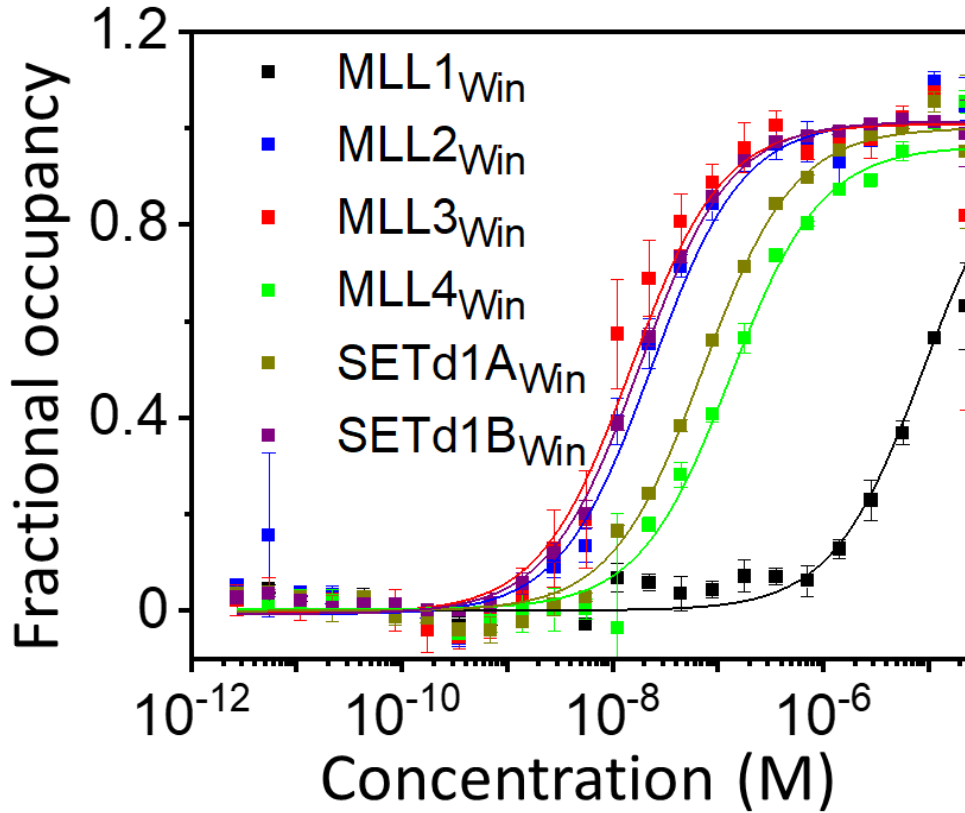


Figure 4: Steady-state FP curves of the WDR5-SET1_{Win} interactions. The N terminus of the SET1_{Win} peptides was tagged with sulforhodamine B, whereas the C terminus was amidated. The final concentration of labeled SET1_{Win} peptides in each well was 10 nM. Three independent experiments were conducted to obtain the WDR5 dose response.

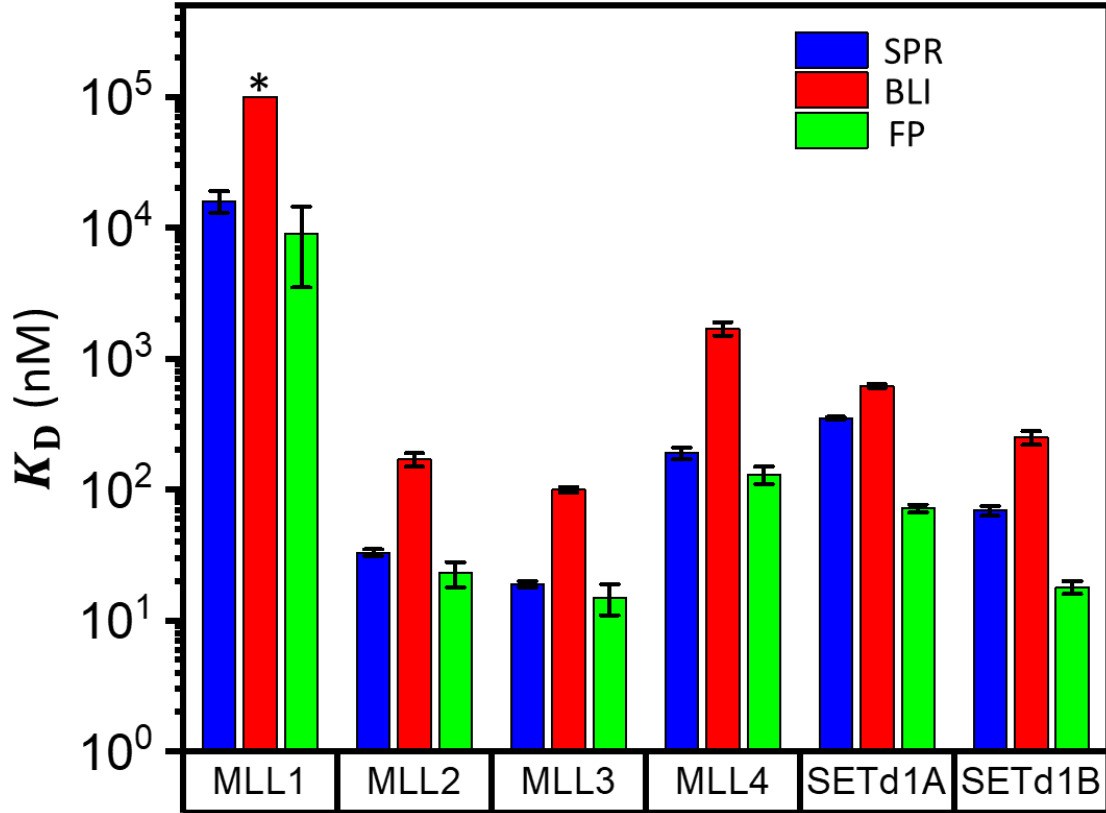


Figure 5: Quantitative comparisons of dissociation equilibrium constants of WDR5-SET1_{Win} interactions using BLI, SPR, and steady-state FP measurements. "*" is the upper-limit value for the detection of K_{D-BLI} . This value results from dividing the upper-limit value of the detection of k_{off} by the value of the k_{on} approximation (Table 2).

Comparisons of binding affinities of WDR5-SET1_{Win} interactions in restricted and unrestricted conditions

Next, we asked how immobilization-free (i.e., unrestricted) conditions influence the binding affinities. It is expected that the equilibrium dissociation constant slightly decreases if both WDR5 and SET1_{Win} move freely in solution. Hence, we determined equilibrium dissociation constant values using steady-state FP measurements, K_{D-FP} (Materials and Methods) [80-82]. This fluorescence technique monitors changes in the polarity of the emitted light due to modifications

in the rotational diffusion coefficient of a fluorescently labeled ligand. For example, the formation of the ligand-receptor complex is accompanied by a decline in the rotational mobility of the ligand, increasing the polarity of the emitted light. Here, Sulforhodamine B, an optically stable and bright fluorophore [83], was chemically attached to the N terminus of SET1_{win} via a 9-residue Gly/Ser-rich flexible spacer, whereas their C terminus was amidated. WDR5 concentration-dependent, steady-state FP binding curves were collected using a plate reader in a high-throughput setting (**Fig. 4**). In this way, we determined the immobilization-free K_{D-FP} (**Supplementary Table S2**). In accord with our anticipation, K_{D-FP} values were slightly lower than those acquired by SPR, K_{D-SPR} , meaning that WDR5-SET1_{win} interactions appeared somewhat stronger when probed in unrestricted conditions.

The K_{D-FP} values are also in agreement with results of prior ITC measurements (e.g., in immobilization-free conditions) at either lower [65] or higher salt concentrations [24]. It is worth mentioning that we preferred replacing Arg by Ser at the C terminus of MLL1_{win} and MLL4_{win} to avoid potential rebinding events of the native Arg at P₆ to the WDR5 cavity (**Table 1**). Regardless, we employed similar peptide sequences and identical buffer conditions to obtain meaningful comparisons among the three approaches. Then, we have discovered the following relationship for each WDR5-SET1_{win} interaction:

$K_{D-BLI} > K_{D-SPR} > K_{D-FP}$ (**Fig. 5; Supplementary Table S2**). In addition, numerical values of

K_{D-FP} replicated similar trends noted with different SET1_{win} peptides using both BLI and SPR.

Tentative interpretations

The kinetics and affinity measurements of the WDR5-SET1_{win} interactions were conducted with no significant variation among independently recorded BLI sensorgrams. The precision of this technique allowed us to quantitatively compare kinetics that were within the same order of magnitude. The SET1_{win} motif is located about 60 residues N-terminal to the SET domain, both of which are at the C-terminal end of the large SET1 proteins. These proteins range between ~1,700 – 5,500 amino acids in length. The rotational and diffusional rates of SET1 proteins relative to WDR5 are slow enough that these proteins can be considered as stationary compared to WDR5. Therefore, a more physiologically-relevant approach that recapitulates the binding of the full-length SET1 is that in which the 14-residue SET1_{win} peptide is attached onto a surface, whereas WDR5 is free in solution. In this way, the actual k_{on} measured by BLI would be conceivably closer to that value in physiological conditions. In addition, it should be mentioned that SET1_{win} is physically restrained at both ends when it is part of the SET1 subunit, suggesting an even lower k_{on} value. However, SET1_{win} may have stabilized conformations that promote binding within the context of the large SET1 subunit. In other words, the unrestricted SET1_{win} may undergo significantly greater degrees of freedom to adopt numerous non-productive conformations. Furthermore,

binding of SET1 proteins to WDR5 may be coupled with additional interaction pockets that can amplify the binding strength either by increasing k_{on} or by decreasing k_{off} or both. For example, prior sedimentation velocity experiments have shown that a 225-residue MLL1_{Win}-containing polypeptide exhibits a binding affinity of ~120 nM to WDR5 [22].

k_{on} values measured by SPR are yet at least an order of magnitude lower than those predicted for a protein-peptide interaction system ($10^7 - 10^8 \text{ M}^{-1}\text{s}^{-1}$) [84-88]. Here, WDR5-SET1_{Win} interactions require a precise insertion of the 6-residue, Arg-containing SET1_{Win} peptide into the WDR5 cavity. Therefore, we interpret that k_{on} values are limited by the entropic penalty determined by the SET1_{Win} partitioning into the Win binding site. The high-affinity Win binding site features a conical geometry with a maximum internal diameter of ~1.5 nm, as measured from side chain to side chain. For example, MLL1_{Win} partitions ~1.0 nm into the Win binding site (**Fig. 1**) [24]. In support to this interpretation, previous single-molecule studies have shown that k_{on} values of the interactions of peptides, up to 25 residues in length, with a narrow 2 nm-wide nanopore are in the order of $10^5 \text{ M}^{-1}\text{s}^{-1}$ [89, 90]. This is the same order of magnitude with k_{on} values that we determined by SPR.

However, the k_{on} is a composite parameter, which includes contributions of the diffusion-limited rate factor, $k_{\text{on}0}$, and electrostatic free energy of the WDR5-SET1_{Win} complex, ΔG_{el}^* . Zhou and coworkers have demonstrated that the rate

constant of association of two proteins can be accurately computed using the following expression: $k_{\text{on}} = k_{\text{on}0} \exp(-\Delta G_{\text{el}}^*/k_{\text{B}}T)$, where k_{B} and T are Boltzmann's constant and the absolute temperature, respectively [91, 92]. For this equation, they employed kinetic-rate theory of rigid-body docking and Poisson-Boltzmann formalism [93-95]. Using the same approach [93] and crystallographic information of the WDR5-SET1_{win} complex [24], we found k_{on} values of several SET1_{win} peptides (**Supplementary Table S3**). For example, computed k_{on} values for MLL2_{win} and MLL3_{win} were $2.9 \times 10^5 \text{ M}^{-1}\text{s}^{-1}$ and $1.2 \times 10^5 \text{ M}^{-1}\text{s}^{-1}$, respectively. These values compare well with our corresponding experimental data determined by SPR, which were $(3.7 \pm 0.3) \times 10^5 \text{ M}^{-1}\text{s}^{-1}$ and $(4.9 \pm 0.4) \times 10^5 \text{ M}^{-1}\text{s}^{-1}$, respectively. Yet, computed k_{on} values for MLL1_{win} and MLL4_{win} were in the order of $10^4 \text{ M}^{-1}\text{s}^{-1}$. The TransComp server: Web Server for Predicting Protein Association Rate Constants [91, 93] was not able to produce computed k_{on} values for SETd1A_{win} and SETd1B_{win}, likely because these WDR5-SET1_{win} complex formations do not undergo a single-step association mechanism. This outcome suggests that the WDR5-SET1_{win} interactions of SETd1A_{win} and SETd1B_{win} exhibit some subtle structural distinctions with respect to MLL1_{win}, MLL2_{win}, MLL3_{win}, and MLL4_{win}, which is in accord with prior crystallographic data [24, 65].

2.5 Concluding remarks, practical implications, and future prospects

In summary, we present a detailed kinetic fingerprint of the multitasking high-affinity Win binding site of WDR5, a protein with major regulatory implications in the methylation of H3K4 and in multiple physical associations with other proteins. This study reveals slow kinetics of association and dissociation of the SET1_{win} peptides with WDR5. It is known that WDR5 bridges the interaction between the SET domain of large SET1 subunits and other WRAD₂ constituents. A long-binding time of WDR5-SET1_{win} interaction, meaning slow dissociation kinetics of the high-affinity Win binding site, is a pivotal mechanism by which WDR5 assists the functional integrity of the multisubunit WRAD₂ complex. Furthermore, slow dissociation rates detected in this study point out a fundamental consideration for future therapeutics aimed at targeting interactions of the Win binding site with other proteins. The stability of these multisubunit complexes would decrease the opportunities for inhibitors to interfere in WDR5-SET1/MLL interactions. Consequently, this stresses the need for both fast association rates and slow dissociation rates when designing potential inhibitors to modulate WDR5 function. Newly designed small-molecule drugs would need to bind strongly to the WDR5 cavity and stave off other binding partners. Slow dissociation rate constants also reiterate the efficacy of SET1_{win} peptidomimetics as a fundamental platform for such drugs. Modifications of these sequences that enhance the association rates, while maintaining the disassociation rates, could be very effective at inhibiting Win binding site interactions. A good place to start would be the alteration of either the net charge or charge distribution of these peptides for amplifying the rate constants

of association. Any approach employed in this work can be used in the high-throughput screening of libraries of small-molecule compounds against WDR5-SET1_{win} interactions. However, WDR5 is a more relevant target for drug discovery when immobilized onto the SPR sensor, where the free inhibitor in solution would better mimic *in vivo* function. This experimental design enables determinations of kinetic rate constants, contrasting the steady-state FP measurements. Our results also indicate that WDR5 did not undergo denaturation upon its immobilization onto the SPR sensor. In the future, it would be desirable to extend these kinetic studies to full-length WRAD₂ subunits, because of the suitability of these high-throughput approaches for examining long-lived protein-protein interactions. For instance, it would be interesting to conduct SPR measurements, in which a full-length SET1 subunit is immobilized on the chip surface and use WDR5 as analyte in solution.

ABBREVIATIONS

AUC, analytical ultracentrifugation; BLI, Biolayer Interferometry; FP, Fluorescence polarization anisotropy; H3K4, histone 3 lysine 4; ITC, isothermal titration calorimetry; KMT, lysine methyltransferases of histones; k_{on} , the association rate constant; k_{off} , the dissociation rate constant; K_D , the equilibrium dissociation constant; K_{D-BLI} , the equilibrium dissociation constant obtained by biolayer interferometry; K_{D-SPR} , the equilibrium dissociation constant obtained by surface plasmon resonance; K_{D-FP} , the equilibrium dissociation constant obtained by steady-state fluorescence polarization; MLL, Mixed lineage leukemia; MYC, transcription factor oncoprotein; PDK1, 3- phosphoinositide-dependent protein kinase 1; PI3K, phosphatidylinositol 3-kinase; SET1, Suppressor of Variegation, Enhancer of Zeste, and Trithorax 1 lysine methyltransferases of histones; SET1_{Win}, 14-residue WDR5 interaction (Win) motif peptides of each SET1 protein; SPR, Surface plasmon resonance; WDR5, WD40 repeat protein 5; Win, evolutionarily conserved WDR5-interaction motif found in all SET1 family members; WRAD₂, subcomplex consisting of WDR5, retinoblastoma binding protein-5 (RbBP5), absent-small-homeotic-2-like protein (Ash2L), and dumpy-30 (DPY-30)

2.6 SUPPORTING INFORMATION

Kinetics of the multitasking high-affinity Win binding site of WDR5 in restricted and unrestricted conditions

**Ali Imran,¹ Brandon S. Moyer,² Ashley J. Canning,³ Dan Kalina,^{2,4}
Thomas M. Duncan,³ Kelsey J. Moody,^{1,2,4} Aaron J. Wolfe,^{1,2,4}
Michael S. Cosgrove,³ and Liviu Movileanu^{1,5,6*}**

¹*Department of Physics, Syracuse University, 201 Physics Building, Syracuse, New York 13244-1130, USA*

²*Ichor Therapeutics, Inc., 2521 US Route 11, LaFayette, New York 13084, USA*

³*Department of Biochemistry and Molecular Biology, State University of New York - Upstate Medical University, 4249 Weiskotten Hall, 766 Irving Avenue, Syracuse, New York 13210, USA*

⁴*Department of Chemistry, State University of New York, College of Environmental Science and Forestry, 1 Forestry Dr., Syracuse, New York 13210, USA*

⁵*The BioInspired Institute, Syracuse University, Syracuse, New York, 13244, USA*

⁶*Department of Biomedical and Chemical Engineering, Syracuse University, 329 Link Hall, Syracuse, New York 13244, USA*

CONTENTS OF THE SUPPLEMENTARY INFORMATION

1. Complex formation of WDR5 with SET1_{win} peptides (**Figures S1-S2**).
2. List of hydrogen bonds at the WDR5-SET1_{win} protein interface (**Table S1, Figure S3**).
3. Negative control of BLI measurements using an arginine-replaced MLL3_{win} derivative (**Figure S4**).
4. Quantitative kinetic determinations of WDR5-SET1_{win} interactions using SPR (**Figure S5**).
5. Determination of the equilibrium dissociation constant of WDR5 - MLL1_{win} interactions using SPR (**Figure S6**).
6. Quantitative comparisons of kinetic rate constants of WDR5-SET1_{win} interactions between BLI and SPR measurements (**Figure S7**).
7. Quantitative comparisons of the binding affinities of WDR5-SET1_{win} interactions among BLI, SPR, and steady-state FP (**Table S2**).
8. Computational predictions of the association rate constants of WDR5-SET1_{win} interactions using the basal rate constants and electrostatic energies of the transient WDR5-SET1_{win} complex (**Table S3**).
9. Accession codes.
10. Supporting references.

1. Complex formation of WDR5 with SET1_{win} peptides.

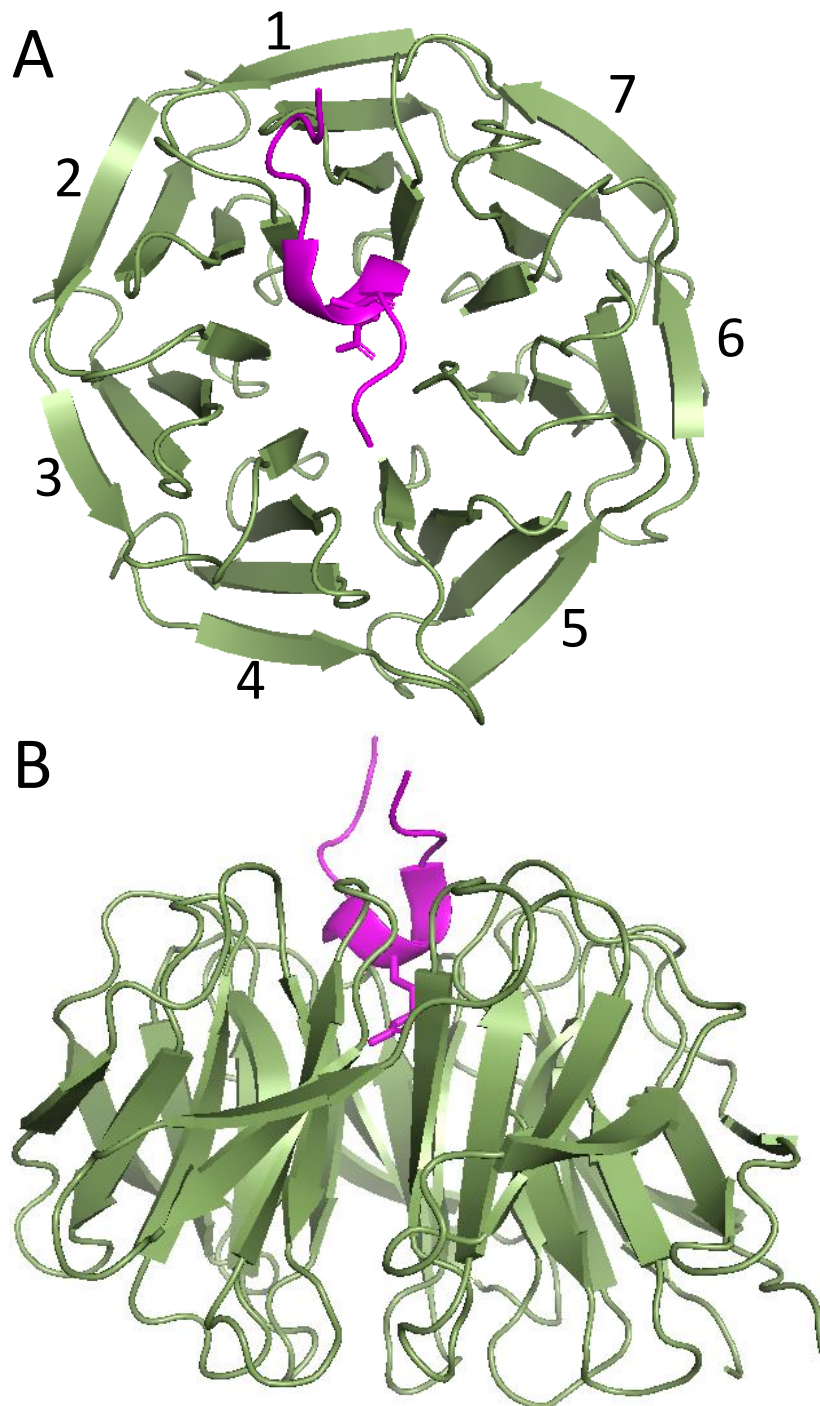


Figure S1: Structures of WDR5 (green) complexed with MLL1_{win} peptide (magenta). (A) The insertion of MLL1_{win} into the WDR5 cavity is shown from the top. (B) The same interaction is shown from the side. These graphic representations were made using the pdb code 4ESG [1].

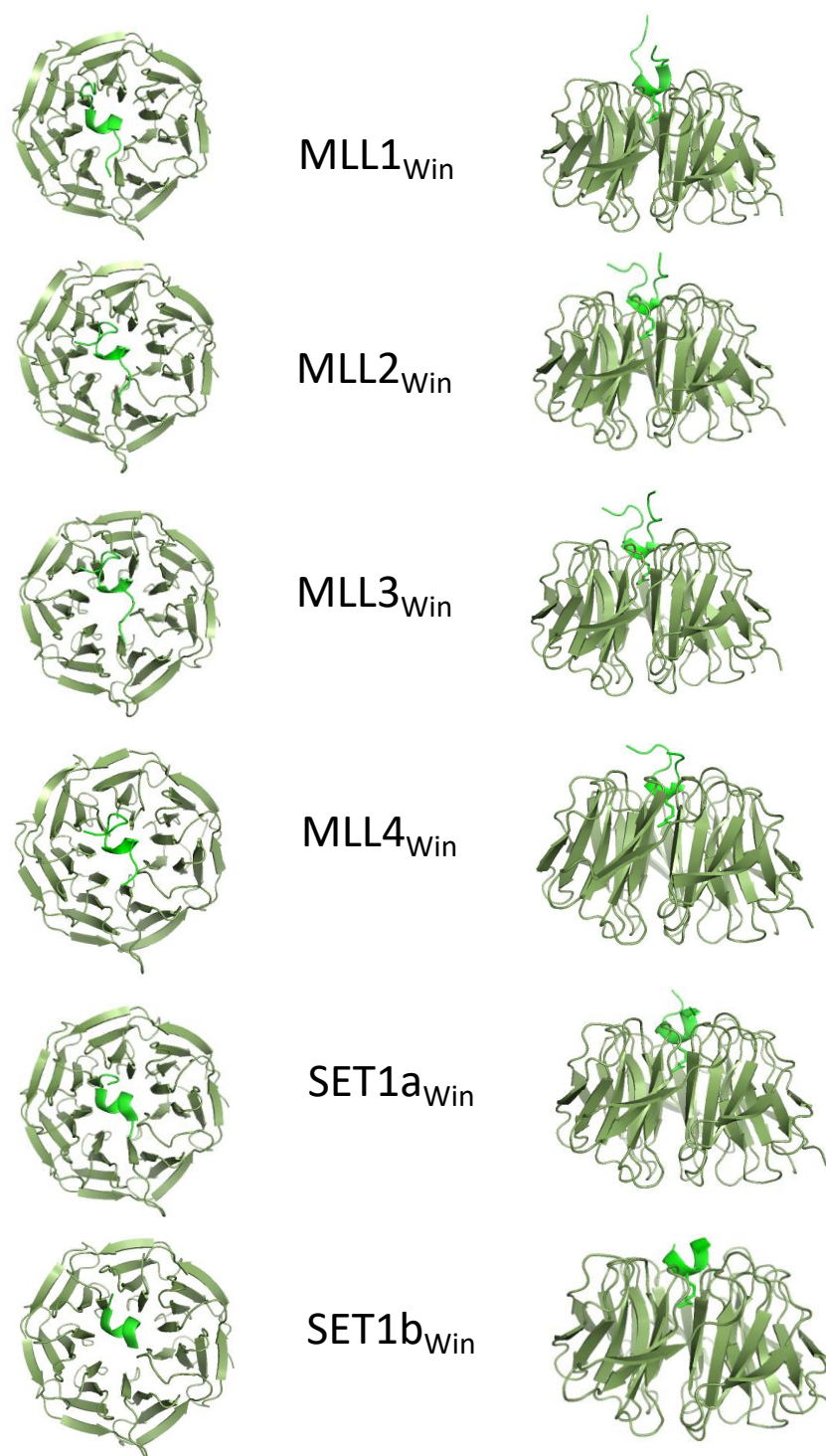


Figure S2: Structures of WDR5 complexed with SET1_{win} peptides. MLL1_{Win}, MLL2_{Win}, MLL3_{Win}, MLL4_{Win}, SETd1A_{Win}, and SETd1B_{Win} are inserted into the WDR5 cavity. Structures correspond to protein data bank codes: 3EG6, 4ESG, 4ERQ, 4ERY, 4ERZ, 4EWR and 4ES0 [1, 2].

2. List of hydrogen bonds at the WDR5-SET1_{win} protein interface.

Table S1: Comprehensive mapping of hydrogen bonding at the WDR5-SET1_{win} interface. These results were obtained using previously published co-crystallization data of Dharmarajan and coworkers [1]. The structures were not always able to model the whole sequence of the peptides, so these hydrogen bonds are not comprehensive. The first residue in each bond belongs to the SET1_{win} peptide, whereas the second one belongs to WDR5. Only peptide sequences of the segments that were able to model these interactions are listed below. Entries with two distances represent two different hydrogen bonds formed by the same residues. The cut-off distance for identifying these hydrogen bonds was 3.2 Å. Here, BB and SC denote backbone and side chain, respectively.

Peptide	Hydrogen Bonds	Distance (Å)	Type
MLL1 _{win} LNPHGSARAEVHL	H3761 – D107	2.7	SC-SC
	G3762 – G89	3.0	BB-BB
	A3764 – D107	3.0	BB-SC
	R3765 – S91	3.0, 2.8	BB-SC, SC-BB
	R3765 – C261	2.9	SC-BB
	R3765 – F133	3.0	SC-BB
MLL2 _{win} INPTGCARSEPKI	G5337 – G89	3.1	BB-BB
	A5339 – D107	2.9	BB-SC
	R5340 – S91	3.1, 2.8	BB-SC, SC-BB
	R5340 – C261	2.9	SC-BB
	R5340 – F133	3.0	SC-BB
	K5344 – K259	2.9	BB-BB
MLL3 _{win} VNPTGCARSEPKMS	A4709 – D107	2.9	BB-SC
	R4710 – S91	3.1, 2.8	BB-SC, SC-BB
	R4710 – C261	2.9	SC-BB
	R4710 – F133	2.9	SC-BB
	K4714 – K259	2.9	BB-BB
MLL4 _{win} LNPHGAARAEVY	A2510 – D107	3.0	BB-SC
	R2511 – S91	3.0, 2.8	BB-SC, SC-BB
	R2511 – C261	2.9	SC-BB
	R2511 – F133	3.0	SC-BB
SETd1A _{win} QTGSARSEGY	A1494 – D107	3.0	BB-SC
	R1495 – S91	3.0, 2.8	BB-SC, SC-BB
	R1495 – C261	2.9	SC-BB
	R1495 – F133	3.1	SC-BB
	Y1499 – K259	2.8	BB-BB
SETd1B _{win} GCARSEG	A1704 – D107	3.0	BB-SC
	R1705 – S91	3.2, 2.8	BB-SC, SC-BB
	R1705 – C261	2.8	SC-BB
	R1705 – F133	3.1	SC-BB

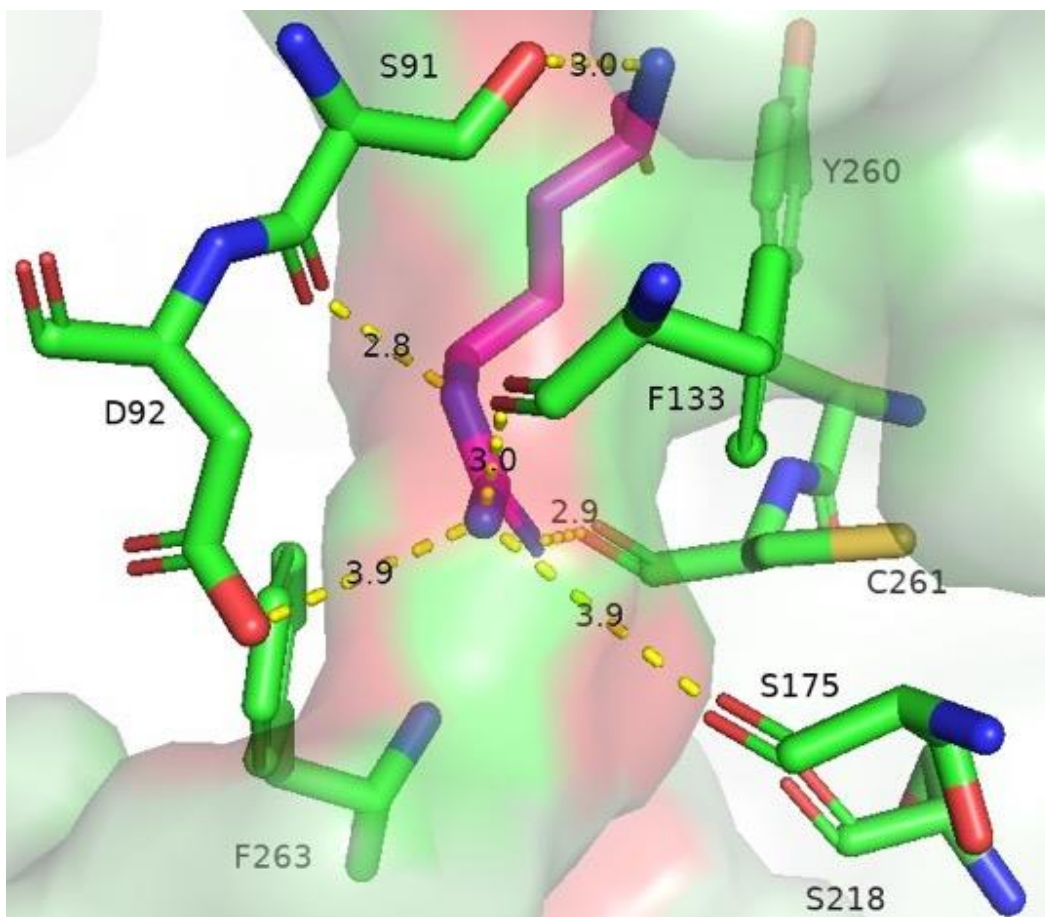


Figure S3: Structure of the binding cavity of WDR5. It illustrates its key residues involved in hydrogen bonding with the evolutionarily conserved Arg residue of MLL1_{win} at position P₀. The Arg residue is marked in magenta. The hydrogen bonds are indicated by thick dashed lines marked in yellow. The cut-off distance for identifying these hydrogen bonds was 4.0 Å. This graphic representation was made using the pdb code 4ESG [1].

3. Negative control of BLI measurements using an arginine-replaced MLL3_{win} derivative.

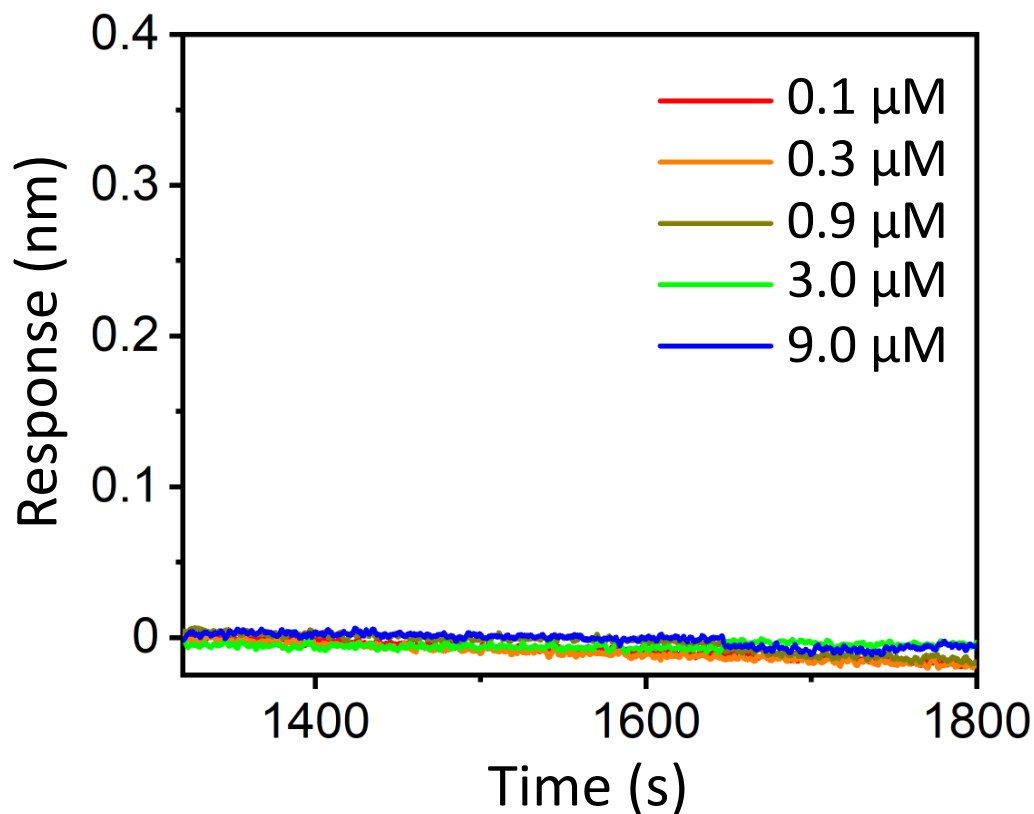


Figure S4: Arginine is a key side chain in trapping the MLL3_{win} peptide within the WDR5 cavity. This figure shows the BLI sensorgram, which includes the association and disassociation curves for the negative-control MLL3_{win} peptide interacting with WDR5. The sequence of this control peptide was (GGS)₃VNPTGCAASEPKMS, where Arg was substituted by Ala at P₀ of MLL3_{win} (Table 1). For pursuing BLI measurements, this control peptide was biotinylated at the N terminus and amidated at the C terminus. 5 nM negative-control MLL3_{win}-mutated peptide was loaded onto streptavidin (SA) sensors and allowed to associate with WRD5, whose concentrations ranged from 0.1 μM to 9 μM. Then, a dissociation process followed. The figure provides compelling evidence that no association phase was detected, illustrating that no binding interactions occurred in this case.

4. Quantitative kinetic determinations of WDR5-SET1_{win} interactions using SPR.

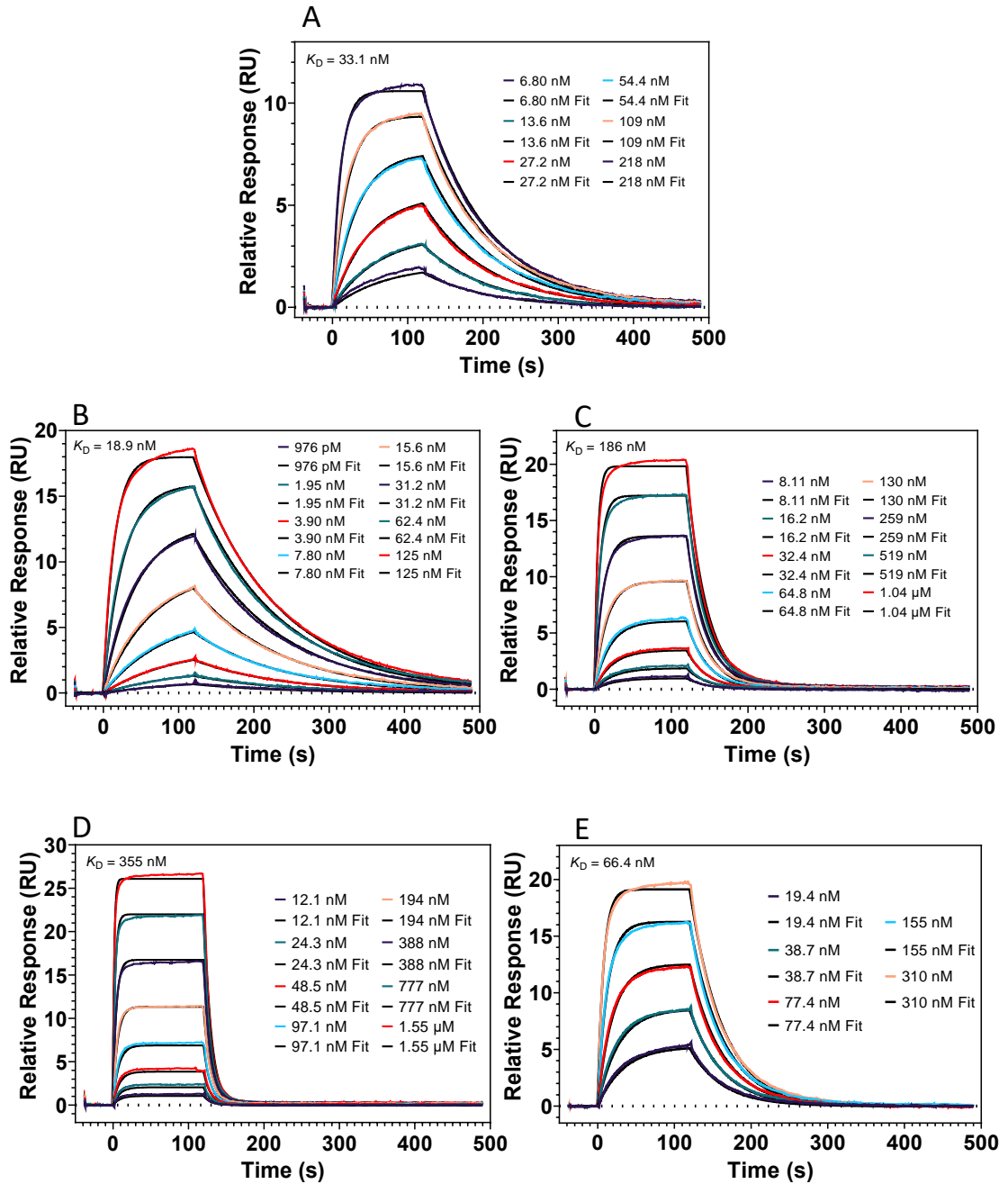


Figure S5: Representative SPR sensorgrams and their kinetic fits for the interactions of SET1_{win} peptides with WDR5. WDR5 was immobilized onto CM5 chips and allowed to associate with SET1_{win} peptides. Each panel indicates the peptide concentrations, the association and disassociation curves, as well as the fits of data to obtain k_{on} and k_{off} . While these are single runs for each peptide, at

least three independent runs were conducted to obtain the average kinetic values. (A) MLL2_{Win}, (B) MLL3_{Win}, (C) MLL4_{Win}, (D) SETd1A_{Win}, and (E) SETd1B_{Win}.

5. Determination of the equilibrium dissociation constant of WDR5 - MLL1_{Win} interactions using SPR.

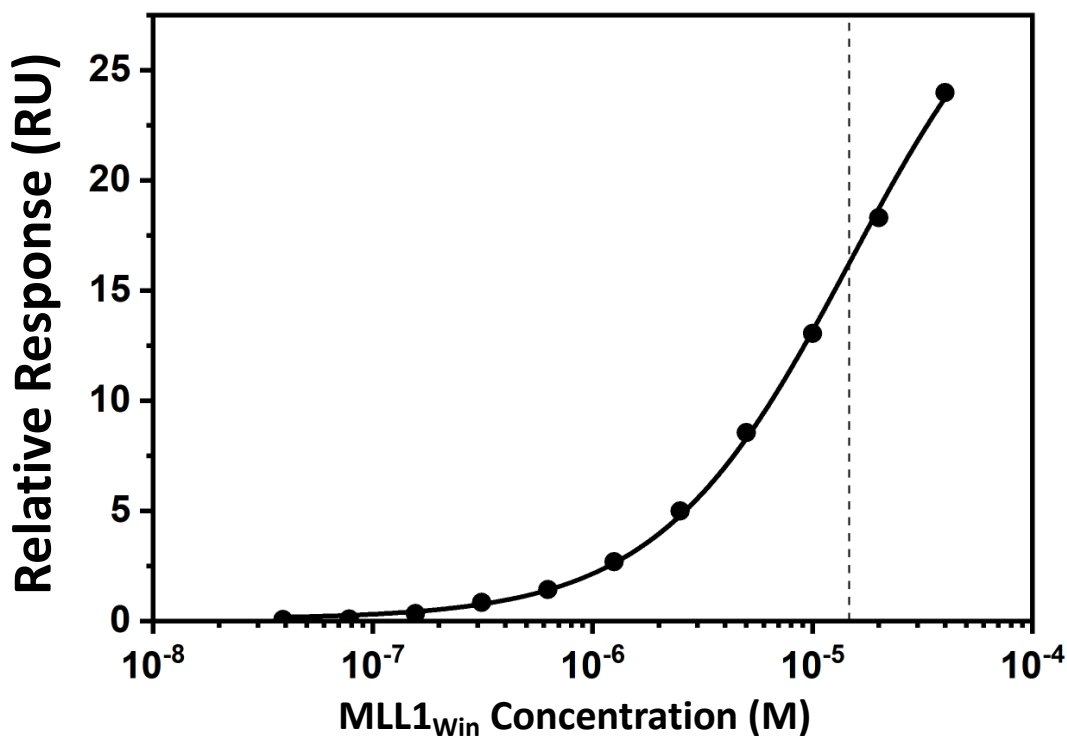


Figure S6: Steady-state SPR measurements for the quantification of the interactions between MLL1_{Win} peptide and WDR5. WDR5 was immobilized onto CM5 chips and allowed to associate with MLL1_{Win} peptide, whose concentration was varied in the range of 4×10^{-8} through 4×10^{-5} M (the horizontal axis). The resultant maximum relative responses were plotted and fitted to obtain the K_D of the interaction. Although this set of illustrated data resulted from a single experiment, three independent data acquisitions were employed to obtain the average value of K_D

6. Quantitative comparisons of kinetic rate constants of WDR5-SET1_{win} interactions between BLI and SPR measurements.

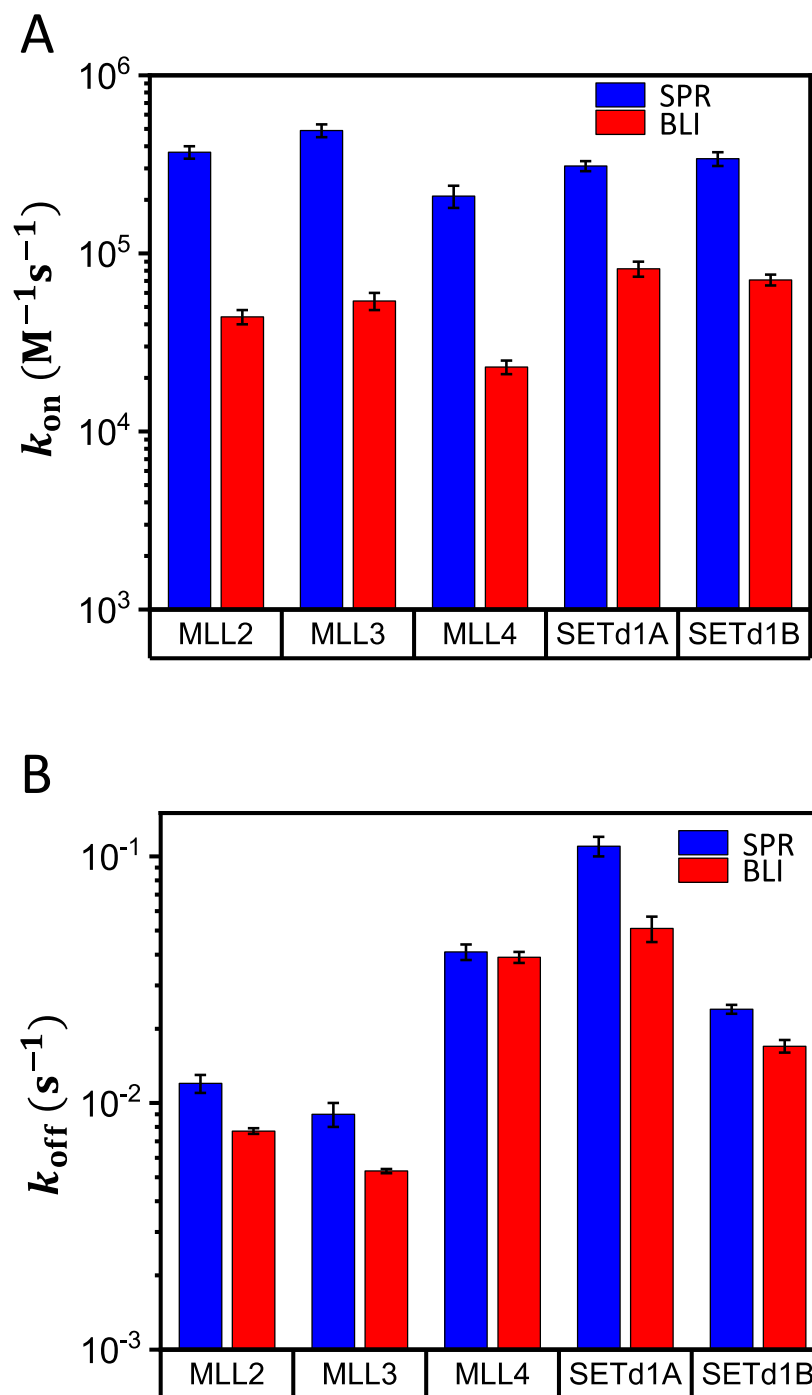


Figure S7: Comparisons of kinetic rate constants of association and dissociation between restricted BLI and unrestricted SPR conditions. (A) Association rate constants. **(B)** Dissociation rate constants. All experimental details are provided in **Materials and Methods**.

7. Quantitative comparisons of the binding affinities of WDR5-SET1_{win} interactions among BLI, SPR, and steady-state FP.

Table S2: Quantitative comparisons of K_D obtained via BLI, SPR, and steady-state FP. K_{D-BLI} , K_{D-SPR} , and K_{D-FP} are the equilibrium dissociation constants measured via BLI, SPR, and steady-state FP, respectively.

Peptide	K_{D-BLI} (nM)	K_{D-SPR} (nM)	K_{D-FP} (nM)
MLL1 _{win}	$\geq 100,000^*$	$16,000 \pm 3,000^{**}$	$9,000 \pm 5,500^{***}$
MLL2 _{win}	170 ± 20	33 ± 2	23 ± 5
MLL3 _{win}	100 ± 5	19 ± 1	15 ± 4
MLL4 _{win}	$1,700 \pm 200$	190 ± 20	130 ± 20
SETd1A _{win}	620 ± 20	350 ± 10	72 ± 5
SETd1B _{win}	250 ± 30	69 ± 6	18 ± 2

*This is the upper-limit value for the detection of K_{D-BLI} . It results from dividing the upper-limit value of detection of k_{off} by the value of the k_{on} approximation.

** K_{D-SPR} was determined using a steady-state SPR measurement.

***Prior ITC measurements at a slightly increased salt concentration show that data are consistent with the steady-state FP measurements [1].

8. Computational predictions of the association rate constants of WDR5-SET1_{win} interactions using the basal rate constants and electrostatic free energies of the transient WDR5-SET1_{win} complex.

Table S3: Determination of the association rate constants using the basal rate constants, k_{on0} , and electrostatic free energies, ΔG^*_{el} , of the transient WDR5-SET1_{win} complex.

Peptide sequence	k_{on0} ($M^{-1} \times s^{-1}$)	ΔG^*_{el} (kcal/mol)	k_{on} ($M^{-1} \times s^{-1}$)
MLL1 _{win}	1.27×10^5	1.412	1.17×10^4
MLL2 _{win}	2.79×10^5	-0.027	2.92×10^5
MLL3 _{win}	2.07×10^5	0.323	1.20×10^5
MLL4 _{win}	2.64×10^4	0.122	2.15×10^4
SETd1A _{win}	ND*	ND*	ND*
SETd1B _{win}	ND*	ND*	ND*

These values were determined using The “TransComp: Web Server for Predicting Protein Association Rate Constants” (<https://pipe.rcc.fsu.edu/transcomp/>) [3-7].

ND* Computational predictions could not be made for these interactions, because the association process of the WDR5-SET1_{Win} complex may not undergo a single-step mechanism.

The calculation of the k_{on} was based on the following equation:

$$k_{on} = k_{on0} \exp(-\Delta G_{el}^*/k_B T)$$

(S1)

Here, k_{on0} is the basal rate constant for attaining the transient WDR5-SET1_{Win} complex. ΔG_{el}^* indicates the electrostatic energy of the transient WDR5-SET1_{Win} complex. The computational process encompasses three components: (i) the generation of the transient WDR5-SET1_{Win} complex, (ii) the calculation of the basal rate constant k_{on0} , and (iii) the determination of the electrostatic interaction energy, ΔG_{el}^* , which is associated with the WDR5-SET1_{Win} transient complex.

9. Accession codes.

WDR5 protein:	UniProtKB - P61964 (WDR5_HUMAN)
MLL1 _{Win} motif :	UniProtKB - Q03164 (KMT2A_HUMAN)
MLL2 _{Win} motif:	UniProtKB - O14686 (KMT2D_HUMAN)
MLL3 _{Win} motif:	UniProtKB - Q8NEZ4 (KMT2C_HUMAN)
MLL4 _{Win} motif:	UniProtKB - Q9UMN6 (KMT2B_HUMAN)
SETd1A _{Win} motif:	UniProtKB - O15047 (SET1A_HUMAN)
SETd1B _{Win} motif:	UniProtKB - Q9UPS6 (SET1B_HUMAN)

10. Supporting references.

- 1 Dharmarajan, V., Lee, J. H., Patel, A., Skalnik, D. G. and Cosgrove, M. S. (2012) Structural basis for WDR5 interaction (Win) motif recognition in human SET1 family histone methyltransferases. *J. Biol. Chem.* **287**, 27275-27289
- 2 Patel, A., Dharmarajan, V. and Cosgrove, M. S. (2008) Structure of WDR5 bound to mixed lineage leukemia protein-1 peptide. *J. Biol. Chem.* **283**, 32158-32161
- 3 Alsallaq, R. and Zhou, H. X. (2008) Electrostatic rate enhancement and transient complex of protein-protein association. *Proteins.* **71**, 320-335
- 4 Zhou, H. X. (2010) Rate theories for biologists. *Q. Rev. Biophys.* **43**, 219-293
- 5 Qin, S., Pang, X. and Zhou, H. X. (2011) Automated prediction of protein association rate constants. *Structure.* **19**, 1744-1751

6 Qin, S. and Zhou, H. X. (2013) PI(2)PE: A Suite of Web Servers for Predictions Ranging From Protein Structure to Binding Kinetics. *Biophys. Rev.* **5**, 41-46

7 Pang, X. and Zhou, H. X. (2017) Rate Constants and Mechanisms of Protein-Ligand Binding. *Annu. Rev. Biophys.* **46**, 105-130

2.7 REFERENCES

- 1 Trievel, R. C. and Shilatifard, A. (2009) WDR5, a complexed protein. *Nat. Struct. Mol. Biol.* **16**, 678-680
- 2 Crawford, B. D. and Hess, J. L. (2006) MLL core components give the green light to histone methylation. *ACS Chem. Biol.* **1**, 495-498
- 3 Cosgrove, M. S. and Patel, A. (2010) Mixed lineage leukemia: a structure-function perspective of the MLL1 protein. *FEBS J.* **277**, 1832-1842
- 4 Li, Y., Han, J., Zhang, Y., Cao, F., Liu, Z., Li, S., Wu, J., Hu, C., Wang, Y., Shuai, J., Chen, J., Cao, L., Li, D., Shi, P., Tian, C., Zhang, J., Dou, Y., Li, G., Chen, Y. and Lei, M. (2016) Structural basis for activity regulation of MLL family methyltransferases. *Nature.* **530**, 447-452
- 5 Vedadi, M., Blazer, L., Eram, M. S., Barsyte-Lovejoy, D., Arrowsmith, C. H. and Hajian, T. (2017) Targeting human SET1/MLL family of proteins. *Protein Sci.* **26**, 662-676
- 6 Xue, H., Yao, T., Cao, M., Zhu, G., Li, Y., Yuan, G., Chen, Y., Lei, M. and Huang, J. (2019) Structural basis of nucleosome recognition and modification by MLL methyltransferases. *Nature.* **573**, 445-449
- 7 Jiang, H. (2020) The complex activities of the SET1/MLL complex core subunits in development and disease. *Biochim. Biophys. Acta. Gene. Regul. Mech.* **1863**, 194560
- 8 Sha, L., Ayoub, A., Cho, U. S. and Dou, Y. (2020) Insights on the regulation of the MLL/SET1 family histone methyltransferases. *Biochim. Biophys. Acta Gene. Regul. Mech.* **1863**, 194561
- 9 Dou, Y., Milne, T. A., Ruthenburg, A. J., Lee, S., Lee, J. W., Verdine, G. L., Allis, C. D. and Roeder, R. G. (2006) Regulation of MLL1 H3K4 methyltransferase activity by its core components. *Nat. Struct. Mol. Biol.* **13**, 713-719
- 10 Lee, J. H., Tate, C. M., You, J. S. and Skalnik, D. G. (2007) Identification and characterization of the human Set1B histone H3-Lys4 methyltransferase complex. *J. Biol. Chem.* **282**, 13419-13428
- 11 Patel, A., Dharmarajan, V., Vought, V. E. and Cosgrove, M. S. (2009) On the mechanism of multiple lysine methylation by the human mixed lineage leukemia protein-1 (MLL1) core complex. *J. Biol. Chem.* **284**, 24242-24256
- 12 Odho, Z., Southall, S. M. and Wilson, J. R. (2010) Characterization of a novel WDR5-binding site that recruits RbBP5 through a conserved motif to enhance methylation of histone H3 lysine 4 by mixed lineage leukemia protein-1. *J. Biol. Chem.* **285**, 32967-32976
- 13 Avdic, V., Zhang, P., Lanouette, S., Groulx, A., Tremblay, V., Brunzelle, J. and Couture, J. F. (2011) Structural and biochemical insights into MLL1 core complex assembly. *Structure.* **19**, 101-108
- 14 Patel, A., Vought, V. E., Dharmarajan, V. and Cosgrove, M. S. (2011) A novel non-SET domain multi-subunit methyltransferase required for sequential nucleosomal histone H3 methylation by the mixed lineage leukemia protein-1 (MLL1) core complex. *J. Biol. Chem.* **286**, 3359-3369
- 15 van Nuland, R., Smits, A. H., Pallaki, P., Jansen, P. W., Vermeulen, M. and

- Timmers, H. T. (2013) Quantitative dissection and stoichiometry determination of the human SET1/MLL histone methyltransferase complexes. *Mol. Cell Biol.* **33**, 2067-2077
- 16 Zhang, P., Bergamin, E. and Couture, J. F. (2013) The many facets of MLL1 regulation. *Biopolymers.* **99**, 136-145
- 17 Froimchuk, E., Jang, Y. and Ge, K. (2017) Histone H3 lysine 4 methyltransferase KMT2D. *Gene.* **627**, 337-342
- 18 Ali, A. and Tyagi, S. (2017) Diverse roles of WDR5-RbBP5-ASH2L-DPY30 (WRAD) complex in the functions of the SET1 histone methyltransferase family. *J. Biosci.* **42**, 155-159
- 19 Han, J., Li, T., Li, Y., Li, M., Wang, X., Peng, C., Su, C., Li, N., Li, Y., Xu, Y. and Chen, Y. (2019) The internal interaction in RBBP5 regulates assembly and activity of MLL1 methyltransferase complex. *Nucleic Acids Res.* **47**, 10426-10438
- 20 Kaustov, L., Lemak, A., Wu, H., Faini, M., Fan, L., Fang, X., Zeng, H., Duan, S., Allali-Hassani, A., Li, F., Wei, Y., Vedadi, M., Aebersold, R., Wang, Y., Houlston, S. and Arrowsmith, C. H. (2019) The MLL1 trimeric catalytic complex is a dynamic conformational ensemble stabilized by multiple weak interactions. *Nucleic Acids Res.* **47**, 9433-9447
- 21 Patel, A., Dharmarajan, V. and Cosgrove, M. S. (2008) Structure of WDR5 bound to mixed lineage leukemia protein-1 peptide. *J. Biol. Chem.* **283**, 32158-32161
- 22 Patel, A., Vought, V. E., Dharmarajan, V. and Cosgrove, M. S. (2008) A conserved arginine-containing motif crucial for the assembly and enzymatic activity of the mixed lineage leukemia protein-1 core complex. *J. Biol. Chem.* **283**, 32162-32175
- 23 Song, J. J. and Kingston, R. E. (2008) WDR5 interacts with mixed lineage leukemia (MLL) protein via the histone H3-binding pocket. *J. Biol. Chem.* **283**, 35258-35264
- 24 Dharmarajan, V., Lee, J. H., Patel, A., Skalnik, D. G. and Cosgrove, M. S. (2012) Structural basis for WDR5 interaction (Win) motif recognition in human SET1 family histone methyltransferases. *J. Biol. Chem.* **287**, 27275-27289
- 25 Alicea-Velázquez, N. L., Shinsky, S. A., Loh, D. M., Lee, J. H., Skalnik, D. G. and Cosgrove, M. S. (2016) Targeted Disruption of the Interaction between WD-40 Repeat Protein 5 (WDR5) and Mixed Lineage Leukemia (MLL)/SET1 Family Proteins Specifically Inhibits MLL1 and SETd1A Methyltransferase Complexes. *J. Biol. Chem.* **291**, 22357-22372
- 26 Shinsky, S. A., Monteith, K. E., Viggiano, S. and Cosgrove, M. S. (2015) Biochemical reconstitution and phylogenetic comparison of human SET1 family core complexes involved in histone methylation. *J. Biol. Chem.* **290**, 6361-6375
- 27 Stirnimann, C. U., Petsalaki, E., Russell, R. B. and Müller, C. W. (2010) WD40 proteins propel cellular networks. *Trends Biochem. Sci.* **35**, 565-574
- 28 Santosh Kumar, H. S., Kumar, V., Pattar, S. and Telkar, S. (2016) Towards the construction of an interactome for Human WD40 protein family. *Bioinformatics.* **12**, 54-61
- 29 Jain, B. P. and Pandey, S. (2018) WD40 Repeat Proteins: Signalling Scaffold with Diverse Functions. *Protein J.* **37**, 391-406

- 30 Ullius, A., Luscher-Firzlaff, J., Costa, I. G., Walsemann, G., Forst, A. H., Gusmao, E. G., Kapelle, K., Kleine, H., Kremmer, E., Vervoorts, J. and Luscher, B. (2014) The interaction of MYC with the trithorax protein ASH2L promotes gene transcription by regulating H3K27 modification. *Nucleic Acids Res.* **42**, 6901-6920
- 31 Thomas, L. R., Foshage, A. M., Weissmiller, A. M. and Tansey, W. P. (2015) The MYC-WDR5 Nexus and Cancer. *Cancer Res.* **75**, 4012-4015
- 32 Thomas, L. R., Wang, Q., Grieb, B. C., Phan, J., Foshage, A. M., Sun, Q., Olejniczak, E. T., Clark, T., Dey, S., Lorey, S., Alicie, B., Howard, G. C., Cawthon, B., Ess, K. C., Eischen, C. M., Zhao, Z., Fesik, S. W. and Tansey, W. P. (2015) Interaction with WDR5 promotes target gene recognition and tumorigenesis by MYC. *Mol. Cell. Biochem.* **58**, 440-452
- 33 Aho, E. R., Weissmiller, A. M., Fesik, S. W. and Tansey, W. P. (2019) Targeting WDR5: A WINning Anti-Cancer Strategy? *Epigenet. Insights.* **12**, 2516865719865282
- 34 Thomas, L. R., Adams, C. M., Wang, J., Weissmiller, A. M., Creighton, J., Lorey, S. L., Liu, Q., Fesik, S. W., Eischen, C. M. and Tansey, W. P. (2019) Interaction of the oncoprotein transcription factor MYC with its chromatin cofactor WDR5 is essential for tumor maintenance. *Proceedings of the National Academy of Sciences of the United States of America.* **116**, 25260-25268
- 35 Thomas, L. R., Adams, C. M., Fesik, S. W., Eischen, C. M. and Tansey, W. P. (2020) Targeting MYC through WDR5. *Mol. Cell. Oncol.* **7**, 1709388
- 36 Guarnaccia, A. D., Rose, K. L., Wang, J., Zhao, B., Popay, T. M., Wang, C. E., Guerrazzi, K., Hill, S., Woodley, C. M., Hansen, T. J., Lorey, S. L., Shaw, J. G., Payne, W. G., Weissmiller, A. M., Olejniczak, E. T., Fesik, S. W., Liu, Q. and Tansey, W. P. (2021) Impact of WIN site inhibitor on the WDR5 interactome. *Cell Rep.* **34**, 108636
- 37 Downing, T. L., Soto, J., Morez, C., Houssin, T., Fritz, A., Yuan, F., Chu, J., Patel, S., Schaffer, D. V. and Li, S. (2013) Biophysical regulation of epigenetic state and cell reprogramming. *Nat. Mater.* **12**, 1154-1162
- 38 Wang, P., Dreger, M., Madrazo, E., Williams, C. J., Samaniego, R., Hodson, N. W., Monroy, F., Baena, E., Sánchez-Mateos, P., Hurlstone, A. and Redondo-Muñoz, J. (2018) WDR5 modulates cell motility and morphology and controls nuclear changes induced by a 3D environment. *Proceedings of the National Academy of Sciences of the United States of America.* **115**, 8581-8586
- 39 Guarnaccia, A. D. and Tansey, W. P. (2018) Moonlighting with WDR5: A Cellular Multitasker. *J. Clin. Med.* **7**
- 40 Bryan, A. F., Wang, J., Howard, G. C., Guarnaccia, A. D., Woodley, C. M., Aho, E. R., Rellinger, E. J., Matlock, B. K., Flaherty, D. K., Lorey, S. L., Chung, D. H., Fesik, S. W., Liu, Q., Weissmiller, A. M. and Tansey, W. P. (2020) WDR5 is a conserved regulator of protein synthesis gene expression. *Nucleic Acids Res.* **48**, 2924-2941
- 41 Couture, J. F., Collazo, E. and Trievel, R. C. (2006) Molecular recognition of histone H3 by the WD40 protein WDR5. *Nat. Struct. Mol. Biol.* **13**, 698-703
- 42 Han, Z., Guo, L., Wang, H., Shen, Y., Deng, X. W. and Chai, J. (2006) Structural basis for the specific recognition of methylated histone H3 lysine 4 by the WD-40 protein WDR5. *Mol. Cell.* **22**, 137-144

- 43 Schuetz, A., Allali-Hassani, A., Martín, F., Loppnau, P., Vedadi, M., Bochkarev, A., Plotnikov, A. N., Arrowsmith, C. H. and Min, J. (2006) Structural basis for molecular recognition and presentation of histone H3 by WDR5. *EMBO J.* **25**, 4245-4252
- 44 Ruthenburg, A. J., Wang, W., Graybosch, D. M., Li, H., Allis, C. D., Patel, D. J. and Verdine, G. L. (2006) Histone H3 recognition and presentation by the WDR5 module of the MLL1 complex. *Nat. Struct. Mol. Biol.* **13**, 704-712
- 45 Avdic, V., Zhang, P., Lanouette, S., Voronova, A., Skerjanc, I. and Couture, J. F. (2011) Fine-tuning the stimulation of MLL1 methyltransferase activity by a histone H3-based peptide mimetic. *FASEB J.* **25**, 960-967
- 46 Iberg, A. N., Espejo, A., Cheng, D., Kim, D., Michaud-Levesque, J., Richard, S. and Bedford, M. T. (2008) Arginine methylation of the histone H3 tail impedes effector binding. *J. Biol. Chem.* **283**, 3006-3010
- 47 Ge, Z., Song, E. J., Kawasawa, Y. I., Li, J., Dovat, S. and Song, C. (2016) WDR5 high expression and its effect on tumorigenesis in leukemia. *Oncotarget.* **7**, 37740-37754
- 48 Sun, W., Guo, F. and Liu, M. (2018) Up-regulated WDR5 promotes gastric cancer formation by induced cyclin D1 expression. *J. Cell. Biochem.* **119**, 3304-3316
- 49 Wang, F., Zhang, J., Ke, X., Peng, W., Zhao, G., Peng, S., Xu, J., Xu, B. and Cui, H. (2020) WDR5-Myc axis promotes the progression of glioblastoma and neuroblastoma by transcriptional activating CARM1. *Biochem. Biophys. Res. Commun.* **523**, 699-706
- 50 Karatas, H., Townsend, E. C., Bernard, D., Dou, Y. and Wang, S. (2010) Analysis of the binding of mixed lineage leukemia 1 (MLL1) and histone 3 peptides to WD repeat domain 5 (WDR5) for the design of inhibitors of the MLL1-WDR5 interaction. *J. Med. Chem.* **53**, 5179-5185
- 51 Karatas, H., Townsend, E. C., Cao, F., Chen, Y., Bernard, D., Liu, L., Lei, M., Dou, Y. and Wang, S. (2013) High-affinity, small-molecule peptidomimetic inhibitors of MLL1/WDR5 protein-protein interaction. *J. Am. Chem. Soc.* **135**, 669-682
- 52 Senisterra, G., Wu, H., Allali-Hassani, A., Wasney, G. A., Barsyte-Lovejoy, D., Dombrowski, L., Dong, A., Nguyen, K. T., Smil, D., Bolshan, Y., Hajian, T., He, H., Seitova, A., Chau, I., Li, F., Poda, G., Couture, J. F., Brown, P. J., Al-Awar, R., Schapira, M., Arrowsmith, C. H. and Vedadi, M. (2013) Small-molecule inhibition of MLL activity by disruption of its interaction with WDR5. *Biochem. J.* **449**, 151-159
- 53 Zhou, H., Liu, L., Huang, J., Bernard, D., Karatas, H., Navarro, A., Lei, M. and Wang, S. (2013) Structure-based design of high-affinity macrocyclic peptidomimetics to block the menin-mixed lineage leukemia 1 (MLL1) protein-protein interaction. *J. Med. Chem.* **56**, 1113-1123
- 54 Cao, F., Townsend, E. C., Karatas, H., Xu, J., Li, L., Lee, S., Liu, L., Chen, Y., Ouillette, P., Zhu, J., Hess, J. L., Atadja, P., Lei, M., Qin, Z. S., Malek, S., Wang, S. and Dou, Y. (2014) Targeting MLL1 H3K4 methyltransferase activity in mixed-lineage leukemia. *Mol. Cell.* **53**, 247-261
- 55 Karatas, H., Li, Y., Liu, L., Ji, J., Lee, S., Chen, Y., Yang, J., Huang, L.,

- Bernard, D., Xu, J., Townsend, E. C., Cao, F., Ran, X., Li, X., Wen, B., Sun, D., Stuckey, J. A., Lei, M., Dou, Y. and Wang, S. (2017) Discovery of a Highly Potent, Cell-Permeable Macrocyclic Peptidomimetic (MM-589) Targeting the WD Repeat Domain 5 Protein (WDR5)-Mixed Lineage Leukemia (MLL) Protein-Protein Interaction. *J. Med. Chem.* **60**, 4818-4839
- 56 Wang, F., Jeon, K. O., Salovich, J. M., Macdonald, J. D., Alvarado, J., Gogliotti, R. D., Phan, J., Olejniczak, E. T., Sun, Q., Wang, S., Camper, D., Yuh, J. P., Shaw, J. G., Sai, J., Rossanese, O. W., Tansey, W. P., Stauffer, S. R. and Fesik, S. W. (2018) Discovery of Potent 2-Aryl-6,7-dihydro-5 H-pyrrolo[1,2-a]imidazoles as WDR5-WIN-Site Inhibitors Using Fragment-Based Methods and Structure-Based Design. *J. Med. Chem.* **61**, 5623-5642
- 57 Aho, E. R., Wang, J., Gogliotti, R. D., Howard, G. C., Phan, J., Acharya, P., Macdonald, J. D., Cheng, K., Lorey, S. L., Lu, B., Wenzel, S., Foshage, A. M., Alvarado, J., Wang, F., Shaw, J. G., Zhao, B., Weissmiller, A. M., Thomas, L. R., Vakoc, C. R., Hall, M. D., Hiebert, S. W., Liu, Q., Stauffer, S. R., Fesik, S. W. and Tansey, W. P. (2019) Displacement of WDR5 from Chromatin by a WIN Site Inhibitor with Picomolar Affinity. *Cell Rep.* **26**, 2916-2928.e2913
- 58 Dennis, M. L., Morrow, B. J., Dolezal, O., Cuzzupe, A. N., Stuppel, A. E., Newman, J., Bentley, J., Hattarki, M., Nuttall, S. D., Foitzik, R. C., Street, I. P., Stuppel, P. A., Monahan, B. J. and Peat, T. S. (2019) Fragment screening for a protein-protein interaction inhibitor to WDR5. *Struct. Dyn.* **6**, 064701
- 59 Tian, J., Teuscher, K. B., Aho, E. R., Alvarado, J. R., Mills, J. J., Meyers, K. M., Gogliotti, R. D., Han, C., Macdonald, J. D., Sai, J., Shaw, J. G., Sensintaffar, J. L., Zhao, B., Rietz, T. A., Thomas, L. R., Payne, W. G., Moore, W. J., Stott, G. M., Kondo, J., Inoue, M., Coffey, R. J., Tansey, W. P., Stauffer, S. R., Lee, T. and Fesik, S. W. (2020) Discovery and Structure-Based Optimization of Potent and Selective WD Repeat Domain 5 (WDR5) Inhibitors Containing a Dihydroisoquinolinone Bicyclic Core. *J. Med. Chem.* **63**, 656-675
- 60 Bolshan, Y., Getlik, M., Kuznetsova, E., Wasney, G. A., Hajian, T., Poda, G., Nguyen, K. T., Wu, H., Dombrovski, L., Dong, A., Senisterra, G., Schapira, M., Arrowsmith, C. H., Brown, P. J., Al-Awar, R., Vedadi, M. and Smil, D. (2013) Synthesis, Optimization, and Evaluation of Novel Small Molecules as Antagonists of WDR5-MLL Interaction. *ACS Med. Chem. Lett.* **4**, 353-357
- 61 Getlik, M., Smil, D., Zepeda-Velázquez, C., Bolshan, Y., Poda, G., Wu, H., Dong, A., Kuznetsova, E., Marcellus, R., Senisterra, G., Dombrovski, L., Hajian, T., Kiyota, T., Schapira, M., Arrowsmith, C. H., Brown, P. J., Vedadi, M. and Al-Awar, R. (2016) Structure-Based Optimization of a Small Molecule Antagonist of the Interaction Between WD Repeat-Containing Protein 5 (WDR5) and Mixed-Lineage Leukemia 1 (MLL1). *J. Med. Chem.* **59**, 2478-2496
- 62 Schapira, M. and Arrowsmith, C. H. (2016) Methyltransferase inhibitors for modulation of the epigenome and beyond. *Curr. Opin. Chem. Biol.* **33**, 81-87
- 63 Schapira, M., Tyers, M., Torrent, M. and Arrowsmith, C. H. (2017) WD40 repeat domain proteins: a novel target class? *Nat. Rev. Drug Discov.* **16**, 773-786
- 64 Gupta, A., Xu, J., Lee, S., Tsai, S. T., Zhou, B., Kurosawa, K., Werner, M. S., Koide, A., Ruthenburg, A. J., Dou, Y. and Koide, S. (2018) Facile target validation in an animal model with intracellularly expressed monobodies. *Nat.*

Chem. Biol. **14**, 895-900

- 65 Zhang, P., Lee, H., Brunzelle, J. S. and Couture, J. F. (2012) The plasticity of WDR5 peptide-binding cleft enables the binding of the SET1 family of histone methyltransferases. *Nucleic Acids Res.* **40**, 4237-4246
- 66 Wu, X. H., Chen, R. C., Gao, Y. and Wu, Y. D. (2010) The effect of Asp-His-Ser/Thr-Trp tetrad on the thermostability of WD40-repeat proteins. *Biochemistry.* **49**, 10237-10245
- 67 Xu, C. and Min, J. (2011) Structure and function of WD40 domain proteins. *Protein & cell.* **2**, 202-214
- 68 Denesyuk, A., Denessiouk, K. and Johnson, M. S. (2018) Top surface blade residues and the central channel water molecules are conserved in every repeat of the integrin-like β -propeller structures. *J. Struct. Biol.* **201**, 155-161
- 69 Shinsky, S. A., Hu, M., Vought, V. E., Ng, S. B., Bamshad, M. J., Shendure, J. and Cosgrove, M. S. (2014) A non-active-site SET domain surface crucial for the interaction of MLL1 and the RbBP5/Ash2L heterodimer within MLL family core complexes. *J. Mol. Biol.* **426**, 2283-2299
- 70 Shinsky, S. A. and Cosgrove, M. S. (2015) Unique Role of the WD-40 Repeat Protein 5 (WDR5) Subunit within the Mixed Lineage Leukemia 3 (MLL3) Histone Methyltransferase Complex. *J. Biol. Chem.* **290**, 25819-25833
- 71 Weeramange, C. J., Fairlamb, M. S., Singh, D., Fenton, A. W. and Swint-Kruse, L. (2020) The strengths and limitations of using biolayer interferometry to monitor equilibrium titrations of biomolecules. *Protein Sci.* **29**, 1018-1034
- 72 Concepcion, J., Witte, K., Wartchow, C., Choo, S., Yao, D., Persson, H., Wei, J., Li, P., Heidecker, B., Ma, W., Varma, R., Zhao, L. S., Perillat, D., Carricato, G., Recknor, M., Du, K., Ho, H., Ellis, T., Gamez, J., Howes, M., Phi-Wilson, J., Lockard, S., Zuk, R. and Tan, H. (2009) Label-free detection of biomolecular interactions using BioLayer interferometry for kinetic characterization. *Comb. Chem. High Throughput Screen.* **12**, 791-800
- 73 Shah, N. B. and Duncan, T. M. (2014) Bio-layer interferometry for measuring kinetics of protein-protein interactions and allosteric ligand effects. *J. Vis. Exp.*, e51383
- 74 Movileanu, L., Cheley, S., Howorka, S., Braha, O. and Bayley, H. (2001) Location of a Constriction in the Lumen of a Transmembrane Pore by Targeted Covalent Attachment of Polymer Molecules. *J. Gen. Physiol.* **117**, 239-251
- 75 Wolfe, A. J., Gugel, J. F., Chen, M. and Movileanu, L. (2018) Kinetics of Membrane Protein-Detergent Interactions Depend on Protein Electrostatics. *J. Phys. Chem. B.* **122**, 9471-9481
- 76 Jarmoskaite, I., AlSadhan, I., Vaidyanathan, P. P. and Herschlag, D. (2020) How to measure and evaluate binding affinities. *eLife.* **9**
- 77 Boozer, C., Kim, G., Cong, S., Guan, H. and Londergan, T. (2006) Looking towards label-free biomolecular interaction analysis in a high-throughput format: a review of new surface plasmon resonance technologies. *Curr. Opin. Biotechnol.* **17**, 400-405
- 78 Masson, J. F. (2017) Surface Plasmon Resonance Clinical Biosensors for Medical Diagnostics. *ACS Sens.* **2**, 16-30
- 79 Drescher, D. G., Selvakumar, D. and Drescher, M. J. (2018) Analysis of

Protein Interactions by Surface Plasmon Resonance. *Adv. Protein Chem. Struct. Biol.* **110**, 1-30

80 Wolfe, A. J., Si, W., Zhang, Z., Blanden, A. R., Hsueh, Y. C., Gugel, J. F., Pham, B., Chen, M., Loh, S. N., Rozovsky, S., Aksimentiev, A. and Movileanu, L. (2017) Quantification of membrane protein-detergent complex interactions. *J. Phys. Chem. B.* **121**, 10228-10241

81 Wolfe, A. J., Hsueh, Y. C., Blanden, A. R., Mohammad, M. M., Pham, B., Thakur, A. K., Loh, S. N., Chen, M. and Movileanu, L. (2017) Interrogating Detergent Desolvation of Nanopore-Forming Proteins by Fluorescence Polarization Spectroscopy. *Analytical chemistry.* **89**, 8013-8020

82 Rossi, A. M. and Taylor, C. W. (2011) Analysis of protein-ligand interactions by fluorescence polarization. *Nat. Protoc.* **6**, 365-387

83 Wolfe, A. J., Gugel, J. F., Chen, M. and Movileanu, L. (2018) Detergent Desorption of Membrane Proteins Exhibits Two Kinetic Phases. *J. Phys. Chem. Lett.* **9**, 1913-1919

84 Tolkatchev, D., Xu, P. and Ni, F. (2003) Probing the kinetic landscape of transient peptide-protein interactions by use of peptide (15)*n* NMR relaxation dispersion spectroscopy: binding of an antithrombin peptide to human prothrombin. *J. Am. Chem. Soc.* **125**, 12432-12442

85 Gianni, S., Engström, A., Larsson, M., Calosci, N., Malatesta, F., Eklund, L., Ngang, C. C., Travaglini-Allocatelli, C. and Jemth, P. (2005) The kinetics of PDZ domain-ligand interactions and implications for the binding mechanism. *J. Biol. Chem.* **280**, 34805-34812

86 Eildal, J. N., Hultqvist, G., Balle, T., Stuhr-Hansen, N., Padrah, S., Gianni, S., Strømgaard, K. and Jemth, P. (2013) Probing the role of backbone hydrogen bonds in protein-peptide interactions by amide-to-ester mutations. *J. Am. Chem. Soc.* **135**, 12998-13007

87 Paul, F., Wehmeyer, C., Abualrous, E. T., Wu, H., Crabtree, M. D., Schöneberg, J., Clarke, J., Freund, C., Weikl, T. R. and Noé, F. (2017) Protein-peptide association kinetics beyond the seconds timescale from atomistic simulations. *Nat. Commun.* **8**, 1095

88 Stadmiller, S. S., Aguilar, J. S., Parnham, S. and Pielak, G. J. (2020) Protein-Peptide Binding Energetics under Crowded Conditions. *J. Phys. Chem. B.* **124**, 9297-9309

89 Mohammad, M. M. and Movileanu, L. (2008) Excursion of a Single Polypeptide into a Protein Pore: Simple Physics, but Complicated Biology. *Eur. Biophys. J.* **37**, 913-925

90 Bikwemu, R., Wolfe, A. J., Xing, X. and Movileanu, L. (2010) Facilitated Translocation of Polypeptides Through a Single Nanopore. *J. Phys.: Condens. Matter.* **22**, 454117

91 Qin, S., Pang, X. and Zhou, H. X. (2011) Automated prediction of protein association rate constants. *Structure.* **19**, 1744-1751

92 Alsallaq, R. and Zhou, H. X. (2008) Electrostatic rate enhancement and transient complex of protein-protein association. *Proteins.* **71**, 320-335

93 Qin, S. and Zhou, H. X. (2013) PI(2)PE: A Suite of Web Servers for Predictions Ranging From Protein Structure to Binding Kinetics. *Biophys. Rev.* **5**,

41-46

94 Zhou, H. X. (2010) Rate theories for biologists. *Q. Rev. Biophys.* **43**, 219-293

95 Pang, X. and Zhou, H. X. (2017) Rate Constants and Mechanisms of Protein-Ligand Binding. *Annu. Rev. Biophys.* **46**, 105-130

Chapter 3: Convergent Oncogenic Alterations of a Protein Hub Produce Divergent Effects Within a Binding Site

Ali Imran,¹ Brandon S. Moyer,² Dan Kalina,^{2,3} Thomas M. Duncan,⁴ Kelsey J. Moody,^{1,2,3,5} Aaron J. Wolfe,^{1,2,3,5} Michael S. Cosgrove,^{4*} and Liviu Movileanu^{1,6,7*}

¹*Department of Physics, Syracuse University, 201 Physics Building, Syracuse, New York 13244-1130, USA*

²*Ichor Life Sciences, Inc., 2651 US Route 11, LaFayette, New York 13084, USA*

³*Department of Chemistry, State University of New York College of Environmental Science and Forestry, 1 Forestry Dr., Syracuse, New York 13210, USA*

⁴*Department of Biochemistry and Molecular Biology, State University of New York Upstate Medical University, 4249 Weiskotten Hall, 766 Irving Avenue, Syracuse, New York 13210, USA*

⁵*Lewis School of Health Sciences, Clarkson University, 8 Clarkson Avenue, Potsdam, New York 13699*

⁶*Department of Biomedical and Chemical Engineering, Syracuse University, 329 Link Hall, Syracuse, New York 13244, USA*

⁷*The BioInspired Institute, Syracuse University, Syracuse, New York, 13244, USA*

This chapter is adapted from “Imran, A; Moyer, B. S.; Kalina, D.; Duncan, T. M.; Moody, K. J.; Wolfe, A. J.; Cosgrove, M. S.; Movlineau, L., Convergent Oncogenic Alterations of a Protein Hub Produce Divergent Effects Withing a Binding Site, *ACS Chem. Bio*, 2022”

<https://doi.org/10.1021/acscchembio.2c00273>

3.1 Abstract

Progress in tumor sequencing and cancer databases has created an enormous amount of information that scientists struggle to sift through. While several research groups have created computational methods to analyze large databases, much work still remains in distinguishing key implications of pathogenic mutations. Here, we describe an approach to identify and evaluate clinically significant mutations of WD40 repeat protein 5 (WDR5), a chromatin-associated protein hub. This multitasking protein maintains the functional integrity of large multi-subunit enzymatic complexes of the six human SET1 methyltransferases. Remarkably, the somatic cancer mutations of WDR5 preferentially distribute within and around an essential cavity, which hosts the WDR5 interaction (Win) binding site. Hence, we assessed the real-time binding kinetics of the interactions of key clustered WDR5 mutants with the Win motif peptide ligands of the SET1 family members (SET1_{Win}). Our measurements highlight that this subset of cancer mutants not only exhibits divergent perturbations in the kinetics and strength of interactions relative to those of the native WDR5, but also among the SET1_{Win} ligands. The immediate outcomes of this study could be used further for accelerated discoveries in precision medicine.

3.2 Introduction

WD40 repeat proteins (WDRs) are among the most abundant protein-protein interaction (PPI) domains in the human proteome (1-3). WDRs are either implicated in numerous cell signaling pathways (4,5) or in scaffolding large multi-subunit enzymatic complexes (6,7). Notably, WD40 repeat protein 5 (WDR5) is a highly conserved nuclear hub, which is primarily known for its regulatory role in histone 3 lysine 4 (H3K4) mono- and di-methylation (8-13). In this process, WDR5 bridges the interaction between the catalytic domain of mixed lineage leukemia MLL/SET1 family proteins and other subunits of the large methyltransferase complex. The assembly and stability of this enzymatic complex is necessary for optimal methyltransferase activity (14-16). In addition, WDR5 interacts with other protein partners, such as transcription factor MYC (17-20) and 3-phosphoinositide-dependent protein kinase 1 (PDK1) (21). Two highly conserved motifs of these protein binders, the WDR5 interaction (Win) motif (22-24) and WDR5-binding motif (WBM) (18,25,26), are deemed responsible for the vast majority of their interactions with WDR5. Interactions corresponding to these motifs are mediated by the Win and WBM sites, respectively (**Fig. 1a**).

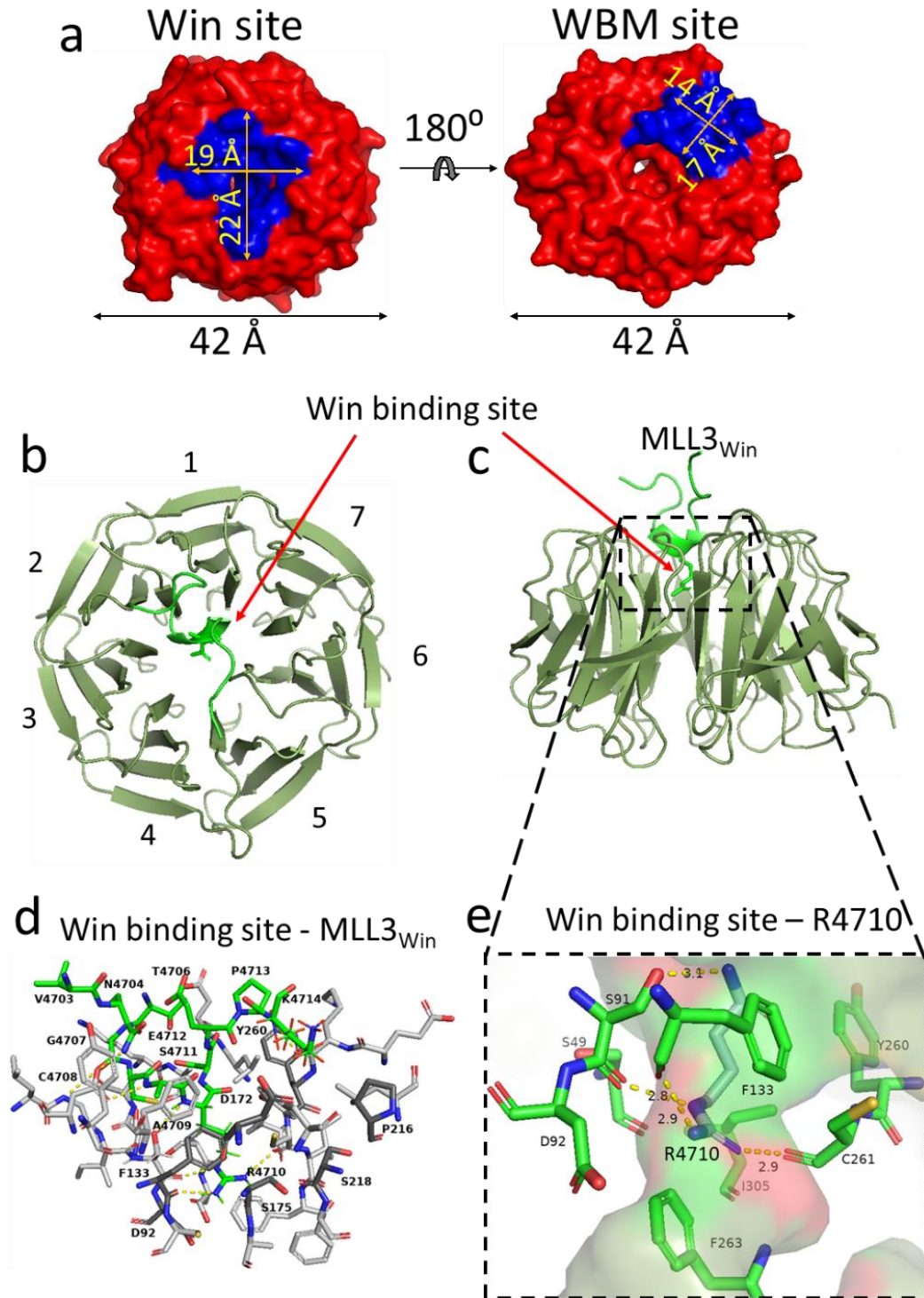


Figure 1: The two binding sites of WDR5 and the structure of the WDR5-MLL3_{Win} complex. (a) Representations of the Win and WBM binding sites of WDR5. Orientations of WDR5 in the two cartoons are 180° with respect to each other. (b) The top view of the WDR5-MLL3_{Win} complex. (c) The side view of the WDR5-MLL3_{Win} complex. (d) The side view of the interaction sites between

MLL3_{Win} (green) and WDR5 (gray). All presented residues are within 5 Å of the other binding partner. The residues corresponding to the WDR5 mutations explored in this study are marked in dark gray. MLL3_{Win} residues are labeled as well. Potential hydrogen bonds between the two binding partners are shown as yellow dotted lines. (e) Key residues of the WDR5 binding cavity involved in hydrogen bonding with the evolutionarily conserved Arg residue (R4710) of MLL3_{Win} at position P₀ (**Supplementary Table S1**). The hydrogen bonds are indicated by thick dashed lines marked in yellow. The cut-off distance for identifying these hydrogen bonds was 4.0 Å. WDR5 was represented using pdb entry 4ERY (35).

For oncoproteins, the driver cancer mutations preferentially populate either within an active site or on their binding surface (27,28). Based upon this argument, we postulated that missense somatic cancer mutations of WDR5 form a dense cluster either within one or both binding sites. Databases, such as Catalogue of Somatic Mutations in Cancer (COSMIC) (29,30), have become instrumental resources for unraveling the influential roles of specific proteins in different cancers (31-33). However, by determining the density and location of known mutations, their important subsets under disease-like conditions can potentially be identified. Using the clustering of mutations in protein structures (CLUMPS) method (34), we were able to identify, in accord with our hypothesis, that the high-density distribution of WDR5 cancer missense alterations occurs within and around the Win binding site.

The Win binding site is located within a central cavity and facilitates high-affinity interactions of WDR5 with each of the six human histone methyltransferases (HMTs; MLL1-4 and SETd1A-B), participating in the formation of corresponding six SET1 enzymatic complexes (35,36). Rearrangements in the MLL1 gene lead to solid tumors and aggressive lymphocytic

leukemias in humans (37). Moreover, WDR5 is overexpressed under various oncogenic conditions and its upregulation catalyzes cancer development (38-42). In recent years, the multitasking Win binding site has received a lot of interest (21,43-45), because it is a promising target for anti-cancer drug discovery (46-53). Therefore, a quantitative understanding of the WDR5 interactions with other Win motif partners has wide-ranging fundamental and clinical significance (50,54-57). For example, the kinetic fingerprints and affinities of the interactions of WDR5 with Win motif peptides of SET1 family members ($SET1_{Win}$) have been previously reported (22,35,36,44,45).

Stimulated by our finding using the CLUMPS method (34), we explored the impact of somatic cancer mutations of WDR5 on its interactions with 14-residue $SET1_{Win}$ peptide ligands of the six SET1 proteins (**Fig. 1b-c; Supplementary Table S1**). The WDR5-SET1 interaction requires the precise insertion of a highly-conserved Arg residue of SET1 proteins into the Win binding site (**Fig. 1d-e**) (23). This key interaction is a prerequisite for the structural and functional integrity of the C-terminal catalytic domain of SET1 proteins (15,22,23). $SET1_{Win}$ ligands recapitulate the native interactions of the six SET1 proteins with WDR5 through the Win binding site (35,36). Therefore, we utilized the benefit of biolayer interferometry (BLI) (58,59) for high-throughput settings and immobilized these $SET1_{Win}$ ligands onto the sensor surface. In this way, we probed the real-time kinetics and dynamics of their interactions with a subset of WDR5 cancer mutants, whose missense alterations are located within and around the Win binding site.

Remarkably, while these clustered mutations feature spatial proximity, they exhibit divergent effects on interactions with each of the six SET1_{win} ligands. Finally, the results of this scalable kinetic platform were confirmed by orthogonal determinations of affinity constants of these interactions using steady-state fluorescence polarization (FP) spectroscopy (60,61).

3.3 Materials and Methods

Clustering of Mutations in Protein Structures (CLUMPS). This approach was used as previously reported (34). WDR5 mutations were obtained using the COSMIC database (29,30,62) and available X-ray crystallographic information (PDB code 4ERY) (35). A weighted average proximity (WAP) score was generated for the distribution of mutations using the following equation:

$$WAP = \sum_{\substack{i,j \\ i \neq j}} s_i s_j e^{-\frac{d_{i,j}^2}{2r^2}}$$

(1)

where i and j iterated over all residues of WDR5. Here, $d_{i,j}$ is the Euclidean distance between residues i and j in Angstroms, and r denotes the distance threshold set to a constant value of 6 Å (34). s_i represents the normalized number of samples, in which the residue i was mutated. This parameter is given by:

$$s_i = \frac{n_i^3}{2^3 + n_i^3}$$

(2)

where n_i represents the number of samples, in which the residue i was mutated. The P -value was determined by calculating the WAP score for 10^6 random distributions of mutations, and then by comparing it with that value of the known distribution.

Protein Expression and Purification. All expression plasmids were synthesized, codon optimized, and sequence verified by GenScript (Piscataway, NJ). Human WDR5 (UniProtKB - P61964; WDR5_HUMAN) and its mutants were expressed and purified as described previously (22,23,44).

Peptide synthesis, labeling, purification, and analysis. For BLI measurements, 14-residue SET1_{win} peptide ligands were biotinylated at their N terminus and amidated at their C terminus. They were synthesized and purified to $\geq 95\%$ purity by GenScript (Piscataway, NJ). Purity confirmation, amino acid analysis, and solubility testing were conducted and provided by GenScript. For steady-state FP measurements, details on peptide synthesis, labeling, purification, and analysis were previously published (44). In brief, peptides were synthesized using a Biotage Syro I peptide synthesizer (Biotage, Charlotte, NC). Then, the peptides were purified using reversed-phase chromatography in two steps: (i) flash chromatography using a Biotage Isolera One (Biotage AB, Uppsala, Sweden), and (ii) semi-preparative HPLC using a Waters 2695 separations module equipped with a Waters 2996 photodiode array detector (PDA). A Sulforhodamine B fluorophore was chemically attached at the N terminus of the 14-residue SET1_{win} peptides, whereas their C terminus was amidated. A 9-residue Gly/Ser-rich peptide sequence

was introduced between the fluorophore and the SET1_{win} sequence (**Supplementary Methods**). Fluorophore-containing peptide fractions were analyzed by MALDI-TOF mass spectroscopy for the identity and purity tests.

Biolayer interferometry (BLI). Octet RED384 (FortéBio, Fremont, CA) was employed for the BLI studies (58,59). The assay buffer contained 150 mM NaCl, 20 mM Tris-HCl, 1 mM TCEP, 1 mg/mL bovine serum albumin (BSA), pH 7.5. Streptavidin-coated biosensors were incubated for 15 minutes with 5 nM biotin-tagged SET1_{win} peptide to specifically immobilize an optimal level of peptide. Sensors were then rinsed briefly in assay buffer to remove unbound peptides. Next, sensors were exposed to 3-fold serial dilutions of WDR5 for the association process. The dissociation phase was initiated by transferring the BLI sensors into WDR5-free buffer. For all WDR5 concentrations, binding curves were recorded by subtracting the baseline and the drift in the sensorgrams acquired with unloaded sensors. These BLI measurements were conducted at 24°C. For various WDR5 concentrations, [C], the association phases were fitted using the following equation (63):

$$Y = Y_{\infty} - (Y_{\infty} - Y_0)e^{-k_{\text{obs}}t}$$

(3)

where Y_0 and Y_{∞} are the response signals at the initial time and infinity, respectively. t is the cumulative time of the association phase, whereas k_{obs} denotes the apparent first-order reaction rate constant of the association phase. The dissociation phases were fitted using the following equation:

$$Y = Y_{\infty} + (Y_0 - Y_{\infty})e^{-k_{\text{off}}t}$$

(4)

where Y_0 and Y_{∞} denote the responses at the initial time and infinity, respectively.

k_{off} is the dissociation rate constant. The association rate constant, k_{on} , was determined using the slope of the linear curve (61,64):

$$k_{\text{obs}} = k_{\text{on}}[C] + k_{\text{off}}$$

(5)

Using several WDR5 concentrations, we also conducted global fittings, which provided the corresponding k_{on} and k_{off} values. The equilibrium dissociation constants, K_D , were indirectly determined using the k_{on} and k_{off} values ($K_D = k_{\text{off}}/k_{\text{on}}$). In each case, three independent BLI recordings were acquired for further determinations of the kinetics and dynamics of WDR5-SET1_{win} interactions.

Steady-state fluorescence polarization (steady-state FP) measurements.

Steady-state fluorescence polarization (FP) recordings were performed using a SpectraMax i3x plate reader (Molecular Devices, San Jose, CA) (60,65). All steady-state FP measurements were conducted using a buffer that contained 20 mM Tris-HCl (pH 7.5), 150mM NaCl, 1 mM TCEP, 0.005% Tween 20, and 96-well black untreated polystyrene microplates (Corning Inc., Corning, NY). Other details of steady-state FP measurements were previously reported (44). 100 μ L of each 20 nM labeled SET1_{win} peptide was added to individual wells at a final concentration of 10 nM. The steady-state FP anisotropy was measured on the plates after a 1 h incubation at room temperature in the dark. WDR5-dependent dose-response data

were averaged and then fitted using a four-parameter logistic function to acquire the binding affinity (K_D) for each interaction pairs.

Molecular graphics. In this study, molecular graphics was conducted using the PyMOL Molecular Graphics System (Version 2.4.0 Schrödinger, LLC).

3.4 Results and Discussion

The use of CLUMPS for the identification of mutation clustering in WDR5.

We employed the CLUMPS method (34) to investigate the 3D clustering of 68 WDR5 mutations identified in 68 tumors. The missense mutations were comprehensively compiled using the COSMIC database (29,30,62). Information collected for each mutation included the residue number, the number of tumor samples, in which a certain mutation was noted, and the total number of mutations, N , in a tumor sample. N was used as a measure of the accumulation of genetic damage in a tumor sample, in which a certain mutation was sequenced. Four overlapping subsets of mutations were created from the total set of known mutations with the following conditions: $N < 10,000$, $N < 5,000$, $N < 1,000$, and $N < 500$ (**Table 1**). For each subset, we calculated the WAP score and the corresponding P -value (**Materials and Methods; Supplementary Fig. S1**). We found that a subset of WDR5 mutations with a relatively low N ($N < 500$) is more likely to show mutation clustering, because P -value was smaller than 0.03. Notably, the low- N subset also showed a substantial presence of mutations within and around the Win binding site (**Supplementary Tables S2-S3**). Therefore, a subset of seven

mutations were selected from all known WDR5 cancer mutations within and around the Win binding site (**Supplementary Table S4**). This approach allowed us to study the effects of these somatic cancer mutations on the kinetics and dynamics of WDR5-SET1_{win} interactions.

Table 1: Results of mutation clustering of WDR5 for different subsets of N. WAP scores were calculated using 4 different subsets of mutations divided on the basis of the genetic damage, N , in their corresponding tumors. The P -values were calculated by comparison to configurations with random permutations of the distribution of mutations. 10^6 configurations were used for each subset. N is the total number of mutations in a given tumor sample. m is the total number of mutations that met the condition $N < N_{\max}$, where N_{\max} is the upper limit of the number of mutations in a given tumor sample. N_{\max} values are listed below for four data subsets on the first column. m was kept constant for all configurations of a subset.

N	m	WAP Score	P -value
< 10,000	51	2.258	0.403
< 5,000	33	0.931	0.206
< 1,000	11	0.095	0.111
< 500	8	0.072	0.025

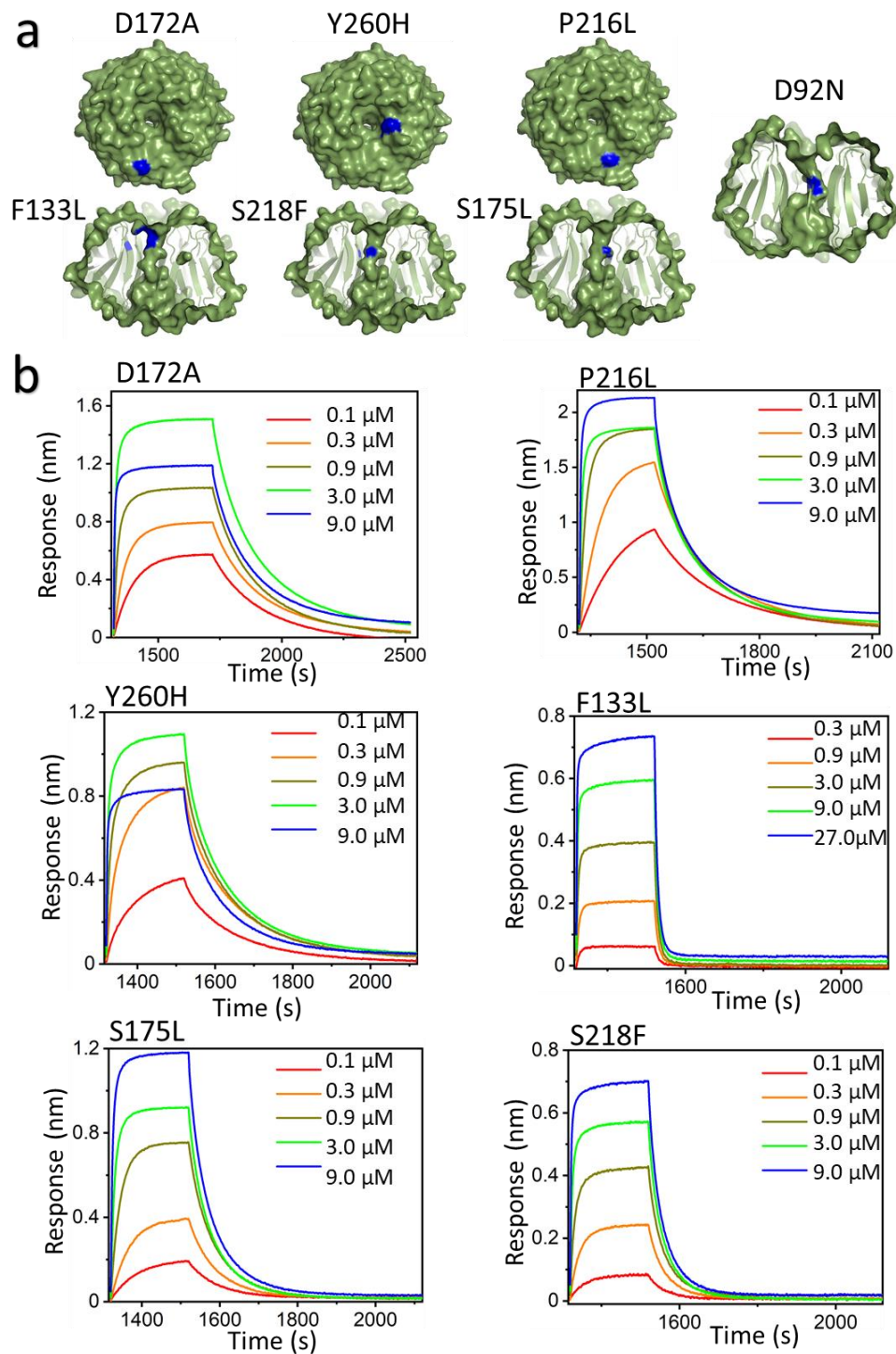


Figure 2: Label-free optical BLI sensorgrams of the WDR5 mutant-MLL3_{win} interactions. (a) Locations of the surface and cavity WDR5 mutations are shown in blue using surface and cross-sectional views of WDR5, respectively. (b) BLI sensorgrams showing the association and dissociation phases. For each WDR5

mutation, sensors with immobilized MLL3_{win} ligand were immersed in buffers containing different WDR5 concentrations (listed on sensorgrams) to monitor association kinetics. Sensors were then transferred to buffer alone to monitor dissociation kinetics.

Biolayer interferometry (BLI) measurements. In this study, targeted mutations have locations either within the WDR5 cavity (F133L, S175L, S218F, and D92N) or on the external surface and near the cavity (D172A, Y260H, and P216L) (**Fig. 2a; Supplementary Table S4**). These mutants were chosen based on their proximal locations to residues deemed to play roles in SET1_{win} interactions with the native WDR5 protein (**Supplementary Fig. S2 Tables S5-S6**) (22,23,35,36). BLI measurements were used to determine the association (k_{on}) and dissociation (k_{off}) rate constants of WDR5-SET1_{win} interactions (58,59). 14-residue SET1_{win} peptide ligands, namely MLL1_{win}, MLL2_{win}, MLL3_{win}, MLL4_{win}, SETd1A_{win}, and SETd1B_{win}, were biotinylated at the N terminus and amidated at the C-terminus (**Supplementary Table S1**). A 9-residue Gly/Ser-rich peptide spacer was inserted between the biotinylated site and the SET1_{win} sequence to avoid any steric hindrance of WDR5-SET1_{win} interactions from the sensor surface. Biotinylated SET1_{win} peptides were then tethered to the surface of streptavidin-coated sensors. Binding interactions of WDR5 with SET1_{win} ligands attached to the sensor surface were monitored through changes in the optical interference pattern generated by reflected light waves at the sensor surface (**Fig. 2b**). The association binding curves were acquired by placing the BLI sensors in distinct wells of varying WDR5 concentration. The dissociation binding curves were

collected by placing the BLI sensors in wells containing WDR5-free buffer. It should be mentioned that all association and dissociation phases obeyed single-exponential fits, suggesting bimolecular association processes and unimolecular dissociation mechanisms of these binding phases, respectively.

Interestingly, we noted very weak binding interactions of all SET1_{win} peptides with D92N, a cavity WDR5 mutant (**Fig. 2a; Supplementary Fig. S3**). While these interactions are detectable, they cannot be accurately quantified using BLI likely due to either a very low k_{on} or a very high k_{off} , or both. A couple of possibilities could explain this interesting outcome. First, Asn-92 might interfere with the two hydrogen bonds between the Arg residue at the P₀ position of the SET1_{win} ligand (**Supplementary Table S1**) and S91, a neighboring residue of WDR5 (**Supplementary Table S5**). Second, the positively charged guanidinium group of Arg at P₀ of SET1_{win} might make an N-O salt bridge with the negatively charged carboxyl group of Asp-92 (**Supplementary Table S6**) (66). In addition, Asp-92 forms a salt bridge with Lys-52 located between β strands. Therefore, the absence of Asp-92 might alter the local conformation of the binding pocket.

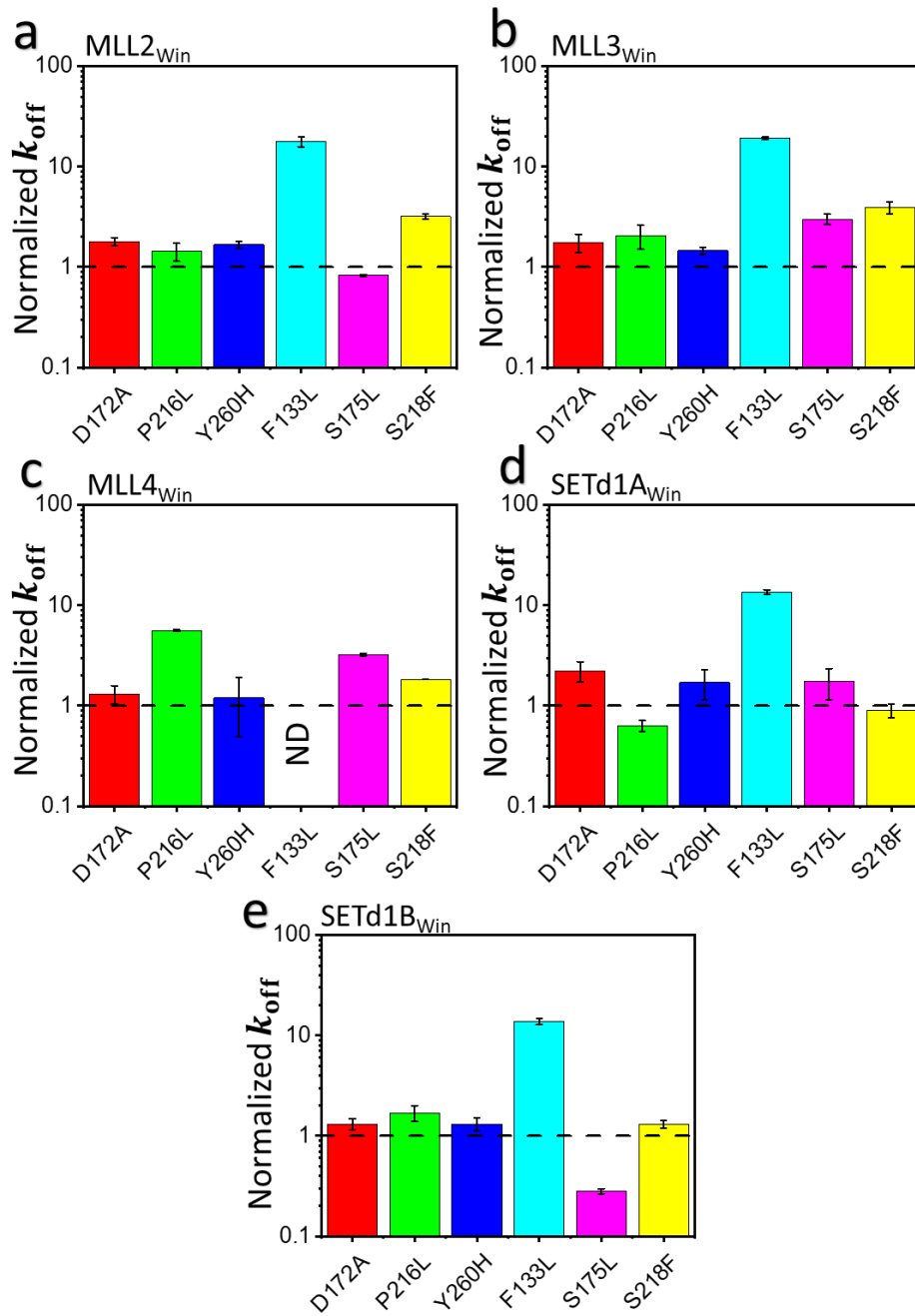


Figure 3: Normalized dissociation rate constants of the WDR5 mutant-SET1_{win} interactions using BLI sensorgrams. The k_{off} values for each SET1_{win} ligand's interaction with mutants have been divided by the k_{off} of that SET1_{win} ligand's interaction with the native WDR5 protein. (a) MLL2_{win}, (b) MLL3_{win}, (c) MLL4_{win}, (d) SETd1A_{win}, and (e) SETd1B_{win}. ND stands for "Not Determined." Using a BLI measurement, the interaction between F133L and MLL4_{win} was detectable, but not quantifiable.

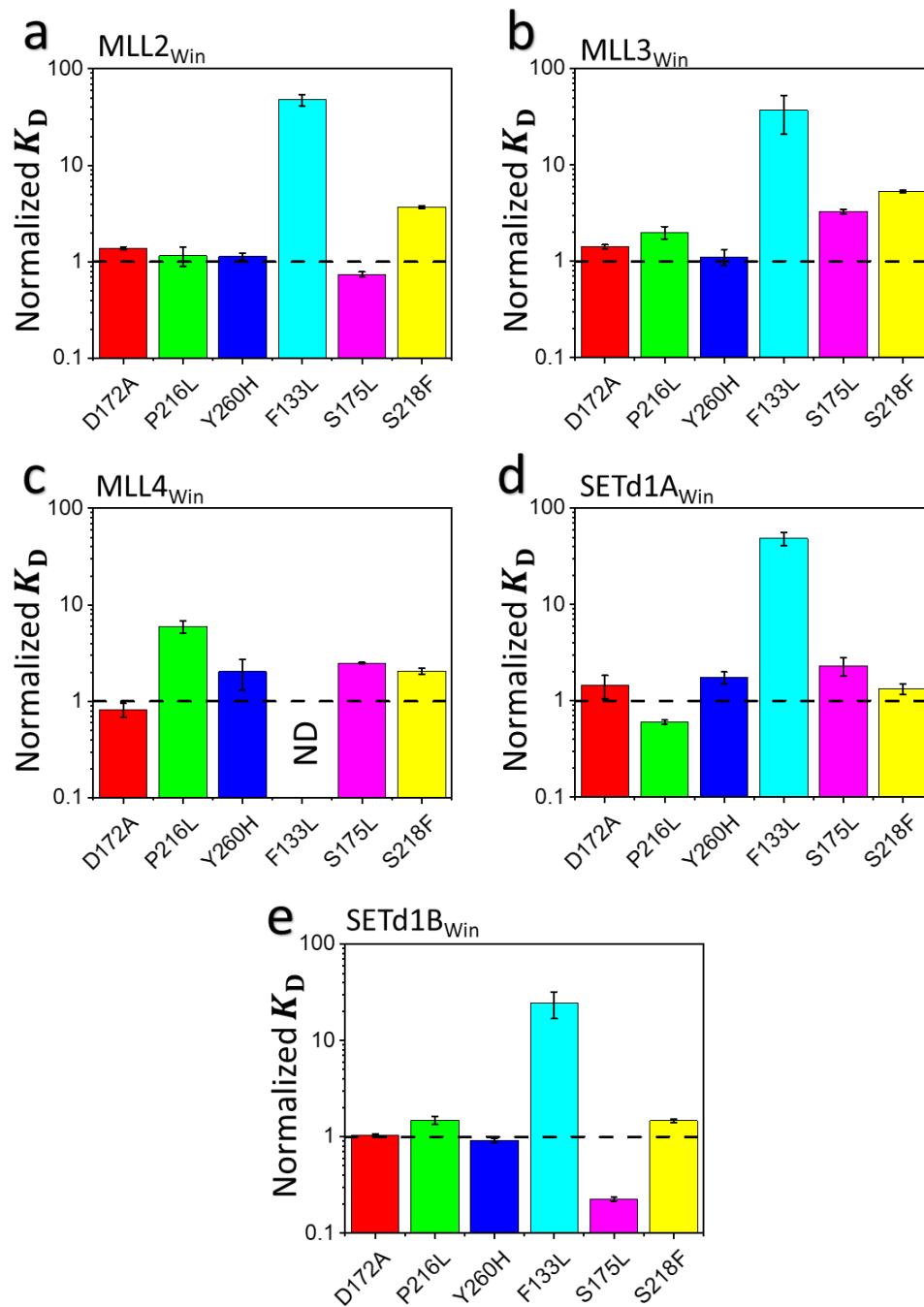


Figure 4: Normalized K_D of the WDR5 mutant-SET1_{win} interactions using BLI sensorgrams. The K_D values for each SET1_{win} ligand's interaction with WDR5 mutants have been divided by the K_D of that SET1_{win} ligand's interaction with the native WDR5 protein.

(a) MLL2_{win}, (b) MLL3_{win}, (c) MLL4_{win}, (d) SETd1A_{win}, and (e) SETd1B_{win}. ND stands for "Not Determined." Using a BLI measurement, the interaction between F133L and MLL4_{win} was detectable, but not quantifiable.

Surface mutants. We first looked at surface mutants and the effects of these mutations on the WDR5-SET1_{Win} interaction. The normalized values of k_{on} (**Supplementary Fig. S4**), k_{off} (**Fig. 3**), and dissociation constant $K_{\text{D-BLI}}$ (**Fig. 4**) for these WDR5 mutants are the values of these parameters of the SET1_{Win}-WDR5 mutant pair interactions divided by those values corresponding to the SET1_{Win}-native WDR5 pair interactions. In general, surface mutants D172A, P216L, and Y260H exhibited closely similar values of k_{on} , k_{off} , and $K_{\text{D-BLI}}$ to those obtained for the native WDR5 protein (**Supplementary Tables S7-S9**) (44). Again, we were not able to obtain a quantifiable k_{on} for the MLL1_{Win}-WDR5 mutant pair interactions due to limited time resolution of BLI. Interestingly, k_{on} followed the same trend with respect to SET1_{Win} peptides, as established in our previous study (44), with the lowest values for the neutrally charged MLL4_{Win}, the highest values for the acidic SETd1A_{Win} and SETd1B_{Win}, and the intermediate values for the positively charged MLL2_{Win} and MLL3_{Win}. For example, for P216L-MLL4_{Win} interactions, k_{on} was $(1.9 \pm 0.3) \times 10^4 \text{ M}^{-1}\text{s}^{-1}$. Yet, for the interactions of P216 L with MLL2_{Win}, MLL3_{Win}, SETd1A_{Win}, and SETd1B_{Win} k_{on} was $(5.6 \pm 0.8) \times 10^4 \text{ M}^{-1}\text{s}^{-1}$, $(5.3 \pm 0.7) \times 10^4 \text{ M}^{-1}\text{s}^{-1}$, $(8.6 \pm 0.8) \times 10^4 \text{ M}^{-1}\text{s}^{-1}$, $(8.0 \pm 0.8) \times 10^4 \text{ M}^{-1}\text{s}^{-1}$, respectively. We conclude that $k_{\text{on}}(0) < k_{\text{on}}(+1) < k_{\text{on}}(-1)$ for surface mutants, where the number between parentheses is the overall charge of the SET1_{Win} peptides (**Supplementary Table S1**). In other words, $k_{\text{on}}(\text{MLL1}_{\text{Win}}, \text{MLL4}_{\text{Win}}) < k_{\text{on}}(\text{MLL2}_{\text{Win}}, \text{MLL3}_{\text{Win}}) < k_{\text{on}}(\text{SETd1A}_{\text{Win}}, \text{SETd1B}_{\text{Win}})$ for surface mutants. This k_{on} rule is likely determined by an asymmetric charge distribution in SET1_{Win} with respect to the highly conserved 6-residue Win motif peptide segment (P-3 through

P₂). Specifically, this is because of a positive charge located on the C-terminal flanking side in P₄ (MLL2_{win} and MLL3_{win}) and a negative charge located on the N-terminal flanking side in P₋₇ (SETd1A_{win} and SETd1B_{win}). Asp-172 is located within the A pocket of WDR5. SET1_{win} ligands show no difference in their interactions with D172A as compared to the native WDR5 protein. We did not see any significant changes in the k_{on} and k_{off} for this pocket mutant. In addition, we noted a significantly weakened interaction of P216L with MLL4_{win}. Pro-216 is located within the B pocket.

Cavity mutants. In addition to D92N, we examined three WDR5 cancer mutations within the WDR5 cavity, such as F133L, S175L, and S218F (**Fig. 2b**). It has been previously reported that F133A significantly deteriorates the strength of the interactions of the MLL1 subunit with the WDR5-RbBP5-Ash2L subcomplex *in vitro* (23). Phe-133 is a critical neighboring WDR5 residue of the evolutionarily conserved Arg at P₀ of SET1_{win} ligands, contributing to a potentially strong cation- π interaction. Very weak interactions of F133L with MLL1_{win} and MLL4_{win} were not quantifiable using BLI. Here, F133L showed a decreased normalized k_{on} with MLL2_{win}, MLL3_{win}, SETd1A_{win}, and SETd1B_{win} (**Supplementary Fig. S4**). As expected, F133L exhibited a noteworthy change in the k_{off} with respect to the native WDR5 protein (**Fig. 3**), leading to a significant increase in the K_{D-BLI} . For MLL2_{win}, MLL3_{win}, SETd1A_{win}, and SETd1B_{win}, these increased values spanned a range between one and two orders of magnitude (**Fig. 4; Supplementary Table S9**). This outcome indirectly confirms their close similarity in sequence and interaction

mechanisms with WDR5 (35,36). Their distinctions in binding affinities with respect to the other SET1_{win} ligands can be attributed to the interaction of their flanking sides with the WDR5 surface.

However, the most interesting mutational effect is that of S175L, which has a more divergent impact on interactions of the SET1_{win} peptides with respect to the native WDR5 protein. For example, S175L selectively weakens the interactions with MLL3_{win}, MLL4_{win}, and SETd1A_{win}, while substantially strengthening the interactions with SETd1B_{win} (**Fig. 3, Fig. 4; Supplementary Table S9**). Moreover, this change is primarily associated with a change in the k_{off} . Ser-175 is part of a cluster of neighboring residues that co-participate in an array of hydrogen bonds, π - π , cation- π , and hydrophobic interactions with the conserved Arg in P₀. These include Ser-91, Phe-133, Ser-175, Ser-218, Cys-261, Phe-263, and Ile-305 (35). For example, Arg at P₀ makes a water-mediated hydrogen bond with the Ser-175 backbone carbonyl group (36).

Known SETd1B-WDR5 crystal structures suggest that replacing Ser-175 with Leu creates steric clashes that affect the structure of the B pocket (**Supplementary Fig. S5**) (35,36). Specifically, it could displace Tyr-191 and make the pocket more hydrophobic, which would explain the increased affinity with SETd1B. It is worth mentioning that SETd1B is unique, because it has a Phe residue at P₄ (**Supplementary Table S1**) that inserts into the hydrophobic B-pocket, while the other B-pocket binders have a more polar residue (Lys or Tyr) in that position.

Interestingly, the increased affinity is made possible through a 4-fold decrease in the dissociation rate constant with no change in the association rate constant. Given the importance of slow dissociation rates for effective therapeutics (50), we predict molecules designed to take advantage of this interaction will improve dwell times and make more effective inhibitors (21).

In agreement with prior crystallographic studies (35,36), S218F exhibited weakened interactions with MLL2_{win}, MLL3_{win}, and MLL4_{win}. However, its interactions with SETd1A_{win} and SETd1B_{win} were closely similar to those with the native WDR5 protein (**Figs. 3-4; Supplementary Table S9**). This finding is in accordance with a different mechanism of binding interactions of SETd1A_{win} and SETd1B_{win} with respect to the other SET1_{win} ligands, likely due to an intermediate orientation of the C-terminal ends of SETd1A_{win} and SETd1B_{win} on the surface of blades 4 and 5.

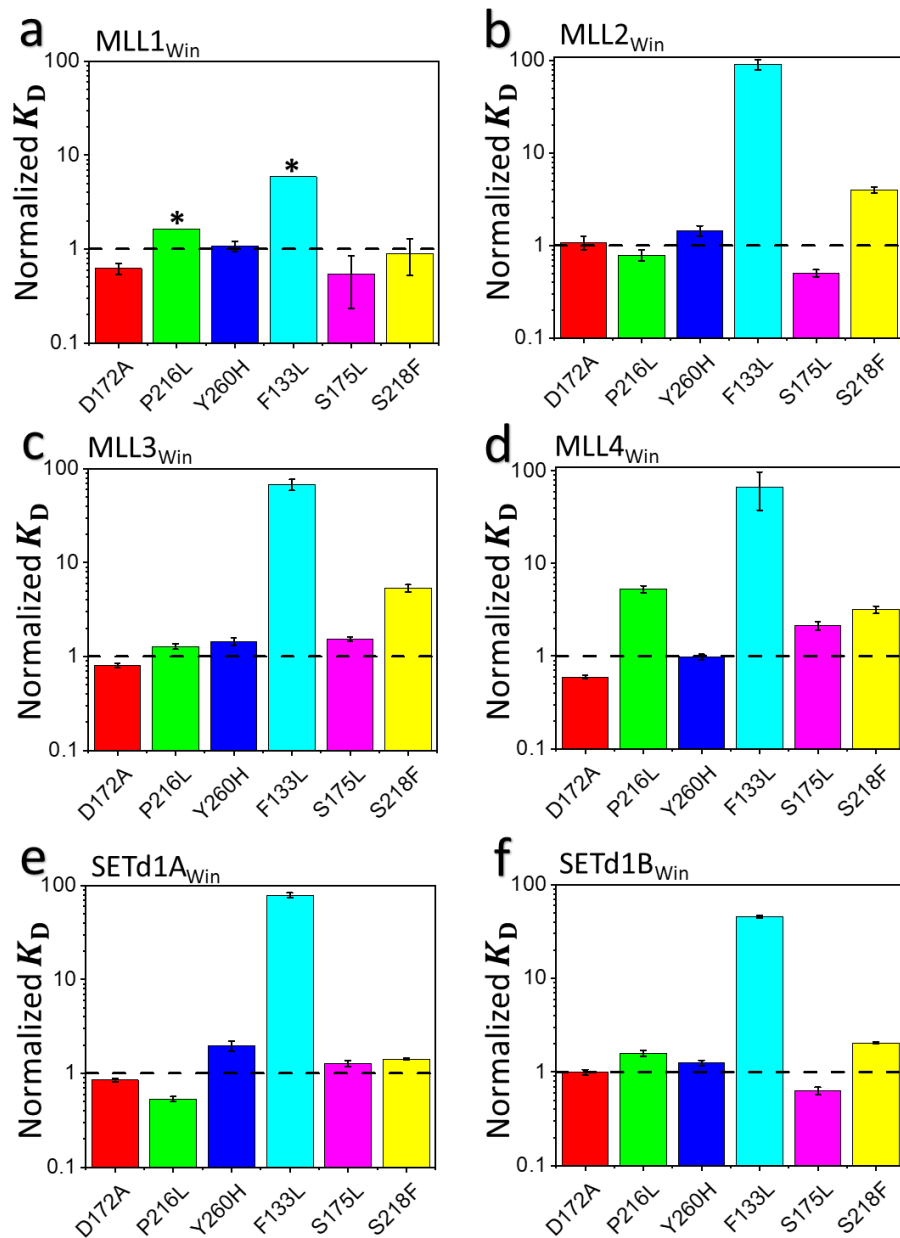


Figure 5: Normalized K_D of the WDR5 mutant-SET1_{Win} interactions using steady-state FP spectroscopy. The K_D values for each SET1_{Win} ligand's interaction with WDR5 mutants have been divided by the K_D of that SET1_{Win} ligand's interaction with the native WDR5 protein.

(a) MLL1_{Win}, (b) MLL2_{Win}, (c) MLL3_{Win}, (d) MLL4_{Win}, (e) SETd1A_{Win}, and (f) SETd1B_{Win}. For vertical bars marked by "*", the K_D of those interactions could not be determined. Those values represent the lower-limit of the K_D based on the highest WDR5 mutant concentrations used in this study.

Validations of BLI data and qualitative comparisons between competing techniques. To validate the outcomes of BLI measurements, we next used steady-state FP spectroscopy as an orthogonal technique (**Supplementary Fig. S6**) to determine binding affinities, K_{D-FP} , of the interactions of SET1_{win} ligands with WDR5 cancer mutants (**Fig. 5; Supplementary Table S10**). 14-residue SET1_{win} peptide ligands were fluorescently labeled with Sulforhodamine B at the N terminus and amidated at the C terminus. A 3 nm-long Gly/Ser-rich peptide spacer was inserted between the fluorophore site and the SET1_{win} sequence. Then, steady-state FP anisotropy, r , values were collected at increasing WDR5 concentrations. Dose-response FP measurements enabled determinations of the K_{D-FP} . Remarkably, the FP experiments validated all qualitative findings acquired by BLI. These include the confirmation of very weak binding interactions of D92N with all SET1_{win} peptides (**Supplementary Fig. S7**). In addition, we always found that the absolute K_D values (i.e., not normalized) obeyed the following inequality: $K_{D-BLI} > K_{D-FP}$. This outcome validates our previous results, indicating that measured interactions are stronger in unrestricted conditions than those corresponding to restrained conditions (**Supplementary Tables S11-S12**) (44). Because these WDR5 mutants have been examined using BLI and FP, we can compare these approaches quantitatively and qualitatively (67). For example, using BLI we can determine the kinetic fingerprint of these interactions. Yet, this cannot be inferred using steady-state FP spectroscopy. BLI is an immobilization-based technique, whereas FP is a method that probes binding affinity in solution under unrestricted conditions. This is likely the reason why the K_{D-BLI} is always about one order of magnitude greater

than the K_{D-FP} (**Supplementary Tables S9-S10**). In addition, FP measurements enabled us to measure some weaker interactions, which had kinetics that were too fast for the BLI time resolution (e.g., for MLL1_{Win}). Furthermore, these approaches probe distinctive physical processes. On one hand, BLI is a real-time technique that samples both the association and dissociation phases based on alterations in the interference pattern of white light reflected on the sensor surface. On the other hand, steady-state FP is a time-independent technique that monitors changes in the rotational diffusion of a fluorescently labeled molecule upon its binding to another molecule. We calculated the ratio K_{D-BLI}/K_{D-FP} (**Supplementary Fig. S8**).

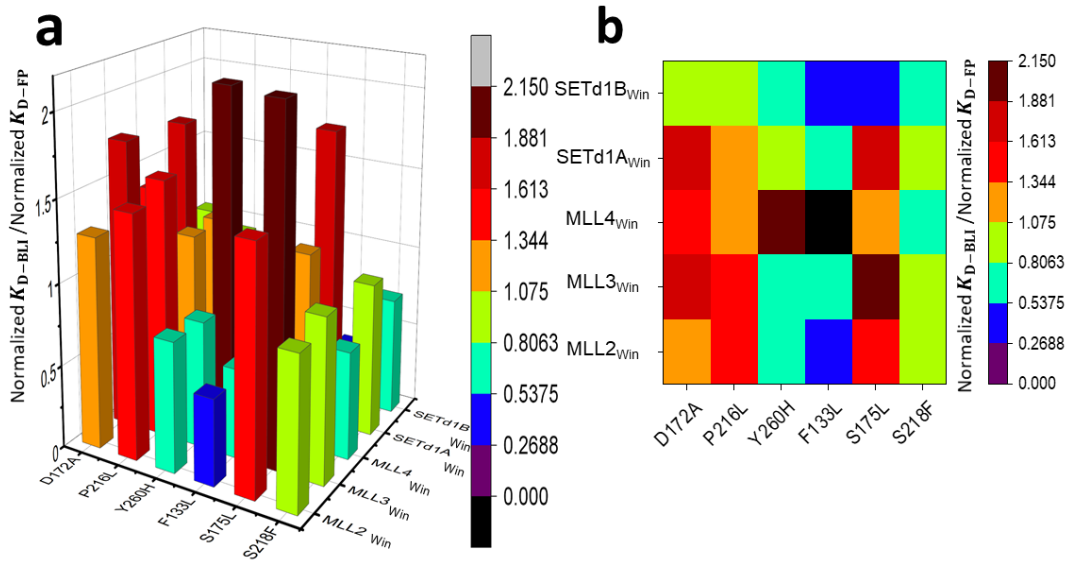


Figure 6: Quantitative comparison between affinity data resulting from BLI and FP measurements. (a) A 3D graph of the ratio of the normalized K_{D-BLI} to the normalized K_{D-FP} . (b) A 2D heat map of the ratio of the normalized K_{D-BLI} to the normalized K_{D-FP} . Normalized K_D values are the K_D measured for a specific WDR5 mutant-SET1_{Win} interaction pair divided by the K_D value corresponding to the native WDR5 protein.

The variability of the K_{D-BLI}/K_{D-FP} ratio for different interacting pairs was likely caused by two determinants: (i) the difference in mobility of each SET1_{Win} ligand

with respect to WDR5 mutants, and (ii) the distinction in physical processes probed by the two methods. To cancel the effect of these two determinants, we determined another dimensionless parameter, the ratio of normalized K_{D-BLI} /normalized K_{D-FP} , which spanned a much narrower spectrum, between 0.36 and 2.15 (**Fig. 6; Supplementary Table S12**). This finding illuminates the qualitative agreement of data resulting from BLI and FP measurements, fortifying our conclusions on the effect of introducing these missense mutations on SET1_{win} - WDR5 interactions. Moreover, these BLI and FP data are in accordance with a recent single-molecule study using an engineered protein nanopore (45), which indicated unaffected D172A-MLL4_{win} interactions and weak D92N-MLL4_{win} interactions with respect to those of the native WDR5 protein. Taken together, these findings demonstrate the critical role of a negative charge located within the acidic WDR5 cavity for the strength of WDR5-SET1_{win} interactions.

Oncogenic potential of Win binding site mutants. While the impact of the WDR5 cancer mutations on WDR5-SET1_{win} interactions is readily distinguishable, their effect on the overall assembly of the SET1 complexes and their functional features is a bit more nuanced. Given our understanding of SET1 family complex behavior (16,48), we can say that these inspected WDR5 mutations have a divergent impact. The absence of WDR5 (16) and/or the inhibition of SET1_{win}-WDR5 interactions (48) downregulates the H3K4 di-methylation function of MLL1 and SETd1A, while this upregulates the H3K4 mono-methylation function of MLL3 (16,68). Therefore, mutations that significantly disrupt SET1_{win}-WDR5

interactions are likely to have similar effects. Consequently, F133L and D92N should disrupt di-methylation by MLL1 and SETd1A. Furthermore, mono-methylation function of MLL3 would be upregulated in the case of F133L, S218F, S175L and D92N. Moreover, our results show that even within the Win binding site, given their effect on SET1_{win}-WDR5 interactions, cavity mutations are more likely to be driver mutations instead of passenger mutations. This holds especially true for D92N, F133L, and S175L. For example, Ali and coworkers (2014) found that F133L disrupts the mitotic progression in the cell cycle process (69).

The information that concerns the K_D values of mutations within the B pocket is critical for future drug development. Precision medicine depends on understanding the unique biophysical impacts of each missense mutation on the structure and function of putative oncogene proteins. Our data suggests that this knowledge would help researchers and eventually clinicians in deciding which inhibitors to use as potential therapeutic approaches. For example, this work suggests that individuals harboring a breast cancer S175L mutation in WDR5 (**Table S4**) are more likely to respond to inhibitors targeting the hydrophobic interactions in the B pocket than other inhibitors. Furthermore, the unique impacts of S175L in SETd1b suggests that those cancers are due to perturbations in the SETd1B-catalyzed H3K4 methylation pathway. This type of information would greatly enhance our ability to prioritize cellular and animal-based follow-up studies that can address more specific hypotheses.

3.5 Concluding remarks. In this study, we evaluated key somatic cancer mutations of WDR5. Specifically, we used the CLUMPS approach to identify that cancer mutations accumulate within the Win binding site and extracted a representative subset of WDR5 mutants for determining the real-time kinetics of their interactions using high-throughput techniques. Our work shows that the total number of mutations in a tumor sample can be used as a parameter to filter out mutations more likely to be driver mutations. Furthermore, we noted that the Win site shows a substantial presence of low- N mutations, while the WBM site shows none. This helped us to exclusively focus on Win binding site mutants for further biophysical measurements. Therefore, we explored the effect of mutations in this binding site by presenting a detailed kinetic fingerprint of the interactions of these mutants with various SET1_{Win} ligands. We provide experimental evidence for influential roles of the residues within the WDR5 cavity on the strength of these interactions. Steady-state FP spectroscopy measurements also confirmed outcomes resulting from BLI experiments. Finally, the interactions of WDR5 cavity mutants depended on the nature of the SET1_{Win} peptides. These divergent effects have distinctive impacts on H3K4 methylation, and therefore for the downstream expression of genes. This is a finding that can reconfigure future strategies for the design, development, and optimization of inhibitors that are aimed at targeting the multitasking high-affinity Win binding site under oncogenic conditions. In the future, it would be interesting to examine the impact of the Win binding site cancer mutations on the kinetics and strength of the interactions of WDR with other protein partners and Win motif ligands.

3.6 SUPPLEMENTARY INFORMATION

Convergent Oncogenic Alterations of a Protein Hub Produce Divergent Effects Within a Binding Site

Ali Imran,¹ Brandon S. Moyer,² Dan Kalina,^{2,3} Thomas M. Duncan,⁴ Kelsey J. Moody,^{1,2,3,5} Aaron J. Wolfe,^{1,2,3,5} Michael S. Cosgrove,⁴ and Liviu Movileanu^{1,6,7*}

¹*Department of Physics, Syracuse University, 201 Physics Building, Syracuse, New York 13244-1130, USA*

²*Ichor Life Sciences, Inc., 2651 US Route 11, LaFayette, New York 13084, USA*

³*Department of Chemistry, State University of New York College of Environmental Science and Forestry, 1 Forestry Dr., Syracuse, New York 13210, USA*

⁴*Department of Biochemistry and Molecular Biology, State University of New York Upstate Medical University, 4249 Weiskotten Hall, 766 Irving Avenue, Syracuse, New York 13210, USA*

⁵*Lewis School of Health Sciences, Clarkson University, 8 Clarkson Avenue, Potsdam, New York 13699*

⁶*Department of Biomedical and Chemical Engineering, Syracuse University, 329 Link Hall, Syracuse, New York 13244, USA*

⁷*The BioInspired Institute, Syracuse University, Syracuse, New York, 13244, USA*

CONTENTS OF THE SUPPORTING INFORMATION

1. Sequence of 14-residue SET1_{win} peptide ligands (**Supplementary Table S1**).
2. Location of somatic cancer mutations from tumor samples with $N < 500$ and their distributions with a well-defined upper limit of mutations (**Supplementary Tables S2-S3**).
3. Results of mutation clustering for different N_{\max} -based mutation subsets (**Supplementary Fig. S1**).
4. List of tumor locations associated with missense WDR5 cancer mutations within and around the Win binding site (**Supplementary Table S4**).
5. List of noncovalent bonds at the WDR5-SET1_{win} protein interface (**Supplementary Tables S5-S6**).
6. Location of surface WDR5 mutations within the A and B pockets (**Supplementary Fig. S2**).
7. Very weak interactions of D92N with SET1_{win} ligands are detected by BLI measurements (**Supplementary Fig. S3**).
8. Kinetic rate constants of association of WDR5 mutants with SET1_{win} ligands using BLI measurements (**Supplementary Table S7**).
9. Kinetic rate constants of dissociation of WDR5 mutants with SET1_{win} ligands using BLI measurements (**Supplementary Table S8**).
10. Normalized kinetic rate constants of association of WDR5 mutants with SET1_{win} ligands using BLI measurements (**Supplementary Fig. S4**).
11. Equilibrium dissociation constants of WDR5 mutants with SET1_{win} ligands using BLI measurements (**Supplementary Table S9**).
12. Structural information on the effect of the S175L mutation (**Supplementary Fig. S5**).
13. Steady-state FP spectroscopy curves for the interactions of WDR5 mutants with SET1_{win} ligands (**Supplementary Fig. S6**).
14. Very weak interactions of D92N with SET1_{win} ligands are detected by steady-state FP spectroscopy measurements (**Supplementary Fig. S7**).
15. Equilibrium dissociation constants of WDR5 mutants with SET1_{win} ligands using steady-state FP spectroscopy measurements (**Supplementary Table S10**).
16. Quantitative comparisons of affinity data acquired with BLI and FP (**Supplementary Fig. S8 Tables S11-S12**).
17. Supplementary methods (**Supplementary Table S13**).
18. Supporting references.

1. Sequence of 14-residue SET1_{Win} peptide ligands

Table S1: Amino acid sequences of SET1_{Win} motif peptide ligands. Here, MLL1_{Win}, MLL2_{Win}, MLL3_{Win}, MLL4_{Win}, SETd1A_{Win} and SETd1B_{Win} are the following 14-residue SET1 Win motif ligands: MLL1³⁷⁵⁸⁻³⁷⁷¹, MLL2⁵³³³⁻⁵³⁴⁶, MLL3⁴⁷⁰³⁻⁴⁷¹⁶, MLL4²⁵⁰⁴⁻²⁵¹⁷, SETd1A¹⁴⁸⁸⁻¹⁵⁰¹, and SETd1B¹⁶⁹⁸⁻¹⁷¹¹ (1-3).

SET1 _{Win}	P ₋₇	P ₋₆	P ₋₅	P ₋₄	P ₋₃	P ₋₂	P ₋₁	P ₀	P ₁	P ₂	P ₃	P ₄	P ₅	P ₆	Charge
MLL1 _{Win}	L	N	P	H	G	S	A	R	A	E	V	H	L	S*	0
MLL2 _{Win}	I	N	P	T	G	C	A	R	S	E	P	K	I	L	+1
MLL3 _{Win}	V	N	P	T	G	C	A	R	S	E	P	K	M	S	+1
MLL4 _{Win}	L	N	P	H	G	A	A	R	A	E	V	Y	L	S**	0
SETd1A _{Win}	E	H	Q	T	G	S	A	R	S	E	G	Y	Y	P	-1
SETd1B _{Win}	E	H	V	T	G	C	A	R	S	E	G	F	Y	T	-1

S* This is an R3771S-substituted MLL1_{Win} peptide ligand.

S** This is an R2517S-substituted MLL4_{Win} peptide ligand.

2. Location of somatic cancer mutations from tumor samples with $N < 500$ and their distributions with a well-defined upper limit of mutations

Table S2: Location of mutations from tumor samples with $N < 500$. The mutation distribution from tumor samples with low N values is shown below. Out of 8 such somatic cancer mutations, 5 were within or around the Win binding site, while 3 were found elsewhere. Mutated residues are either inside the WDR5 cavity (■), have established interactions with SET1_{Win} (□), or sequentially are one residue away from residues with established interactions with SET1_{Win} (°) (1,4).

Mutations within and around the Win binding site	Independent Mutations
F133L ■ □ S175L ■ □ A264V ■ N130Y ° D150G °	S54N G254D L282P

Table S3: Distributions of somatic cancer mutations in tumors with a well-defined upper limit of mutations. Diverse mutation clusters correspond to different maximum number of mutations, N_{\max} . The mutations highlighted in yellow were studied further using BLI and steady-state FP spectroscopy. S218F and D92N mutations, which are located within the WDR5 cavity, were found in tumors with $N > 10,000$. For compiling these mutations, the COSMIC database was used (5-7).

Condition	Mutations
$N < 10,000$	N130Y S54N S175L G254D A264V D150G F133L L282P L185F R181C E292Q S184F D333Y S148F I327V S318P P311Q S223Y S202L D213N P139H Y75H V217M T253A L143F R181C Y260H P224S A201T D172A L102V R196C V275L G226V G299C D172N E279K L206P D302E Q289E S278L K245N H255N G277D I274F S91F S171L P216L L102F L230P G147E
$N < 5,000$	N130Y S54N S175L G254D A264V D150G F133L L282P L185F R181C E292Q S184F D333Y S148F I327V S318P P311Q S223Y S202L D213N P139H Y75H V217M T253A L143F R181C Y260H P224S A201T D172A L102V R196C V275L
$N < 1,000$	N130Y S54N S175L G254D A264V D150G F133L L282P L185F R181C E292Q
$N < 500$	N130Y S54N S175L G254D A264V D150G F133L L282P

3. Results of mutation clustering for different N_{\max} -based mutation subsets

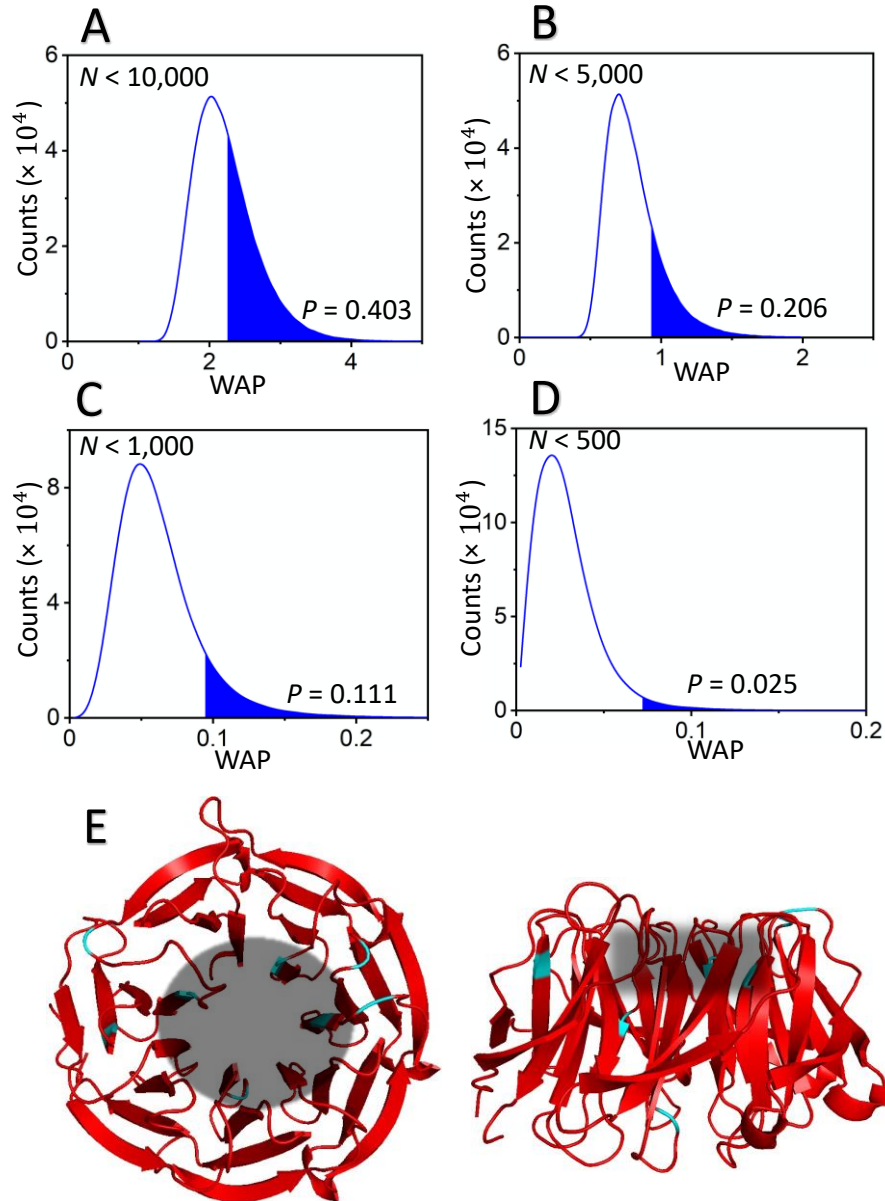


Figure S1: Results of mutation clustering for different N_{\max} -based mutation subsets. (A) WAP scores were calculated using 4 different subsets of mutations divided on the basis of the genetic damage, N , in their corresponding tumors. The P -values were calculated by comparing to the calculated WAP scores to those corresponding to random permutations of the mutation distribution. 10^6 configurations were used for $N < 10,000$ (A), $N < 5,000$ (B), $N < 1,000$ (C), and $N < 500$ (D). (E) The top and side views of WDR5 shown in red, on the left and right sides, respectively. The locations of low- N mutations are marked in cyan. The shaded region in dark grey represents the Win binding site of WDR5. These representations were made using pdb entry code 4ERY (1).

4. List of tumor locations associated with missense WDR5 cancer mutations within and around the Win binding site

Table S4: Tumor locations associated with missense WDR5 cancer mutations. The table shows the location of the tumors in which the mutations were found.

Mutation	Tumor Location	Other information
D172A***	Kidney	Studied experimentally by BLI and steady-state FP
P216L	Skin	
Y260H	Large Intestine	
S218F	Skin	
D92N***	Endometrium	
F133L*	Kidney	
S175L*	Breast	
A264V	Soft Tissue	Clustering with $N < 500$
N130Y	Breast	
D150G	Stomach	
S54N	Biliary Tract	
G254D	Haematopoietic and Lymphoid Tissue	
L282P	Kidney	This mutant disrupts known Win binding site interactions
S91F**	Skin	

*F133L and S175L also meet the clustering with $N < 500$ condition. It was found that F133L disrupts the mitotic progression in the cell cycle process (8).

S91F was not studied experimentally. It does not meet the clustering with the $N < 500$ condition, yet it can disrupt known Win site interactions (Supplementary Table S5**). For example, a related mutant, S91K, is not able to make interactions with a minimal C-terminal SET catalytic domain of MLL1 (9).

***D172A and D92N were experimentally studied using single-molecule electrical recordings and an MLL4_{Win}-containing engineered nanopore (3). In addition, D172A was recently studied using pull-down assays, showing declined interactions with histone H3 peptides with respect to the native WDR5 protein (10).

5. List of noncovalent bonds at the WDR5-SET1_{Win} protein interface

Table S5: Mapping of hydrogen bonds at the WDR5-SET1_{Win} interface. These results were obtained using previously published co-crystallization data of Dharmarajan and co-workers (1). The cut-off distance for identifying these

hydrogen bonds was 4.0 Å. Here, BB and SC denote backbone and side chain, respectively. These interactions were determined using protein interactions calculator (PIC) (11). The structures were not always able to model the whole sequence of the peptides, so the list of these hydrogen bonds is not comprehensive. The first residue in each bond belongs to the SET1_{win} ligand, whereas the second one belongs to WDR5. Only peptide sequences of the segments that were able to model these interactions are listed below. Entries with multiple distances represent multiple different hydrogen bonds formed by the same residues.

Peptide	Hydrogen Bonds	Distance (Å)	Type
MLL1 _{win} LNPHGSARAEVHL	G3762-G89	3.0	BB-BB
	H3761-K46	3.3	BB-SC
	S3763-I90	3.2	BB-SC
	A3764-S91	3.3,	BB-SC
	A3764-D107	3.0, 3.3	BB-SC
	R3765-S91	3.0, 2.8	BB-SC
	R3765-F133	3.0	BB-SC
	R3765-C261	2.9	BB-SC
	H3761-D107	2.7	SC-SC
MLL2 _{win} INPTGCARSEPKI	G5337 – G89	3.1	BB-BB
	K5344 – K259	2.9	BB-BB
	C5338-I90	3.7	BB-SC
	A5339 – D107	2.9	BB-SC
	R5340 – S91	3.1, 2.8	BB-SC
	R5340 – F133	3.0	BB-SC
	R5340 – C261	2.9	BB-SC
	C5338-S91	3.7	SC-SC
	N5334-D107	2.8	SC-SC
MLL3 _{win} VNPTGCARSEPKMS	G4707-G89	3.3	BB-BB
	K4714 – K259	2.9	BB-BB
	C4708-I90	3.5	BB-SC
	A4709 – D107	2.9, 3.5	BB-SC
	R4710 – S91	3.1, 2.8	BB-SC
	R4710 – F133	2.9	BB-SC
	R4710 – C261	2.9	BB-SC
	C4708-S91	3.7	SC-SC
	N4704-D107	2.8	SC-SC
MLL4 _{win} LNPHGAARAEVY	G2508-G89	3.3	BB-BB
	A2510-S91	3.4	BB-SC
	A2510 – D107	3.0	BB-SC
	R2511 – S91	3.0, 2.8	BB-SC
	R2511 – F133	3.0	BB-SC
	R2511 – C261	2.9	BB-SC
	N2505-D107	2.7	SC-SC
	Y2515-D172	3.2	SC-SC
SETd1A _{win}	G1492-G89	3.3	BB-BB

QTGSARSEGY	Y1499 – K259	2.8	BB-BB
	T1491-G322	3.5	BB-SC
	A1494-S91	3.4	BB-SC
	A1494 – D107	3.0, 3.4	BB-SC
	R1495 – S91	3.0, 2.8	BB-SC
	R1495 – F133	3.1	BB-SC
	R1495 – C261	2.9	BB-SC
SETd1B _{win} GCARSEG	G1702-G89	3.3	BB-BB
	C1703-I90	3.4	BB-SC
	A1704-S91	3.5	BB-SC
	A1704 – D107	3.0, 3.3	BB-SC
	R1705 – S91	3.2, 2.8	BB-SC
	R1705 – F133	3.1	BB-SC
	R1705 – C261	2.8	BB-SC
	C1703-S91	3.7	SC-SC

Table S6: List of all known noncovalent interactions. These results were obtained in a similar method as that for **Table S5**. For each interaction, the first residue corresponds to the SET1_{win} ligand, while the second residue corresponds to WDR5. The cut-off radii for the ionic and cation-pi interactions were 6 Å. Also, the cut-off radii for the hydrophobic and aromatic-aromatic interactions were 5 and 7 Å, respectively.

Peptide	Ionic	Cation-Pi	Hydrophobic	Aromatic-Aromatic
MLL1 _{win} LNPHGSARAEVHL	R3765-D92 H3761-D107 H3769-D172	R3765-F133 R3765-F263	A3766-A47 A3766-A65 A3764-Y131 A3764-F133 A3764-D149 V3768-Y260 A3766-K321	
MLL2 _{win} INPTGCARSEPKI	R5340-D92	R5340-F133 R5340-F263 K5344-Y191	A5339-Y131 A5339-F133 A5339-F149 P5343-Y260	
MLL3 _{win} VNPTGCARSEPKMS	R4710-D92	R4710-F133 R4710-F263 K4714-Y191	A4709-Y131 A4709-F133 A4709-F149 P4713-Y260	
MLL4 _{win} LNPHGAARAEVY	R2511-D92 H2507-Q322	R2511-F133 R2511-F263	A2512-A47 A2509-A65 A2512-A65 A2510-Y131	Y2515-F149 Y2515-Y191

			A2510-F133 A2510-F149 Y2515-F149 Y2515-P173 Y2515-Y191 V2514-Y260 A2512-L321	
SETd1A _{win} QTGSARSEGY	R1495-D92	R1495-F133 R1495-F263	A1494-Y131 A1494-F133 A1494-F149 Y1499-Y191 Y1499-P216 Y1499-L234	Y1499-Y191
SETd1B _{win} GCARSEG	R1705-D92	R1705-F133 R1705-F263	A1704-Y131 A1704-F133 A1704-F149	

6. Location of surface WDR5 mutations within the A and B pockets

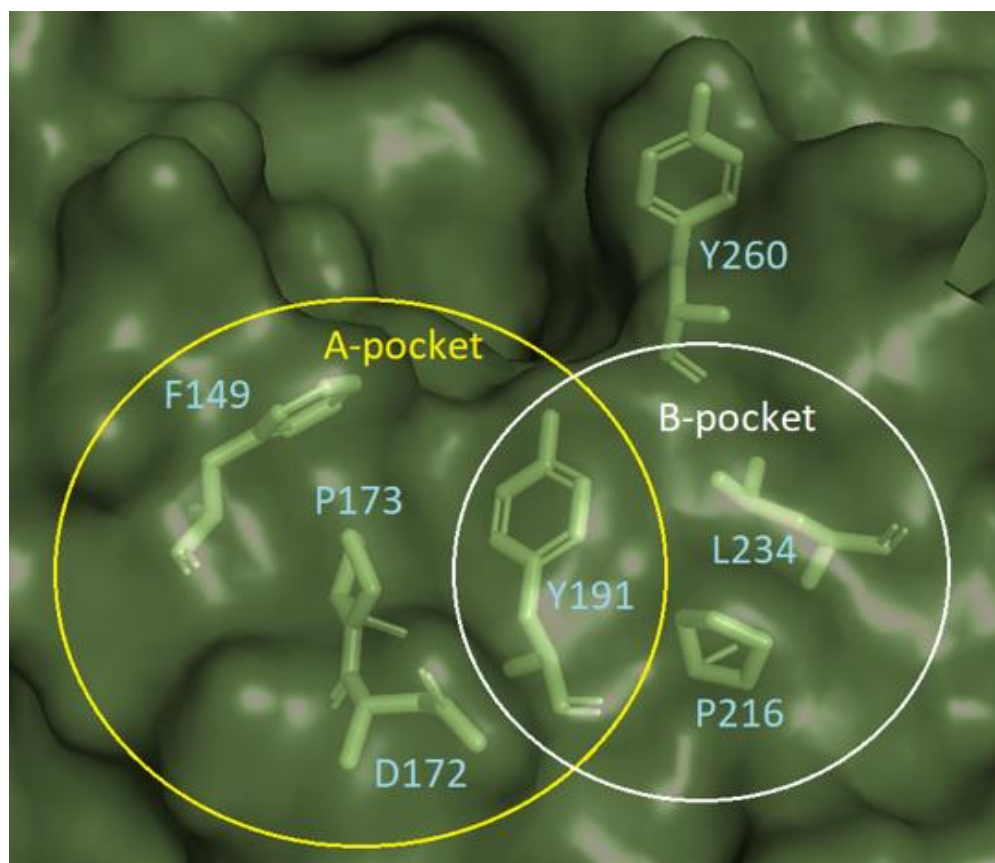


Figure S2: Cartoon illustrating the location of key residues present in the A and B pockets of the WDR5 protein.

7. Very weak interactions of D92N with SET1_{Win} ligands are detected by BLI measurements

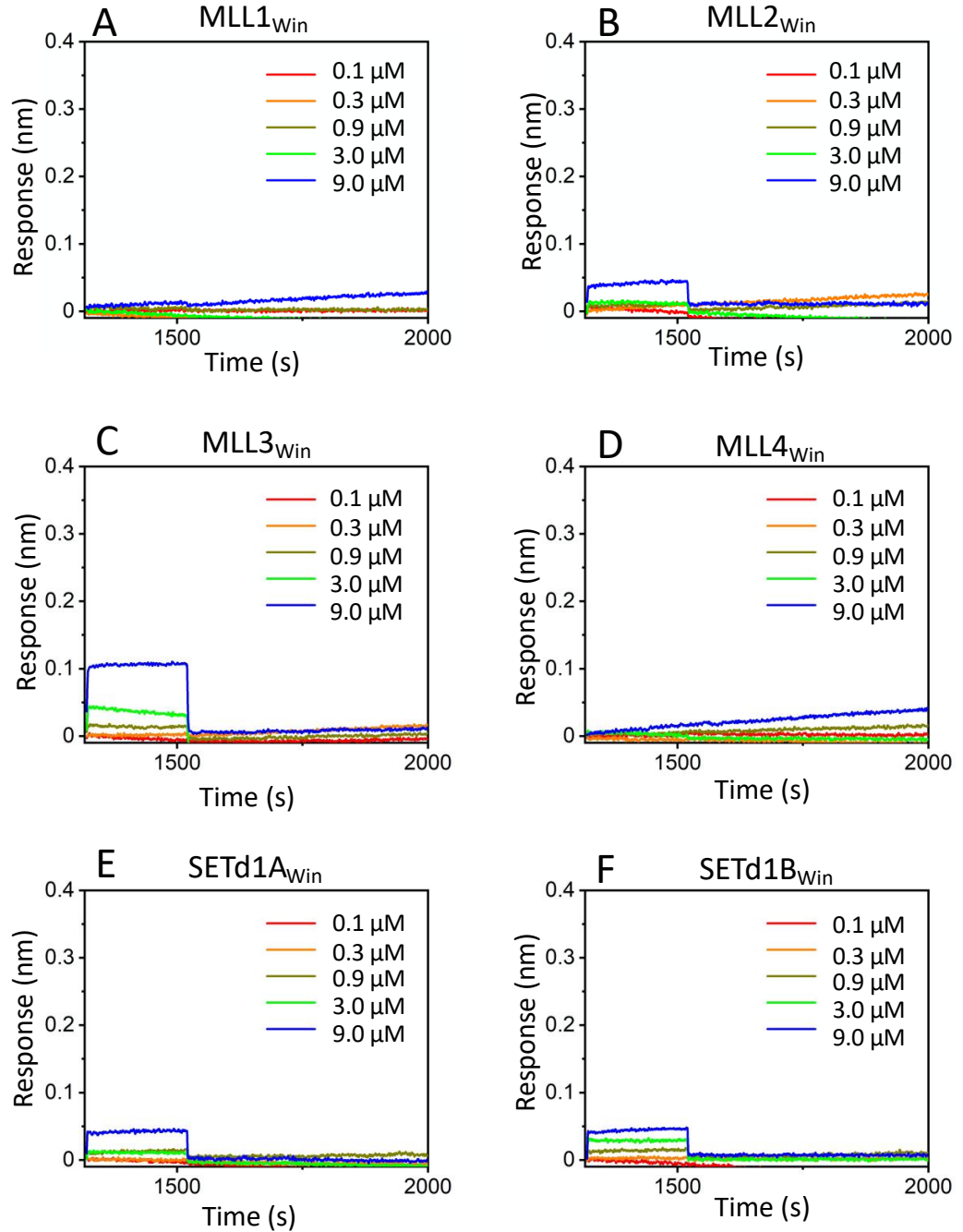


Figure S3: BLI sensorgrams show either nondetectable or weakly detectable interactions of D92N with SET1_{Win} ligands. 5 nM biotin-tagged peptides were

loaded onto streptavidin (SA) sensors for 15 minutes. A 3-fold serial dilution of D92N ranging from 0.1 μM to 9 μM was used to obtain individual binding curves. These sensorgrams show no binding interactions for MLL1_{Win} and MLL4_{Win}. For the other SET1_{Win} ligands, the binding interactions were visible, yet quantitative kinetic determinations were not possible.

(A) MLL1_{Win}, (B) MLL2_{Win}, (C) MLL3_{Win}, (D) MLL4_{Win}, (E) SETd1A_{Win}, and (F) SETd1B_{Win}.

8. Kinetic rate constants of association of WDR5 mutants with SET1_{Win} ligands using BLI measurements

Table S7: Kinetic rate constants of association, k_{on} , of WDR5 mutants with the SETd1A_{Win} ligands using BLI measurements. k_{on} values were provided in $10^4 \text{ M}^{-1}\text{s}^{-1}$. Results for WDR5 mutants were obtained the same way as those for the native WDR5 protein. For F133L, 3-fold serial dilutions ranging from 0.3 μM to 27 μM were used. Numbers represent mean \pm s.d. determined from three independent experimental observations. D92N did not show any measurable binding interactions using BLI, so it was not included in this table.

Ligand	WDR5*	D172A	P216L	Y260H	F133L	S175L	S218F
MLL1 _{Win}	~ 1**	~ 1**	~ 1**	~ 1**	NO***	~ 1**	~ 1**
MLL2 _{Win}	4.4 \pm 0.4	5.7 \pm 0.6	5.6 \pm 0.8	6.6 \pm 0.9	1.6 \pm 0.1	4.9 \pm 0.4	4.0 \pm 0.2
MLL3 _{Win}	5.4 \pm 0.6	6.5 \pm 1.3	5.3 \pm 0.7	6.4 \pm 0.2	3.6 \pm 2.1	4.9 \pm 0.3	3.9 \pm 0.5
MLL4 _{Win}	2.3 \pm 0.2	3.7 \pm 0.4	1.9 \pm 0.3	2.4 \pm 0.3	~ 1	3.0 \pm 0.1	2.0 \pm 0.2
SETd1A _{Win}	8.2 \pm 0.8	13 \pm 1	8.6 \pm 0.8	8.8 \pm 1.3	2.6 \pm 0.3	6.1 \pm 0.7	5.6 \pm 0.4
SETd1B _{Win}	7.1 \pm 0.5	8.9 \pm 1.4	8.0 \pm 0.8	10 \pm 1	4.3 \pm 1.2	8.4 \pm 0.6	6.3 \pm 0.6

*This data are from Imran and co-workers (2021) (2).

**In this case, k_{on} was in the order of $10^4 \text{ M}^{-1}\text{s}^{-1}$ assuming that the association process is in the range of values determined with the other SET1_{Win} ligands.

***NO stands for “Not Observed.”

9. Kinetic rate constants of dissociation of WDR5 mutants with SET1_{Win} ligands using BLI measurements.

Table S8: Kinetic rate constants of dissociation, k_{off} , of WDR5 mutants with the SET1_{Win} ligands using BLI measurements. k_{off} values were provided in 10^{-3} s^{-1} . Numbers represent mean \pm s.d. determined from three independent experimental observations. D92N did not show any measurable binding interactions using BLI, so it was not included in this table.

Ligand	WDR5*	D172A	P216L	Y260H	F133L	S175L	S218F
MLL1 _{win}	> 1000**	> 1000**	> 1000**	> 1000**	NO***	> 1000**	> 1000**
MLL2 _{win}	7.7 ± 0.2	14 ± 1	11 ± 2	13 ± 1	140 ± 20	6.3 ± 0.1	25 ± 2
MLL3 _{win}	5.3 ± 0.1	9.3 ± 1.9	11 ± 3	7.7 ± 0.6	100 ± 10	16 ± 2	21 ± 3
MLL4 _{win}	39 ± 2	51 ± 10	220 ± 50	47 ± 28	> 1000*	130 ± 4	71 ± 1
SETd1A _{win}	51 ± 6	110 ± 30	33 ± 4	98 ± 29	690 ± 40	89 ± 30	46 ± 7
SETd1B _{win}	17 ± 1	23 ± 3	30 ± 5	23 ± 3	240 ± 20	4.9 ± 0.3	23 ± 2

*This data are from Imran and co-workers (2021) (2).

**This upper-limit value for the detection of k_{off} is set according to instrument specifications.

***NO stands for “Not Observed.”

10. Normalized kinetic rate constants of association of WDR5 mutants with $SET1_{Win}$ ligands using BLI measurements

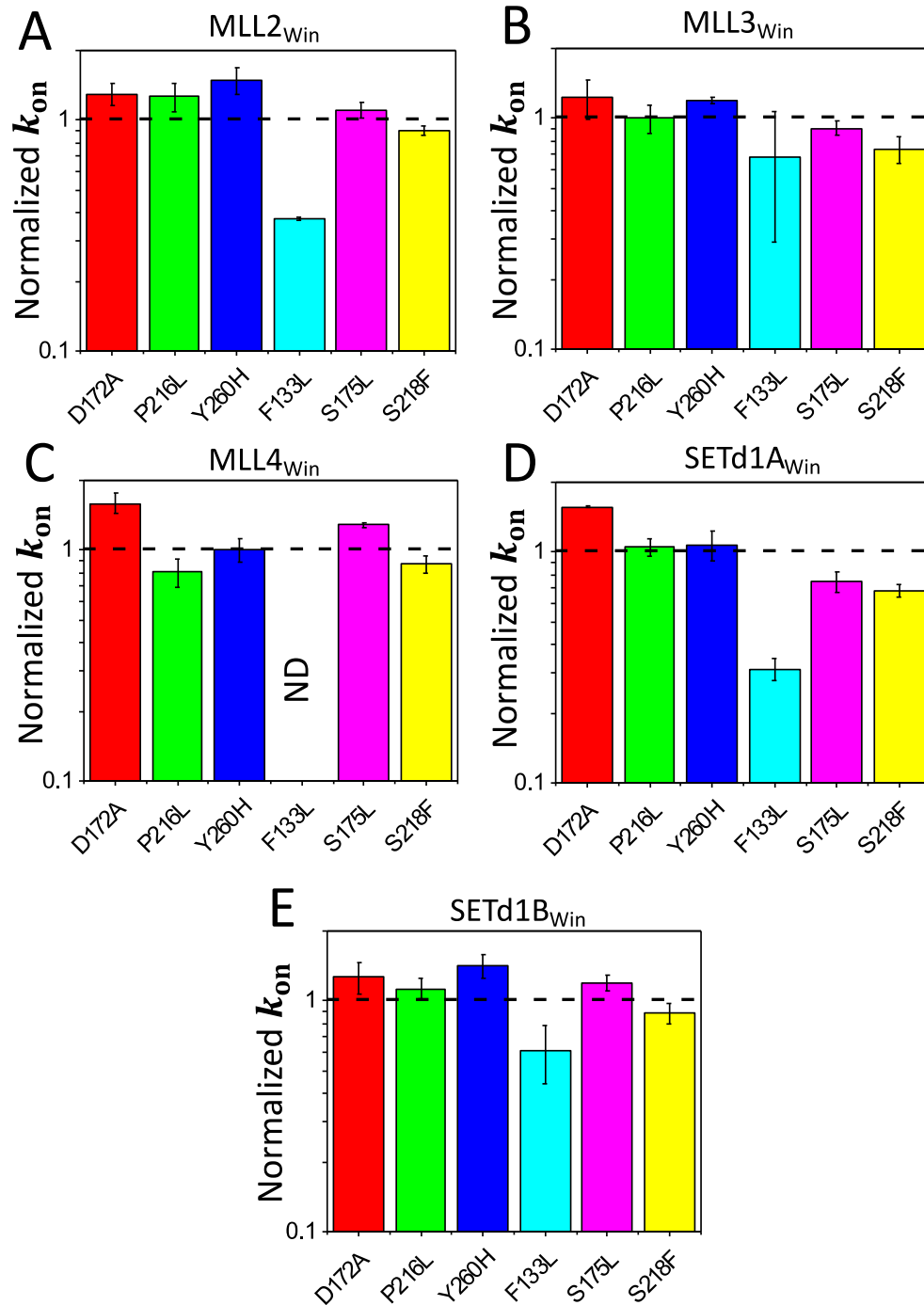


Figure S4: Normalized association rate constants of the WDR5- $SET1_{Win}$ interactions using BLI sensorgrams. The k_{on} values for each $SET1_{Win}$ ligand's interaction with WDR5 mutants have been divided by the k_{on} of that $SET1_{Win}$ ligand's interaction with the native WDR5 protein. ND stands for "Not

Determined.” Interaction between F133L and MLL4 was detectable, but not quantifiable, using a BLI measurement.

11. Equilibrium dissociation constants of WDR5 mutants with SET1_{win} ligands using BLI measurements.

Table S9: Equilibrium dissociation constants, K_{D-BLI} , of the WDR5 mutants with the SET1_{win} ligands determined from BLI measurements. K_{D-BLI} values are provided in nM. Numbers represent mean \pm s.d. determined from three independent experimental determinations. D92N did not show any measurable binding interactions using the BLI, so it was not included in this table.

Ligand	WDR5 [#]	D172A	P216L	Y260H	F133L	S175L	S218F
MLL1 _{win}	$\geq 100,000^*$	$\geq 100,000^*$	$\geq 100,000^*$	$\geq 100,000^*$	NO**	$\geq 100,000^*$	$\geq 100,000^*$
MLL2 _{win}	170 ± 20	240 ± 10	200 ± 50	200 ± 20	$8,300 \pm 1,000$	130 ± 10	640 ± 20
MLL3 _{win}	100 ± 5	140 ± 10	200 ± 30	110 ± 20	$3,700 \pm 1,600$	330 ± 20	530 ± 20
MLL4 _{win}	$1,700 \pm 200$	$1,400 \pm 200$	$9,900 \pm 1,400$	$3,400 \pm 1,200$	$\geq 100,000^*$	$4,200 \pm 100$	$3,400 \pm 300$
SETd1A _{win}	620 ± 20	900 ± 240	380 ± 20	$1,100 \pm 200$	$30,000 \pm 5,000$	$1,400 \pm 300$	830 ± 110
SETd1B _{win}	250 ± 30	260 ± 10	370 ± 40	230 ± 10	$6,000 \pm 1,900$	56 ± 3	360 ± 20

[#]These data are from the reference (2).

*This upper-limit value for the detection of K_{D-BLI} results from dividing the upper-limit value of the detection of k_{off} by the value of the k_{on} approximation.

**NO stands for “Not Observed.”

12. Structural information on the effect of the S175L mutation.

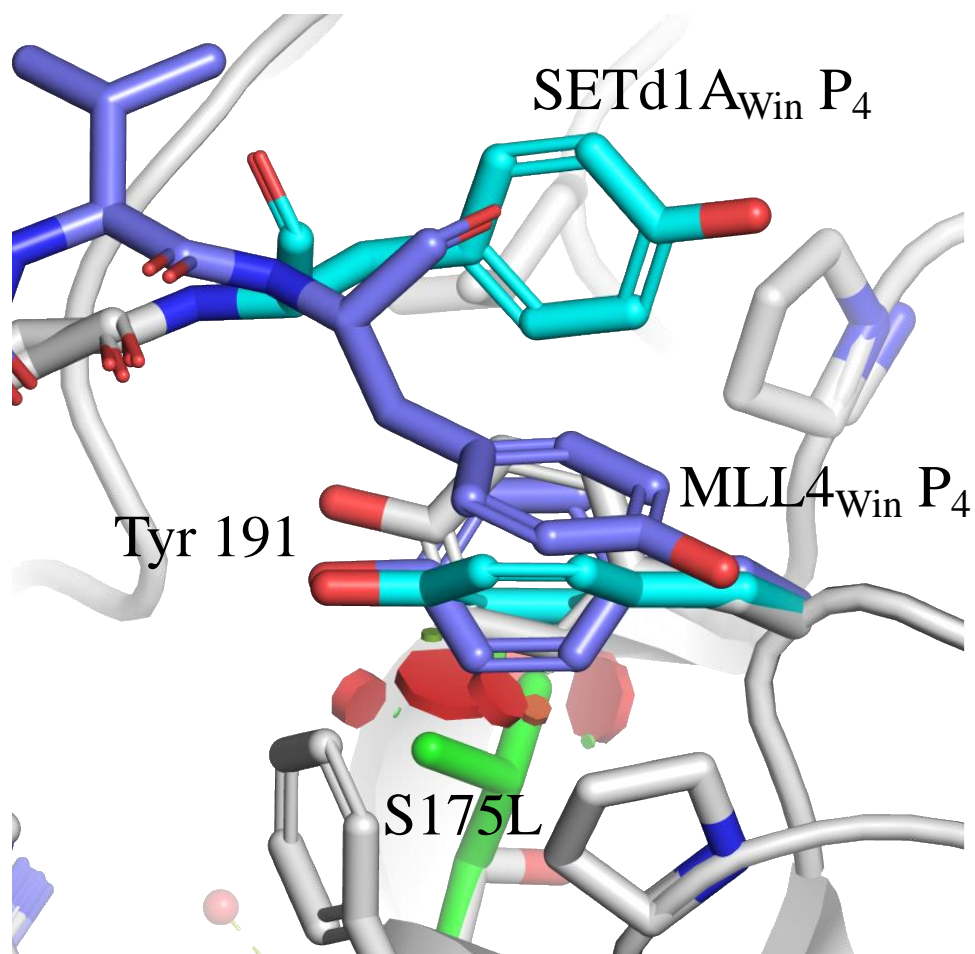


Figure S5: The effect of the S175L mutation on the SETd1A_{win}-S175L interaction. The figure shows the effect of the S175L mutation on neighboring residues. It shows superimposed structures from PDB 4es0, 4ewr and 4erz. SETd1A_{win} is marked in cyan, while MLL4_{win} is marked in light blue. The red circles show the steric clashes created by replacing Ser-175 with Leu-175 (green). Superimposed Tyr-191 side chains from the three PDB files are shown. SETd1A_{win} was used, instead of SETd1B_{win}, to show the B-pocket interactions, because the P₆ residue in the SETd1B_{win} structure is disordered (1).

13. Steady-state FP spectroscopy curves for the interactions of WDR5 mutants with SET1_{win} ligands

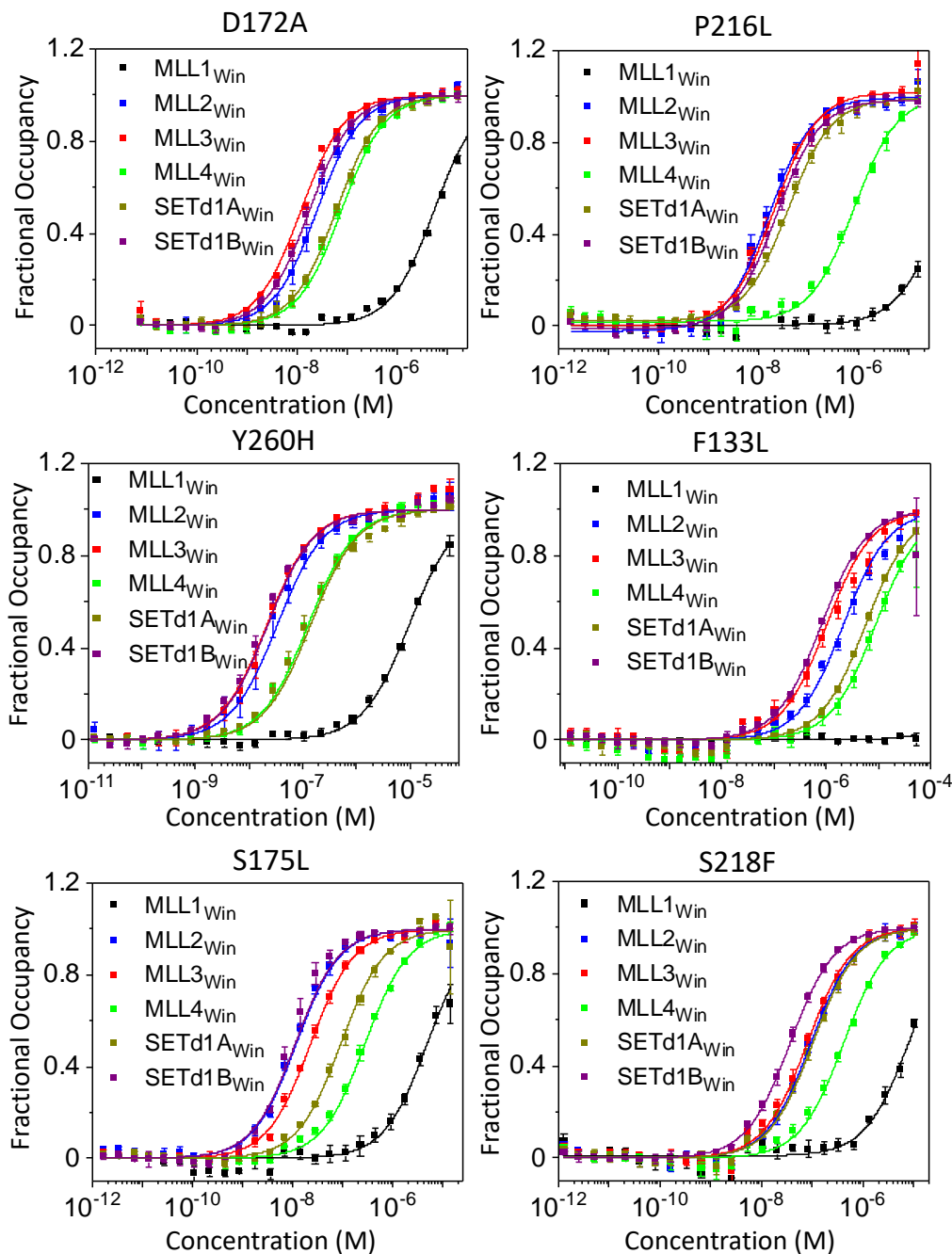


Figure S6: Steady-state FP anisotropy curves for WDR5-SET1_{win} ligand interactions. The N terminus of the SET1_{win} ligands was tagged with Sulforhodamine B, whereas the C terminus was amidated. The final concentration of the labeled SET1_{win} ligands in each well was 10 nM. Each SET1_{win} ligand – WDR5 run involved a 2-fold serial dilution of WDR5 over 24 wells. Three independent experiments were conducted to obtain the dose response, which was fitted using a four-parameter logistic model to get the **K_D**.

14. Very weak interactions of D92N with SET1_{win} ligands are detected by steady-state FP spectroscopy measurements

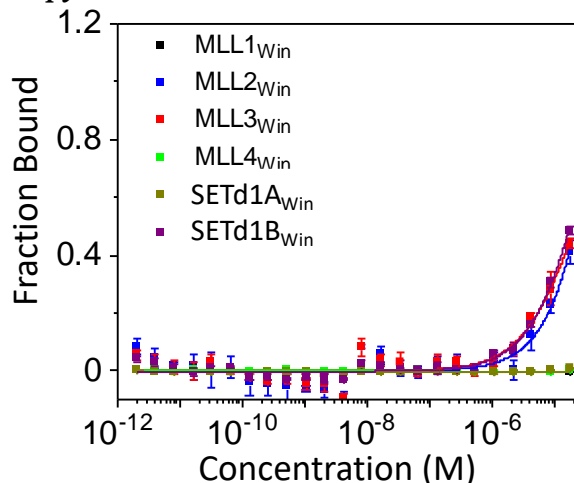


Figure S7: Fraction bound of SET1_{win} ligands to D92N using steady-state FP spectroscopy experiments. These experiments showed either nondetectable or very weak interactions of D92N with all SET1_{win} ligands. The final SET1_{win} ligand concentration was 10 nM. The WDR5 concentration (horizontal axis) spanned from low μ M to low pM. No FP signal was detectable for MLL1_{win}, MLL4_{win}, and SETd1A_{win}. Very weak interactions with D92N were detected in the case of MLL2_{win}, MLL3_{win}, and SETd1B_{win}. For these SET1_{win} ligands, K_D was greater than 10 μ M.

15. Equilibrium dissociation constants of WDR5 mutants with SET1_{win} ligands using FP measurements

Table S10: Equilibrium dissociation constants, K_{D-FP} , of WDR5 mutants with SET1_{win} ligands determined from steady-state FP measurements. Three independent experiments were conducted to obtain the dose response, which was fitted using a four-parameter logistic model. K_{D-FP} values are provided in nM. For D92N, the K_D values were greater than 17,000 nM. Numbers represent mean \pm s.e.m. from three individual experimental determinations.

Ligand	WDR5 [#]	D172A	P216L	Y260H	F133L	S175L	S218F
MLL1 _{win}	9,000 \pm 5,500	5,600 \pm 800	> 14,650*	9,700 \pm 1,200	> 53,000*	4,800 \pm 2,800	8,100 \pm 3,400
MLL2 _{win}	23 \pm 5	25 \pm 4	18 \pm 3	34 \pm 4	2,100 \pm 300	11 \pm 1	94 \pm 7
MLL3 _{win}	15 \pm 4	12 \pm 1	19 \pm 1	22 \pm 2	1,000 \pm 100	23 \pm 1	80 \pm 7
MLL4 _{win}	130 \pm 20	78 \pm 3	690 \pm 60	130 \pm 10	8,800 \pm 3,900	280 \pm 30	420 \pm 40
SETd1A _{win}	72 \pm 5	61 \pm 2	39 \pm 2	140 \pm 20	5,700 \pm 300	92 \pm 7	100 \pm 10
SETd1B _{win}	18 \pm 2	18 \pm 1	28 \pm 2	23 \pm 2	820 \pm 30	11 \pm 1	37 \pm 1

[#]These data are from the reference (2).

*These low-value limits are based on the highest concentrations of WDR5 mutants employed in this study.

16. Quantitative comparisons of affinity data acquired with BLI and FP.

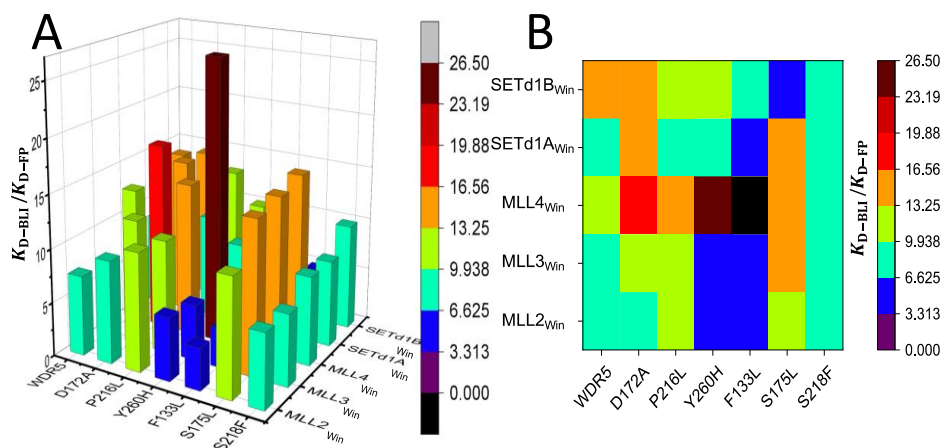


Figure S8: Quantitative comparison between affinity data resulting from BLI and FP measurements. (A) A 3D graph of the ratio of the K_{D-BLI} to the K_{D-FP} . (B) A 2D heat map of the ratio of the K_{D-BLI} to the K_{D-FP} .

Table S11: Quantitative comparisons between affinity data resulting from BLI and FP measurements in terms of the ratio of the K_{D-BLI} to the K_{D-FP} .

Protein	MLL2 _{win}	MLL3 _{win}	MLL4 _{win}	SETd1A _{win}	SETd1B _{win}
WDR5	7.43	6.68	12.7	8.60	13.8
D172A	9.51	11.7	17.5	14.7	14.4
P216L	10.9	10.5	14.3	9.73	12.9
Y260H	5.81	5.15	26.4	7.68	10.1
F133L	3.90	3.62	ND*	5.28	7.40
S175L	10.9	14.4	14.9	15.6	4.97
S218F	6.83	6.63	8.25	8.05	9.92

ND* stands for not determined.

Table S12: Quantitative comparisons between affinity data resulting from BLI and FP measurements in terms of the ratio of the normalized K_{D-BLI} to the normalized K_{D-FP} . A normalized K_D of the binding interactions of a SET1_{win} ligand with a WDR5 mutant is the K_D measured for this interaction pair divided by the K_D value measured with the same SET1_{win} ligand interacting with the native WDR5 protein.

Protein	MLL2 _{win}	MLL3 _{win}	MLL4 _{win}	SETd1A _{win}	SETd1B _{win}
D172A	1.28	1.76	1.37	1.71	1.04
P216L	1.47	1.57	1.13	1.13	0.94
Y260H	0.78	0.77	2.09	0.89	0.73

F133L	0.52	0.54	ND*	0.61	0.54
S175L	1.47	2.15	1.18	1.82	0.36
S218F	0.92	0.99	0.65	0.94	0.72

ND* stands for not determined.

17. Supporting methods.

Table S13: List of fluorescently labeled SET1_{Win} ligands for steady-state FP studies. All ligands were fluorescently labeled at the N terminus and amidated at the C terminus. A 9-residue Gly-Ser-based peptide spacer was inserted between Sulforhodamine B and SET1_{Win} ligand.

	<u>Ligand</u>	<u>Sequence</u>
1	MLL1 _{Win}	Sulforhodamine B-(GGS) ₃ LNPHGSARAEVHLS-NH ₂
2	MLL2 _{Win}	Sulforhodamine B -(GGS) ₃ INPTGCARSEPKIL-NH ₂
3	MLL3 _{Win}	Sulforhodamine B -(GGS) ₃ VNPTGCARSEPKMS-NH ₂
4	MLL4 _{Win}	Sulforhodamine B -(GGS) ₃ LNPHGAARAEVYLS-NH ₂
5	SETd1A _{Win}	Sulforhodamine B -(GGS) ₃ EHQTGSARSEGYYYP-NH ₂
6	SETd1B _{Win}	Sulforhodamine B -(GGS) ₃ EHVTGCARSEGYYT-NH ₂

18. Supporting references.

1. Dharmarajan, V., Lee, J.H., Patel, A., Skalnik, D.G. and Cosgrove, M.S. (2012) Structural basis for WDR5 interaction (Win) motif recognition in human SET1 family histone methyltransferases. *J. Biol. Chem.*, **287**, 27275-27289.
2. Imran, A., Moyer, B.S., Canning, A.J., Kalina, D., Duncan, T.M., Moody, K.J., Wolfe, A.J., Cosgrove, M.S. and Movileanu, L. (2021) Kinetics of the multitasking high-affinity Win binding site of WDR5 in restricted and unrestricted conditions. *Biochem. J.*, **478**, 2145-2161.
3. Mayse, L.A., Imran, A., Larimi, M.G., Cosgrove, M.S., Wolfe, A.J. and Movileanu, L. (2022) Disentangling the recognition complexity of a protein hub using a nanopore. *Nature Commun.*, **13**, 978.
4. Zhang, P., Lee, H., Brunzelle, J.S. and Couture, J.F. (2012) The plasticity of WDR5 peptide-binding cleft enables the binding of the SET1 family of histone methyltransferases. *Nucleic Acids Res.*, **40**, 4237-4246.
5. Forbes, S.A., Beare, D., Bindal, N., Bamford, S., Ward, S., Cole, C.G., Jia, M., Kok, C., Boutselakis, H., De, T. *et al.* (2016) COSMIC: High-Resolution Cancer Genetics Using the Catalogue of Somatic Mutations in Cancer. *Curr. Protoc. Hum Genet.*, **91**, 10.11.11-10.11.37.

6. Forbes, S.A., Beare, D., Boutselakis, H., Bamford, S., Bindal, N., Tate, J., Cole, C.G., Ward, S., Dawson, E., Ponting, L. *et al.* (2017) COSMIC: somatic cancer genetics at high-resolution. *Nucleic Acids Res.*, **45**, D777-d783.
7. Tate, J.G., Bamford, S., Jubb, H.C., Sondka, Z., Beare, D.M., Bindal, N., Boutselakis, H., Cole, C.G., Creatore, C., Dawson, E. *et al.* (2019) COSMIC: the Catalogue Of Somatic Mutations In Cancer. *Nucleic Acids Res.*, **47**, D941-d947.
8. Ali, A., Veeranki, S.N. and Tyagi, S. (2014) A SET-domain-independent role of WRAD complex in cell-cycle regulatory function of mixed lineage leukemia. *Nucleic Acids Res.*, **42**, 7611-7624.
9. Patel, A., Vought, V.E., Dharmarajan, V. and Cosgrove, M.S. (2008) A conserved arginine-containing motif crucial for the assembly and enzymatic activity of the mixed lineage leukemia protein-1 core complex. *J. Biol. Chem.*, **283**, 32162-32175.
10. Zhao, J., Chen, W., Pan, Y., Zhang, Y., Sun, H., Wang, H., Yang, F., Liu, Y., Shen, N., Zhang, X. *et al.* (2021) Structural insights into the recognition of histone H3Q5 serotonylation by WDR5. *Science advances*, **7**.
11. Tina, K.G., Bhadra, R. and Srinivasan, N. (2007) PIC: Protein Interactions Calculator. *Nucleic Acids Res.*, **35**, W473-476.

3.7 REFERENCES

1. Xu, C. and Min, J. (2011) Structure and function of WD40 domain proteins. *Protein & cell*, **2**, 202-214.
2. Zhang, C. and Zhang, F. (2015) The Multifunctions of WD40 Proteins in Genome Integrity and Cell Cycle Progression. *J. Genomics*, **3**, 40-50.
3. Afanasieva, E., Chaudhuri, I., Martin, J., Hertle, E., Ursinus, A., Alva, V., Hartmann, M.D. and Lupas, A.N. (2019) Structural diversity of oligomeric β -propellers with different numbers of identical blades. *eLife*, **8**.
4. Stirnimann, C.U., Petsalaki, E., Russell, R.B. and Müller, C.W. (2010) WD40 proteins propel cellular networks. *Trends Biochem. Sci.*, **35**, 565-574.
5. Santosh Kumar, H.S., Kumar, V., Pattar, S. and Telkar, S. (2016) Towards the construction of an interactome for Human WD40 protein family. *Bioinformatics*, **12**, 54-61.
6. Migliori, V., Mapelli, M. and Guccione, E. (2012) On WD40 proteins: propelling our knowledge of transcriptional control? *Epigenetics*, **7**, 815-822.
7. Jain, B.P. and Pandey, S. (2018) WD40 Repeat Proteins: Signalling Scaffold with Diverse Functions. *Protein J.*, **37**, 391-406.
8. Cosgrove, M.S. and Patel, A. (2010) Mixed lineage leukemia: a structure-function perspective of the MLL1 protein. *FEBS J.*, **277**, 1832-1842.
9. Li, Y., Han, J., Zhang, Y., Cao, F., Liu, Z., Li, S., Wu, J., Hu, C., Wang, Y., Shuai, J. *et al.* (2016) Structural basis for activity regulation of MLL family methyltransferases. *Nature*, **530**, 447-452.
10. Vedadi, M., Blazer, L., Eram, M.S., Barsyte-Lovejoy, D., Arrowsmith, C.H. and Hajian, T. (2017) Targeting human SET1/MLL family of proteins. *Protein Sci.*, **26**, 662-676.
11. Xue, H., Yao, T., Cao, M., Zhu, G., Li, Y., Yuan, G., Chen, Y., Lei, M. and Huang, J. (2019) Structural basis of nucleosome recognition and modification by MLL methyltransferases. *Nature*, **573**, 445-449.
12. Jiang, H. (2020) The complex activities of the SET1/MLL complex core subunits in development and disease. *Biochim. Biophys. Acta. Gene. Regul. Mech.*, **1863**, 194560.
13. Sha, L., Ayoub, A., Cho, U.S. and Dou, Y. (2020) Insights on the regulation of the MLL/SET1 family histone methyltransferases. *Biochim. Biophys.*

Acta Gene. Regul. Mech., **1863**, 194561.

14. Dou, Y., Milne, T.A., Ruthenburg, A.J., Lee, S., Lee, J.W., Verdine, G.L., Allis, C.D. and Roeder, R.G. (2006) Regulation of MLL1 H3K4 methyltransferase activity by its core components. *Nat. Struct. Mol. Biol.*, **13**, 713-719.
15. Patel, A., Dharmarajan, V., Vought, V.E. and Cosgrove, M.S. (2009) On the mechanism of multiple lysine methylation by the human mixed lineage leukemia protein-1 (MLL1) core complex. *J. Biol. Chem.*, **284**, 24242-24256.
16. Shinsky, S.A., Monteith, K.E., Viggiano, S. and Cosgrove, M.S. (2015) Biochemical reconstitution and phylogenetic comparison of human SET1 family core complexes involved in histone methylation. *J. Biol. Chem.*, **290**, 6361-6375.
17. Thomas, L.R., Wang, Q., Grieb, B.C., Phan, J., Foshage, A.M., Sun, Q., Olejniczak, E.T., Clark, T., Dey, S., Lorey, S. *et al.* (2015) Interaction with WDR5 promotes target gene recognition and tumorigenesis by MYC. *Mol. Cell. Biochem.*, **58**, 440-452.
18. Thomas, L.R., Adams, C.M., Wang, J., Weissmiller, A.M., Creighton, J., Lorey, S.L., Liu, Q., Fesik, S.W., Eischen, C.M. and Tansey, W.P. (2019) Interaction of the oncoprotein transcription factor MYC with its chromatin cofactor WDR5 is essential for tumor maintenance. *Proceedings of the National Academy of Sciences of the United States of America*, **116**, 25260-25268.
19. Thomas, L.R., Adams, C.M., Fesik, S.W., Eischen, C.M. and Tansey, W.P. (2020) Targeting MYC through WDR5. *Mol. Cell. Oncol.*, **7**, 1709388.
20. Thomas, L.R., Foshage, A.M., Weissmiller, A.M. and Tansey, W.P. (2015) The MYC-WDR5 Nexus and Cancer. *Cancer Res.*, **75**, 4012-4015.
21. Guarnaccia, A.D., Rose, K.L., Wang, J., Zhao, B., Popay, T.M., Wang, C.E., Guerrazzi, K., Hill, S., Woodley, C.M., Hansen, T.J. *et al.* (2021) Impact of WIN site inhibitor on the WDR5 interactome. *Cell Rep.*, **34**, 108636.
22. Patel, A., Dharmarajan, V. and Cosgrove, M.S. (2008) Structure of WDR5 bound to mixed lineage leukemia protein-1 peptide. *J. Biol. Chem.*, **283**, 32158-32161.
23. Patel, A., Vought, V.E., Dharmarajan, V. and Cosgrove, M.S. (2008) A conserved arginine-containing motif crucial for the assembly and enzymatic activity of the mixed lineage leukemia protein-1 core complex. *J. Biol. Chem.*, **283**, 32162-32175.

24. Song, J.J. and Kingston, R.E. (2008) WDR5 interacts with mixed lineage leukemia (MLL) protein via the histone H3-binding pocket. *J. Biol. Chem.*, **283**, 35258-35264.
25. Odho, Z., Southall, S.M. and Wilson, J.R. (2010) Characterization of a novel WDR5-binding site that recruits RbBP5 through a conserved motif to enhance methylation of histone H3 lysine 4 by mixed lineage leukemia protein-1. *J. Biol. Chem.*, **285**, 32967-32976.
26. Chacón Simon, S., Wang, F., Thomas, L.R., Phan, J., Zhao, B., Olejniczak, E.T., Macdonald, J.D., Shaw, J.G., Schlund, C., Payne, W. *et al.* (2020) Discovery of WD Repeat-Containing Protein 5 (WDR5)-MYC Inhibitors Using Fragment-Based Methods and Structure-Based Design. *J. Med. Chem.*, **63**, 4315-4333.
27. Gao, J., Chang, M.T., Johnsen, H.C., Gao, S.P., Sylvester, B.E., Sumer, S.O., Zhang, H., Solit, D.B., Taylor, B.S., Schultz, N. *et al.* (2017) 3D clusters of somatic mutations in cancer reveal numerous rare mutations as functional targets. *Genome Med.*, **9**, 4.
28. Acuner, S.E., Sumbul, F., Torun, H. and Haliloglu, T. (2021) Oncogenic mutations on Rac1 affect global intrinsic dynamics underlying GTP and PAK1 binding. *Biophys. J.*, **120**, 866-876.
29. Forbes, S.A., Beare, D., Bindal, N., Bamford, S., Ward, S., Cole, C.G., Jia, M., Kok, C., Boutselakis, H., De, T. *et al.* (2016) COSMIC: High-Resolution Cancer Genetics Using the Catalogue of Somatic Mutations in Cancer. *Curr. Protoc. Hum Genet.*, **91**, 10.11.11-10.11.37.
30. Tate, J.G., Bamford, S., Jubb, H.C., Sondka, Z., Beare, D.M., Bindal, N., Boutselakis, H., Cole, C.G., Creatore, C., Dawson, E. *et al.* (2019) COSMIC: the Catalogue Of Somatic Mutations In Cancer. *Nucleic Acids Res.*, **47**, D941-d947.
31. Torkamani, A. and Schork, N.J. (2008) Prediction of cancer driver mutations in protein kinases. *Cancer. Res.*, **68**, 1675-1682.
32. Ryslik, G.A., Cheng, Y., Modis, Y. and Zhao, H. (2016) Leveraging protein quaternary structure to identify oncogenic driver mutations. *BMC Bioinformatics*, **17**, 137.
33. Kumar, S., Clarke, D. and Gerstein, M.B. (2019) Leveraging protein dynamics to identify cancer mutational hotspots using 3D structures. *Proceedings of the National Academy of Sciences of the United States of America*, **116**, 18962-18970.
34. Kamburov, A., Lawrence, M.S., Polak, P., Leshchiner, I., Lage, K., Golub, T.R., Lander, E.S. and Getz, G. (2015) Comprehensive assessment of

- cancer missense mutation clustering in protein structures. *Proceedings of the National Academy of Sciences of the United States of America*, **112**, E5486-5495.
35. Dharmarajan, V., Lee, J.H., Patel, A., Skalnik, D.G. and Cosgrove, M.S. (2012) Structural basis for WDR5 interaction (Win) motif recognition in human SET1 family histone methyltransferases. *J. Biol. Chem.*, **287**, 27275-27289.
 36. Zhang, P., Lee, H., Brunzelle, J.S. and Couture, J.F. (2012) The plasticity of WDR5 peptide-binding cleft enables the binding of the SET1 family of histone methyltransferases. *Nucleic Acids Res.*, **40**, 4237-4246.
 37. Muntean, A.G. and Hess, J.L. (2012) The pathogenesis of mixed-lineage leukemia. *Annu. Rev. Pathol.*, **7**, 283-301.
 38. Chen, X., Xie, W., Gu, P., Cai, Q., Wang, B., Xie, Y., Dong, W., He, W., Zhong, G., Lin, T. *et al.* (2015) Upregulated WDR5 promotes proliferation, self-renewal and chemoresistance in bladder cancer via mediating H3K4 trimethylation. *Sci. Rep.*, **5**, 8293.
 39. Chen, X., Gu, P., Li, K., Xie, W., Chen, C., Lin, T. and Huang, J. (2015) Gene expression profiling of WDR5 regulated genes in bladder cancer. *Genom. Data*, **5**, 27-29.
 40. Ge, Z., Song, E.J., Kawasawa, Y.I., Li, J., Dovat, S. and Song, C. (2016) WDR5 high expression and its effect on tumorigenesis in leukemia. *Oncotarget*, **7**, 37740-37754.
 41. Sun, W., Guo, F. and Liu, M. (2018) Up-regulated WDR5 promotes gastric cancer formation by induced cyclin D1 expression. *J. Cell. Biochem.*, **119**, 3304-3316.
 42. Wang, F., Zhang, J., Ke, X., Peng, W., Zhao, G., Peng, S., Xu, J., Xu, B. and Cui, H. (2020) WDR5-Myc axis promotes the progression of glioblastoma and neuroblastoma by transcriptional activating CARM1. *Biochem. Biophys. Res. Commun.*, **523**, 699-706.
 43. Bryan, A.F., Wang, J., Howard, G.C., Guarnaccia, A.D., Woodley, C.M., Aho, E.R., Rellinger, E.J., Matlock, B.K., Flaherty, D.K., Lorey, S.L. *et al.* (2020) WDR5 is a conserved regulator of protein synthesis gene expression. *Nucleic Acids Res.*, **48**, 2924-2941.
 44. Imran, A., Moyer, B.S., Canning, A.J., Kalina, D., Duncan, T.M., Moody, K.J., Wolfe, A.J., Cosgrove, M.S. and Movileanu, L. (2021) Kinetics of the multitasking high-affinity Win binding site of WDR5 in restricted and unrestricted conditions. *Biochem. J.*, **478**, 2145-2161.

45. Mayse, L.A., Imran, A., Larimi, M.G., Cosgrove, M.S., Wolfe, A.J. and Movileanu, L. (2022) Disentangling the recognition complexity of a protein hub using a nanopore. *Nature Commun.*, **13**, 978.
46. Karatas, H., Townsend, E.C., Cao, F., Chen, Y., Bernard, D., Liu, L., Lei, M., Dou, Y. and Wang, S. (2013) High-affinity, small-molecule peptidomimetic inhibitors of MLL1/WDR5 protein-protein interaction. *J. Am. Chem. Soc.*, **135**, 669-682.
47. Cao, F., Townsend, E.C., Karatas, H., Xu, J., Li, L., Lee, S., Liu, L., Chen, Y., Ouillette, P., Zhu, J. *et al.* (2014) Targeting MLL1 H3K4 methyltransferase activity in mixed-lineage leukemia. *Mol. Cell.*, **53**, 247-261.
48. Alicea-Velázquez, N.L., Shinsky, S.A., Loh, D.M., Lee, J.H., Skalnik, D.G. and Cosgrove, M.S. (2016) Targeted Disruption of the Interaction between WD-40 Repeat Protein 5 (WDR5) and Mixed Lineage Leukemia (MLL)/SET1 Family Proteins Specifically Inhibits MLL1 and SETd1A Methyltransferase Complexes. *J. Biol. Chem.*, **291**, 22357-22372.
49. Karatas, H., Li, Y., Liu, L., Ji, J., Lee, S., Chen, Y., Yang, J., Huang, L., Bernard, D., Xu, J. *et al.* (2017) Discovery of a Highly Potent, Cell-Permeable Macrocyclic Peptidomimetic (MM-589) Targeting the WD Repeat Domain 5 Protein (WDR5)-Mixed Lineage Leukemia (MLL) Protein-Protein Interaction. *J. Med. Chem.*, **60**, 4818-4839.
50. Schapira, M., Tyers, M., Torrent, M. and Arrowsmith, C.H. (2017) WD40 repeat domain proteins: a novel target class? *Nat. Rev. Drug Discov.*, **16**, 773-786.
51. Aho, E.R., Weissmiller, A.M., Fesik, S.W. and Tansey, W.P. (2019) Targeting WDR5: A WINning Anti-Cancer Strategy? *Epigenet. Insights*, **12**, 2516865719865282.
52. Aho, E.R., Wang, J., Gogliotti, R.D., Howard, G.C., Phan, J., Acharya, P., Macdonald, J.D., Cheng, K., Lorey, S.L., Lu, B. *et al.* (2019) Displacement of WDR5 from Chromatin by a WIN Site Inhibitor with Picomolar Affinity. *Cell Rep.*, **26**, 2916-2928.e2913.
53. Dennis, M.L., Morrow, B.J., Dolezal, O., Cuzzupe, A.N., Stuppel, A.E., Newman, J., Bentley, J., Hattarki, M., Nuttall, S.D., Foitzik, R.C. *et al.* (2019) Fragment screening for a protein-protein interaction inhibitor to WDR5. *Struct. Dyn.*, **6**, 064701.
54. Bolshan, Y., Getlik, M., Kuznetsova, E., Wasney, G.A., Hajian, T., Poda, G., Nguyen, K.T., Wu, H., Dombrovski, L., Dong, A. *et al.* (2013) Synthesis, Optimization, and Evaluation of Novel Small Molecules as Antagonists of WDR5-MLL Interaction. *ACS Med. Chem. Lett.*, **4**, 353-357.

55. Getlik, M., Smil, D., Zepeda-Velázquez, C., Bolshan, Y., Poda, G., Wu, H., Dong, A., Kuznetsova, E., Marcellus, R., Senisterra, G. *et al.* (2016) Structure-Based Optimization of a Small Molecule Antagonist of the Interaction Between WD Repeat-Containing Protein 5 (WDR5) and Mixed-Lineage Leukemia 1 (MLL1). *J. Med. Chem.*, **59**, 2478-2496.
56. Schapira, M. and Arrowsmith, C.H. (2016) Methyltransferase inhibitors for modulation of the epigenome and beyond. *Curr. Opin. Chem. Biol.*, **33**, 81-87.
57. Gupta, A., Xu, J., Lee, S., Tsai, S.T., Zhou, B., Kurosawa, K., Werner, M.S., Koide, A., Ruthenburg, A.J., Dou, Y. *et al.* (2018) Facile target validation in an animal model with intracellularly expressed monobodies. *Nat. Chem. Biol.*, **14**, 895-900.
58. Concepcion, J., Witte, K., Wartchow, C., Choo, S., Yao, D., Persson, H., Wei, J., Li, P., Heidecker, B., Ma, W. *et al.* (2009) Label-free detection of biomolecular interactions using BioLayer interferometry for kinetic characterization. *Comb. Chem. High Throughput Screen.*, **12**, 791-800.
59. Weeramange, C.J., Fairlamb, M.S., Singh, D., Fenton, A.W. and Swint-Kruse, L. (2020) The strengths and limitations of using biolayer interferometry to monitor equilibrium titrations of biomolecules. *Protein Sci.*, **29**, 1018-1034.
60. Wolfe, A.J., Si, W., Zhang, Z., Blanden, A.R., Hsueh, Y.C., Gugel, J.F., Pham, B., Chen, M., Loh, S.N., Rozovsky, S. *et al.* (2017) Quantification of membrane protein-detergent complex interactions. *J. Phys. Chem. B*, **121**, 10228-10241.
61. Wolfe, A.J., Gugel, J.F., Chen, M. and Movileanu, L. (2018) Kinetics of Membrane Protein-Detergent Interactions Depend on Protein Electrostatics. *J. Phys. Chem. B*, **122**, 9471-9481.
62. Forbes, S.A., Beare, D., Boutselakis, H., Bamford, S., Bindal, N., Tate, J., Cole, C.G., Ward, S., Dawson, E., Ponting, L. *et al.* (2017) COSMIC: somatic cancer genetics at high-resolution. *Nucleic Acids Res.*, **45**, D777-d783.
63. Movileanu, L., Cheley, S., Howorka, S., Braha, O. and Bayley, H. (2001) Location of a Constriction in the Lumen of a Transmembrane Pore by Targeted Covalent Attachment of Polymer Molecules. *J. Gen. Physiol.*, **117**, 239-251.
64. Jarmoskaite, I., AlSadhan, I., Vaidyanathan, P.P. and Herschlag, D. (2020) How to measure and evaluate binding affinities. *eLife*, **9**.
65. Wolfe, A.J., Hsueh, Y.C., Blanden, A.R., Mohammad, M.M., Pham, B.,

- Thakur, A.K., Loh, S.N., Chen, M. and Movileanu, L. (2017) Interrogating Detergent Desolvation of Nanopore-Forming Proteins by Fluorescence Polarization Spectroscopy. *Analytical chemistry*, **89**, 8013-8020.
66. Kumar, S. and Nussinov, R. (2002) Relationship between ion pair geometries and electrostatic strengths in proteins. *Biophys. J.*, **83**, 1595-1612.
67. Nogal, B., Bowman, C.A. and Ward, A.B. (2017) Time-course, negative-stain electron microscopy-based analysis for investigating protein-protein interactions at the single-molecule level. *J. Biol. Chem.*, **292**, 19400-19410.
68. Shinsky, S.A. and Cosgrove, M.S. (2015) Unique Role of the WD-40 Repeat Protein 5 (WDR5) Subunit within the Mixed Lineage Leukemia 3 (MLL3) Histone Methyltransferase Complex. *J. Biol. Chem.*, **290**, 25819-25833.
69. Ali, A., Veeranki, S.N. and Tyagi, S. (2014) A SET-domain-independent role of WRAD complex in cell-cycle regulatory function of mixed lineage leukemia. *Nucleic Acids Res.*, **42**, 7611-7624.

Chapter 4: The Interplay of Affinity and Surface Tethering in Protein Recognition

Ali Imran,¹ Brandon S. Moyer,^{2,3} Aaron J. Wolfe,^{1,2,3,4}
Michael S. Cosgrove,⁵ Dmitrii E. Makarov,^{6,7} and Liviu Movileanu^{1,8,9,*}

¹*Department of Physics, Syracuse University, 201 Physics Building, Syracuse, New York 13244-1130, USA*

²*Ichor Life Sciences, Inc., 2651 US Route 11, LaFayette, New York 13084, USA*

³*Lewis School of Health Sciences, Clarkson University, 8 Clarkson Avenue, Potsdam, New York 13699*

⁴*Department of Chemistry, State University of New York College of Environmental Science and Forestry, 1 Forestry Dr., Syracuse, New York 13210, USA*

⁵*Department of Biochemistry and Molecular Biology, State University of New York Upstate Medical University, 4249 Weiskotten Hall, 766 Irving Avenue, Syracuse, New York 13210, USA*

⁶*Department of Chemistry, University of Texas at Austin, Austin, Texas 78712, USA*

⁷*Oden Institute for Computational Engineering and Sciences, University of Texas at Austin, Austin, Texas 78712, USA.*

⁸*Department of Biomedical and Chemical Engineering, Syracuse University, 329 Link Hall, Syracuse, New York 13244, USA*

⁹*The BioInspired Institute, Syracuse University, Syracuse, New York 13244, USA*

This chapter is adapted from “Imran, A; Moyer, B. S.; Wolfe, A. J.; Cosgrove, M. S.; Makarov, D. E.; Movileanu, L. The Interplay of Affinity and Surface Tethering in Protein Recognition, *J. Phys. Chem. Lett.*, 2022, 13(18), 4021-4028.” <https://doi.org/10.1021/acs.jpcclett.2c00621>

4.1 Abstract

Surface-tethered ligand-receptor complexes are key components in biological signaling and adhesion. They also find increasing utility in single-molecule assays and biotechnological applications. Here, we study the real-time binding kinetics between various surface-immobilized peptide ligands and their unrestrained receptors. A long peptide tether increases the association of ligand-receptor complexes, experimentally proving the fly-casting mechanism where the disorder accelerates protein recognition. On the other hand, a short peptide tether enhances the complex dissociation. Notably, the rate constants measured for the same receptor, but under different spatial constraints, are strongly correlated with one another. Furthermore, this correlation can be used to predict how surface tethering on a ligand-receptor complex alters its binding kinetics. Our results have immediate implications in the broad areas of biomolecular recognition, intrinsically disordered proteins, and biosensor technology.

4.2 Introduction

Tethered ligand-receptor complexes are common in protein recognition^{1,2} and cellular adhesion.³ Surface-bound ligand-protein complexes are also the basis for biotechnological applications, such as biosensors⁴⁻⁹ and cell-targeted therapeutic proteins,^{10,11} as well as for single-molecule techniques that probe the dynamics and thermodynamics of protein binding.¹²⁻¹⁶ Yet, how the presence of spatial constraints imposed by the surface and/or the tether affects the thermodynamics and, especially, kinetics of binding is largely an open experimental question. Most of the current insight in this topic comes from theoretical¹⁷⁻²¹ and computational^{10,22-24} studies. However, experimental examinations of tethered ligand-protein interactions are mostly limited to measuring macroscopic intermolecular forces,²⁵⁻²⁸ equilibrium dissociation constants,²⁹ and effective protein concentrations.^{29,30}

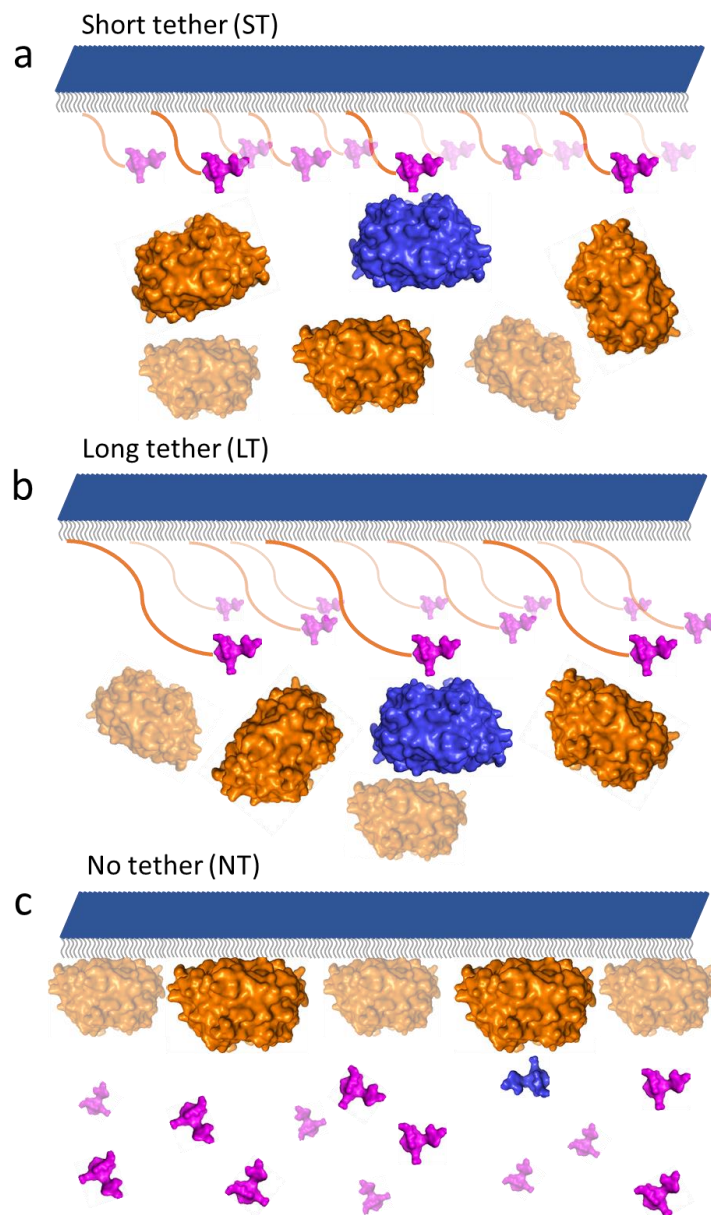


Figure 1: WDR5 protein interacting with the SET1_{win} peptide ligands under different conditions. WDR5 is shown in orange, while SET1_{win} ligands are shown in magenta. Bound interacting partners are shown in blue. Lightly colored receptors and ligands indicate interacting partners in the background. **(a)** Biotinylated ST-SET1_{win} ligands were chemically attached onto a streptavidin-coated biolayer interferometry (BLI) sensor surface. Either WDR5 proteins or one of its mutants were freely movable in solution. **(b)** The same system as in (a), but with LT-SET1_{win} ligands. **(c)** Either WDR5 proteins or one of its mutants were immobilized onto a surface plasmon resonance (SPR) chip surface, whereas the NT-SET1_{win} ligands were freely movable in solution.

In contrast to the earlier experimental work, this study focuses on the question of how the kinetics of binding and unbinding is altered by the tethering of one of the binding partners to a surface. To this end, we measure the real-time kinetics of tethered ligand-receptor complexes using surface immobilization-based sensing approaches. In our case, the receptor is WD40 repeat protein 5 (WDR5),^{31,32} a chromatin-associated hub that is primarily known for its regulatory role in histone methylation.^{33,34} The 334-residue WDR5 features a seven-bladed β propeller circular structure and a central cavity. The WDR5 cavity hosts the binding site for the WDR5-interaction (Win) motif of human mixed lineage leukemia (MLL/SET1) methyltransferases, also named the Win binding site. We examined details of the interactions of five 14-residue Win motif peptide ligands of SET1 proteins (SET1_{Win} ligands; **Supplementary Table 1** and **Supplemental Methods**)^{35,36} with WDR5 via its Win binding site. SET1_{Win} ligands were chemically attached to a streptavidin-coated surface. Either a 3-residue short peptide tether (ST-SET1_{Win} ligands; **Fig. 1a**) or a 9-residue long peptide tether (LT-SET1_{Win} ligands; **Fig. 1b**) was inserted between the biotinylated attachment site of the SET1_{Win} ligand to the surface and the SET1_{Win} sequence. In this way, the binding kinetics of the WDR5-SET1_{Win} complex were probed using biolayer interferometry (BLI).³⁷ The association and dissociation phases of the tethered ligand-receptor complex were discriminated optically using changes in the interference pattern of reflected light waves at the sensor surface. Hence, these interactions were monitored using WDR5-containing and WDR5-free assay buffers, respectively. Tethered ligand-receptor interactions were also evaluated

using Win binding site-directed WDR5 mutants (**Supplementary Table 2** and **Supplemental Methods**). To further examine the binding kinetics in the absence of restraining tethers, WDR5 proteins were immobilized on the surface plasmon resonance (SPR) sensors³⁸ (no tether, NT-SET1_{win} ligands; **Fig. 1c**).

4.3 Results and Discussion

We obtained the real-time kinetics of five SET1_{win} peptide ligands (MLL2_{win}, MLL3_{win}, MLL4_{win}, SETd1A_{win}, and SETd1B_{win}) with four WDR5 proteins (wild-type and 3 mutants of the Win binding site, P216L, F133L, and S218F) using ST and LT constraints (**Supplementary Figs. 1-2 Tables 3-5**). Later, we validated the outcomes of this study using S175L, a fourth WDR5 mutant of unknown affinity. Interestingly, the association rate constants, k_a , acquired with LT-SET1_{win} ligands (k_{a-LT}) were on average higher than those corresponding values recorded with ST-SET1_{win} ligands (k_{a-ST}) (**Fig. 2a; Supplementary Table 6**). To explain this observation, we considered the general framework of diffusion-controlled reactions,³⁹⁻⁴¹ which gives the following association rate constant:

$$k_a = (k_D^{-1} + k_R^{-1})^{-1}$$

(1)

where k_R is the reaction-controlled rate constant and

$$k_D = 4\pi D_{rel} a$$

(2)

is the diffusion-controlled rate constant that depends on the relative diffusion coefficient of the two reacting species, D_{rel} , and on a “geometric” parameter, a . In the limit $k_{\text{R}} \gg k_{\text{D}}$, the association is purely diffusion controlled and $k_{\text{a}} \approx k_{\text{D}}$.⁴²

Eq. 2 may be loosely interpreted as the rate constant of the association process happening instantaneously upon the reactants diffusing into a favorable relative configuration. This configuration is characterized by a linear length scale, a .

Notably, simple dimensionality arguments require that the diffusion-controlled rate constant, k_{D} , must be of the form of **Eq. 2**. Hence, **Eq. 2** can be viewed as the definition of the *effective* “target” size of the diffusion-controlled reaction.

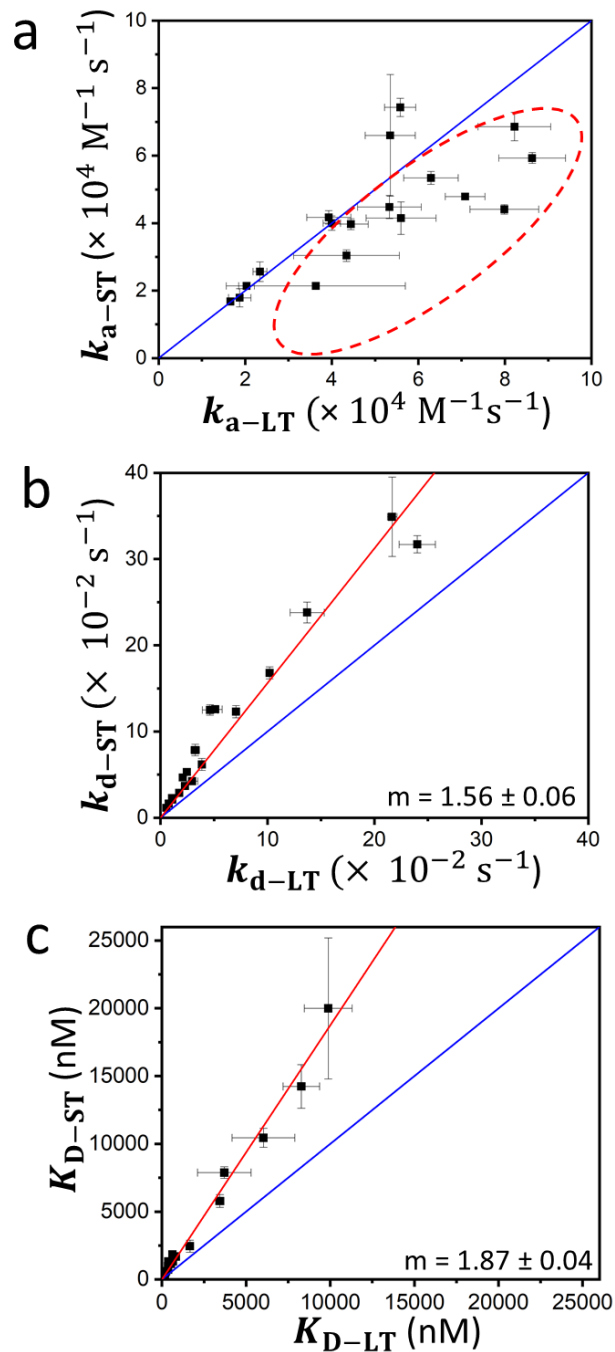


Figure 2: Scatter plots of kinetic and equilibrium constants for ST-SET1_{win} and LT-SET1_{win} ligands. (a) Association rate constants k_{a-ST} of ST-SET1_{win}-WDR5 complexes plotted against association rate constants k_{a-LT} of LT-SET1_{win}-WDR5 complexes. Points above the blue line correspond to complexes with faster association rate constants for ST-SET1_{win} ligands, while points below correspond to interactions with slower association rate constants for ST-SET1_{win} ligands. (b) Dissociation rate constants k_{d-ST} of ST-SET1_{win}-WDR5 complexes plotted against

dissociation rate constants k_{d-LT} of LT-SET1_{win}-WDR5 complexes. Points above the blue line correspond to complexes with faster dissociation rate constants for ST-SET1_{win} ligands. (c) Equilibrium dissociation constants K_{D-ST} of ST-SET1_{win}-WDR5 complexes plotted against equilibrium dissociation constants K_{D-LT} of LT-SET1_{win}-WDR5 complexes. Points above the blue line correspond to less stable complexes with ST-SET1_{win} ligands. m indicate the slopes of linear fits in panels (b) and (c). Data represent mean \pm s.d. that resulted from three independent BLI sensorgrams.

There are two notable examples of this equation. First, Smoluchowski (1917) has obtained a formula for the diffusion-controlled rate constant, where the association process between two spherically symmetrical reactants takes place whenever their distance reaches the “capture radius” value a .^{43,44} Second, Berg and Purcell (1977) derived a formula for the rate constant of the process where a freely diffusing particle hits a patch on a planar wall, with a being the linear size of the patch.⁴⁵ The Berg and Purcell's scenario can be viewed as a prototype for the system studied here, as one of the reactants is surface immobilized. It should be noted that the length parameter, a , generally depends on the interaction between the reactants.^{39,41} For example, the electrostatic attraction between them leads to a larger “capture radius”.

Equipped with these ideas, we consider the difference between the cases of ST- and LT-SET1_{win} ligands. The much smaller, surface-attached SET1_{win} ligand diffuses rapidly, with a diffusion coefficient $D_{SET1win} \gg D_{WDR5}$. Diffusion of the SET1_{win} ligand occurs around its attachment point within a certain volume, which depends on the tether length. This suggests a simple model of association, as follows. Like in Berg and Purcell's model,⁴⁵ the surface-attached SET1_{win} ligand

appears as target with a characteristic size, a , to a freely diffusing WDR5. Because of the complicated geometry of the system, it is challenging to derive a simple expression for a . LT-SET1_{win} can deviate further from the attachment point than ST-SET1_{win}. Therefore, LT-SET1_{win} is a bigger “target” for the WDR5 than ST-SET1_{win} (i.e., $a_{LT} > a_{ST}$), so the association rate constant for LT-SET1_{win}, k_{a-LT} , is higher than that for ST-SET1_{win}, k_{a-ST} , as observed in **Fig. 2a**. Note, however, that this picture is expected to break down in the limit of long tethers where further increase of the tether length results in a larger search volume that has to be explored by the binding partners, reducing the overall association rate. Indeed, as recently discussed by Misiura and Kolomeisky,⁴⁶ the dependence of the association rate constant on the tether length is non-monotonic, with the maximum association speedup occurring at an intermediate tether length.

The association speedup induced by a longer tether found here is an experimental validation of the “fly-casting association mechanism,” which was proposed earlier by Wolynes and coworkers on theoretical grounds and computational analysis⁴⁷⁻⁴⁹ and discussed later by others.^{13,46,50-54} This mechanism explains how intrinsically disordered proteins with random-coil conformations can bind faster to their targets.^{12,55} Because of the geometric nature of the parameter a , it is expectable that the ratio of a values for LT-SET1_{win} and ST-SET1_{win}, a_{LT}/a_{ST} , is nearly the same for all SET1_{win} ligands. Indeed, we observe a linear correlation between the association rate constants for LT-SET1_{win} and ST-SET1_{win}, k_{a-LT} and k_{a-ST} , respectively (**Fig. 2a**). But recalling that the

parameter a also depends on the energetics of the interactions, deviations from a perfectly linear correlation are not surprising.

In contrast to the association rate constants, the dissociation rate constants for ST-SET1_{win} ligands, k_{d-ST} , were consistently higher than those for LT-SET1_{win} ligands, k_{d-LT} (**Fig. 2b; Supplementary Tables 7-8**). Furthermore, k_{d-ST} and k_{d-LT} values closely followed a proportionality relationship. To explain these observations, we start with the Arrhenius law for the unimolecular dissociation process:⁴²

$$k_d = \nu \exp\left(-\frac{\Delta G_a}{k_B T}\right),$$

(3)

where ν is a prefactor, and ΔG_a is the activation free energy, which is determined by the strength of cohesive interactions between SET1_{win} and WDR5. It is known that a microscopic object (e.g., a Brownian particle) attached to a surface via a flexible polymer tether experiences a repulsive net force that pushes it away from the surface even when the surface is perfectly neutral. This force is "entropic" in its nature, originating from the fact that the object has more space available when it is further away from the surface. The properties of this force have been theoretically studied by Segall and coworkers,⁵⁶ who showed that it is roughly inversely proportional to the distance from the surface.

Based on the above argument, as the force pushes WDR5 away from the surface, and thus from SET1_{win}, it enhances dissociation by lowering the

dissociation barrier. The simplest approximate description of this mechanochemical effect for the dissociation rate constant, k_d , is the Eyring-Zhurkov-Bell formula:⁵⁷

$$k_d = \nu \exp\left(-\frac{\Delta G_a - f\Delta x}{k_B T}\right) = k_d^0 \exp\left(\frac{f\Delta x}{k_B T}\right), \quad (4)$$

where k_d^0 is k_d at $f = 0$. Here, f is the magnitude of the force, and Δx is an activation length. Hence, k_d^0 is the dissociation rate constant in the absence of the surface. Clearly, the force f for ST-SET1_{win}, f_{ST} , is higher than that for LT-SET1_{win}, f_{LT} . Therefore, the dissociation rate constant for ST-SET1_{win}, k_{d-ST} , is greater than that for LT-SET1_{win}, k_{d-LT} , as observed in **Fig. 2b**. Assuming that the activation length Δx , being again a geometric parameter, is approximately the same for different constructs, the ratio of the two dissociation rate constants should be close to a constant. This should happen even though the rate constants themselves may vary considerably owing to the variation of the activation free energy, ΔG_a , and to exponential sensitivity of the dissociation rate constant to the energetics of interaction. Indeed, this is what we observe in **Fig. 2b**. Despite almost two orders of magnitude variation between the individual k_d constants for each construct, k_{d-ST} and k_{d-LT} remain proportional to each other. Note that the k_a constants for the same constructs vary within a much narrower range, within a maximum factor of ~ 4 , supporting the above proposal that the association process is near the diffusion-controlled limit and thus less sensitive to energetics.

These results suggest that the length of the tether plays a significant role in modulating the interactions of the SET1_{win}-WDR5 complex. An increased physical constraint as a result of a decreased tether length not only reduces the rate constant of complex formation, as established earlier, but also substantially decreases the stability of the complex. Consequently, the overall impact of reducing the tether length is an increase in K_D (**Fig. 2c; Supplementary Tables 9-10**). Changes observed for k_a should normally be independent from those noted for k_d , because the mechanisms of changing the corresponding activation free energies are different. Indeed, we observed no correlation between the k_a and k_d values (**Supplementary Figs. 3-4**).

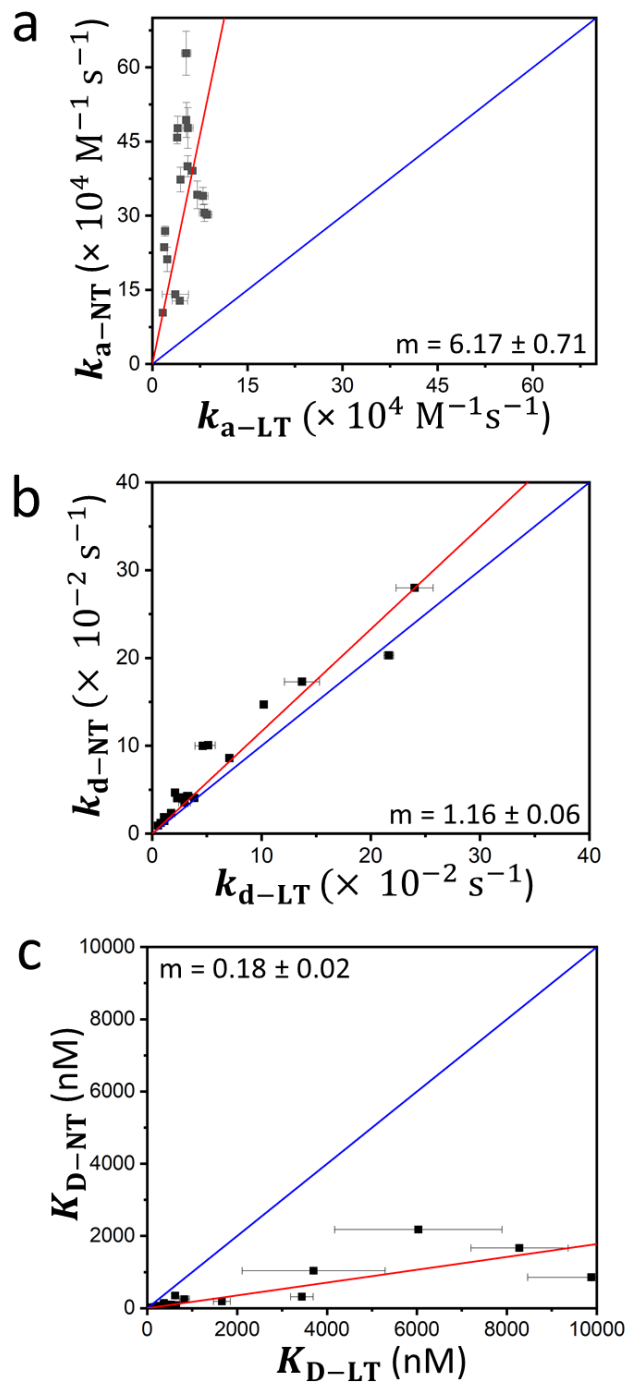


Figure 3: Scatter plots of kinetic and equilibrium constants for NT-SET1_{win} and LT-SET1_{win} ligands. (a) Association rate constants k_{a-NT} of NT-SET1_{win}-WDR5 complexes plotted against association rate constants k_{a-LT} of LT-SET1_{win}-WDR5 complexes. Points above the blue line correspond to interactions with faster association rate constants for NT-SET1_{win} ligands. (b) Dissociation rate constants k_{d-NT} of NT-SET1_{win}-WDR5 complexes plotted against dissociation rate constants k_{d-LT} of LT-SET1_{win}-WDR5 complexes. Points

above the blue line correspond to interactions with faster dissociation rate constants for NT-SET1_{win} ligands.

(c) Equilibrium dissociation constants K_{D-NT} values of NT-SET1_{win}-WDR5 complexes plotted against equilibrium dissociation constants K_{D-LT} of LT-SET1_{win}-WDR5 complexes. Points below the blue line correspond to more stable complexes with LT-SET1_{win} ligands. m indicate the slopes of linear fits in all panels. Data represent mean \pm s.d. that resulted from three independent BLI sensorgrams.

We then measured the kinetic rate constants for 20 ligand-receptor complexes using unrestricted conditions (no tether, NT-SET1_{win} ligands) (**Supplementary Fig. 5 Tables 11-13**). In this case, BLI was not used, because it does not have a satisfactory sensitivity to reliably detect a short-peptide binding to the surface. The SPR,³⁸ with its greater sensitivity, was a more effective choice for this case. Accumulation of ligand-receptor complexes onto the surface of the SPR sensor was monitored by changes in the refractive index. Therefore, WDR5 was immobilized onto the surface of the SPR chips (**Fig. 1c**), and the association and dissociation phases were probed in real time. As established by our previous work,⁵⁸ the k_a values for NT-SET1_{win} ligands were substantially greater than those for LT-SET1_{win} ligands (**Fig. 3a; Supplementary Table 14**). This significant difference is due to the increased translational and rotational diffusion coefficients of NT-SET1_{win} ligands relative to WDR5 and its derivatives. Moreover, our previous work⁵⁸ also showed, by comparison with values obtained from fluorescence polarization (FP) spectroscopy, that immobilizing WDR5 onto the sensor surface does not impact its functional integrity. Let's assume that $D_{NT-SET1win}$ and D_{WDR5} are the translational diffusion coefficients of NT-SET1_{win} and WDR5, respectively. For applying **Eq. 2** to this problem, one now has to consider that $D_{NT-SET1win} \gg D_{WDR5}$, since either WDR5 or one of its

derivatives was immobilized on the sensor surface. Therefore, the unrestrained NT-SET1_{win} was responsible for the diffusion-mediated mutual approach of the reacting species, so $D_{\text{rel}} \approx D_{\text{NT-SET1}_{\text{win}}}$. Again, **Eq. 2** predicts proportionality between $k_{\text{a-NT}}$ and $k_{\text{a-LT}}$, as noted in **Fig. 3a**, with the ratio of the two roughly equal to the ratio of SET1_{win}'s and WDR5's diffusion coefficients.

Remarkably, the k_{d} values using NT-SET1_{win} and LT-SET1_{win} ligands were closely similar (**Fig. 3b; Supplementary Table 15**). Our interpretation of this finding is in terms of **Eq. 4**. In the case of LT-SET1_{win} ligands, but not for ST-SET1_{win} ligands, the repulsive force f is negligible as the complex is far enough from the surface. Hence, the dissociation rate constant is near that value corresponding to the zero-force limit, k_{d}^0 , which is the dissociation rate constant for NT-SET1_{win} ligands, $k_{\text{d-NT}}$. In other words, at long enough tether lengths, the experimental system approaches that of NT-SET1_{win} ligands in terms of the dissociation rate constant, k_{d} . Therefore, the equilibrium dissociation constant, K_{D} , of the ligand-receptor complex becomes larger as we go from NT-SET1_{win} ligands to LT-SET1_{win} ligands (**Fig. 3c; Supplementary Tables 16-17**).

Moreover, the differential free energy of the ligand-receptor complex formation, $\Delta\Delta G$, for NT-SET1_{win} ligands with respect to LT-SET1_{win} ligands is in the range -0.3 through -1.5 kcal/mol. The primary contribution to this change results from the considerable increase in the k_{a} in the absence of the tether. This shows how the attachment of a binding partner to a surface influences the overall dynamic equilibrium of the interaction. In our case, the effect is substantial given the large

difference in size between the two binding partners. Even though for NT-SET1_{win} ligands the WDR5 is restricted to the surface, the comparison between similar restriction and steady-state fluorescence polarization (FP) data of freely interacting SET1_{win} and WDR5 in solution shows that this condition can be thought as that of an unrestricted interaction.⁵⁸

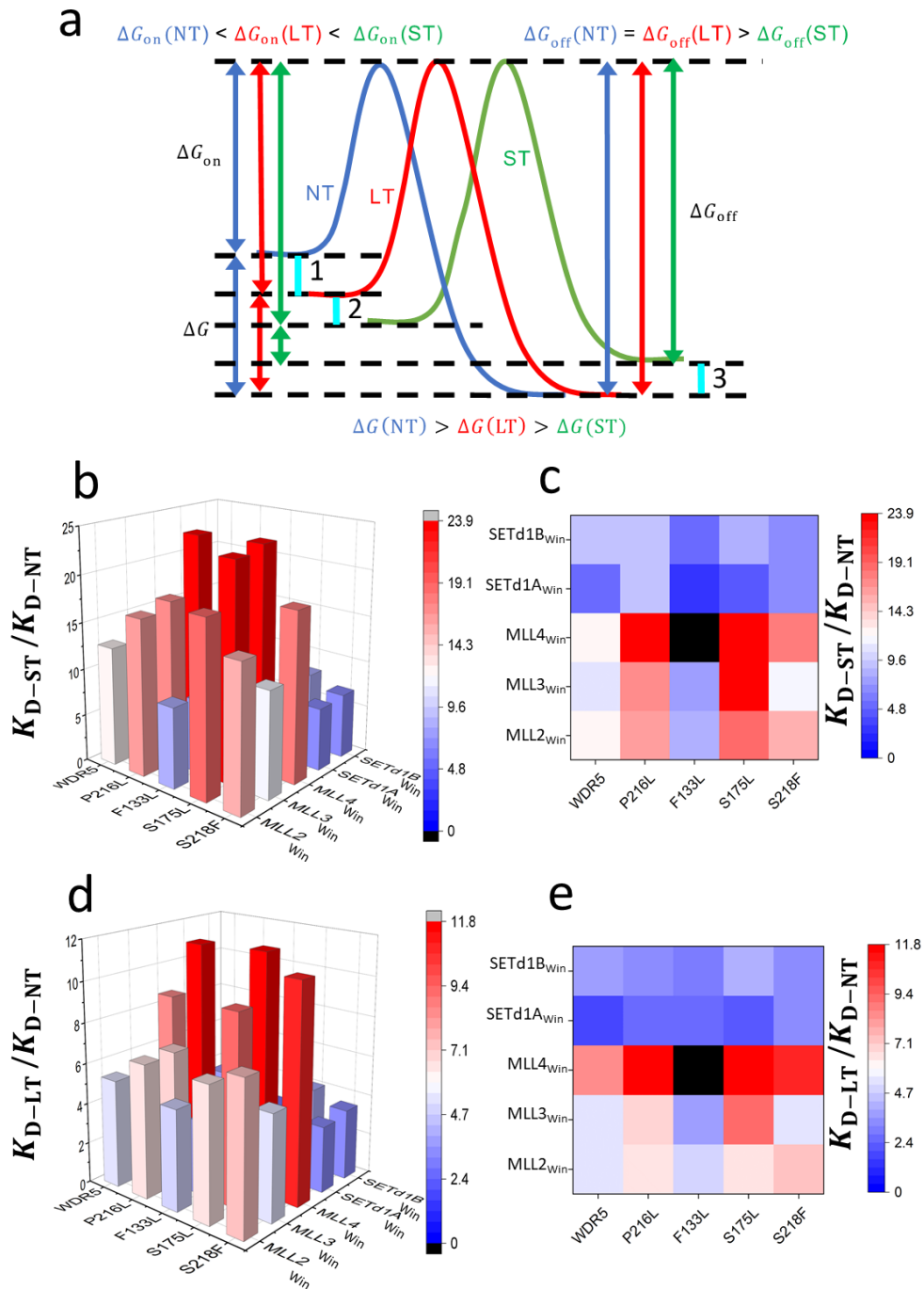


Figure 4: 3D plots and contour maps of normalized K_D constants. (a) Qualitative free energy landscapes of SET1_{win}-WDR5 interactions when NT-SET1_{win} (NT), ST-SET1_{win} (ST), and LT-SET1_{win} (LT) peptide ligands were used. Vertical lines 1, 2, and 3, which are marked in cyan, indicate the differential free energy barriers due to unrestrained diffusion of the ligand, fly-casting mechanism, and repulsion entropic forces of the receptor from the sensor surface, respectively. (b) Bar graph and (c) contour map of K_{D-ST} values for the interaction

of ST-SET1_{Win} ligands, with WDR5 and its mutants, divided by their corresponding K_{D-NT} values measured with the corresponding NT-SET1_{Win} ligands. **(d)** Bar graph and **(e)** contour map of K_{D-LT} values for the interaction of LT-SET1_{Win} ligands, with WDR5 and its mutants, divided by their corresponding K_{D-NT} values measured with the corresponding NT-SET1_{Win} ligands. K_{D-ST} and K_{D-LT} for MLL4_{Win}-F133L interactions could not be quantitatively determined using BLI measurements. These data points are colored in black.

In **Fig. 4a**, we illustrate a qualitative comparison of the free energy landscapes that correspond to NT-SET1_{Win}, ST-SET1_{Win}, and LT-SET1_{Win} ligands. For short and long tethers, the presence of the flexible tether reduces the association rate constant of the SET1_{Win}-WDR5 complex with respect to that in the absence of the tether (**Supplementary Fig. 6**). Further increase in the k_{d-ST} with respect to k_{d-LT} (**Supplementary Fig. 7**) due to repulsion forces of WDR5 proteins from the sensor surface explains the relative increase in the normalized values $(K_{D-ST}/K_{D-NT}) > (K_{D-LT}/K_{D-NT})$ (**Fig. 4b-e**). Because there are linear correlations between measured affinities of various SET1_{Win}-WDR5 pairs with specified constraints, we can advantageously utilize these findings to predict the k_d and K_D for a given tethered ligand-receptor complex. To demonstrate this, we examined the interactions of SET1_{Win} ligands with S175L, a WDR5 derivative, whose single-site mutation is located within the Win binding site. Using the kinetic and equilibrium parameters measured for NT-SET1_{Win}-S175L interactions via SPR (**Supplementary Tables 12-13**), we established the proportionality relationships with their corresponding parameters for ST-SET1_{Win} ligands (**Supplementary Fig. 8**). Remarkably, our experimental determinations of k_{d-ST} for S175L against 5 ST-SET1_{Win} ligands are closely similar to corresponding anticipated values

(**Table 1**). Furthermore, using the same method we demonstrate the predictive power of this approach for the K_{D-ST} values (**Table 2**). Therefore, the binding affinity of tethered ligand-receptor interactions can be precisely modulated by changing the tether length (**Supplementary Fig. 9**).

Table 1: Table showing the predicted and experimental values of the k_{d-ST} for S175L interacting with ST-SET1_{win}. k_{d-ST} are the dissociation rate constants corresponding to ST-SET1_{win} ligands. Predicted values of k_{d-ST} were obtained using the proportionality relationship between k_{d-ST} and k_{d-NT} (**Supplementary Fig. 8**) and the experimentally determined values of k_{d-NT} (**Supplementary Table 12**). Triplicate k_{d-NT} values were used to calculate corresponding k_{d-ST} values by linear interpolation. Values indicate mean \pm s.d., which were calculated using these triplicates.

Parameter	SET1 _{win}	Predicted values $\times 10^3$ (s ⁻¹)	Experimental values $\times 10^3$ (s ⁻¹)
k_{d-ST}	MLL2 _{win}	14 \pm 1	12 \pm 1
	MLL3 _{win}	36 \pm 1	28 \pm 1
	MLL4 _{win}	190 \pm 10	180 \pm 10
	SETd1A _{win}	300 \pm 10	160 \pm 10
	SETd1B _{win}	13 \pm 1	5.4 \pm 0.2

Table 2: Table showing the predicted and experimental values of the K_{D-ST} for S175L interacting with ST-SET1_{win}. K_{D-ST} are the equilibrium dissociation constants corresponding to ST-SET1_{win} ligands. Predicted values of K_{D-ST} were obtained using the proportionality relationship between K_{D-ST} and K_{D-NT} (**Supplementary Fig. 8**) and the experimentally determined values of K_{D-NT} (**Supplementary Table 13**). Triplicate K_{D-NT} values were used to calculate corresponding K_{D-ST} values by linear interpolation. Values indicate mean \pm s.d., which were calculated using these triplicates.

Parameter	SET1 _{win}	Predicted values $\times 10^9$ (M)	Experimental values $\times 10^9$ (M)
K_{D-ST}	MLL2 _{win}	150 \pm 10	360 \pm 30
	MLL3 _{win}	270 \pm 10	810 \pm 90
	MLL4 _{win}	2,800 \pm 100	8,500 \pm 300
	SETd1A _{win}	5,500 \pm 200	2,900 \pm 100
	SETd1B _{win}	110 \pm 10	110 \pm 6

4.4 Conclusion

In summary, we provide compelling experimental evidence for the fly-casting mechanism of association between surface-attached peptide ligands and their receptors. The observed speedup in the association rate k_a when using a longer tether is rather modest for the tether lengths employed here, which agrees with previous computational work.⁴⁷ We also found that the dissociation rate constant was greater in the case of a short tether length as a result of entropic repulsion forces acting on the receptor pulling it away from the surface. Accordingly, this resulted in a weakened interaction of the tethered ligand-protein complex. As a longer tether accelerates the association but decelerates the dissociation, the binding affinity of the ligand-receptor complex is greater at increased tether lengths. Our experimental approach can be used to predict dissociation rate constants and binding affinities of ligand-protein interactions for specified physicochemical properties of the tether. Therefore, our method can be employed in biosensor technology to modulate the interaction strength of a ligand-protein complex on a sensing surface by modifying the tether length. Finally, this result has been successfully validated using a test WDR5 mutant of unknown dissociation constant for five ST-SET1_{win} ligands.

4.5 SUPPLEMENTARY INFORMATION

The Interplay of Affinity and Surface Tethering in Protein Recognition

**Ali Imran,¹ Brandon S. Moyer,² Aaron J. Wolfe,^{1,2,3,4} Michael S. Cosgrove,⁵
Dmitrii E. Makarov,^{6,7} and Liviu Movileanu^{1,8,9,*}**

¹*Department of Physics, Syracuse University, 201 Physics Building, Syracuse,
New York 13244-1130, USA*

²*Ichor Life Sciences, Inc., 2651 US Route 11, LaFayette, New York 13084, USA*

³*Department of Chemistry, State University of New York College of
Environmental Science and Forestry, 1 Forestry Dr., Syracuse, New York 13210,
USA*

⁴*Lewis School of Health Sciences, Clarkson University, 8 Clarkson Avenue,
Potsdam, New York 13699*

⁵*Department of Biochemistry and Molecular Biology, State University of New York
Upstate Medical University, 4249 Weiskotten Hall, 766 Irving Avenue, Syracuse, New
York 13210, USA*

⁶*Department of Chemistry, University of Texas at Austin, Austin, Texas 78712,
USA*

⁷*Oden Institute for Computational Engineering and Sciences, University of Texas
at Austin, Austin, Texas 78712, USA.*

⁸*Department of Biomedical and Chemical Engineering, Syracuse University, 329
Link Hall, Syracuse, New York 13244, USA*

⁹*The BioInspired Institute, Syracuse University, Syracuse, New York 13244, USA*

Table of Contents (TOC) - Supplementary Information

1. Materials and Methods (**Supplementary Tables S1-S2**).
 - 1.1. Peptide synthesis, purification, and analysis
 - 1.2. Protein expression and purification.
 - 1.3. Biolayer interferometry (BLI).
 - 1.4. Surface plasmon resonance (SPR).
2. Examples of BLI sensorgrams for probing real-time kinetics of SET1_{win}-WDR5 interactions (**Supplementary Figs. S1-S2**).
3. Determinations of the kinetic and equilibrium constants of the interactions of ST-SET1_{win} ligands with WDR5 receptors using BLI measurements (**Supplementary Tables S3-S5**).
4. The kinetic and equilibrium constants of the interactions of ST-SET1_{win} ligands with WDR5 receptors normalized to the corresponding values of LT-SET1_{win} ligands (**Supplementary Tables S6-S10**).
5. Scatter plots of the association rate constants versus the dissociation rate constants using linear- and logarithm-scale representations (**Supplementary Figs. S3-S4**).
6. Examples of SPR sensorgrams for probing real-time kinetics of NT-SET1_{win}-WDR5 interactions (**Supplementary Fig. S5**).
7. Determinations of the kinetic and equilibrium constants of the interactions of NT-SET1_{win} ligands with WDR5 receptors using SPR measurements (**Supplementary Tables S11-S13**).
8. The kinetic and equilibrium constants of the interactions of NT-SET1_{win} ligands with WDR5 receptors normalized to the corresponding values of LT-SET1_{win} ligands (**Supplementary Tables S14-S17**).
9. The 3D plots and contour maps of the association rate constants under ST and LT conditions normalized to those recorded under NT conditions (**Supplementary Fig. S6**).
10. The 3D plots and contour maps of the dissociation rate constants under ST and LT conditions normalized to those recorded under NT conditions (**Supplementary Fig. S7**).
11. Scatter plots of kinetic and equilibrium constants for the ST, LT, and NT experiments (**Supplementary Figs. S8-S9**).

12. Supporting references.

1. Materials and Methods

1.1. Peptide synthesis, purification, and analysis. For BLI measurements, 14-residue SET1_{win} peptide ligands were synthesized and purified to $\geq 95\%$ purity by GenScript (Piscataway, NJ). These peptide ligands were biotinylated at their N terminus and amidated at their C terminus. Their sequence is provided in **Table S1**, which is displayed below.

Table S1: List of 14-residue SET1_{win} peptide ligands used in biolayer interferometry (BLI) measurements. An either a 3-residue short tether (ST) or a 9-residue long tether (LT) was inserted between the biotinylated attachment site and SET1_{win} sequence. The tether sequence is marked in blue. The SET1_{win} sequence is marked in red.

#	SET1 _{win}	Tether length	Ligand sequence
1	ST-MLL2 _{win}	ST	Biotinyl-(GGS)INPTGCARSEPKIL _{NH2}
2	ST-MLL3 _{win}	ST	Biotinyl-(GGS)VNPTGCARSEPKMS _{NH2}
3	ST-MLL4 _{win}	ST	Biotinyl-(GGS)LNPHGAARAEVYLS _{NH2}
4	ST-SETd1A _{win}	ST	Biotinyl-(GGS)EHQTGSARSEGYY _{NH2}
5	ST-SETd1B _{win}	ST	Biotinyl-(GGS)EHVTGCARSEGFYT _{NH2}
6	LT-MLL2 _{win}	LT	Biotinyl-(GGS) ₃ INPTGCARSEPKIL _{NH2}
7	LT-MLL3 _{win}	LT	Biotinyl-(GGS) ₃ VNPTGCARSEPKMS _{NH2}
8	LT-MLL4 _{win}	LT	Biotinyl-(GGS) ₃ LNPHGAARAEVYLS _{NH2}
9	LT-SETd1A _{win}	LT	Biotinyl-(GGS) ₃ EHQTGSARSEGYY _{NH2}
10	LT-SETd1B _{win}	LT	Biotinyl-(GGS) ₃ EHVTGCARSEGFYT _{NH2}

Purity confirmation, amino acid analysis, and solubility testing were conducted and provided by GenScript. For SPR measurements, SET1_{win} peptide ligands were synthesized, purified, and analyzed in-house at Ichor Life Sciences (LaFayette, NY). Details on these procedures and protocols were previously provided¹. Peptide synthesis was performed using a Biotage Syro I peptide synthesizer (Biotage, Charlotte, NC). Peptide purification was achieved using reversed-phase chromatography in two steps: (1) flash chromatography employing a Biotage Isolera One (Biotage AB, Uppsala, Sweden), and (2) semi-preparative high-performance liquid chromatography (HPLC) using a Waters 2695 separations module, which was coupled with a Waters 2996 photodiode array detector (PDA).

1.2. Protein expression and purification. In this study, all expression plasmids were synthesized, codon optimized, and sequence verified by GenScript (Piscataway, NJ). Human WDR5 (UniProtKB - P61964; WDR5_HUMAN) and its mutants were expressed and purified as described previously.¹⁻³ WDR5 construct design has the following sequence:

6H-TEV-WDR5 in pET3aTr vector (Addgene, Watertown, MA). The detailed WDR5 sequence (sequence fragments marked in yellow are linkers) is the following:

MHHHHHSSGVDLGTENLYFQSNGATEEKKPETEAARAQPTPSSSATQ
 SKPTPVKPNYALKFTLAGHTKAVSSVKFSPNGEWLASSADKLIKIWG
 AYDGKFEKTISGHKLGISDVAWSSDSNLLVSASDDKTLKIWDVSSGKC
 LKTLKGHSNYVFCNFPQSNLIVSGSFDESRIWDVKTGKCLKTLPA
 HSDPVSAVHFNRDGLIVSSSYDGLCRIWDTASGQCLKTLIDDDNPPVS
 FVKFSPNGKYILAAATLDNTLKLWDYSKGKCLKTYTGHKNEKYCIFAN
 FSVTGGKWIVSGSEDNLVYIWNLQTKEIVQKLQGHTDVVISTACHPT
 ENIIASAALENDKTIKLWKSDC

Table S2: This table shows WDR5 mutants used in this study. These WDR5 mutants involve amino acid side chains within the Win binding site of WDR5.⁴⁻⁶

Entry	WDR5 Mutant
1	P216L
2	F133L
3	S218F
4	S175L

1.3. Biolayer interferometry (BLI). These measurements were conducted using an Octet RED384 instrument (FortéBio, Fremont, CA) at 24°C.⁷ The assay buffer included 150 mM NaCl, 20 mM Tris-HCl, 1 mM TCEP, 1 mg/mL bovine serum albumin (BSA), pH 7.5. Streptavidin-coated biosensors were incubated with 5 nM biotinylated SET1_{Win} for 15 minutes. Then, the unbound peptides were washed out by rinsing the sensors in assay buffer. These experimental conditions were optimized to amplify the signal-to-noise ratio while preventing potential artifacts. These include the rebinding of receptors to the surface-immobilized peptide ligands during the dissociation phase. Prior crystallographic studies demonstrated that these ligand-receptor interactions follow a 1:1 binding model.⁸⁻⁹ The association process was monitored by exposing the sensors to 3-fold serial dilutions of WDR5 proteins. The dissociation phase was probed by transferring the sensors into WDR5-free assay buffer. The association phases were fitted using the equation:¹⁰

$$Y = Y_{\infty} - (Y_{\infty} - Y_0)e^{-k_{\text{obs}}t} \quad (\text{S1})$$

Here, Y_0 and Y_{∞} denote the responses at the initial time and infinity, respectively. k_{obs} is the apparent first-order reaction rate constant of the association phase. t represents the cumulative time of the association reaction. The dissociation phases were fitted using the equation:

$$Y = Y_{\infty} + (Y_0 - Y_{\infty})e^{-k_{\text{off}}t} \quad (\text{S2})$$

Here, k_{off} indicates the dissociation rate constant. Y_0 and Y_{∞} are the responses at the initial time and infinity, respectively. Finally, the association rate constant, k_{on} , was determined using the slope of the linear curve:¹¹⁻¹²

$$k_{\text{obs}} = k_{\text{on}}[C] + k_{\text{off}}$$

(S3)

Then, global fittings were achieved using several WDR5 (or WDR5 mutant) concentrations. These fittings provided the corresponding k_{on} and k_{off} values. Equilibrium dissociation constant values, K_{D} , were indirectly determined using the k_{on} and k_{off} values ($K_{\text{D}} = k_{\text{off}}/k_{\text{on}}$). Three independent BLI measurements were conducted for all conditions in this study.

1.4. Surface plasmon resonance (SPR). In this study, all SPR measurements were conducted using a Cytiva Biacore 8K instrument (Cytiva Life Sciences, Marlborough, MA), as previously reported.¹ WDR5 proteins were immobilized onto the active flow cell of each channel of a Cytiva Series S Sensor Chip CM5 (Cytiva Life Sciences). The sensor surface was then activated using an injection of 1:1 N-hydroxysuccinimide (NHS)/1-ethyl-3-(3-dimethylaminopropyl)carbodiimide (EDC) (Cytiva Amine Coupling Kit, Cytiva Life Sciences). The protein sample was then injected across the active flow cell. Finally, both active and passive flow cells were chemically deactivated. Multicycle kinetic analyses were conducted at a flow cell temperature of 25°C and a sample compartment temperature of 20°C in a running buffer composed of 20 mM Tris-HCl (pH 7.5), 150 mM NaCl, 1 mM TCEP, 0.05% Tween 20. Biacore™ Insight Evaluation Software v3 (Cytiva Life Sciences) was employed to analyze and fit the sensorgrams using a 1:1 binding interaction model to provide the association (k_{a}) and dissociation (k_{d}) rate constants. The K_{D} were calculated indirectly using $K_{\text{D}} = k_{\text{d}}/k_{\text{a}}$.

2. Examples of BLI sensorgrams and fittings for probing the real-time kinetics of $SET1_{win}$ -WDR5 interactions.

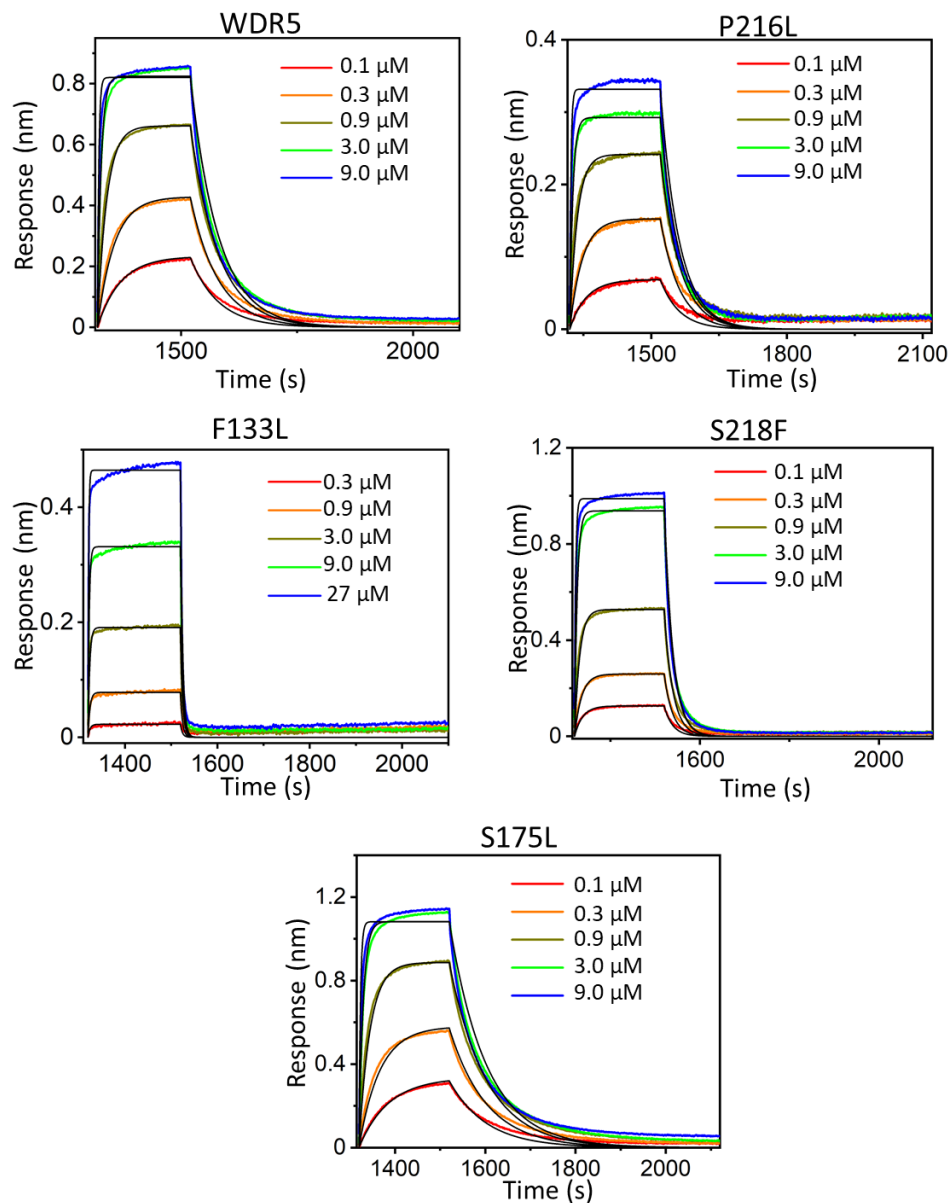


Figure S1: BLI sensorgrams of ST-MLL2_{win} interacting with WDR5 and its mutants. 5 nM biotinylated ST-MLL2_{win} was loaded onto streptavidin-coated sensors for 15 minutes. 3-fold serial dilutions of WDR5 and its mutants were used to obtain individual binding curves. These sensorgrams were fitted to obtain k_{a-ST} , k_{d-ST} , and K_{D-ST} (eqns. (S1)-(S3)). The fits are shown in black.

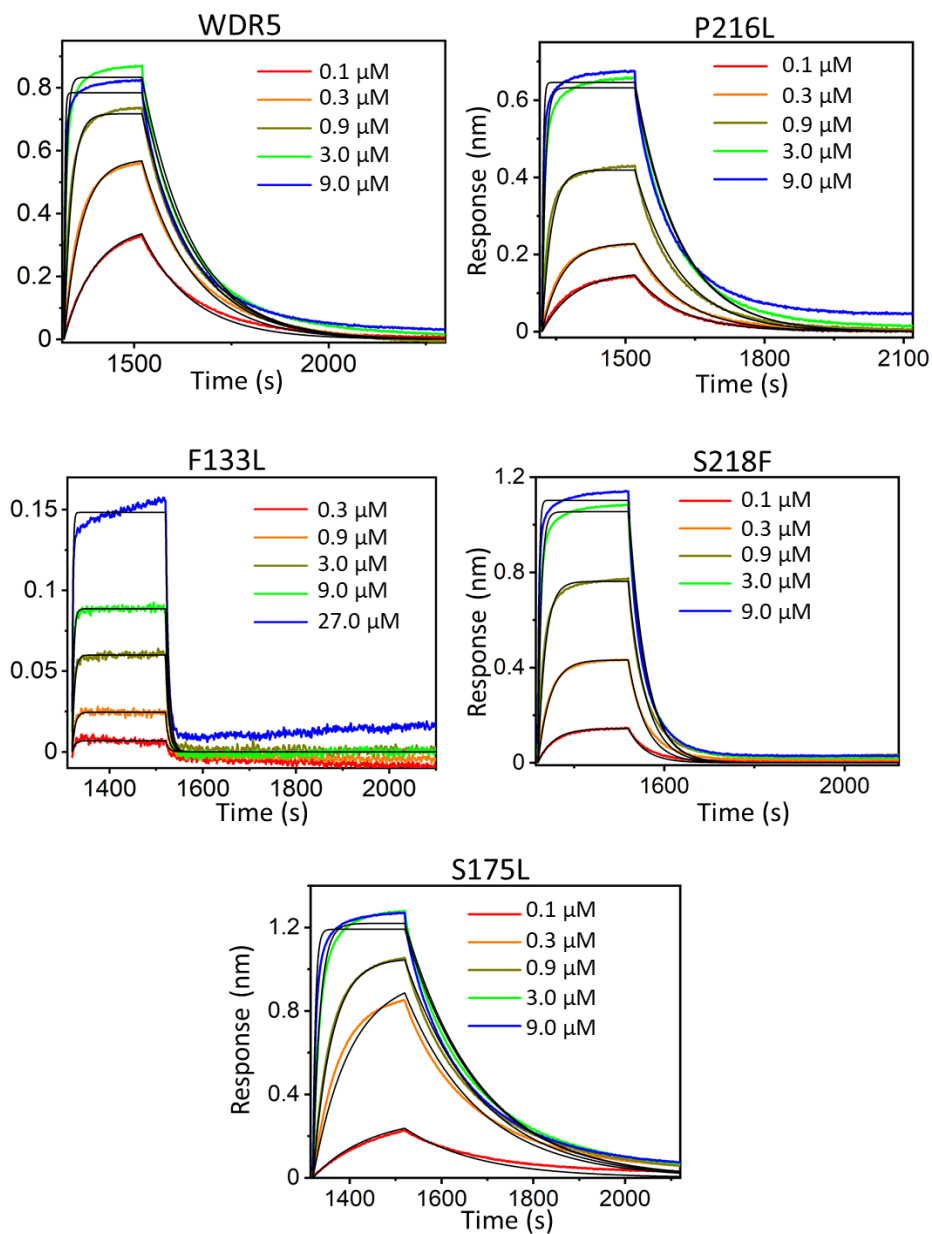


Figure S2: BLI sensorgrams of LT-MLL2_{win} interacting with WDR5 and its mutants. 5 nM biotinylated LT-MLL2_{win} was loaded onto streptavidin-coated sensors for 15 minutes. 3-fold serial dilutions of WDR5 and its mutants were used to obtain individual binding curves. These sensorgrams were fitted to obtain k_{a-LT} , k_{d-LT} , and K_{D-LT} (eqns. (S1)-(S3)). The fits are shown in black.

3. Determinations of the kinetic and equilibrium constants of the interactions of ST-SET1_{win} ligands with WDR5 receptors using BLI measurements.

Table S3: Kinetic rate constants of association, k_{a-ST} , of WDR5 and its mutants with ST-SET1_{win} ligands using BLI measurements. 5 nM biotinylated ST-SET1_{win} were loaded onto streptavidin-coated sensors for 15 minutes. 3-fold serial dilutions of WDR5 and its mutants, ranging from 0.1 μ M to 9 μ M, were used to obtain individual binding curves. The buffer solution contained 150 mM NaCl, 20 mM Tris-HCl, 1 mM TCEP, 1 mg/ml bovine serum albumin (BSA), pH 7.5. The binding curves were fitted using the Octet Data Analysis software. k_{a-ST} values were provided in $(M^{-1} s^{-1}) \times 10^{-4}$. For F133L, 3-fold serial dilutions ranging from 0.3 μ M to 27 μ M were used. Numbers represent mean \pm s.d. determined from three independent BLI experimental determinations.

Peptide	WDR5	P216L	F133L*	S175L**	S218F
MLL2	4.0 \pm 0.2	4.2 \pm 0.5	1.7 \pm 0.1	3.4 \pm 0.3	4.0 \pm 0.2
MLL3	6.6 \pm 1.8	4.5 \pm 0.3	2.1 \pm 0.1	3.5 \pm 0.3	4.2 \pm 0.2
MLL4	2.6 \pm 0.3	1.8 \pm 0.3	~ 1	2.0 \pm 0.1	2.1 \pm 0.1
SETd1A	6.9 \pm 0.4	5.9 \pm 0.2	2.7 \pm 0.4	5.7 \pm 0.4	7.4 \pm 0.3
SETd1B	4.8 \pm 0.1	4.4 \pm 0.1	3.0 \pm 0.2	4.8 \pm 0.1	5.3 \pm 0.2

*In this case, k_{a-ST} was in the order of $10^4 M^{-1} s^{-1}$ assuming that the association process is in the range of values determined with the other MLL peptides.

**Experimental values of the test mutant of WDR5.

Table S4: Kinetic rate constants of dissociation, k_{d-ST} , of WDR5 and its mutants with ST-MLL ligands using BLI measurements. The N terminus of ST-SET1_{win} ligands were tagged with biotin and their C-terminus were amidated. 5 nM biotinylated ST-SET1_{win} ligands were loaded onto streptavidin-coated sensors for 15 minutes. 3-fold serial dilutions of WDR5 and its mutants, ranging from 0.1 μ M to 9 μ M, were used to obtain individual binding curves. The buffer solution contained 150 mM NaCl, 20 mM Tris-HCl, 1 mM TCEP, 1 mg/ml bovine serum albumin (BSA), pH 7.5. The binding curves were fitted using the Fortebio Octet Data Analysis software. k_{d-ST} values were provided in $(s^{-1}) \times 10^3$. For F133L, 3-fold serial dilutions ranging from 0.3 μ M to 27 μ M were used. Numbers represent mean \pm s.d. determined from three independent BLI experimental determinations.

Peptide	WDR5	P216L	F133L	S175L**	S218F
MLL2	16 \pm 1	21 \pm 3	240 \pm 10	12 \pm 1	53 \pm 3
MLL3	12 \pm 2	23 \pm 2	170 \pm 10	28 \pm 1	47 \pm 1
MLL4	62 \pm 7	350 \pm 50	> 1000*	180 \pm 10	120 \pm 10

SETd1A	130 ± 10	79 ± 7	760 ± 120	160 ± 10	130 ± 10
SETd1B	29 ± 1	42 ± 3	320 ± 10	5.4 ± 0.2	37 ± 3

*This upper-limit value for the detection of k_{d-ST} is set according to instrument specifications.

**Experimental values of the test mutant of WDR5.

Table S5: Equilibrium dissociation constants, K_{D-ST} , of WDR5 and its mutants with ST-SET1_{win} ligands determined from BLI measurements. The N terminus of ST-SET1_{win} ligands were tagged with biotin and their C-terminus were amidated. 5 nM biotinylated ST-SET1_{win} ligands were loaded onto streptavidin-coated sensors for 15 minutes. 3-fold serial dilutions of WDR5 and its mutants, ranging from 0.1 μM to 9 μM, were used to obtain individual binding curves. The buffer solution contained 150 mM NaCl, 20 mM Tris-HCl, 1 mM TCEP, 1 mg/ml bovine serum albumin (BSA), pH 7.5. The binding curves were fitted using the ForteBio Octet Data Analysis software. For F133L, 3-fold serial dilutions ranging from 0.3 μM to 27 μM were used. K_{D-ST} values were provided in nM. Numbers represent mean ± s.d. determined from three independent BLI experimental determinations.

Peptide	WDR5	P216L	F133L	S175L**	S218F
MLL2	410 ± 22	510 ± 50	14,000 ± 2,000	360 ± 30	1,300 ± 10
MLL3	190 ± 57	530 ± 30	7,900 ± 400	810 ± 90	1,100 ± 100
MLL4	2500 ± 400	20000 ± 5200	≥ 100,000*	8,500 ± 300	5,800 ± 500
SETd1A	1800 ± 200	1300 ± 100	29,000 ± 10,000	2,900 ± 100	1,700 ± 100
SETd1B	600 ± 30	960 ± 100	10,000 ± 1,000	110 ± 6	720 ± 80

*This upper-limit value for the detection of K_{D-ST} results from dividing the upper-limit value of the detection of k_{a-ST} by the value of the k_{a-ST} approximation.

**Experimental values of the test mutant of WDR5.

4. The kinetic and equilibrium constants of the interactions of ST-SET1_{win} ligands with WDR5 receptors normalized to those values corresponding to LT-SET1_{win} ligands.

Table S6: Kinetic rate constant of association, k_{a-ST} , of WDR5 and its mutants, for ST-SET1_{win} ligands divided by the corresponding k_{a-LT} for LT-SET1_{win} ligands. Numbers represent mean ± s.d. determined from three independent BLI experimental determinations.

Peptide	WDR5	P216L	F133L	S175L**	S218F
MLL2	0.89 ± 0.04	0.74 ± 0.10	1.0 ± 0.1	0.69 ± 0.07	1.0 ± 0.1
MLL3	1.2 ± 0.4	0.84 ± 0.08	0.59 ± 0.02	0.71 ± 0.08	1.0 ± 0.1
MLL4	1.1 ± 0.2	0.96 ± 0.17	ND*	0.68 ± 0.03	1.1 ± 0.1
SETd1A	0.83 ± 0.06	0.69 ± 0.02	1.07 ± 0.19	0.93 ± 0.07	1.3 ± 0.1
SETd1B	0.68 ± 0.01	0.55 ± 0.02	0.70 ± 0.05	0.57 ± 0.01	0.85 ± 0.04

*ND stands for “Not Determined.” Interaction between F133L and MLL4 was detectable using a BLI measurement. However, no statistically significant accurate determinations were made due to limited resolution of the approach.

**Experimental values of the test mutant of WDR5.

Table S7: Kinetic rate constant of disassociation, k_{d-ST} , of WDR5 and its mutants interacting with ST-SET1_{win} ligands divided by the corresponding k_{d-LT} for LT-SET1_{win} ligands. Numbers represent mean \pm s.d. determined from three independent BLI experimental determinations.

Peptide	WDR5	P216L	F133L	S175L**	S218F
MLL2	2.1 \pm 0.1	1.9 \pm 0.4	1.7 \pm 0.1	2.0 \pm 0.1	2.2 \pm 0.1
MLL3	2.2 \pm 0.4	2.1 \pm 0.2	1.6 \pm 0.1	1.7 \pm 0.1	2.2 \pm 0.1
MLL4	1.6 \pm 0.2	1.6 \pm 0.2	ND*	1.4 \pm 0.1	1.7 \pm 0.1
SETd1A	2.5 \pm 0.3	2.4 \pm 0.3	1.1 \pm 0.2	1.8 \pm 0.1	2.7 \pm 0.2
SETd1B	1.7 \pm 0.1	1.4 \pm 0.1	1.3 \pm 0.1	1.1 \pm 0.1	1.6 \pm 0.1

*ND stands for “Not Determined.” Interaction between F133L and MLL4 was detectable using a BLI measurement. However, no statistically significant accurate determinations were made due to limited resolution of the approach.

**Experimental values of the test mutant of WDR5.

Table S8: Calculations of the differential activation free energies of the dissociation processes, $\Delta\Delta G_d$, of the interactions of ST-SET1_{win} ligands with respect to those of LT-SET1_{win} ligands. Calculated values of $\Delta\Delta G_d$ are given in kcal/mol. Data are provided as mean \pm s.d. from three independent BLI experimental determinations.

Peptide	WDR5	P216L	F133L	S175L**	S218F
MLL2	-0.45 \pm 0.01	-0.38 \pm 0.12	-0.33 \pm 0.04	-0.40 \pm 0.02	-0.45 \pm 0.04
MLL3	-0.45 \pm 0.10	-0.43 \pm 0.07	-0.30 \pm 0.03	-0.32 \pm 0.02	-0.47 \pm 0.01
MLL4	-0.28 \pm 0.08	-0.28 \pm 0.10	ND*	-0.19 \pm 0.01	-0.33 \pm 0.04
SETd1A	-0.53 \pm 0.06	-1.88 \pm 0.06	-0.04 \pm 0.11	-0.36 \pm 0.03	-0.59 \pm 0.04
SETd1B	-0.30 \pm 0.03	-0.21 \pm 0.06	-0.16 \pm 0.02	-0.06 \pm 0.03	-0.28 \pm 0.05

*ND stands for “Not Determined.” Interaction between F133L and MLL4 was detectable using a BLI measurement. However, no quantitative determinations were made due to limited time resolution of the approach. **Experimental values of the test mutant of WDR5.

Table S9: K_{D-ST} measured with ST-SET1_{win} ligands normalized to the corresponding K_{D-LT} values measured with LT-SET1_{win} ligands. Numbers represent mean \pm s.d. determined from three independent BLI experimental determinations.

Peptide	WDR5	P216L	F133L	S175L**	S218F
MLL2	2.4 \pm 0.2	2.5 \pm 0.3	1.7 \pm 0.2	2.8 \pm 0.3	2.1 \pm 0.1
MLL3	1.9 \pm 0.7	2.6 \pm 0.2	2.1 \pm 0.1	2.5 \pm 0.3	2.2 \pm 0.2
MLL4	1.5 \pm 0.3	2.0 \pm 0.6	ND*	2.0 \pm 0.1	1.7 \pm 0.2
SETd1A	3.0 \pm 0.4	3.5 \pm 0.4	0.96 \pm 0.39	2.0 \pm 0.1	2.0 \pm 0.1
SETd1B	2.4 \pm 0.1	2.6 \pm 0.3	1.7 \pm 0.1	2.0 \pm 0.1	2.0 \pm 0.3

*ND stands for “Not Determined.” Interaction between F133L and MLL4 was detectable using a BLI measurement. However, no quantitative determinations were made due to limited time resolution of the approach. **Experimental values of the test mutant of WDR5.

Table S10: Calculations of the differential activation free energies of the ligand-receptor complex formation, $\Delta\Delta G$, of WDR5-SET1_{win} interactions of ST-SET1_{win} ligands with respect to those of LT-SET1_{win} ligands. Calculated values of $\Delta\Delta G$ are given in kcal/mol. Data are provided as mean \pm s.d. from three independent BLI experimental determinations.

Peptide	WDR5	P216L	F133L	S175L**	S218F
MLL2	0.51 \pm 0.04	0.54 \pm 0.07	0.32 \pm 0.08	0.61 \pm 0.06	0.43 \pm 0.01
MLL3	0.37 \pm 0.21	0.57 \pm 0.05	0.45 \pm 0.04	0.53 \pm 0.08	0.45 \pm 0.05
MLL4	0.22 \pm 0.13	0.40 \pm 0.20	ND*	0.42 \pm 0.02	0.30 \pm 0.06
SETd1A	0.64 \pm 0.07	0.74 \pm 0.07	-0.05 \pm 0.22	0.42 \pm 0.02	0.42 \pm 0.03
SETd1B	0.53 \pm 0.03	0.57 \pm 0.08	0.32 \pm 0.05	0.40 \pm 0.04	0.40 \pm 0.08

*ND stands for “Not Determined.” Interaction between F133L and MLL4 was detectable using a BLI measurement. However, no quantitative determinations were made due to limited time resolution of the approach. **Experimental values of the test mutant of WDR5.

5. Scatter plots of the association rate constants versus the dissociation rate constants using linear- and logarithm-scale representations.

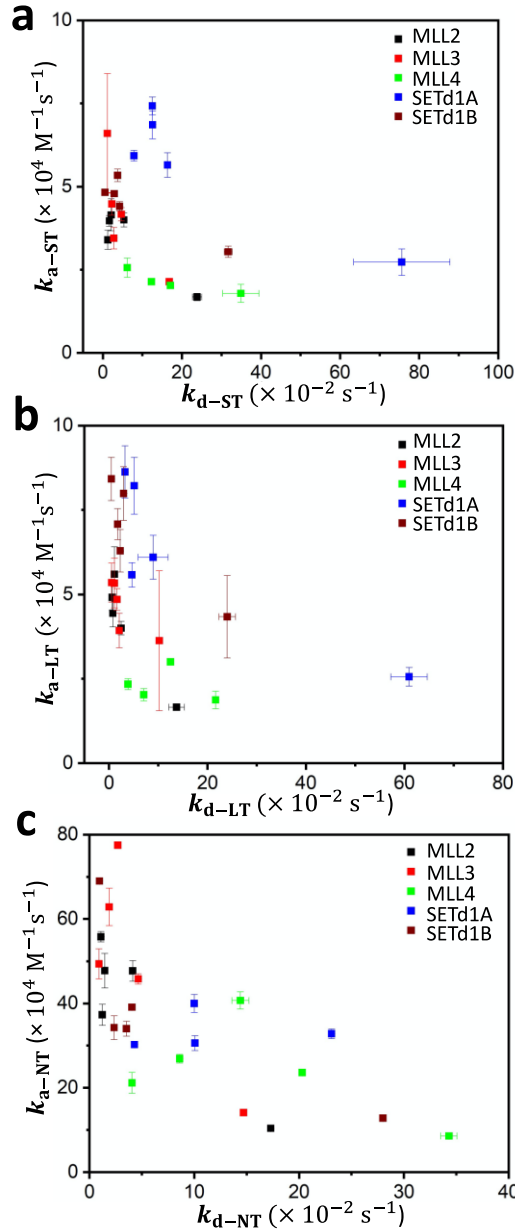


Figure S3: Scatter plots of the association rate constants versus the dissociation rate constants using a linear-scale representation. (a) Data resulted from short-tether (ST) experiments. **(b)** Data resulted from long-tether (LT) experiments. **(c)** Data resulted from no tether (NT) experiments. For ST and LT experiments, MLL4_{Win}-F133L interactions were not quantitatively determined. Hence, they only have four points each for MLL4 (for WDR5, P216L, S218F and S175L). For NT experiments, SETd1A_{Win}-F133L interactions were not quantitatively determined. Therefore, they only have four points for SETd1A (for WDR5, P216L, S218F and S175L). Data are provided as mean \pm s.d. from three independent experimental determinations.

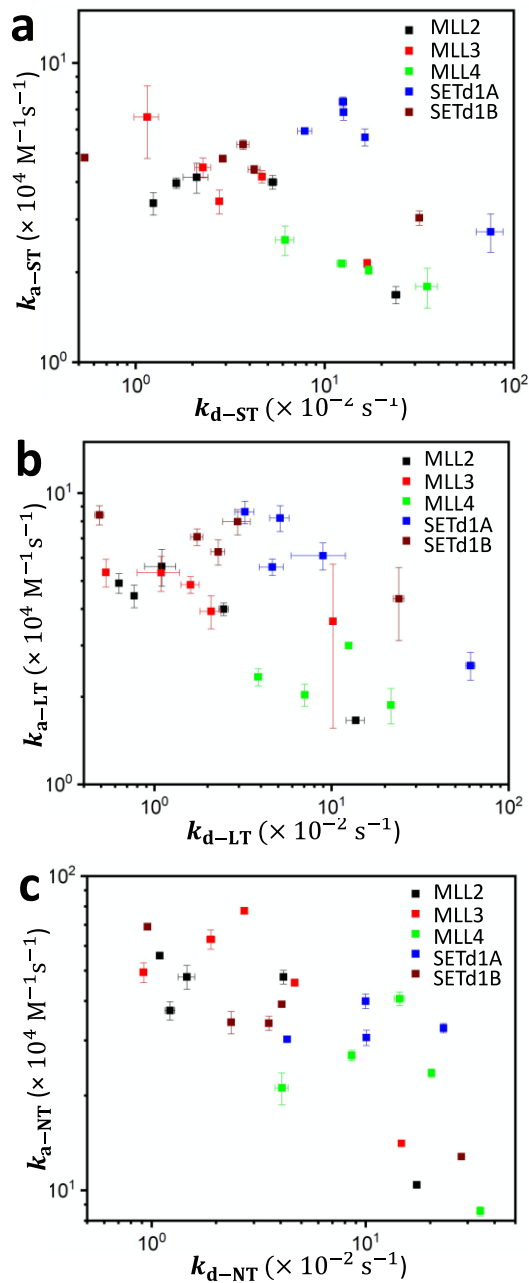


Figure 4: Scatter plots of the association rate constants versus the dissociation rate constants using a logarithm-scale representation. (a) Data resulted from short-tether (ST) experiments. **(b)** Data resulted from long-tether (LT) experiments. **(c)** Data resulted from no tether (NT; SPR) experiments. For ST and LT experiments, MLL4_{win}-F133L interactions were not quantitatively determined. Hence, they only have four points each for MLL4 (for WDR5, P216L, S218F and S175L). For NT experiments, SETd1A_{win}-F133L interactions were not quantitatively determined. Therefore, they only have four points for

SETd1A (for WDR5, P216L, S218F and S175L). Data are provided as mean \pm s.d. from three independent experimental determinations.

6. Examples of SPR sensorgrams and fittings for probing the real-time kinetics of NT-SET1_{win}-WDR5 interactions.

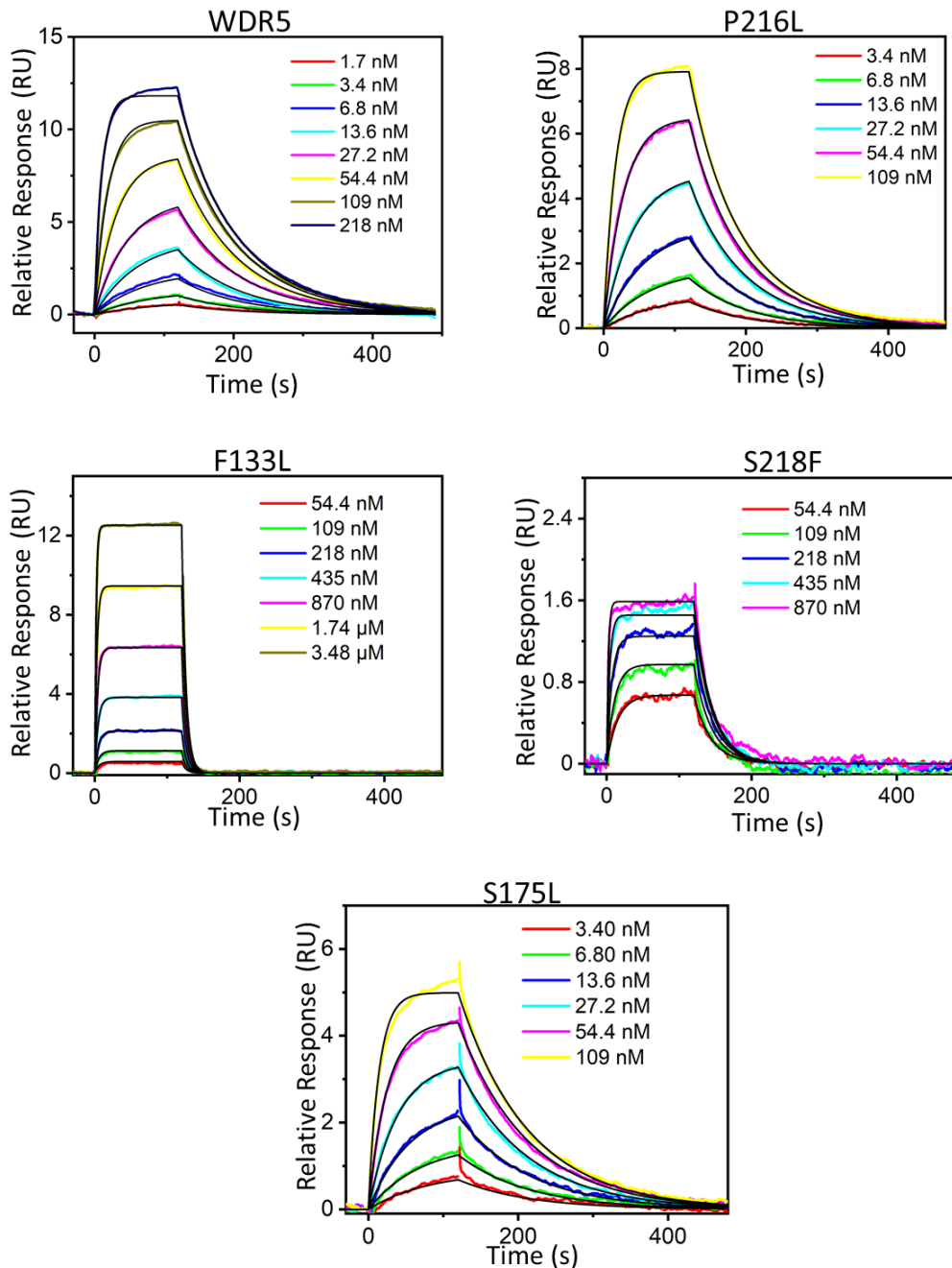


Figure S5: SPR sensorgrams of NT-MLL2_{win} interacting with immobilized WDR5 proteins. WDR5 and its mutants were immobilized onto Cytiva Series S CM5 chips using EDC/NHS amine coupling chemistry in separate experiments. Titration series of no-tether MLL2_{win} (NT-MLL2_{win}) was injected as analyte and

the corresponding association (120 sec.) and dissociation (360 sec.) curves are shown. Data for WDR5 is taken from Imran and co-workers (2021).¹ These sensorgrams were fitted to obtain k_{a-NT} , k_{d-NT} , and K_{D-NT} (eqns. (S1)-S3)). The fits are shown in black.

7. Determinations of the kinetic and equilibrium constants of the interactions of NT-SET1_{win} ligands with WDR5 receptors using SPR measurements.

Table S11: Kinetic rate constants of association, k_{a-NT} , of immobilized WDR5 receptor and its mutants with NT-SET1_{win} ligands using SPR measurements. WDR5 and its mutants were immobilized onto Cytiva Series S CM5 chips using EDC/NHS amine coupling chemistry. Titration series of the respective NT-SET1_{win} ligands were injected as analytes. In the case of the SETd1A-F133L binding interaction, the kinetic constants were outside the limits that could be measured by the instrument. k_{a-NT} values were provided in ($M^{-1}s^{-1}$) $\times 10^{-4}$. Values represent mean \pm s.d. acquired from three independent SPR experimental determinations.

Peptide	WDR5*	P216L	F133L	S175L***	S218F
MLL2	37 \pm 3	48 \pm 4	10 \pm 1	56 \pm 1	48 \pm 2
MLL3	49 \pm 4	63 \pm 4	14 \pm 1	78 \pm 1	46 \pm 1
MLL4	21 \pm 2	24 \pm 1	8.6 \pm 0.3	41 \pm 2	27 \pm 1
SETd1A	31 \pm 2	30 \pm 1	$\sim 10^{**}$	33 \pm 1	40 \pm 2
SETd1B	34 \pm 3	34 \pm 2	13 \pm 1	69 \pm 1	39 \pm 1

*Data from Imran and co-workers.¹ **Interaction between wild-type F133L and SETd1A was detectable using a SPR measurement. However, no quantitative determinations were made due to limited time resolution of the approach. In this case, k_{a-NT} was in the order of $10^5 M^{-1}s^{-1}$ assuming that the association process is in the range of values determined with the other NT-SET1_{win} ligands. ***The test mutant of WDR5.

Table S12: Kinetic rate constants of dissociation, k_{d-NT} , of WDR5 and its mutants with the NT-SET1_{win} ligands using SPR measurements. WDR5 proteins were immobilized onto Cytiva Series S CM5 chips using EDC/NHS amine coupling chemistry. Titration series of the respective SET1_{win} peptide ligands were injected as analytes. In the case of the SETd1A-F133L binding interaction, the kinetic constants were outside the limits that could be measured by the instrument. k_{d-NT} values were provided in (s^{-1}) $\times 10^3$. Values represent mean \pm s.d. acquired from three independent SPR experimental determinations.

Peptide	WDR5*	P216L	F133L	S175L***	S218F
MLL2	12 \pm 1	15 \pm 1	170 \pm 10	11 \pm 1	41 \pm 1
MLL3	9.2 \pm 0.1	19 \pm 1	150 \pm 10	27 \pm 1	47 \pm 1
MLL4	41 \pm 3	200 \pm 10	340 \pm 10	140 \pm 10	86 \pm 2

SETd1A	110 ± 10	43 ± 1	> 500**	230 ± 10	100 ± 10
SETd1B	24 ± 1	35 ± 1	280 ± 10	9.6 ± 0.3	41 ± 1

*Data from Imran and co-workers.¹ **The upper-limit value for the detection of k_{d-NT} using SPR experiments is explicitly specified by the instrument manufacturer. The Biacore 8K+ cannot measure rate constants of dissociation, k_{d-NT} , faster than 0.5 s^{-1} . ***The test mutant of WDR5.

Table S13: Equilibrium dissociation constants, K_{D-NT} , of WDR5 and its mutants with the NT-SET1_{win} ligands using SPR measurements. Either WDR5 or its derivatives was immobilized onto Cytiva Series S CM5 chips using EDC/NHS amine coupling chemistry. Titration series of the respective NT-SET1_{win} ligands were injected as analytes. K_{D-NT} was calculated directly from these kinetic rate constants using $K_D = k_d/k_a$. In the case of the SETd1A-F133L binding interaction, the kinetic constants were outside the limits that could be measured by the instrument. Therefore, an affinity analysis (relative response vs. concentration dose-response curve) was used to calculate the K_{D-NT} . K_{D-NT} values were provided in nM. Values represent mean ± s.d. acquired from three independent SPR experimental determinations.

Peptide	WDR5*	P216L	F133L	S175L***	S218F
MLL2	33 ± 2	31 ± 1	1,700 ± 100	20 ± 1	87 ± 5
MLL3	19 ± 1	30 ± 1	1,000 ± 100	35 ± 1	100 ± 10
MLL4	190 ± 20	860 ± 20	4,000 ± 100	350 ± 10	320 ± 10
SETd1A	350 ± 10	140 ± 10	11,000 ± 1,000**	710 ± 20	250 ± 10
SETd1B	69 ± 6	110 ± 10	2,200 ± 100	14 ± 1	100 ± 10

*Data from Imran and co-workers.¹ **Here, K_{D-NT} was determined using a steady-state SPR measurement. ***The test mutant of WDR5.

8. The kinetic and equilibrium constants of the interactions of NT-SET1_{win} ligands with WDR5 receptors normalized to the corresponding of LT-SET1_{win} ligands.

Table S14: Kinetic rate constant of association, k_{a-NT} , of WDR5 and its mutants, determined by SPR measurements divided by the corresponding k_{a-LT} determined by BLI sensorgrams. Data are provided as mean ± s.d. from three independent experiments.

Peptide	WDR5	P216L	F133L	S175L***	S218F
MLL2	8.4 ± 0.7	8.5 ± 0.7	6.2 ± 0.1	11 ± 1	12 ± 1
MLL3	9.2 ± 0.7	12 ± 1	3.9 ± 0.1	16 ± 1	12 ± 1
MLL4	9.0 ± 1.1	12 ± 1	ND*	14 ± 1	13 ± 1
SETd1A	3.7 ± 0.2	3.5 ± 0.1	ND**	5.4 ± 0.2	7.2 ± 0.4
SETd1B	4.8 ± 0.4	4.3 ± 0.2	3.0 ± 0.1	8.2 ± 0.1	6.2 ± 0.1

*ND stands for “Not Determined.” Interaction between F133L and MLL4 was detectable using a BLI measurement. However, this interaction was not quantitatively determined using BLI due to the limited time resolution of the approach. ** Interaction between F133L and SETd1A was detectable using a SPR measurement. However, this interaction was not quantitatively determined using SPR due to the limited resolution of the approach. ***The test mutant of WDR5.

Table S15: Kinetic rate constants of dissociation, k_{d-NT} , of WDR5 and its mutants, determined by SPR, normalized to the corresponding k_{d-LT} values.

Data are provided as mean \pm s.d. from three independent experiments.

Peptide	WDR5	P216L	F133L	S175L***	S218F
MLL2	1.6 \pm 0.1	1.3 \pm 0.1	1.3 \pm 0.1	1.7 \pm 0.1	1.7 \pm 0.1
MLL3	1.7 \pm 0.1	1.7 \pm 0.1	1.4 \pm 0.1	1.7 \pm 0.1	2.2 \pm 0.1
MLL4	1.1 \pm 0.1	0.94 \pm 0.01	ND*	1.2 \pm 0.1	1.2 \pm 0.1
SETd1A	2.1 \pm 0.1	1.3 \pm 0.1	ND**	2.6 \pm 0.1	2.2 \pm 0.1
SETd1B	1.3 \pm 0.1	1.2 \pm 0.1	1.2 \pm 0.1	2.0 \pm 0.1	1.8 \pm 0.1

*ND stands for “Not Determined.” **The interaction between F133L and SETd1A was detectable using an SPR measurement. Yet, this interaction was not quantitatively determined using BLI due to the limited time resolution of the approach. ***The test mutant of WDR5.

Table S16: K_{D-NT} values determined by SPR measurements, which were normalized to the corresponding K_{D-LT} values determined by BLI measurements.

Data are provided as mean \pm s.d. from three independent experiments.

Peptide	WDR5	P216L	F133L	S175L**	S218F
MLL2	0.19 \pm 0.01	0.15 \pm 0.01	0.20 \pm 0.01	0.15 \pm 0.01	0.13 \pm 0.01
MLL3	0.19 \pm 0.01	0.15 \pm 0.01	0.28 \pm 0.01	0.11 \pm 0.01	0.19 \pm 0.01
MLL4	0.12 \pm 0.01	0.087 \pm 0.002	ND*	0.085 \pm 0.001	0.093 \pm 0.002
SETd1A	0.56 \pm 0.02	0.38 \pm 0.01	0.37 \pm 0.01	0.49 \pm 0.02	0.30 \pm 0.02
SETd1B	0.27 \pm 0.02	0.29 \pm 0.01	0.36 \pm 0.01	0.25 \pm 0.01	0.28 \pm 0.01

ND stands for “Not Determined.” The interaction between F133L and MLL4 was detectable, but not quantifiable using BLI. **The test mutant of WDR5.

Table S17: Differential activation free energies of the ligand-receptor complex formation, $\Delta\Delta G$ (kcal/mol), determined for NT conditions with respect to LT conditions. Data are provided as mean \pm s.d. using three independent experiments.

Peptide	WDR5	P216L	F133L	S175L**	S218F
MLL2	-0.98 \pm 0.03	-1.1 \pm 0.1	-0.94 \pm 0.01	-1.1 \pm 0.1	-1.2 \pm 0.1
MLL3	-0.99 \pm 0.02	-1.1 \pm 0.1	-0.75 \pm 0.01	-1.3 \pm 0.1	-0.97 \pm 0.02
MLL4	-1.3 \pm 0.1	-1.4 \pm 0.1	ND*	-1.5 \pm 0.1	-1.4 \pm 0.1
SETd1A	-0.34 \pm 0.02	-0.57 \pm 0.01	-0.58 \pm 0.01	-0.42 \pm 0.02	-0.70 \pm 0.03
SETd1B	-0.76 \pm 0.05	-0.73 \pm 0.02	-0.60 \pm 0.01	-0.83 \pm 0.02	-0.74 \pm 0.01

*ND stands for “Not Determined.” The interaction between F133L and MLL4 was detectable, but not quantifiable using BLI. **The test mutant of WDR5.

9. The 3D plots and contour maps of the association rate constants under ST and LT conditions normalized to those recorded under NT conditions.

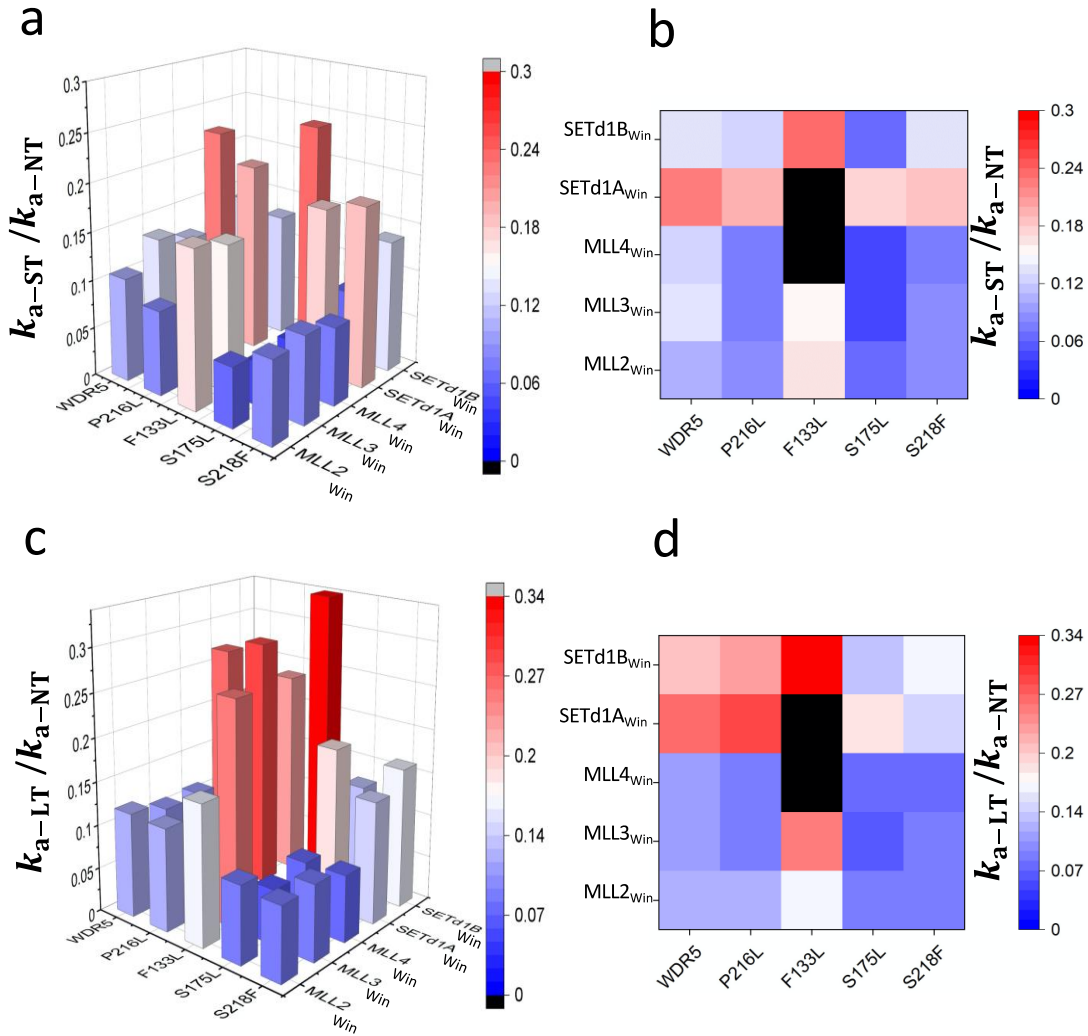


Figure S6: 3D plots and contour maps of the normalized association rate constants. (a) Bar graph and (b) contour map of k_{a-ST} values for the interaction of ST-SET1_{Win} ligands, with WDR5 and its mutants, divided by their corresponding k_{a-NT} values. (c) Bar graph and (d) contour map of k_{a-LT} values for the interaction of LT-SET1_{Win} ligands, with WDR5 and its mutants, divided by their corresponding k_{a-NT} values. k_{a-ST} for the MLL4_{Win}-F133L interactions could not be determined using BLI, while k_{a-NT} of the SETd1A_{Win}-F133L interactions could not be determined using SPR. Therefore, those values are colored in black.

10. The 3D plots and contour maps of the dissociation rate constants under ST and LT conditions normalized to those recorded under NT conditions.

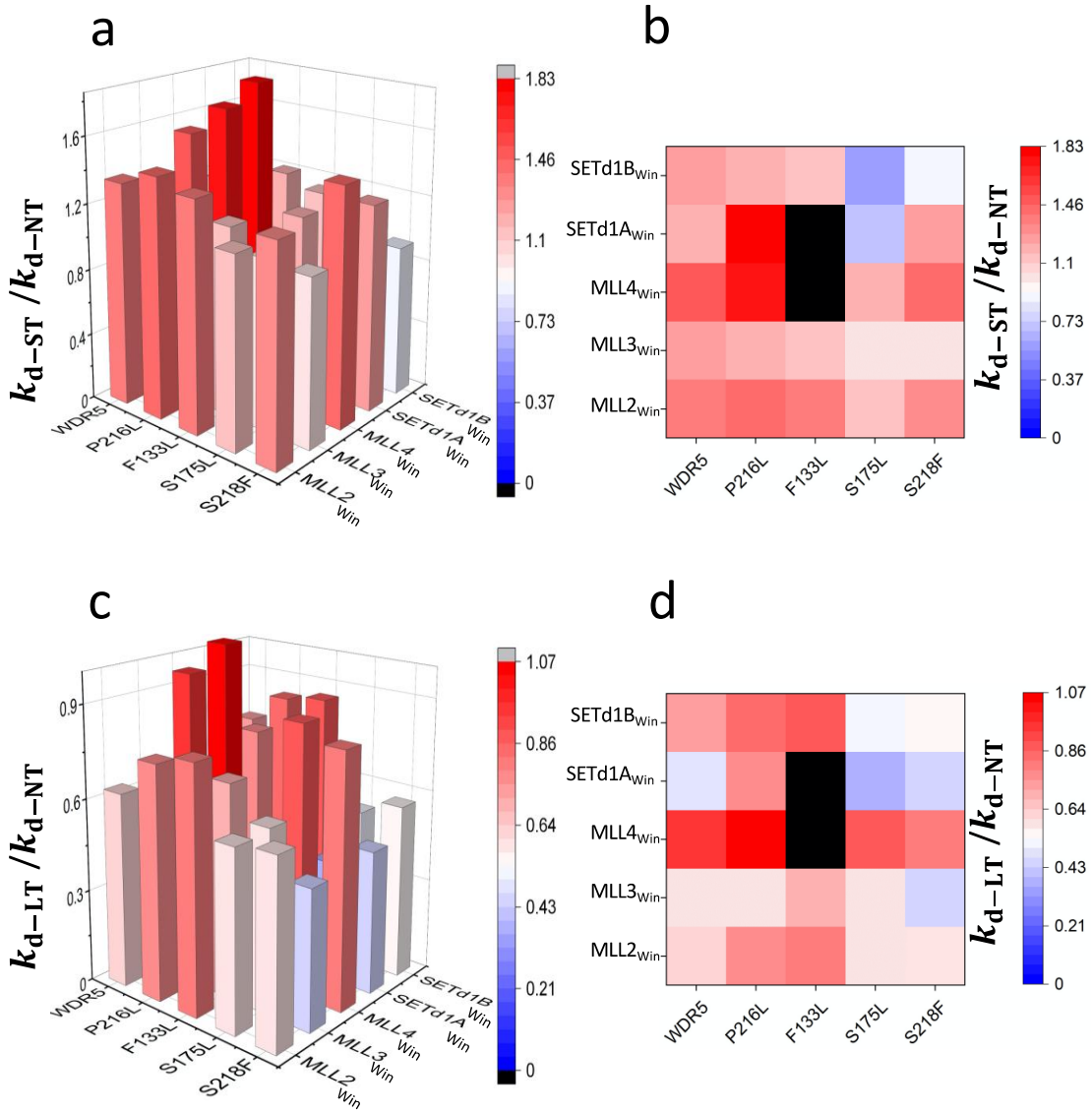


Figure S7: 3D plots and contour maps of the normalized association rate constants. (a) Bar graph and (b) contour map of k_{d-ST} values for the interaction of ST-SET1_{Win} ligands, with WDR5 and its mutants, divided by their corresponding k_{d-NT} values. (c) Bar graph and (d) contour map of k_{d-LT} values for the interaction of LT-SET1_{Win} ligands, with WDR5 and its mutants, divided by their corresponding k_{d-NT} values. k_{d-ST} for the MLL4_{Win}-F133L interactions could not be determined using BLI, while k_{d-NT} of the SETd1A_{Win}-F133L interactions could not be determined using SPR. Therefore, those values are colored in black.

11. Scatter plots of kinetic and equilibrium constants for the ST, LT, and NT experiments.

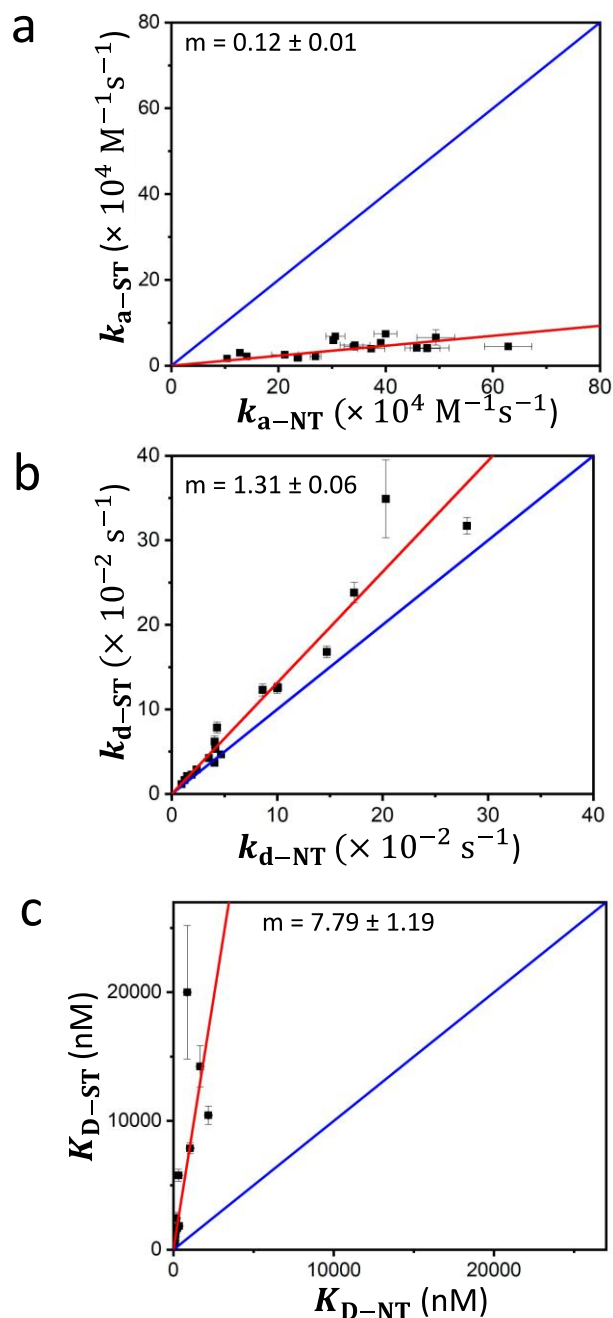


Figure S8: Scatter plots of the k_a , k_d , and K_D for the ST and NT conditions. (a) k_{a-ST} values plotted against the corresponding k_{a-NT} values. Points below this line correspond to interactions with slower association rates for the ST experiments. (b) k_{d-ST} values plotted against the corresponding k_{d-NT} values. Points above this line correspond to interactions with faster disassociation rate constants for the ST experiments. (c) K_{D-ST} values plotted against the corresponding K_{D-NT} values. Points above this line correspond to interactions that were weaker in the

ST experiments. Data are provided as mean \pm s.d. from three independent experiments.

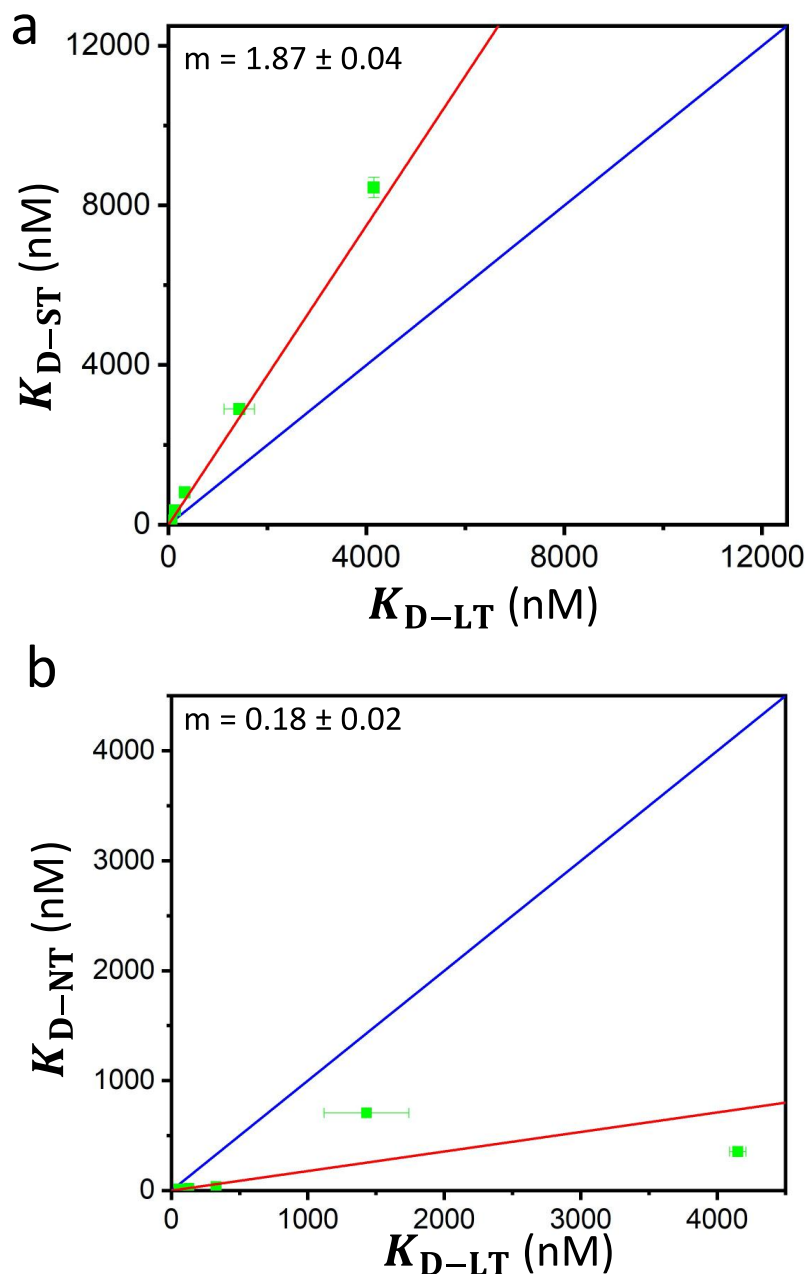


Figure S9: Scatter plots of the equilibrium dissociation constants of S175L data. (a) K_{D-ST} values plotted against the K_{D-LT} values. The red line is the fit resulted from interactions of WDR5, P216L, S218F and F133L with SET1_{win} under ST and LT conditions. The green points represent interactions of S175L. Points above this blue line correspond to interactions which were weakened by reducing tether length. (b) K_{D-NT} values plotted against the K_{D-LT} values. The red line is the fit resulted from interactions of WDR5, P216L, S218F and F133L with SET1_{win} under NT and LT conditions. The green points represent interactions of S175L. Points below this blue line correspond to interactions that were stronger

under NT conditions. *m* indicates the slope of curves in both panels. Data are provided as mean \pm s.d. from three independent experiments.

12. Supporting references.

1. Imran, A.; Moyer, B. S.; Canning, A. J.; Kalina, D.; Duncan, T. M.; Moody, K. J.; Wolfe, A. J.; Cosgrove, M. S.; Movileanu, L., Kinetics of the multitasking high-affinity Win binding site of WDR5 in restricted and unrestricted conditions. *Biochem. J.* **2021**, *478* (11), 2145-2161.
2. Patel, A.; Dharmarajan, V.; Cosgrove, M. S., Structure of WDR5 bound to mixed lineage leukemia protein-1 peptide. *J. Biol. Chem.* **2008**, *283* (47), 32158-61.
3. Patel, A.; Vought, V. E.; Dharmarajan, V.; Cosgrove, M. S., A conserved arginine-containing motif crucial for the assembly and enzymatic activity of the mixed lineage leukemia protein-1 core complex. *J. Biol. Chem.* **2008**, *283* (47), 32162-75.
4. Tate, J. G.; Bamford, S.; Jubb, H. C.; Sondka, Z.; Beare, D. M.; Bindal, N.; Boutselakis, H.; Cole, C. G.; Creatore, C.; Dawson, E.; Fish, P.; Harsha, B.; Hathaway, C.; Jupe, S. C.; Kok, C. Y.; Noble, K.; Ponting, L.; Ramshaw, C. C.; Rye, C. E.; Speedy, H. E.; Stefancsik, R.; Thompson, S. L.; Wang, S.; Ward, S.; Campbell, P. J.; Forbes, S. A., COSMIC: the Catalogue Of Somatic Mutations In Cancer. *Nucleic Acids Res.* **2019**, *47* (D1), D941-d947.
5. Forbes, S. A.; Beare, D.; Boutselakis, H.; Bamford, S.; Bindal, N.; Tate, J.; Cole, C. G.; Ward, S.; Dawson, E.; Ponting, L.; Stefancsik, R.; Harsha, B.; Kok, C. Y.; Jia, M.; Jubb, H.; Sondka, Z.; Thompson, S.; De, T.; Campbell, P. J., COSMIC: somatic cancer genetics at high-resolution. *Nucleic Acids Res.* **2017**, *45* (D1), D777-d783.
6. Goldman, M. J.; Zhang, J.; Fonseca, N. A.; Cortés-Ciriano, I.; Xiang, Q.; Craft, B.; Piñero-Yáñez, E.; O'Connor, B. D.; Bazant, W.; Barrera, E.; Muñoz-Pomer, A.; Petryszak, R.; Füllgrabe, A.; Al-Shahrour, F.; Keays, M.; Haussler, D.; Weinstein, J. N.; Huber, W.; Valencia, A.; Park, P. J.; Papatheodorou, I.; Zhu, J.; Ferretti, V.; Vazquez, M., A user guide for the online exploration and visualization of PCAWG data. *Nat. Commun.* **2020**, *11* (1), 3400.
7. Weeramange, C. J.; Fairlamb, M. S.; Singh, D.; Fenton, A. W.; Swint-Kruse, L., The strengths and limitations of using biolayer interferometry to monitor equilibrium titrations of biomolecules. *Protein Sci.* **2020**, *29* (4), 1018-1034.
8. Dharmarajan, V.; Lee, J. H.; Patel, A.; Skalnik, D. G.; Cosgrove, M. S., Structural basis for WDR5 interaction (Win) motif recognition in human SET1 family histone methyltransferases. *J. Biol. Chem.* **2012**, *287* (33), 27275-89.

9. Zhang, P.; Lee, H.; Brunzelle, J. S.; Couture, J. F., The plasticity of WDR5 peptide-binding cleft enables the binding of the SET1 family of histone methyltransferases. *Nucleic Acids Res.* **2012**, *40* (9), 4237-46.
10. Movileanu, L.; Cheley, S.; Howorka, S.; Braha, O.; Bayley, H., Location of a Constriction in the Lumen of a Transmembrane Pore by Targeted Covalent Attachment of Polymer Molecules. *J. Gen. Physiol.* **2001**, *117* (3), 239-251.
11. Wolfe, A. J.; Gugel, J. F.; Chen, M.; Movileanu, L., Kinetics of Membrane Protein-Detergent Interactions Depend on Protein Electrostatics. *J. Phys. Chem. B* **2018**, *122* (41), 9471-9481.
12. Jarmoskaite, I.; AlSadhan, I.; Vaidyanathan, P. P.; Herschlag, D., How to measure and evaluate binding affinities. *eLife* **2020**, *9*.

4.6 REFERENCES

- (1) Erlendsson, S.; Teimum, K. Binding Revisited-Avidity in Cellular Function and Signaling. *Front. Mol. Biosci.* **2020**, *7*, 615565.
- (2) Reiner, A.; Isacoff, E. Y. Tethered ligands reveal glutamate receptor desensitization depends on subunit occupancy. *Nat. Chem. Biol.* **2014**, *10*, 273-280.
- (3) Jurchenko, C.; Chang, Y.; Narui, Y.; Zhang, Y.; Salaita, K. S. Integrin-generated forces lead to streptavidin-biotin unbinding in cellular adhesions. *Biophys. J.* **2014**, *106*, 1436-1446.
- (4) Movileanu, L.; Howorka, S.; Braha, O.; Bayley, H. Detecting protein analytes that modulate transmembrane movement of a polymer chain within a single protein pore. *Nat. Biotechnol.* **2000**, *18*, 1091-1095.
- (5) Komatsu, N.; Aoki, K.; Yamada, M.; Yukinaga, H.; Fujita, Y.; Kamioka, Y.; Matsuda, M. Development of an optimized backbone of FRET biosensors for kinases and GTPases. *Mol. Biol. Cell* **2011**, *22*, 4647-4656.
- (6) Watkins, H. M.; Vallee-Belisle, A.; Ricci, F.; Makarov, D. E.; Plaxco, K. W. Entropic and electrostatic effects on the folding free energy of a surface-attached biomolecule: an experimental and theoretical study. *J. Am. Chem. Soc.* **2012**, *134*, 2120-2126.
- (7) Schena, A.; Griss, R.; Johnsson, K. Modulating protein activity using tethered ligands with mutually exclusive binding sites. *Nat. Commun.* **2015**, *6*, 7830.
- (8) Fahie, M. A.; Yang, B.; Pham, B.; Chen, M. Tuning the selectivity and sensitivity of an OmpG nanopore sensor by adjusting ligand tether length. *ACS Sens.* **2016**, *1*, 614-622.
- (9) Kang, D.; Sun, S.; Kurnik, M.; Morales, D.; Dahlquist, F. W.; Plaxco, K. W. New Architecture for Reagentless, Protein-Based Electrochemical Biosensors. *J. Am. Chem. Soc.* **2017**, *139*, 12113-12116.
- (10) Robinson-Mosher, A.; Chen, J. H.; Way, J.; Silver, P. A. Designing cell-targeted therapeutic proteins reveals the interplay between domain connectivity and cell binding. *Biophys. J.* **2014**, *107*, 2456-2466.
- (11) Nagamune, T. Biomolecular engineering for nanobio/bionanotechnology. *Nano Converg.* **2017**, *4*, 9.
- (12) Kim, J. Y.; Meng, F.; Yoo, J.; Chung, H. S. Diffusion-limited association of disordered protein by non-native electrostatic interactions. *Nat.*

Commun. **2018**, *9*, 4707.

(13) Borgia, A.; Borgia, M. B.; Bugge, K.; Kissling, V. M.; Heidarsson, P. O.; Fernandes, C. B.; Sottini, A.; Soranno, A.; Buholzer, K. J.; Nettels, D.; Kragelund, B. B.; Best, R. B.; Schuler, B. Extreme disorder in an ultrahigh-affinity protein complex. *Nature* **2018**, *555*, 61-66.

(14) Sturzenegger, F.; Zosel, F.; Holmstrom, E. D.; Buholzer, K. J.; Makarov, D. E.; Nettels, D.; Schuler, B. Transition path times of coupled folding and binding reveal the formation of an encounter complex. *Nat. Commun.* **2018**, *9*, 4708.

(15) Zosel, F.; Mercadante, D.; Nettels, D.; Schuler, B. A proline switch explains kinetic heterogeneity in a coupled folding and binding reaction. *Nat. Commun.* **2018**, *9*, 3332.

(16) Mayse, L. A.; Imran, A.; Larimi, M. G.; Cosgrove, M. S.; Wolfe, A. J.; Movileanu, L. Disentangling the recognition complexity of a protein hub using a nanopore. *Nature Commun.* **2022**, *13*, 978.

(17) De Gennes, P.-G. Kinetics of diffusion-controlled processes in dense polymer systems. I. Nonentangled regimes. *J. Chem. Phys.* **1982**, *76*, 3316-3321.

(18) Van Valen, D.; Haataja, M.; Phillips, R. Biochemistry on a leash: the roles of tether length and geometry in signal integration proteins. *Biophys. J.* **2009**, *96*, 1275-1292.

(19) Ren, C. L.; Carvajal, D.; Shull, K. R.; Szleifer, I. Streptavidin-biotin binding in the presence of a polymer spacer. A theoretical description. *Langmuir* **2009**, *25*, 12283-12292.

(20) Kane, R. S. Thermodynamics of multivalent interactions: influence of the linker. *Langmuir* **2010**, *26*, 8636-8640.

(21) Reeves, D.; Cheveralls, K.; Kondev, J. Regulation of biochemical reaction rates by flexible tethers. *Phys. Rev. E Stat. Nonlin. Soft Matter Phys.* **2011**, *84*, 021914.

(22) Levin, M. D.; Shimizu, T. S.; Bray, D. Binding and diffusion of CheR molecules within a cluster of membrane receptors. *Biophys. J.* **2002**, *82*, 1809-1817.

(23) Windisch, B.; Bray, D.; Duke, T. Balls and chains--a mesoscopic approach to tethered protein domains. *Biophys. J.* **2006**, *91*, 2383-2392.

(24) Shewmake, T. A.; Solis, F. J.; Gillies, R. J.; Caplan, M. R. Effects of linker length and flexibility on multivalent targeting. *Biomacromolecules* **2008**,

9, 3057-3064.

(25) Wong, J. Y.; Kuhl, T. L.; Israelachvili, J. N.; Mullah, N.; Zalipsky, S. Direct measurement of a tethered ligand-receptor interaction potential. *Science* **1997**, *275*, 820-822.

(26) Jeppesen, C.; Wong, J. Y.; Kuhl, T. L.; Israelachvili, J. N.; Mullah, N.; Zalipsky, S.; Marques, C. M. Impact of polymer tether length on multiple ligand-receptor bond formation. *Science* **2001**, *293*, 465-468.

(27) Leckband, D.; Israelachvili, J. Intermolecular forces in biology. *Q. Rev. Biophys.* **2001**, *34*, 105-267.

(28) Bauer, M.; Kékicheff, P.; Iss, J.; Fajolles, C.; Charitat, T.; Daillant, J.; Marques, C. M. Sliding tethered ligands add topological interactions to the toolbox of ligand-receptor design. *Nat. Commun.* **2015**, *6*, 8117.

(29) Krishnamurthy, V. M.; Semetey, V.; Bracher, P. J.; Shen, N.; Whitesides, G. M. Dependence of effective molarity on linker length for an intramolecular protein-ligand system. *J. Am. Chem. Soc.* **2007**, *129*, 1312-1320.

(30) Sørensen, C. S.; Kjaergaard, M. Effective concentrations enforced by intrinsically disordered linkers are governed by polymer physics. *Proceedings of the National Academy of Sciences of the United States of America* **2019**, *116*, 23124-23131.

(31) Patel, A.; Dharmarajan, V.; Cosgrove, M. S. Structure of WDR5 bound to mixed lineage leukemia protein-1 peptide. *J. Biol. Chem.* **2008**, *283*, 32158-32161.

(32) Song, J. J.; Kingston, R. E. WDR5 interacts with mixed lineage leukemia (MLL) protein via the histone H3-binding pocket. *J. Biol. Chem.* **2008**, *283*, 35258-35264.

(33) Li, Y.; Han, J.; Zhang, Y.; Cao, F.; Liu, Z.; Li, S.; Wu, J.; Hu, C.; Wang, Y.; Shuai, J.; Chen, J.; Cao, L.; Li, D.; Shi, P.; Tian, C.; Zhang, J.; Dou, Y.; Li, G.; Chen, Y.; Lei, M. Structural basis for activity regulation of MLL family methyltransferases. *Nature* **2016**, *530*, 447-452.

(34) Xue, H.; Yao, T.; Cao, M.; Zhu, G.; Li, Y.; Yuan, G.; Chen, Y.; Lei, M.; Huang, J. Structural basis of nucleosome recognition and modification by MLL methyltransferases. *Nature* **2019**, *573*, 445-449.

(35) Dharmarajan, V.; Lee, J. H.; Patel, A.; Skalnik, D. G.; Cosgrove, M. S. Structural basis for WDR5 interaction (Win) motif recognition in human SET1 family histone methyltransferases. *J. Biol. Chem.* **2012**, *287*, 27275-27289.

(36) Zhang, P.; Lee, H.; Brunzelle, J. S.; Couture, J. F. The plasticity of

WDR5 peptide-binding cleft enables the binding of the SET1 family of histone methyltransferases. *Nucleic Acids Res.* **2012**, *40*, 4237-4246.

(37) Weeramange, C. J.; Fairlamb, M. S.; Singh, D.; Fenton, A. W.; Swint-Kruse, L. The strengths and limitations of using bilayer interferometry to monitor equilibrium titrations of biomolecules. *Protein Sci.* **2020**, *29*, 1018-1034.

(38) Masson, J. F. Surface Plasmon Resonance Clinical Biosensors for Medical Diagnostics. *ACS Sens.* **2017**, *2*, 16-30.

(39) Pang, X.; Zhou, H. X. Rate Constants and Mechanisms of Protein-Ligand Binding. *Annu. Rev. Biophys.* **2017**, *46*, 105-130.

(40) Schreiber, G.; Haran, G.; Zhou, H. X. Fundamental aspects of protein-protein association kinetics. *Chem. Rev.* **2009**, *109*, 839-860.

(41) Nitzan, A.: *Chemical Dynamics in Condensed Phases*; Oxford University Press, 2006.

(42) Zhou, H. X. Rate theories for biologists. *Q. Rev. Biophys.* **2010**, *43*, 219-293.

(43) Smoluchowski, M. Mathematical Theory of the Kinetics of the Coagulation of Colloidal Solutions. *Z. Phys. Chem.* **1917**, *92*, 129-135.

(44) Hanggi, P.; Talkner, P.; Borkovec, M. Reaction-Rate Theory - 50 Years After Kramers. *Rev. Mod. Phys.* **1990**, *62*, 251-341.

(45) Berg, H. C.; Purcell, E. M. Physics of chemoreception. *Biophys. J.* **1977**, *20*, 193-219.

(46) Misiura, M. M.; Kolomeisky, A. B. Role of Intrinsically Disordered Regions in Acceleration of Protein-Protein Association. *J. Phys. Chem. B* **2020**, *124*, 20-27.

(47) Shoemaker, B. A.; Portman, J. J.; Wolynes, P. G. Speeding molecular recognition by using the folding funnel: the fly-casting mechanism. *Proceedings of the National Academy of Sciences of the United States of America* **2000**, *97*, 8868-8873.

(48) Levy, Y.; Onuchic, J. N.; Wolynes, P. G. Fly-casting in protein-DNA binding: frustration between protein folding and electrostatics facilitates target recognition. *J. Am. Chem. Soc.* **2007**, *129*, 738-739.

(49) Trizac, E.; Levy, Y.; Wolynes, P. G. Capillarity theory for the fly-casting mechanism. *Proceedings of the National Academy of Sciences of the United States of America* **2010**, *107*, 2746-2750.

- (50) Sugase, K.; Dyson, H. J.; Wright, P. E. Mechanism of coupled folding and binding of an intrinsically disordered protein. *Nature* **2007**, *447*, 1021-1025.
- (51) Wright, P. E.; Dyson, H. J. Linking folding and binding. *Curr. Opin. Struct. Biol.* **2009**, *19*, 31-38.
- (52) Soranno, A.; Koenig, I.; Borgia, M. B.; Hofmann, H.; Zosel, F.; Nettels, D.; Schuler, B. Single-molecule spectroscopy reveals polymer effects of disordered proteins in crowded environments. *Proceedings of the National Academy of Sciences of the United States of America* **2014**, *111*, 4874-4879.
- (53) Mollica, L.; Bessa, L. M.; Hanouille, X.; Jensen, M. R.; Blackledge, M.; Schneider, R. Binding Mechanisms of Intrinsically Disordered Proteins: Theory, Simulation, and Experiment. *Front. Mol. Biosci.* **2016**, *3*, 52.
- (54) Umezawa, K.; Ohnuki, J.; Higo, J.; Takano, M. Intrinsic disorder accelerates dissociation rather than association. *Proteins* **2016**, *84*, 1124-1133.
- (55) Huang, Y.; Liu, Z. Kinetic advantage of intrinsically disordered proteins in coupled folding-binding process: a critical assessment of the "fly-casting" mechanism. *J. Mol. Biol.* **2009**, *393*, 1143-1159.
- (56) Segall, D. E.; Nelson, P. C.; Phillips, R. Volume-exclusion effects in tethered-particle experiments: bead size matters. *Phys. Rev. Lett* **2006**, *96*, 088306.
- (57) Makarov, D. E. Perspective: Mechanochemistry of biological and synthetic molecules. *J. Chem. Phys.* **2016**, *144*, 030901.
- (58) Imran, A.; Moyer, B. S.; Canning, A. J.; Kalina, D.; Duncan, T. M.; Moody, K. J.; Wolfe, A. J.; Cosgrove, M. S.; Movileanu, L. Kinetics of the multitasking high-affinity Win binding site of WDR5 in restricted and unrestricted conditions. *Biochem. J.* **2021**, *478*, 2145-2161.

Chapter 5: N-terminus IDR of WDR5 Impacts its Function and Kinetic Measurements

Ali Imran,¹ Michael S. Cosgrove,² and Liviu Movileanu^{1,3,4*}

¹*Department of Physics, Syracuse University, 201 Physics Building, Syracuse, New York 13244-1130, USA*

²*Department of Biochemistry and Molecular Biology, State University of New York Upstate Medical University, 4249 Weiskotten Hall, 766 Irving Avenue, Syracuse, New York 13210, USA*

³*The BioInspired Institute, Syracuse University, Syracuse, New York, 13244, USA*

⁴*Department of Biomedical and Chemical Engineering, Syracuse University, 329 Link Hall, Syracuse, New York 13244, USA*

5.1 Abstract

WD40 Repeat Protein 5 (WDR5) is a well-known epigenetic regulator which has recognized interactions with a host of different proteins. It has a 22 residue N-terminus intrinsically disordered tail whose function is unknown. Most available crystal structures of WDR5 use a truncated version similar to WDR5²³⁻³³⁴ (WDR5_{ΔN}) to get around this intrinsically disordered region (IDR). Studies of WDR5's interactions with other proteins do not differentiate between full-length WDR5 (WDR5_{FL}) and WDR5_{ΔN}, ignoring any differences between them. Here we look at the impact of the tail on WDR5's interactions, its effect on our Biolayer Interferometry (BLI) measurements of WBM site kinetics and its role in aiding WDR5 function. We also look at the significance of physiologically relevant salt conditions for quantifying these interactions.

5.2 Introduction

WD40 repeat protein-5 (WDR5) plays established roles in multiple protein complexes. ¹ It is crucial to the regulation of Histone-3 Lysine-4 (H3K4) methylation by SET1 family proteins; MLL1, MLL2, MLL3, MLL4, SETd1A and SETd1B.²⁻⁴ Not only does it interact directly with these SET1 proteins ⁵⁻⁷ it also interacts with retinoblastoma binding protein-5 (RbBP5) which is an integral part of the SET1 complex.^{5, 6, 8, 9} Moreover, it also has known interactions with the transcription factor MYC,¹⁰⁻¹³ 3-phosphoinositide-dependent protein kinase 1 (PDK1)¹⁴ and other interacting partners involved in phosphatidylinositol 3-kinase (PI3K) signaling.¹⁴ These interactions have wide ranging implications for epigenetic regulation and complex assembly among other things.

WDR5 has two known binding sites responsible for all of its interactions: the WDR5 Interacting (Win) site^{2, 3, 15-17} and the WDR5 Binding Motif (WBM) site.^{13, 14, 18} SET1 proteins and histone H3 have the Win sequence which allows them to associate with the Win site.³ These interactions involve precise insertions into the Win site cavity and thus impose an entropic penalty on the binding. The kinetics of these interactions have been explored before and reveal a significantly slow association rate as expected.⁷ On the other hand, RbBP5¹⁸ and MYC¹³ use the WDR5 Binding Motif to bind to the WBM site. These are primarily surface interactions which have not been explored kinetically before.

The N-terminus IDR present on WDR5 has no understood function. These 22 residues are largely ignored when focusing on WDR5's functions. Most available crystal structures work with a truncated version similar to WDR5²³⁻³³⁴ (WDR5_{ΔN}) to get around this region.^{2,15,16,17} This IDR has part of the Win motif and has been seen interacting with the Win site cavity in at least one crystal structure exploration.¹⁹

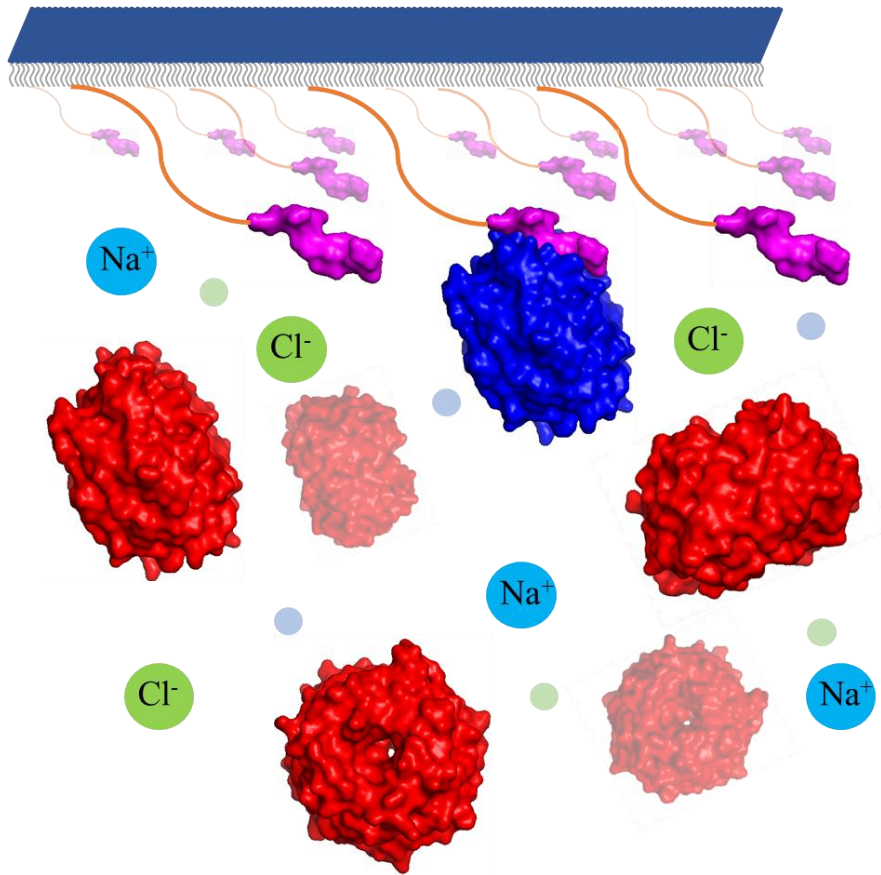


Figure 1: BLI Experiment of RbBP5 interacting with WDR5 in the presence of Salt. The figure shows the RbBP5 peptide interacting with WDR5. RbBP5 (magenta) is immobilized onto the BLI sensor surface with a linker. WDR5 (red), Na⁺ ions (light blue) and Cl⁻ ions (green) are shown freely moving in solution. Bound WDR5 is marked in blue.

In this study we look at the role the intrinsically disordered tail plays in WDR5's interactions, the effect it can have on kinetics measurements of the WBM site and its contribution to the overall function of WDR5 inside the cell. We also look at the importance of maintaining physiologically relevant conditions when looking at these interactions.

5.3 Results and Discussion

WDR5_{FL} and the tale of the N-terminus. We obtained BLI sensorgrams for the interaction of RbBP5 peptide with Full-length WDR5 (WDR5_{FL}) which included the N-terminus tail (**Table 1**). The biotinylated RbBP5 peptide was immobilized onto Streptavidin sensors and then submerged in different concentrations of the analyte, WDR5_{FL}. Once the interaction reached equilibrium, the sensors were moved to an analyte free solution. This allowed us to look at the association and dissociation phases of the interaction in real time. WDR5_{FL} gave us the curves shown in figure (**Figure 2a**). Not only did we see large responses we also saw that as the concentration of WDR5_{FL} was increased, the curves did not show faster saturation. The lower concentrations showed quick saturation while the higher concentrations did not. This was counterintuitive to the expectations we would have for any simple 1:1 protein-protein interaction. The results were reproduced an additional two times to confirm that no experimental errors were responsible for this deviation from normal expected behavior. Optimizing this experiment, by varying loading and association steps, to decrease maximum

response did not improve the results. Decreasing loading peptide concentration to 1 nM reduced the maximum response but did not produce results amenable to 1:1 binding analysis. Reducing the maximum concentration of analyte to 600 nM or 300 nM again did not solve this problem. We hypothesized that there could be another interaction creating an artifact in our BLI data.

Table 1: Peptides. The table shows the peptides used for this work, their sequences and the sites they bind onto on WDR5. The C-terminus of all peptides were amidated. The N-terminus of RbBP5³⁶⁹⁻³⁷⁹ peptide and MLL3⁴⁷⁰³⁻⁴⁷¹⁶ were Biotinylated while that of WBM Inhibitor and ARTEVY were acetylated. The relevant sequences are in black, N-terminal and C-terminal modifications are marked in blue, and the linkers are marked in red.

Peptide Name	Peptide Sequence	Binding Site
RbBP5 ³⁶⁹⁻³⁷⁹ Peptide	Biotinyl- GGSGGSGGS AAEDEEVDVTSVD-NH ₂	WBM
WBM Inhibitor	CH ₃ CO-AAEDEEVDVTSVD-NH ₂	WBM
ARTEVY	CH ₃ CO-ARTEVY-NH ₂	Win
MLL3 ⁴⁷⁰³⁻⁴⁷¹⁶	Biotinyl- GG VNPTGCARSEPKMS-NH ₂	Win

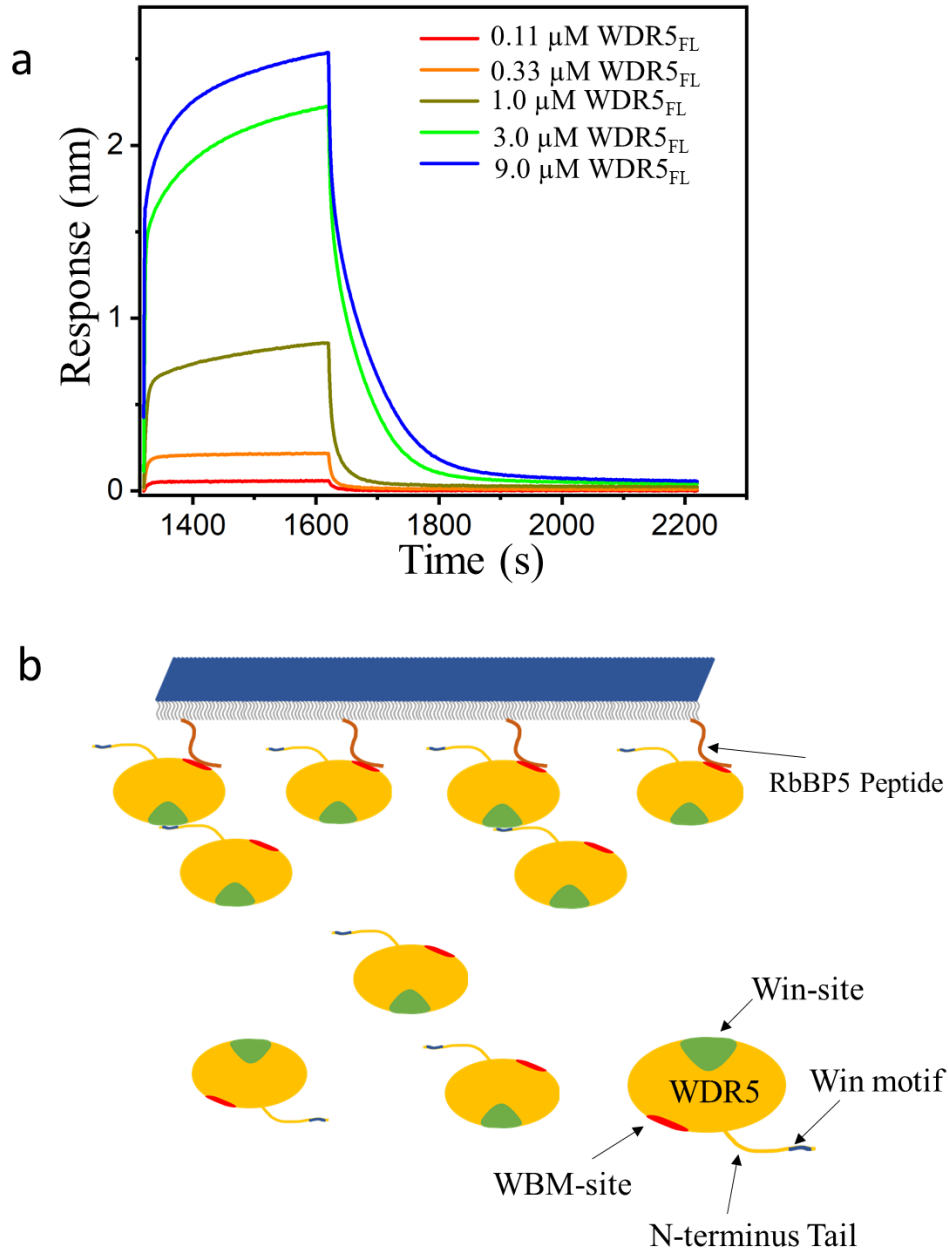


Figure 2: RbBP5 Interaction with WDR5_{FL}. (a) This figure shows BLI sensorgrams obtained for the interaction of RbBP5 with full length WDR5. Biotinylated RbBP5 peptide was immobilized as ligand on to Streptavidin sensors. The sensors were dipped into well containing different concentrations of WDR5_{FL} as analyte. The sensorgrams corresponding to the 5 different concentrations used are shown below. (b) This figure shows the schematic of the interaction and the role the N-terminus IDR plays in our results.

Dimerization. Based on available X-ray crystallography structure, we hypothesized that, in the case of these specific BLI experiments, WDR5 may be binding in such a way that it leaves the Win site open to interactions with the N-terminus tail of other present WDR5s. The N-terminus tail has a Win motif sequence given by EAARAQP that can potentially insert into the Win site cavity.¹⁹ This schematic is shown in figure (**Figure 2b**). Thus, the binding of WDR5 to the immobilized RbBP5 peptide would allow even more WDR5 to bind onto the first one and so on. To test this, we added ARTEVY (win6mer), a Win binding site inhibitor, to the RbBP5-WDR5_{FL} association well, to block the Win site (14). **Figure 3a** shows that ARTEVY successfully brought the interaction to normal behavior. Considering ARTEVY is a Win site binder, normally it would have no effect whatsoever on the WBM interaction making this result very interesting. Moreover, **Figure 3b** also shows that when the same experiment was performed with WDR5²³⁻³³⁴ (WDR5_{ΔN}), not only did ARTEVY have no effect, but the curves seen were similar to the 10 μM ARTEVY spike curve in Figure 3a. This confirms that the interaction between the N-terminus IDR and the Win binding site was responsible for the unexpected results. Furthermore, when the original experiment, shown in **Figure 3a**, was carried out with 20 μM ARTEVY spiked in the association wells we got the sensorgrams shown in figure **Figure S1**. These curves showed a concentration dependent responses and rates of saturation, more amenable to 1:1 binding fitting and gave us kinetics of the interaction.

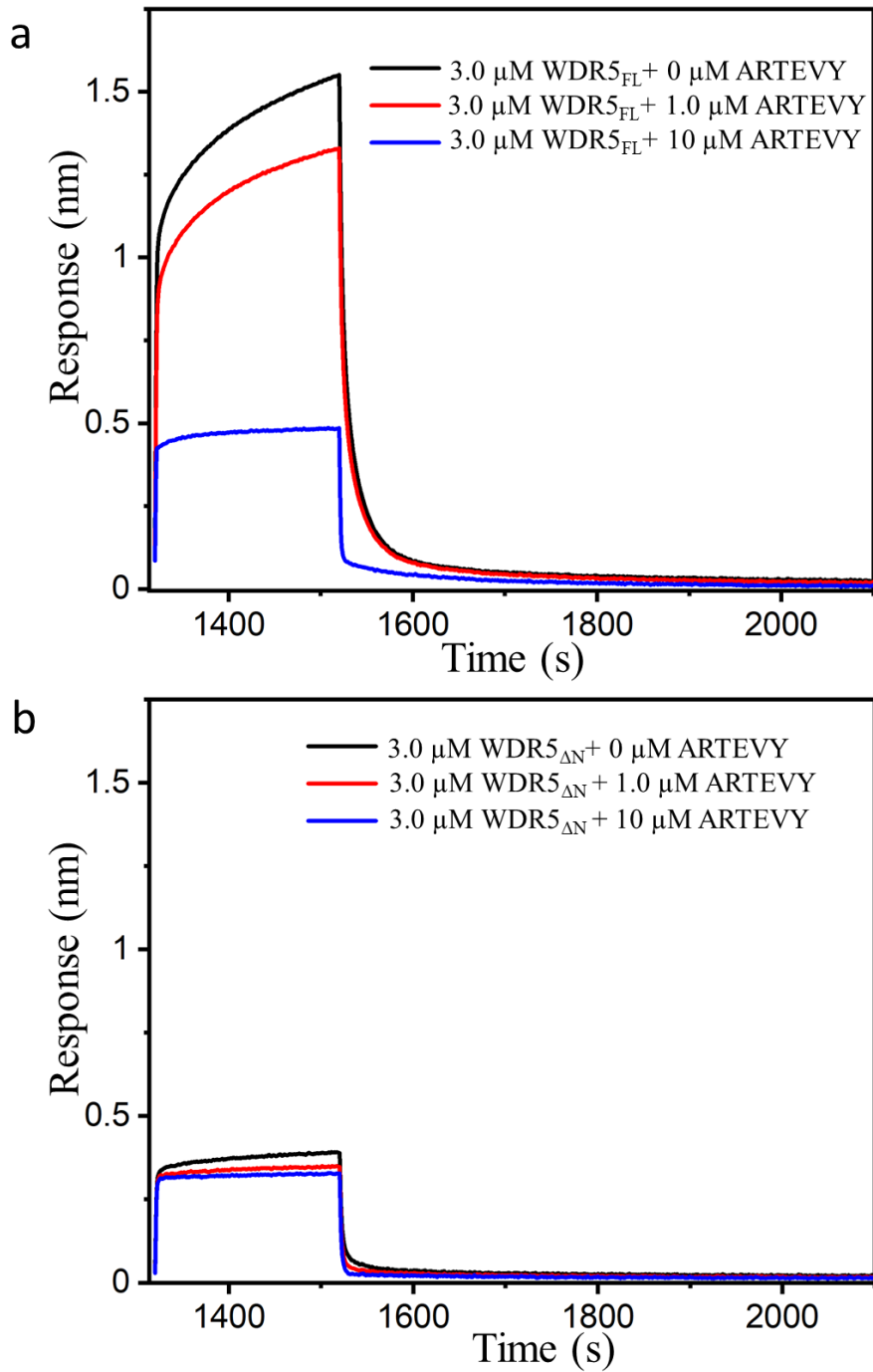
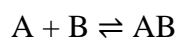


Figure 3: Blocking the Win binding site using ARTEVY. RbBP5's interaction with WDR5 inhibited with different concentrations of ARTEVY peptide. Biotinylated RbBP5 peptide was immobilized onto Streptavidin sensors. 3 μM WDR5 association wells were spiked with different concentrations of ARTEVY (a) WDR5_{FL} (b) WDR5_{ΔN}.

Moreover, we looked at the interaction of RbBP5 with WDR5 $_{\Delta N}$ (**Figure 4a**). These curves were again well behaved, readily analyzable and gave us very similar kinetics (**Table S1**). Additionally, the interaction of MLL3 with WDR5 $_{\Delta N}$ interaction showed no difference from MLL3's interaction with WDR5 $_{FL}$ interaction measured by us previously (**Figure S2, Table S2**), showing that this effect was limited to WBM measurements. These comprehensive results allow us to conclude that WDR5 $_{FL}$ dimerizes due to the interaction between the N-terminus IDR and the Win binding site cavity. This dimerization is amplified in the case of our BLI measurements of the RbBP5-WDR5 $_{FL}$ complex because of the specific configuration WDR5 ends up in after binding with the RbBP5 peptide as shown in figure. We expect this to hold true for most WBM binding measurements through BLI and SPR in which the WBM partner is immobilized.

Two-State Interaction. Another possibility that we explored was that the RbBP5-WDR5 $_{FL}$ interaction was a two-state interaction. It was possible that the complex was going through a conformational change after the initial binding leading to a much more stable complex. Therefore, our interaction model would have changed from



to



Here A and B represent the binding partners RbBP5 and WDR5 respectively, AB represents the complex and AB* represents a more stable complex forming after conformational change i.e the second state. The model fit our optimized data sets really well (**Figure S3**). The figure shows our analysis of one of these curves using this model (**Figure S4a**). It shows that as association proceeds, we get higher and higher percentages of the more stable AB*. Consequently, the dissociation rate constant should decrease the longer the association time or “contact time”. **Figure S4b** shows the two-state test, the contact time was increased and the corresponding dissociation curves were analyzed. Similar tests have been performed before using the SPR (20). We saw that increasing contact time had no effect on the dissociation rate. Therefore, even though the model fit our data well, this interaction was not a two-state interaction. Our results reemphasize the unreliability of picking and choosing models based only on how well they fit the BLI data. Validating models through orthogonal tests is crucial to extracting useful and credible information from data.

Phase Separation and WDR5. These results have significant ramifications for understanding the behavior of WDR5. Previous work⁷ has shown that WDR5’s interactions with SET1 proteins have very low association rates due in part to the entropic cost associated with the SET1 Win motif Arginine inserting into the WDR5 cavity. However, this exploration suggests that the intrinsically disordered tail allows WDR5 to dimerize under certain conditions. This increased inter-molecular affinity could potentially trigger phase-separation and allow WDR5 to

form local hyper-concentrations making up for the slow association rates. Moreover, the connection between the presence of IDRs and the ability to phase separate has been explored extensively before (15-18). This would explain why, despite the low association rates, WDR5 is crucial to the regulation of the histone methylation function of some SET1 proteins.² Phase separation would allow WDR5 to maintain its specificity, granted by the Win binding site cavity, while not compromising on function.

Association and dissociation rate constants. Looking at the kinetics of the RbBP5-WDR5_{ΔN} interaction, we see that that this WBM site interaction had a greater association rate than most of our measured Win binding site interactions. This was in line with our predictions as this surface interaction did not have the same entropic limitations that the Win binding site cavity interactions have. Furthermore, the dissociation rate constant was also in general greater than those of the Win binding site interactions (**Figure 4a, Table S1**). This may be due to a relative lack of hydrogen bonds stabilizing the RbBP5-WDR5 complex (**Table S3**). The complex has several ionic and hydrophobic contributions (**Table S4**), but it seems they do not make this a high-affinity complex. Consequently, the K_D of the interaction was 1.5 μM , making this interaction weaker than most SET1 protein interactions with WDR5 (7, 16, 17).

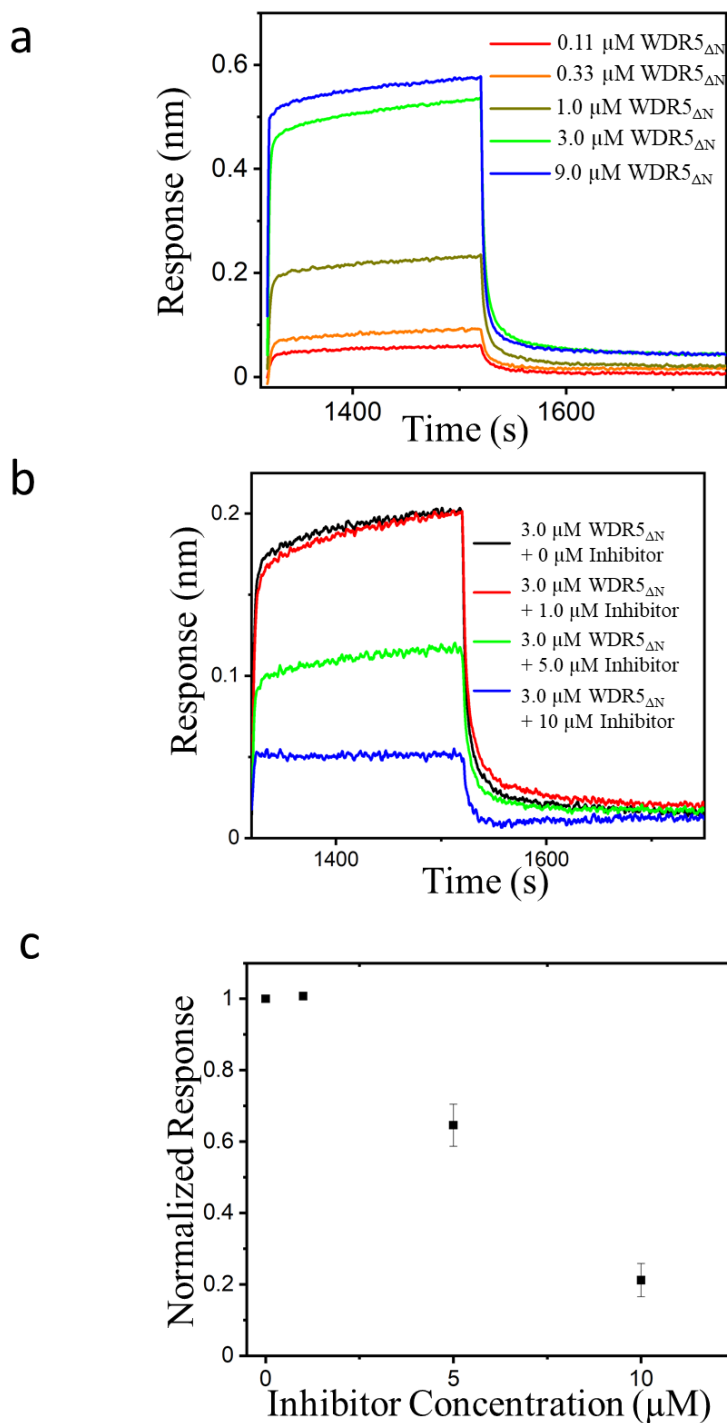


Figure 4: RbBP5 Interaction with WDR5 $_{\Delta\text{N}}$. (a) This figure shows BLI sensorgrams obtained for the interaction of RbBP5 with WDR5 $_{\Delta\text{N}}$. Biotinylated RbBP5 peptide was immobilized as ligand on to Streptavidin sensors. The sensors were dipped into well containing different concentrations of WDR5 $_{\text{FL}}$ as analyte. The sensorgrams corresponding to the 5 different concentrations used are shown

below. **(b)** RbBP5-WDR5 complex inhibited with different concentrations of WBM inhibitor (**Table 1**). Biotinylated RbBP5 peptide was immobilized onto Streptavidin sensors. 3 μM WDR5 association wells were spiked with different concentrations of WBM inhibitor. **(c)** Normalized maximum responses obtained for the inhibition of WDR5-RbBP5 interactions.

Inhibition. Additionally, our data shows that this interaction can be inhibited by using a peptidomimetic inhibitor based on the RbBP5 WBM motif (**Table 1**). We saw that formation of the RbBP5-WDR5 complex was greatly decreased, as the concentration of WBM inhibitor was increased from 1 μM through 10 μM (**Figures 4bc, Table S5**). However, the effect of the inhibitor at 1 μM concentration was insignificant and an order of magnitude higher concentration was required to produce a strong inhibition. This suggests that the WBM inhibitor while capable of inhibition would need some modifications to increase its effectiveness. Our results show that this peptide can serve as the basis for the design of strongly binding molecules.

Effect of salt concentration. The figure shows that the RbBP5-WDR5 interaction is highly aided by electrostatic effects (**Figure S5**). The WBM site on WDR5 is highly positive, while the WBM motif on RbBP5 is highly negative. Moreover, we postulated that this would make the interaction very susceptible to shielding effects from salt. To test this, we measured the kinetics of these interactions in three other buffers. Tris, TCEP and BSA were kept the same while the concentration of NaCl was varied. The three additional NaCl concentrations used were 50 mM, 300 mM, and 600 mM. 150 mM NaCl had already been used,

as mentioned above. Our results, in figure, show that the interaction is significantly affected by salt concentration (**Figure 5, Figure S6, Table S6**). The interaction strength decreased as NaCl was increased, as shown by the figure. The overall change in strength was non-linear with respect to salt. Furthermore, our technique allowed us to further break down this effect in terms of changes in association and dissociation rates. We see that increasing salt-concentration decreases association rate constant. This is to be expected as the higher salt concentration would decrease the Debye screening length, decrease the effective interaction radius of the two binding partners and lead to fewer association events occurring. Surprisingly, the salt also affected the dissociation rate. We see that at 50 mM NaCl, the dissociation rate is 50-fold slower than at 600 mM NaCl. Moreover at 150 mM NaCl and 300 mM NaCl the interaction is ~3 fold slower and ~2 fold slower, respectively, than that at 600 mM NaCl. This explains the overall non-linearity of the change in interaction strength.

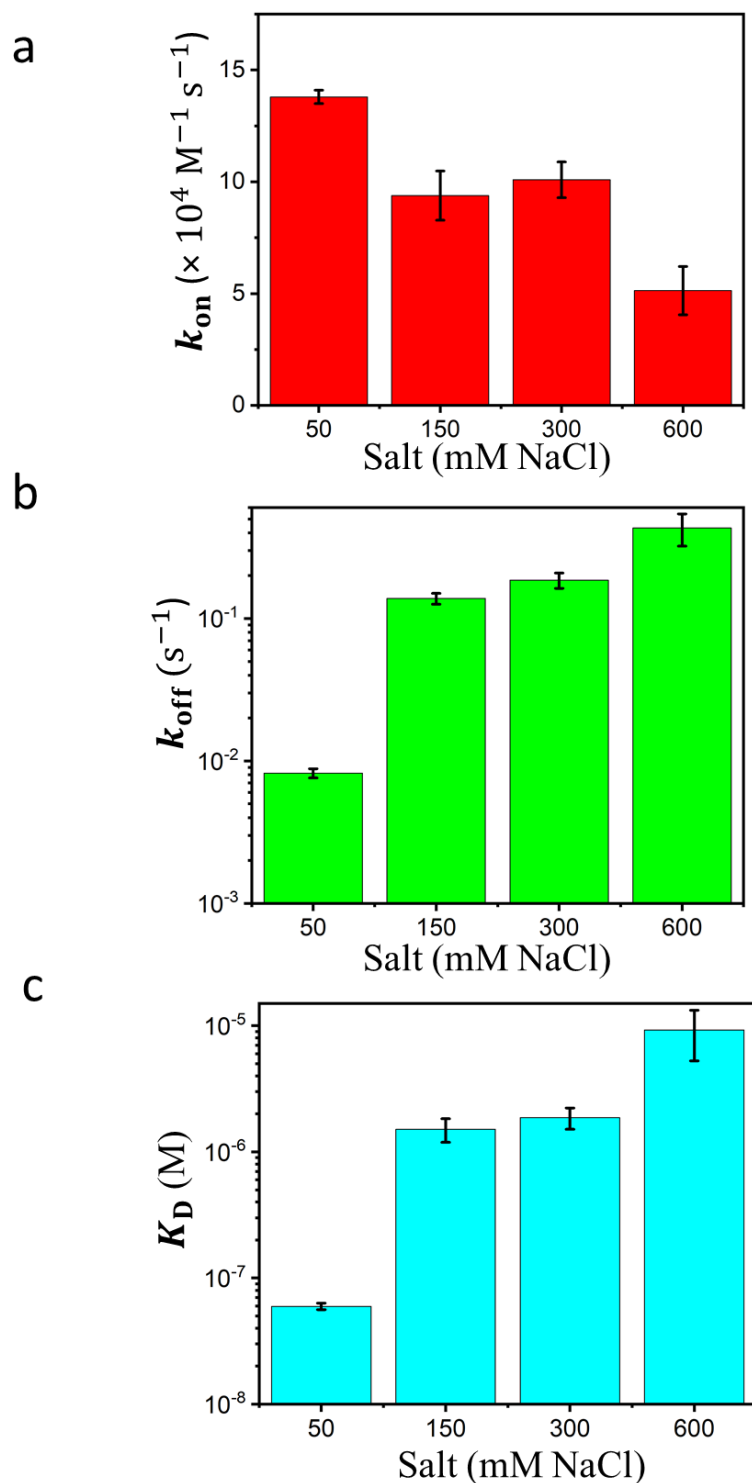


Figure 5: Effect of Salt on the RbBP5 Interaction with WDR5 Δ N. The figure shows the binding constants obtained for the RbBP5 interaction with WDR5 Δ N in different salt concentrations. **(a)** association rate constants **(b)** dissociation rate constants **(c)** equilibrium dissociation constants.

5.4 Conclusions

Our work presents the first ever thorough kinetic study of WDR5 WBM site interactions, explores the impact of salt on WBM site kinetics, and suggests the role the N-terminus IDR of WDR5 plays in governing its overall function. We found that the WBM site association rate constant was higher than those of the Win site, but this increase was countered by a simultaneous increase in the dissociation rate. Furthermore, we see that increasing salt decreases the association rate of the interaction and increases the dissociation rate, greatly weakening the binding affinity. This underscores the importance of maintaining physiologically relevant conditions for *in-vitro* studies, especially for WDR5 work. Additionally, we see that the N-terminus intrinsically disordered tail contributes to the inter molecular affinity of WDR5 increasing the likelihood of phase separation. This increased likelihood of phase separation may explain the unique way with which WDR5 is able to maintain a balance between specificity and function.

5.5 Materials and Methods

Protein Expression and Purification. Full-length WDR5 (WDR5_{FL}) and was expressed and purified in a similar way as described previously.⁷ N-terminus truncated WDR5 (WDR5²³⁻³³⁴, WDR5_{ΔN}) was purified in the same way. pET3aTr vectors containing the 6×His-TEV-WDR5 and 6×His-TEV- WDR5²³⁻³³⁴ sequences

were transformed into Rosetta™ 2 BL21(DE3)pLysS (Novagen, Cat #71403) competent E. coli cells. These cells were then grown overnight on Luria-Bertani (LB) agar carbenicillin/chloramphenicol selection plates at 37°C. Single colonies from these transformations were used for carbenicillin and chloramphenicol inoculated 50 mL Terrific Broth (TB) media starter cultures. This culture was grown overnight at 30°C. Inoculated 1L TB media cultures were seeded by the starter cultures. These expression cultures were grown at 37°C for 2.5 hours and then left at room temperature for 30 minutes. They were induced with 100 µM IPTG and grown at 16°C for 20 hours. Pellets were harvested and lysed using multiple passes through a microfluidizer. The Lysis buffer contained PMSF and EDTA-free protease inhibitor. The lysate was spun down, the supernatant was collected and passed through a Nickel column on an FPLC. WDR5 was eluted using buffer containing imidazole. The Hi-tag was cleaved using TEV Protease. The Nickel column was again used to extract the His-tag and TEV Protease from the proteins.

Peptide synthesis, labeling, purification, and analysis. All peptides for biolayer interferometry, the Fluorescein isothiocyanate (FITC) labelled peptides for FP spectroscopy and the label-free peptides were synthesized and purified by GenScript (Piscataway, NJ). The peptides were purified to $\geq 95\%$ purity. The BLI peptides were Biotinylated at the N-terminus, the FP ones were labelled with FITC at the N-terminus and the un-labelled ones were acetylated at the N-terminus. These were purified to $\geq 90\%$ purity. The label was again added at the N-terminus. All the

peptides were amidated at the C-terminus. Amino acid analysis, purity confirmation, and solubility testing were provided by GenScript.

Biolayer interferometry (BLI). BLI studies were carried out using OctetRED384 (FortéBio, Fremont, CA). The assays were performed the same way as in our previous studies⁷. Peptide's biotinylated at the N-terminus were immobilized onto Streptavidin (SA) sensors as ligands. These sensors were dipped into analyte containing wells (Manufacturer, Town, State) to obtain association curves and then were moved to analyte free wells to obtain dissociation curves. Unless specified otherwise, the running buffer for most experiments contained 150 mM NaCl, 20 mM Tris, 1 mM TCEP and 1mg/ml BSA. The pH of all running buffers was adjusted to 7.5. For the inhibition experiments, additional non-biotinylated peptides were included with the analytes

Molecular graphics. All protein representations were prepared using PyMOL Molecular Graphics System (Version 2.4.0 Schrödinger, LLC).

5.6 SUPPLEMENTARY INFORMATION

N-terminus IDR of WDR5 Impacts its Function and Kinetic Measurements

Ali Imran,¹ Michael S. Cosgrove,² and Liviu Movileanu^{1,3,4*}

¹Department of Physics, Syracuse University, 201 Physics Building, Syracuse, New York 13244-1130, USA

²Department of Biochemistry and Molecular Biology, State University of New York Upstate Medical University, 4249 Weiskotten Hall, 766 Irving Avenue, Syracuse, New York 13210, USA

³The BioInspired Institute, Syracuse University, Syracuse, New York, 13244, USA

⁴Department of Biomedical and Chemical Engineering, Syracuse University, 329 Link Hall, Syracuse, New York 13244, USA

Contents of the Supporting Information.

1. Traces for RbBP5's interaction with ARTEVY saturated WDR5 (**Supplementary Fig. 1**).
2. Kinetics measured for the RbBP5-WDR5 interaction (**Supplementary Table 1**).
3. Traces for the MLL3- WDR5 Δ N Interaction (**Supplementary Fig. 2**).
4. Kinetics measured for the MLL3-WDR5 interactions (**Supplementary Table 2**).
5. Two State Analysis of the RbBP5-WDR5FL Interaction (**Supplementary Fig. 3-4**).
6. Known Interactions at the RbBP5-WDR5 Interface (**Supplementary Table 3-4**).
7. Impact of WBM Inhibitor (**Supplementary Table 5**).
8. Role of Charge Distribution (**Supplementary Fig. 5**).
9. RbBP5-WDR5 Δ N Interactions in different Buffer conditions (**Supplementary Fig. 6, Table 6**).
10. Supporting References.

1. Traces for RbBP5's interaction with ARTEVY saturated WDR5

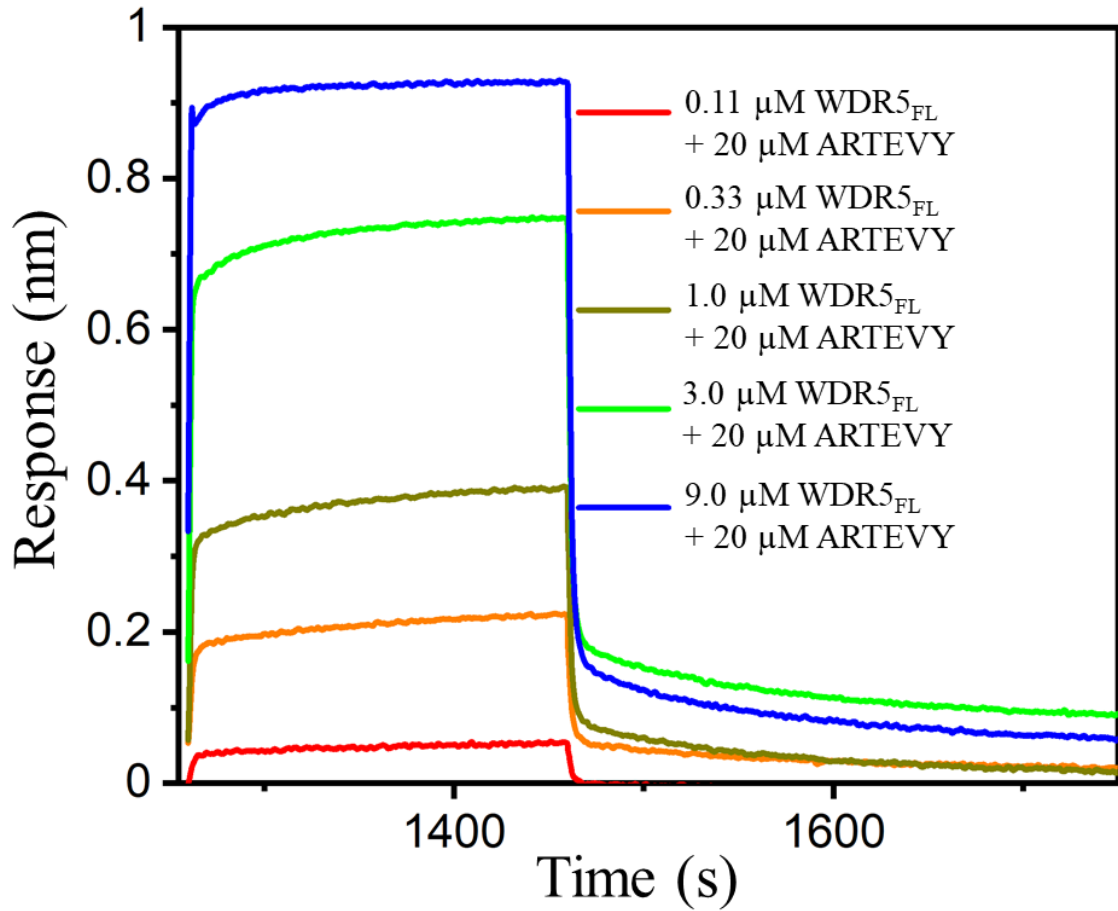


Figure S1: BLI Sensorgrams for RbBP5's interaction with ARTEVY saturated WDR5_{FL}. This figure shows BLI sensorgrams obtained for the interaction of RbBP5 with WDR5_{FL} + ARTEVY. Biotinylated RbBP5 peptide was immobilized as ligand on to Streptavidin sensors. The sensors were dipped into well containing different concentrations of WDR5 as analyte as well as 20 μM ARTEVY. The sensorgrams corresponding to the 5 different WDR5 concentrations used are shown below.

2. Kinetics measured for the RbBP5-WDR5 interaction

Table S1: WDR5_{FL} and WDR5_{ΔN}, kinetics and K_D, with RbBP5. The table shows k_{on} , k_{off} and K_D values for the interaction of RbBP5 peptide with WDR5_{FL} and WDR5_{ΔN}. For WDR5_{FL}, ARTEVY was spiked in the association well to block the Win site and prevent dimerization. Values were obtained using BLI sensorgrams in **figure S1** and **figure 4**. These sensorgrams were fitted to obtain k_{on} and k_{off} , which were used to indirectly obtain K_D . Triplicates were performed and the resultant mean \pm s.d values are shown.

	k_{on} ($\times 10^4 \text{ M}^{-1} \text{ s}^{-1}$)	k_{off} ($\times 10^{-1} \text{ s}^{-1}$)	K_D (μM)
WDR5_{FL}	17 \pm 2	2.4 \pm 0.3	1.4 \pm 0.4
WDR5_{ΔN}	9.4 \pm 1.1	1.4 \pm 0.1	1.5 \pm 0.3

3. Traces for the MLL3- WDR5_{ΔN} Interaction

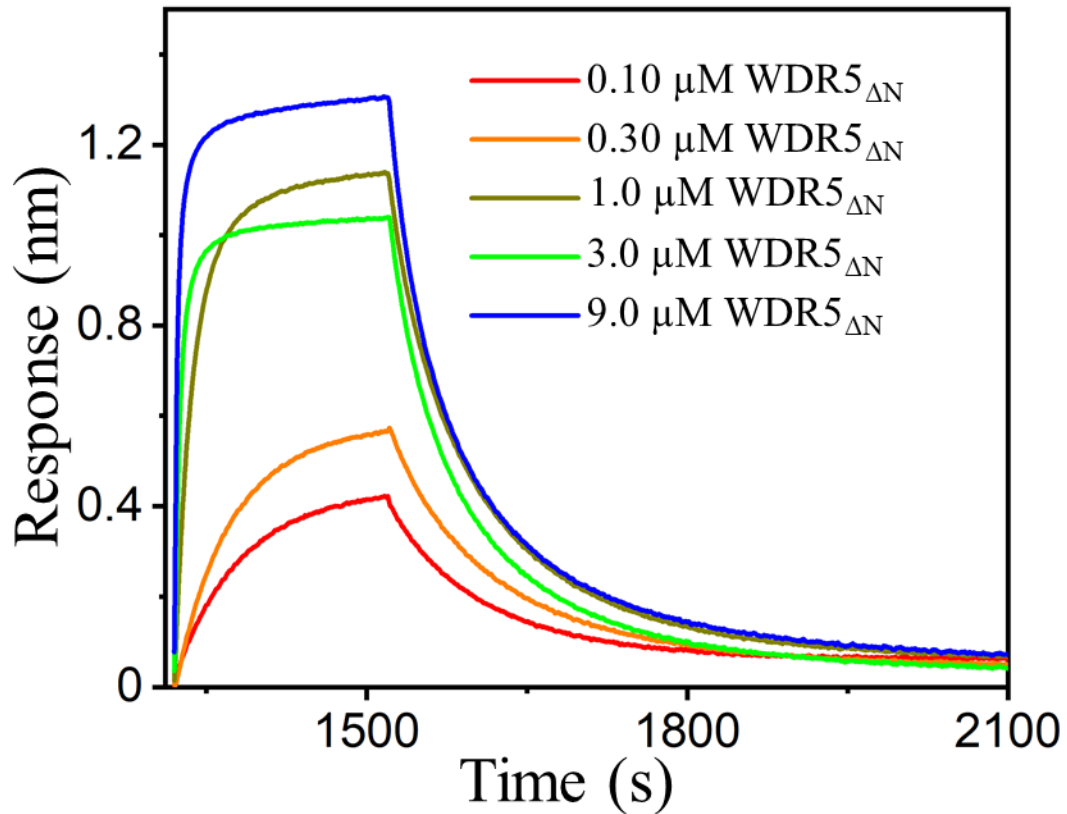


Figure S2: BLI sensorgrams for MLL3's interaction with WDR5_{ΔN}. This figure shows BLI sensorgrams obtained for the interaction of MLL3 with WDR5_{ΔN}. Biotinylated MLL3 peptide was immobilized as ligand on to Streptavidin sensors. The sensors were dipped into well containing different concentrations of WDR5_{ΔN} as analyte. The sensorgrams corresponding to the 5 different concentrations used are shown.

4. Kinetics measured for the MLL3-WDR5 interactions

Table S2: WDR5_{FL} and WDR5_{ΔN}, kinetics and K_D , with MLL3. The table shows k_{on} , k_{off} and K_D values for the interaction of MLL3 with WDR5_{FL}(3) and WDR5_{ΔN}. WDR5_{FL} values were taken from our previous work. WDR5_{ΔN} values were obtained using similarly acquired BLI sensorgrams shown in **figure S2**. These sensorgrams were fitted to obtain k_{on} and k_{off} , which were used to indirectly obtain K_D . Triplicates were performed and the resultant mean \pm s.d values are shown.

	k_{on} ($\times 10^4 M^{-1} s^{-1}$)	k_{off} ($\times 10^{-2} s^{-1}$)	K_D (nM)
WDR5_{ΔN}	6.3 \pm 2.8	0.97 \pm 0.04	170 \pm 70
WDR5_{FL}	6.6 \pm 1.8	1.2 \pm 0.2	190 \pm 60

5. Two state analysis of the RbBP5-WDR5_{FL} interaction

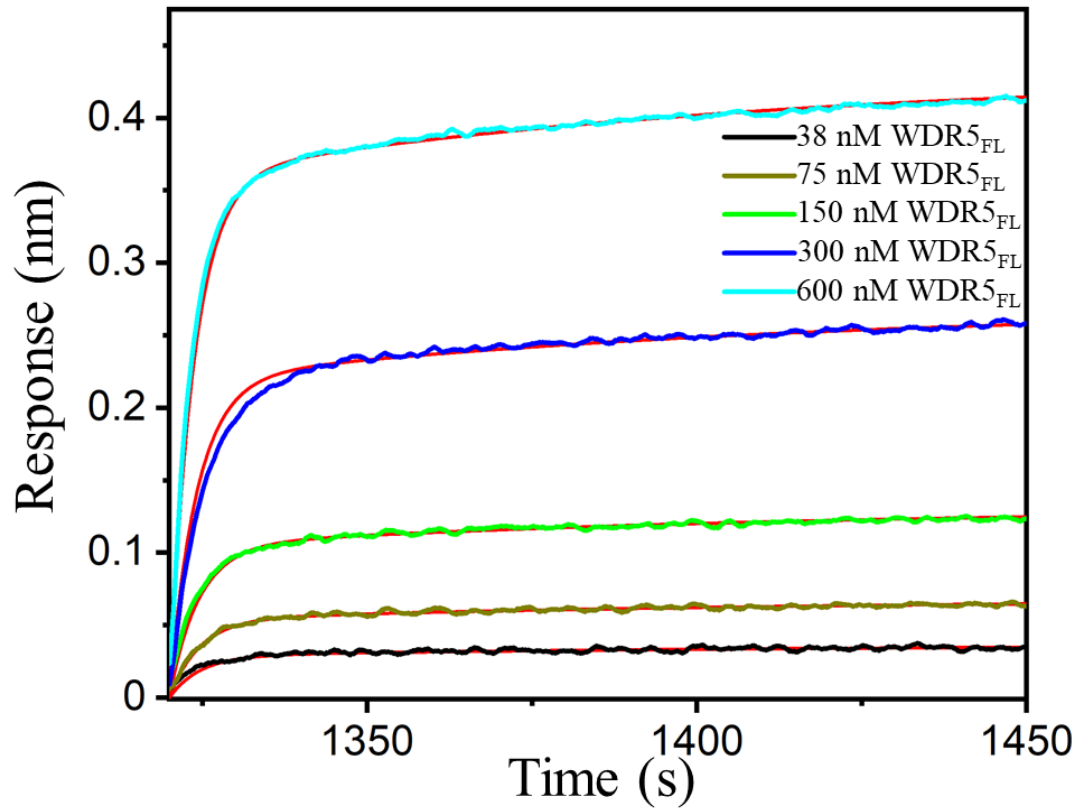


Figure S3: Two state fitted BLI sensorgrams for RbBP5's interaction with WDR5_{FL}. This figure shows BLI sensorgrams obtained for the interaction of RbBP5 with full length WDR5. Biotinylated RbBP5 peptide was immobilized as ligand on to Streptavidin sensors. The sensors were dipped into well containing different concentrations of WDR5_{FL} as analyte. The sensorgrams corresponding to the 5 different concentrations used are shown. Fitting was performed using MatLab and is shown in red.

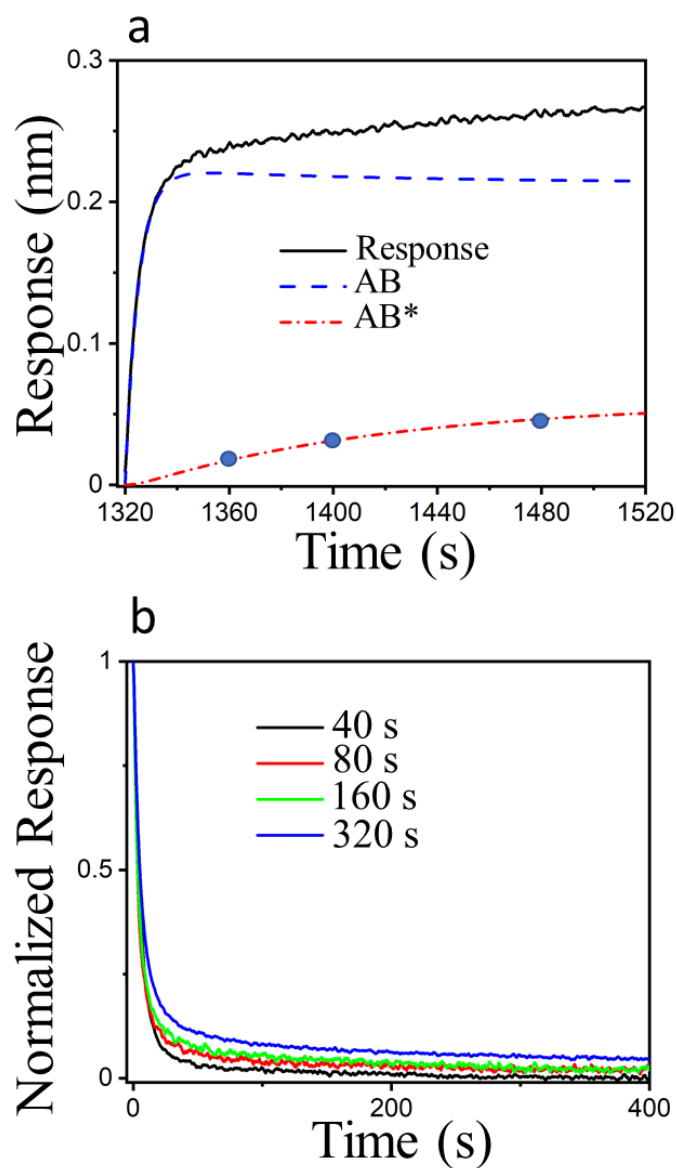


Figure S4: Two state analysis of RbBP5-WDR5_{FL} Interaction. (a) Raw Response and AB vs AB* composition obtained from two-state analysis of the RbBP-WDR5 association. The purple points show the time values chosen for the contact-time analysis and the corresponding AB* response. Analysis was performed using Matlab. (b) Normalized Dissociation curves obtained after different association times. The contact time was increased and the corresponding dissociation curves were analyzed Each curve was normalized using its starting value.

6. Known interactions at the RbBP5-WDR5 interface.

Table S3: Mapping of the Hydrogen bonds at the RbBP5-WDR5 interface.

These results were obtained using previously published co-crystallization data (PDB ID: 6KIW).¹ The cut-off distance for identifying these hydrogen bonds was 4.0 Å. Here, BB and SC denote backbone and side chain, respectively. These interactions were determined using protein interactions calculator (PIC).² The structure was not able to model the whole sequence of RbBP5, so these hydrogen bonds are not comprehensive. The first residue in each bond belongs to RbBP5, whereas the second one belongs to WDR5. BB and SC denote backbone and side chain, respectively.

Hydrogen Bonds	Distance (Å)	Type
S379-N225	3.4	BB-BB
E371-L249	2.5	BB-BB
S379-R181	3.3	BB-SC
D376-N225	3.1	BB-SC
V377-N225	3.5	BB-SC

Table S4: List of all known noncovalent interactions between RbBP5 and WDR5. These results were obtained in a similar method as for **Table S2**. For each interaction, the first residue corresponds to RbBP5 while the second residue corresponds to WDR5. The cut-off for ionic interactions was 6 Å, while for hydrophobic interactions it was 5 Å.

Ionic	Hydrophobic
E373-K245	V375-Y228
E373-K247	V375-L249
D372-K247	V377-Y228
E374-K272	V377-L240
D376-K272	V377-L249
E271-K291	V377-F266
	V377-L288

7. Impact of WBM Inhibitor

Table S5: Impact of WBM Inhibitor on RbBP5-WDR5 interaction. The table shows the impact of RbBP5 based inhibitor on the BLI response. 5 nM RbBP5 peptide was immobilized onto Streptavidin sensors and its interaction with 600 nM WDR5_{ΔN} was disrupted using the WBM inhibitor. The interaction was allowed to reach equilibrium and the highest response values were recorded. The normalized responses were calculated by setting the without inhibitor response to 1. Triplicates were performed and the resultant value mean ± s.d values are shown.

Inhibitor Concentration (μM)	Normalized Response
0	1
1	1.0 ± 0.1
5	0.65 ± 0.06
10	0.21 ± 0.05

8. Role of Charge Distribution

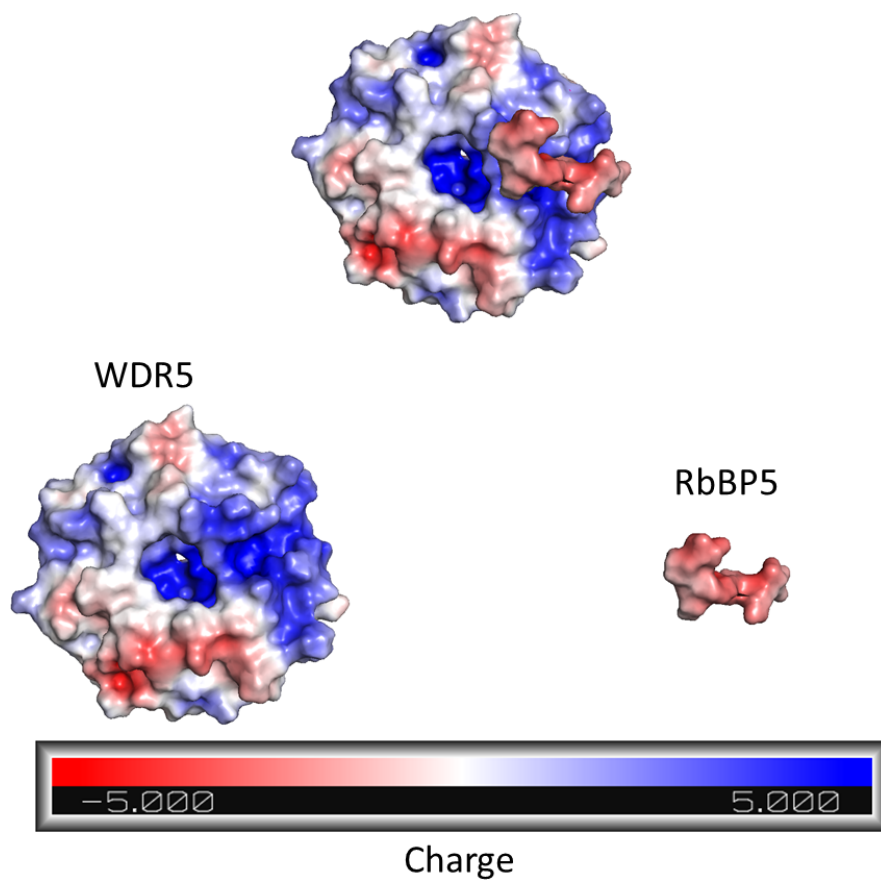


Figure S5: RbBP5 peptide and WDR5 charge distribution. The figures show the charge distributions on RbBP5 and WDR5.

9. RbBP5-WDR5 Δ N interactions in different buffer conditions

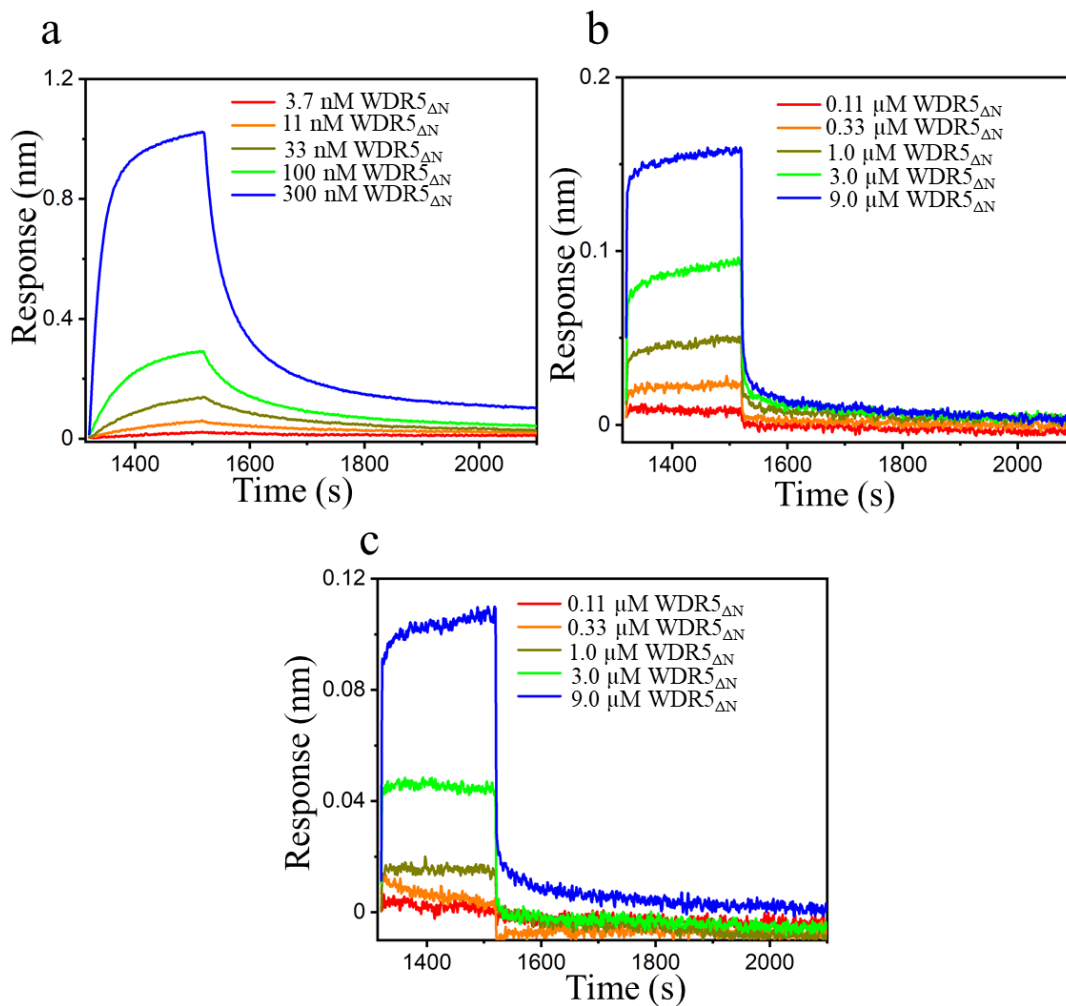


Figure S6: BLI Sensorgrams for different buffer conditions. This figure shows BLI sensorgrams obtained for the interaction of RbBP5 with WDR5 Δ N. Biotinylated RbBP5 peptide was immobilized as ligand on to Streptavidin sensors. The sensors were dipped into well containing different concentrations of WDR5 Δ N as analyte. The sensorgrams corresponding to the 5 different concentrations used are shown below. The NaCl concentration in the buffer was varied. (a) 50 mM NaCl (b) 300 mM NaCl (c) 600 mM NaCl

Table S6: Salt analysis. The table shows k_{on} , k_{off} and K_D values for the interaction of RbBP5 peptide with WDR5 $_{\Delta N}$ under different buffer conditions. The concentration of NaCl in the buffer was varied while other components were kept constant. Values were obtained using BLI. Sensorgrams were fitted to obtain k_{on} and k_{off} , which were used to indirectly obtain K_D . Triplicates were performed and the resultant mean \pm s.d values are shown.

Salt (mM NaCl)	k_{on} ($\times 10^4 \text{ M}^{-1} \text{ s}^{-1}$)	k_{off} ($\times 10^{-2} \text{ s}^{-1}$)	K_D (nM)
50	14 \pm 1	0.82 \pm 0.06	60 \pm 4
150	9.4 \pm 1.1	14 \pm 1	1500 \pm 300
300	10 \pm 1	19 \pm 2	1900 \pm 400
600	5.1 \pm 1.1	43 \pm 11	9300 \pm 4000

Supplementary References

1. Xue, H., Yao, T., Cao, M. *et al.* Structural basis of nucleosome recognition and modification by MLL methyltransferases. *Nature* 573, 445–449 (2019).
2. K. G. Tina, R. Bhadra and N. Srinivasan, PIC: Protein Interactions Calculator, *Nucleic Acids Research*, 2007, Vol. 35, Web Server issue W473–W476
3. Chapter 4

5.7 REFERENCES

1. Guarnaccia, A. D.; Tansey, W. P., Moonlighting with WDR5: A Cellular Multitasker. *J. Clin. Med.* **2018**, *7* (2).
2. Song, J. J.; Kingston, R. E., WDR5 interacts with mixed lineage leukemia (MLL) protein via the histone H3-binding pocket. *J. Biol. Chem.* **2008**, *283* (50), 35258-64.
3. Patel, A.; Vought, V. E.; Dharmarajan, V.; Cosgrove, M. S., A conserved arginine-containing motif crucial for the assembly and enzymatic activity of the mixed lineage leukemia protein-1 core complex. *J. Biol. Chem.* **2008**, *283* (47), 32162-75.
4. Shinsky, S. A.; Monteith, K. E.; Viggiano, S.; Cosgrove, M. S., Biochemical reconstitution and phylogenetic comparison of human SET1 family core complexes involved in histone methylation. *J. Biol. Chem.* **2015**, *290* (10), 6361-75.
5. Ernst, P.; Vakoc, C. R., WRAD: enabler of the SET1-family of H3K4 methyltransferases. *Brief. Funct. Genomics* **2012**, *11* (3), 217-26.
6. Avdic, V.; Zhang, P.; Lanouette, S.; Groulx, A.; Tremblay, V.; Brunzelle, J.; Couture, J. F., Structural and biochemical insights into MLL1 core complex assembly. *Structure* **2011**, *19* (1), 101-8.
7. Imran, A.; Moyer, B. S.; Canning, A. J.; Kalina, D.; Duncan, T. M.; Moody, K. J.; Wolfe, A. J.; Cosgrove, M. S.; Movileanu, L., Kinetics of the multitasking high-affinity Win binding site of WDR5 in restricted and unrestricted conditions. *Biochem. J.* **2021**, *478* (11), 2145-2161.
8. Han, J.; Li, T.; Li, Y.; Li, M.; Wang, X.; Peng, C.; Su, C.; Li, N.; Li, Y.; Xu, Y.; Chen, Y., The internal interaction in RBBP5 regulates assembly and activity of MLL1 methyltransferase complex. *Nucleic Acids Res.* **2019**, *47* (19), 10426-10438.
9. Li, Y.; Han, J.; Zhang, Y.; Cao, F.; Liu, Z.; Li, S.; Wu, J.; Hu, C.; Wang, Y.; Shuai, J.; Chen, J.; Cao, L.; Li, D.; Shi, P.; Tian, C.; Zhang, J.; Dou, Y.; Li, G.; Chen, Y.; Lei, M., Structural basis for activity regulation of MLL family methyltransferases. *Nature* **2016**, *530* (7591), 447-52.
10. Thomas, L. R.; Adams, C. M.; Fesik, S. W.; Eischen, C. M.; Tansey, W. P., Targeting MYC through WDR5. *Mol. Cell. Oncol.* **2020**, *7* (2), 1709388.
11. Thomas, L. R.; Adams, C. M.; Wang, J.; Weissmiller, A. M.; Creighton, J.; Lorey, S. L.; Liu, Q.; Fesik, S. W.; Eischen, C. M.; Tansey, W. P., Interaction of the oncoprotein transcription factor MYC with its chromatin cofactor WDR5 is essential for tumor maintenance. *Proceedings of the National Academy of Sciences*

of the United States of America **2019**, 116 (50), 25260-25268.

12. Thomas, L. R.; Foshage, A. M.; Weissmiller, A. M.; Tansey, W. P., The MYC-WDR5 Nexus and Cancer. *Cancer Res.* **2015**, 75 (19), 4012-5.
13. Thomas, L. R.; Wang, Q.; Grieb, B. C.; Phan, J.; Foshage, A. M.; Sun, Q.; Olejniczak, E. T.; Clark, T.; Dey, S.; Lorey, S.; Alicie, B.; Howard, G. C.; Cawthon, B.; Ess, K. C.; Eischen, C. M.; Zhao, Z.; Fesik, S. W.; Tansey, W. P., Interaction with WDR5 promotes target gene recognition and tumorigenesis by MYC. *Mol. Cell. Biochem.* **2015**, 58 (3), 440-52.
14. Guarnaccia, A. D.; Rose, K. L.; Wang, J.; Zhao, B.; Popay, T. M.; Wang, C. E.; Guerrazzi, K.; Hill, S.; Woodley, C. M.; Hansen, T. J.; Lorey, S. L.; Shaw, J. G.; Payne, W. G.; Weissmiller, A. M.; Olejniczak, E. T.; Fesik, S. W.; Liu, Q.; Tansey, W. P., Impact of WIN site inhibitor on the WDR5 interactome. *Cell Rep.* **2021**, 34 (3), 108636.
15. Patel, A.; Dharmarajan, V.; Cosgrove, M. S., Structure of WDR5 bound to mixed lineage leukemia protein-1 peptide. *J. Biol. Chem.* **2008**, 283 (47), 32158-6
16. Dharmarajan, V.; Lee, J. H.; Patel, A.; Skalnik, D. G.; Cosgrove, M. S., Structural basis for WDR5 interaction (Win) motif recognition in human SET1 family histone methyltransferases. *J. Biol. Chem.* **2012**, 287 (33), 27275-89.
17. Zhang, P.; Lee, H.; Brunzelle, J. S.; Couture, J. F., The plasticity of WDR5 peptide-binding cleft enables the binding of the SET1 family of histone methyltransferases. *Nucleic Acids Res.* **2012**, 40 (9), 4237-46.
18. Odho, Z.; Southall, S. M.; Wilson, J. R., Characterization of a novel WDR5-binding site that recruits RbBP5 through a conserved motif to enhance methylation of histone H3 lysine 4 by mixed lineage leukemia protein-1. *J. Biol. Chem.* **2010**, 285 (43), 32967-76.
19. Schuetz, A.; Allali-Hassani, A.; Martín, F.; Loppnau, P.; Vedadi, M.; Bochkarev, A.; Plotnikov, A. N.; Arrowsmith, C. H.; Min, J., Structural basis for molecular recognition and presentation of histone H3 by WDR5. *EMBO J.* **2006**, 25 (18), 4245-52.
20. Lund-Katz, S.; Nguyen, D.; Dhanasekaran, P.; Kono, M.; Nickel, M.; Saito, H.; Phillips, M. C. Surface Plasmon Resonance Analysis of the Mechanism of Binding of ApoA-I to High Density Lipoprotein Particles. *J Lipid Res* **2010**, 51 (3), 606–617.

Chapter 6: Summary and Future work

In summary, we have extracted the kinetics of WDR5-SET1 interactions as well as of WDR5's interaction with RbBP5. We used SET1_{win} peptides to emulate the binding sites of large SET1 proteins and we studied their interactions with WDR5 using BLI, SPR and FP methods. The use of multiple bulk-phase techniques increased confidence in our findings. It shows how the use of orthogonal approaches ensures that derived results are credible and reproducible across techniques. Furthermore, the exploration of the effects of restrictions on interacting partners provides much-needed information on how to interpret the results derived from different bulk-phase techniques.

Additionally, in the case of the Win site interactions, we have obtained association and dissociation rates for wild-type WDR5 as well WDR5 cancer mutants. These mutants were divided into two categories: surface mutants and cavity mutants. The surface mutants included, D172A, P216L and Y260 H. While the cavity mutants included F133L, S175L, S218F and D92N. We used BLI to extract kinetics and indirectly calculate the K_D , and then we validated our findings using FP. We observed divergent impacts of Win site mutations on the kinetics of the Win site interactions. All of the Win site binders were not always impacted the same way due to these mutations. This study will help lay the groundwork for precision medicine. Understanding the impacts of individual mutations in cancers sets up the base for having tailor made drugs to counter those effects.

Moreover, our work with varying the surface-tethering conditions for these interactions investigated interesting experimental phenomenon. We looked at three conditions: short tether (ST), long tether (LT) and no tether (NT). We studied the interactions of SET1_{win} peptides with WDR5 under these conditions. For the ST case, the peptides were attached to a BLI sensor surface using 3 residue (GGS) tethers. For the LT case the tethers were elongated to 6 residues (GGS)³. While for the NT conditions WDR5 was immobilized onto a SPR sensor and the peptides were free in solution. Our results showed that as the conditions changed, so did the rates of association and dissociation. The LT condition provided faster association rates and slower dissociation rates as compared to the ST condition. However, NT conditions exhibited even faster association rates compared to LT. The dissociation rates under LT and NT conditions were very similar. This work provides experimental evidence of the fly-casting mechanism of association between a surface tethered ligand and its receptor. Furthermore, it looks at the entropic force modulating the dissociation rate constants of these interactions, in a quantifiable way. This approach allowed us to set up a model to predict the effects of surface tethering and then test these using more sets of interactions.

Finally, the exploration of the interaction of RbBP5 with WDR5 showed that WBM interactions are also amenable to study using BLI. We provide kinetics of this interaction for WDR5_{FL} as well as WDR5_{ΔN}, using a peptide containing the RbBP5 WBM sequence. Moreover, we establish that the N-terminus IDR of WDR5 can insert into the Win site cavity. This detailed work shows conclusively that this IDR can impact BLI measurements of WBM site kinetics. Also, it confirms the self-

association behavior of WDR5. This result is also potentially crucial in explaining how WDR5 is able to have a wide range of interacting partners while maintaining specificity.

Future work on in this regard can focus on other yet to be kinetically explored binding partners of WDR5. In this direction, we have already obtained preliminary data for the MYC-WDR5 interaction as shown in figure 1.

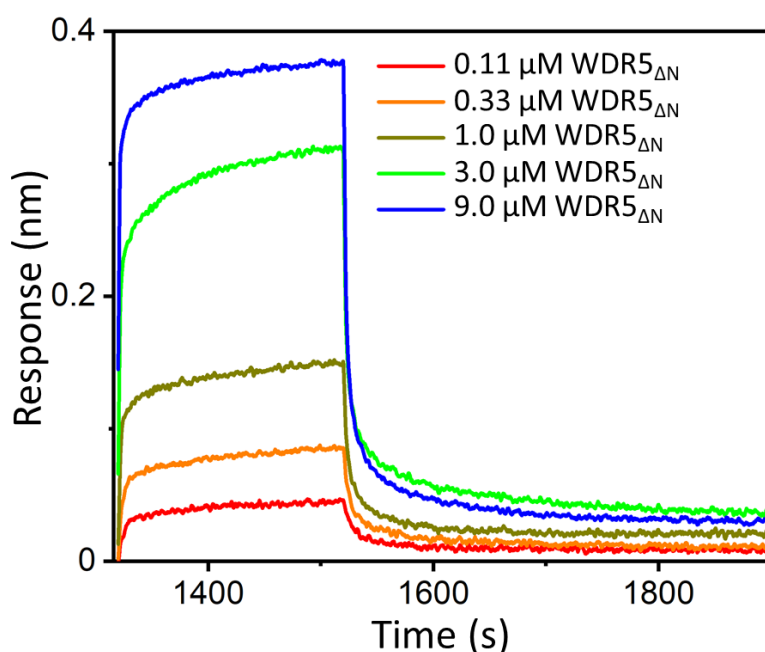


Figure 1: BLI sensorgram of the MYC- WDR5 Δ N interaction. This figure shows BLI sensorgrams obtained for the interaction of MYC with WDR5 Δ N. Biotinylated MYC peptide, containing the WBM motif, was immobilized as ligand on to Streptavidin sensors. The sensors were dipped into well containing different concentrations of WDR5 Δ N as analyte. Here, the sensorgrams corresponding to the 5 different concentrations are shown.

Furthermore, now that we understand of the kinetics of the interactions mediated by the Win site using SET1 representative peptides, we can investigate these kinetics with larger fragment of the SET1 proteins. For this purpose, we can use the

truncated proteins of SET1 family members i.e., MLL1³⁷⁴⁵⁻³⁹⁶⁹, MLL2^{5319- 5537}, MLL3⁴⁶⁸⁹⁻⁴⁹¹¹, MLL4²⁴⁹⁰⁻²⁷¹⁵, SETd1A¹⁴⁷⁴⁻¹⁷⁰⁸, and SETd1B¹⁷²⁷⁻¹⁹⁶⁶. These SET1 fragments include the Win motif, required for binding to WDR5, as well as the SET domain, responsible for catalyzing histone methylation. Studying these larger fragments would bring us one step closer in mimicking *in vivo* conditions for our *in vitro* experiments. Also, we can use these proteins along with the members of the SET1 family core complex to look at the stability of the complexes formed by the SET1 proteins. By immobilizing SET1 fragments onto biosensors and allowing them to interact with combinations of analytes we can study the preference for the formations of different sub-complexes as well as their stabilities.

Curriculum Vitae

Ali Imran

204 Ostrom Ave, Apt 3 | Syracuse, NY, 13210 | 201-993-6432 | aimran@syr.edu

SUMMARY

- Biophysicist with a focus on cancer research
- 3+ years of experience in quantifying protein-protein interactions using multiple in-vitro techniques: BLI, SPR, and FP
- Experienced in creating models and computational simulations
- Designed projects and experiments that addressed knowledge gaps in the field
- Managed research collaborations involving multiple institutions
- Produced 5 papers

EDUCATION

Syracuse University (Syracuse, NY): *PhD Physics* **May 2022**

- Biophysical research quantifying protein-protein interactions
- Research Excellence Doctoral Funding Fellowship 2021
- Public Relations Officer, Physics Graduate Student Organization
- Academic Program Senator, Graduate Student Organization,

Syracuse University (Syracuse, NY): *MS Physics* **Dec 2018**

Lahore University of Management Sciences (LUMS, Lahore, Pakistan): BS Physics **May 2016**

- Minor in Computer Science
- Dean's Honor List: 2013, 2014, 2015, and 2016
- Assistant Director, Blood Link, LUMS Community Service Society

RESEARCH EXPERIENCE

Syracuse University **2016 – Present**

- Established Oncogenic Potential of WDR5 Win-site mutations using multiple in-vitro techniques
- Investigated the modulation of Protein-Protein Interactions Using Tether length as a parameter
- Modelled BLI and SPR results for Two State Protein-Protein Interactions using MATLAB and Python
- Investigated Mutation Clustering of High Probability Driver Mutations by utilizing established computational methods
- Analyzed WBM-site Interactions of WDR5 using BLI
- Characterized Win-site Interactions of WDR5 using BLI, SPR and FP

CERN **June – August 2015**

- Created program that extracted test pulse shape from prototype detectors

- Evaluated Pedestal Noise measurement in detector channels using multiple fitting approaches

WORK EXPERIENCE

Ichor Therapeutics (LaFayette, New York, USA) **March – May 2021**

- Graduate Research Fellow
- Investigated Allosteric Effect in WDR5 using SPR and FP
- Optimized ELISA assays for clients

CERN (Geneva, Switzerland) **June – August 2015**
Summer Student Program

Dollar Industries (Pvt.) Ltd (Karachi, Pakistan) **May – July 2014**

- Quality Assurance Analyst
- Created SOPs for Quality Control

PUBLICATIONS

Imran, A., ... Movileanu, L. (2022). Convergent Oncogenic Alterations of a Protein Hub Produce Divergent Effects Within a Binding Site. (Submitted)

Imran, A., ... Movileanu, L. (2022). The Interplay of Affinity and Physical Restraint in Protein Recognition. (Submitted)

Mayse, L. A., **Imran, A.**, ... & Movileanu, L. (2022). Disentangling the recognition complexity of a protein hub using a nanopore. *Nature Communications*, 978(13).

Imran, A., ... Movileanu, L. (2021). Kinetics of the multitasking high-affinity Win binding site of WDR5 in restricted and unrestricted conditions. *The Biochemical journal*, 478(11).

Imran, A., Popescu, D., & Movileanu, Liviu. (2020). Cyclic Activity of an Osmotically Stressed Liposome in a Finite Hypotonic Environment. *Langmuir*, 36(13).

TECHNICAL SKILLS

Research: Project Design, Collaborative Leadership, Data Analysis, Data Visualization, Communication and Publishing

Biophysical: Biolayer Interferometry (BLI), Fluorescence Polarization (FP), Surface Plasmon Resonance (SPR), ELISA, Isothermal Titration Calorimetry (ITC) and Computational Clustering

Languages: C++, Python, Java, MySQL and Php

Softwares: Pymol, Mathematica, Microsoft Excel, GraphPad, Origin, Labview, Latex and MatLab